Biophysical Studies of Repeats of Marsupial Prion Protein: Application of Low-Resolution Spectroscopy Methods to Low-Complexity Peptide Sequences

Marsia Gustiananda

A thesis submitted for the degree of Doctor of Philosophy
of the Australian National University

June 2003

Statement of Originality

The contents of this thesis are the result of my original research, which has been conducted under the principal supervision of Dr. Jill Gready (John Curtin School of Medical Research, ANU).

Part of the work presented in Chapter III has been published jointly with others:

Gustiananda, M., Haris, P. I., Milburn, P. J. and Gready, J. E. (2002). Copper-induced conformational change in a marsupial prion protein repeat peptide probed using FTIR spectroscopy. *FEBS Letters* **512**: 38-42.

The molecular dynamics simulation presented in Chapter V was performed by Dr. Peter Cummins (John Curtin School of Medical Research, ANU) and analyzed by Dr. John Liggins (John Curtin School of Medical Research, ANU). The experiment of temperature dependence study of the complete peptides set, presented in Chapter V, was performed by Dr. John Liggins.

I declare that the work presented in this thesis is to my belief original, except as acknowledged in the text and above, and that the material has not been submitted, either in whole or in part, for a degree at this or any other university.

Marsia Gustiananda

June 2003

Amendments

To correct the impression that a marsupial is not a mammal, the word 'mammalian' should be added after the word "marsupial' (page iv, first paragraph, line 2). The words 'placental (eutherian)' should be added before 'mammalian' (page iv, first paragraph, line 7). In the rest of the thesis, the word 'mammalian' should be taken to refer to placental (eutherian) mammalian and the word 'marsupial' should be taken to refer to marsupial mammalian.

p127, caption to Figure 5.1, line 3 "λ_{max} 355 nm" should be corrected to "λ_{max} 335 nm".

p180, caption to Table 7.2, add sentences:
The symbols for a free peptide species of PHGGGWGQ-NH_2 and Ac-PHGGGWGQ-NH_2 are HL and L, respectively. The copper complex species of HL and L are CuHL and CuL, respectively. $CuH_{-n}L$, n = 1, 2, 3, 4 indicates sequential deprotonation of amide nitogens in copper complex species.

Acknowledgements

I owe the greatest debt to my supervisor Dr. Jill Gready for her intellectual support, advice, useful criticism, and continuous guidance throughout the duration of my study, and for her patience and generosity with her time, comments, suggestions, and corrections on every draft of my thesis.

I am also indebted to Dr. Parvez I. Haris from the De Montfort University, United Kingdom, for his advice, comments, and suggestions for the interpretation of the FTIR spectra. I thank Dr. Jun Y Fan for her expertise, guidance, and help during the early years of my research. Jun has taught me to use the fluorescence spectrophotometer, the UV/Vis absorption spectrophotometers, and to analyze the binding data. I thank her for her encouragement for me to use the FTIR method, which turned out to be very useful in my research. I also would like to express my gratitude to my advisers Dr. Peter Milburn and Dr. Peter Jeffrey for giving me guidance in the early stage of my research. I thank Dr. John Liggins for doing the lengthy experiments on the temperature dependence of the FRET distances for the complete peptides set. I thank Dr. Peter Cummins, and also Dr. John Liggins, for their contributions to performing the MD simulation of the FRET distances.

Many of the experiments carried out during this project would not have been possible without the help of staff at various research schools and faculties in the Australian National University. I would like to thank Professor Bruce Wild from the Research School of Chemistry (RSC) for generously providing access to his FTIR and CD instruments. I also would like to thank Mr. Paul Gugger and Mr. Horst Neumann from the RSC for assisting me with the experimental set up of FTIR and CD. I also would like to thank all staffs and students of the RSC who, because I was using the FTIR instruments, had to reschedule their work. I thank them for their patience and understanding. I thank Mr. Karl Braybrook, Ms. Jenni Rothschild, Mr. Gordon Lockhart, and Dr. Phil Jackson from the Mass Spectrometry Unit of the RSC, for running my samples. I would like to thank Mr. John Marsh (Forestry Department) for providing me access to his AAS instrument. For generously providing me access to their ICP OES instrument, I thank Dr. Steve Eggins, Dr. Andy Christy, and Mr. Tony Phimpisane (Geology Department). The equilibrium dialysis experiments would not

have been possible without help from Mr. Nick Best (JCSMR workshop), who made all 40 ED chambers and the rotation apparatus. I thank Dr. Karen Edwards and Mr. Kerry McAndrew, from the Biomolecular Resource Facility of the JCSMR, for supplying most of the peptides I used in my research, and for useful consultation on how to handle the peptides.

My study at the Australian National University, Canberra, was made possible by a scholarship from the Australian Government through AusAid to pursue a Masters degree, and payment of tuition fees from my supervisor's funds for upgrading to a PhD degree. For this great and invaluable support I thank them very much.

To all my friends in SCUNA (ANU Choral Society), I enjoyed singing with you, thank you for providing me a cheerful sanctuary full of laugh and song.

I wish to sincerely thank my mother Sulastri and my father Marsel Yacoub for lifelong support and encouragement. I gained mental and physical strength from their prayers so that I could finish the thesis. I thank my elder sister Yuli and her husband Purwadi who have been particularly supportive of my academic pursuits. For a lot of moral support from afar, I thank my husband parents, my little brothers Zeni and Purna, and all my family in Indonesia.

My most heartfelt thank goes to my husband Siswo Pramono for his love, patience, and understanding. He encouraged me and gave me strong motivation to upgrade into PhD degree. I thank him for always be there for me, despite the fact that he has his own PhD thesis to finish at the same time as mine. I would have never seen this thesis through to completion without his unfailing and wonderful support throughout the years of my study. This thesis is dedicated to him.

Abstract

Biophysical properties of the PrP-repeat sequences from the brush-tailed possum (i.e. a marsupial) are reported. The results of several methods (FTIR, fluorescence, FRET, ESI MS, CD, ED, UV/Vis absorption spectroscopy) have been integrated to provide information on the conformation, and conformational changes, of marsupial PrP-repeat (Msp) peptide under various conditions (peptide length, pH and presence of copper ions), and the copper-binding properties (binding strength, stoichiometry, and binding sites). Similarities and differences between the properties of marsupial and mammalian PrP repeats, which have significantly different repeats sequences, were also analyzed.

The conformation of Msp peptides was studied mainly by FTIR spectroscopy, which showed that in the absence of copper ions Msp peptides are disordered throughout pH 6.0-9.0. The presence of disordered structure was also evident in CD spectra. Although they are disordered, inter-residue distance data obtained from FRET experiments combined with MD simulations showed the peptides are loosely folded, and not staggered or fully extended. The simulations also indicated that the peptide does not adopt only one conformation. Copper binding to longer peptides induced the formation of a more hydrogen-bonded structure, as shown by the shift of the IR amide I band toward lower frequency and changes in CD spectra.

Copper-binding strength was measured primarily by fluorescence titration spectroscopy. The shape of the saturation curve indicates that copper binds very tightly to Msp peptides with free imino terminus. Under the experimental conditions, acetylation of the N-terminus abolishes the binding ability of the peptides or suggests far weaker binding. ED was also employed to investigate copper binding to a rather high molecular weight Msp peptide. However, the binding strengths obtained from ED do not agree with the fluorimetry results.

Amidation of the C-terminus does not affect the binding strength but greatly influence the stoichiometry. In the absence of this group, one copper ion binds to more than one molecule of peptide, which suggests multimerisation. However, this multimerisation was not detected when stoichiometry was measured using ESI MS and ED, the last two

methods using peptide concentrations 10-20 times higher than the fluorescence method. Fluorimetry experiments also showed that the stoichiometry as well as the copper-binding affinity depended greatly on the peptide concentration.

FTIR spectra, fluorimetry, and ESI MS data show that the N-terminally free Msp peptides $(PH\underline{P}GGSNWGQ)_{n = 1, 2, 3, 4}$ binds copper ion through the imino end group of Pro as the anchoring site. The amide nitrogen and the N_π atom of the His^2 also participate in copper binding. At higher peptide concentration and pH higher than 8 copper binding to the N-terminally capped Msp peptides was detected by FTIR. The data suggest that the copper-anchoring site in these peptides is the N_π atom of the His^2. The amide nitrogens of the Gly^4 and Gly^5 complete the copper-coordination sphere. Mutation of the Pro^3 into Gly^3 ($^1PH\underline{G}GGSNWGQ^{10}$) increases the ability of the N-terminally capped peptide to bind copper, suggesting that the NH group of the amide backbone of the Gly^3 found naturally in the human PrP octarepeat ($^1PHGGGWGQ^8$), is also a copper-binding site.

This thesis also proposes a possible interaction, which stabilizes the loosely folded structure in PrP-repeat peptides, as cation-π or π-π interactions between Trp and His residues. The influence of cation-π or π-π interactions on the conformational stability of PrP-repeat peptides needs to be investigated further.

Table of Contents

Statement of Originality i
Acknowledgement ii
Abstract iv
Table of Contents vi
List of Figures x
List of Tables xiii
List of Abbreviations xiv

Chapter I Introduction 1
1.1. 3-D structure of PrP 1
1.2. Copper binding and the proposed functions of PrP 3
1.3. Repeats region of PrP 4
1.4. PrP repeats as a segment with low-complexity sequence 4
1.5. Copper binding to PrP repeats 6
1.5.1. Structure of PrP repeats in the absence and presence of copper ion 7
1.5.2. Dissociation constant (K_d) of copper binding to PrP repeats 10
1.5.3. Stoichiometry of copper binding to PrP repeats 14
1.5.4. Copper coordination in PrP repeats 17
1.5.5. Copper binding to post-repeat region 26
1.6. Sugar binding to PrP repeats 27
1.7. Review of low-complexity proteins and methods in general to study them 27
1.8. Copper-binding mode in PrP from species other than mammalian 28

Chapter II Materials and Methods 30
2.1. Instrumentation 30
2.1.1. UV/Vis spectrophotometer 30
2.1.2. High-pressure liquid chromatography (HPLC) 30
2.1.3. Chromatography column 30
2.1.4. Fluorescence spectrophotometer 30
2.1.5. Electrospray ionization mass spectrophotometer (ESI MS) 31
2.1.6. Fourier transform infrared spectrophotometer (FTIR) 31
2.1.7. Circular dichroism spectrophotometer (CD) 31
2.1.8. Equilibrium dialysis (ED) apparatus 31
2.1.9. Inductively coupled plasma optical emission spectrophotometer (ICP OES) 31
2.2. Materials 31
2.2.1. Synthetic peptides 31
2.2.1.1. Peptide synthesis 32
2.2.1.2. Peptide purification: the removal of residual trifluoroacetic acid (TFA) 33
2.2.1.3. Preparation of stock peptide solutions 33
2.2.2. General buffer and reagent solution 34
2.2.2.1. Preparation of stock PBS (phosphate buffered saline) buffer 34
2.2.2.2. Preparation of stock NEM (N-ethylmorpholine) buffer 34
2.2.2.3. Preparation of stock phosphate buffer solutions at pH 6.0, 7.4 and 8.0 35
2.2.2.4. Preparation of stock universal buffer solution pH 3.0-8.0 35
2.2.2.5. Preparation of stock solutions of metal salts 35

Chapter III Fourier Transform Infrared Spectroscopy 36
3.1. Introduction 36
3.2. Aims 37
3.3. Materials and methods 38
3.3.1. Sample preparation 38
3.3.2. Infrared spectroscopic measurement and analysis 39
3.4. Results and discussion 40
3.4.1. FTIR spectra of Msp1 group in the absence and the presence of copper ions 40
3.4.1.1 Conformational analysis - amide I band at ~1650 cm^{-1} 40

3.4.1.2. Assignment of the band at 1611-1617 cm^{-1} 43
3.4.1.3. Assignment of the ~1590 cm^{-1} and 1560 cm^{-1} band 48
3.4.1.4. Tautomeric forms of His ring 53
3.4.1.5. Assignment of the band at 1500-1506 cm^{-1} 58
3.4.1.6. Copper-binding sites in Msp1 group peptides (PHPGGSNWGQG) 59
3.4.2. FTIR spectra of Msp1P3GcapNC (Ac-PHGGGSNWGQG-NH_2) 60
3.4.3. FTIR spectra of Msp_1strepcapNC (Ac-PQGGGTNWGQG-NH_2) 63
3.4.4. FTIR spectra of Msp_4threpcapNC (Ac-PHGGSNWGQG-NH_2) 64
3.4.5. FTIR spectra of Hu1capNC (PHGGGWGQG) 66
3.4.6. Conformational analysis of multi-repeat peptides (Msp2 group, Msp3 group, and Msp4 group) in the absence and presence of copper ions 68
3.4.6.1. Msp2 group peptides 68
3.4.6.2. Msp3 group peptides 73
3.4.6.3. Msp4 group peptides 78
3.4.7. Copper-binding sites in multi-repeat (Msp2, Msp3, and Msp4 group) peptides. 82
3.4.8. Copper titration of Msp1 at pH 8.0 83
3.4.9. Binding of other metals to Msp1 and Msp4 85
3.5. Conclusions 88

Chapter IV Fluorescence Titration Spectrophotometry 90
4.1. Introduction 90
4.2. Aims 93
4.3. Materials and methods 94
4.3.1. Sample preparation 94
4.3.2. Conditions of data acquisition and data analysis 95
4.4. Results and discussion 96
4.4.1. The emission maximum of Msp peptides does not change upon copper addition 96
4.4.2. Titrations have been carried out under stoichiometric binding conditions 96
4.4.3. Different equations used to describe different binding conditions 97
4.4.4. Copper-binding properties of Mspn (n = 1, 2, 3, and 4) group peptides 98
4.4.4.1. The effect of N-terminal capping on copper binding to the peptides 98
4.4.4.2. The K_d values for copper binding to the peptides at pH 6.0, 7.4, and 8.0 98
4.4.4.3. The stoichiometry of the binding (C_s) 109
4.4.5. Effect of peptide concentration on K_d and C_s values 110
4.4.6. Copper binding to mutant and variant Msp1 peptide 114
4.4.7. Copper binding to Msp1 His-methylated peptide 117
4.4.8. Copper binding to repeat peptides with modified sequences 119
4.5. Conclusions 120

Chapter V Fluorescence Resonance Energy Transfer 122
5.1. Introduction 122
5.2. Aims 123
5.3. Materials and methods 123
5.3.1. Sample preparation 123
5.3.2. Fluorescence measurements 124
5.3.3. Calculation of donor-acceptor apparent distance 126
5.4. Results and discussion 127
5.4.1. Spectral overlap between Trp and dansyl 127
5.4.2. CD spectra of dansylated peptide 128
5.4.3. Dansyl fluorescence at 535 nm as other evidence for energy transfer 129
5.4.4. pH effect on the Trp fluorescence emission intensity of dansylated and nondansylated peptides 130
5.4.5. pH dependence of FRET distances 131
5.4.6. Comparison of FRET distances in Msp1capNC, Msp2capNC, and Hu1capNC peptides 133
5.4.7. The FRET distance indicates the peptides are loosely compacted 134
5.4.8. Temperature dependence of FRET distances 135

5.4.9. A comparison of FRET distances and MD simulation 140
5.4.10. Copper-ion binding and FRET distances 140
5.5. Conclusions 141

Chapter VI Electrospray Ionization Mass Spectrometry 143
6.1. Introduction 143
6.1.1. Principles of electrospray ionization mass spectrometry 143
6.1.2. Mass spectrometry in the study of copper binding to PrP-repeat peptides 145
6.2. Aims 146
6.3. Materials and methods 146
6.3.1. Sample preparation 146
6.3.2. Choice of buffers 147
6.3.3. Conditions of data acquisition 147
6.4. Results and discussion 147
6.4.1. Copper binding to Msp2, Msp3, and Msp4 peptides 147
6.4.2. Binding of other metal ions to Msp2 153
6.4.3. Copper ion titration of Msp4 157
6.4.4. Copper binding to Msp1 and its modified peptides 160
6.5. Conclusions 164

Chapter VII Other Approaches: Equilibrium Dialysis, Circular Dichroism, and Visible Absorption Spectroscopy 166
7.1. Equilibrium dialysis 166
7.1.1. Introduction 166
7.1.2. Aims 167
7.1.3. Materials and methods 167
7.1.3.1. Materials and apparatus 167
7.1.3.2. Methods 168
7.1.4. Results and discussion 170
7.1.4.1. Design of the dialysis chamber 170
7.1.4.2. Time for equilibration 171
7.1.4.3. Copper binding to Msp peptides at pH 7.4 171
7.1.5. Conclusions from ED experiments 172
7.2. Circular dichroism spectroscopy 174
7.2.1. Introduction 174
7.2.2. Aims 174
7.2.3. Materials and methods 175
7.2.3.1. Sample preparation 175
7.2.3.2. CD measurement 175
7.2.4. Results and discussion: CD spectral changes associated with copper binding to Msp peptides 175
7.2.5. Conclusions 178
7.3. Visible absorption spectroscopy 179
7.3.1. Introduction 179
7.3.2. Aims 181
7.3.3. Experimental 181
7.3.3.1. Sample preparation 181
7.3.3.2. Spectrum measurement 181
7.3.4. Results and discussion 181
7.3.5. Conclusions 182

Chapter VIII Concluding Essay: Biophysical Properties of Marsupial PrP Repeats 183
8.1. Structure of marsupial PrP repeats 184
8.1.1. Copper-free peptides 184
8.1.2. Copper-complexed peptides 184
8.2. Dissociation constant (K_d) and stoichiometry of copper binding to marsupial PrP repeats 185

8.3. Proposed copper-binding mode in marsupial PrP repeats 188
8.3.1. Copper-binding mode in Msp1 and Msp1capC 190
8.3.2. Copper-binding mode in Msp1capNC 192
8.3.3. Copper-binding mode in Msp1P3GcapNC 193
8.4. Copper-binding mode in Hu1capNC 195
8.5. Suggestion for future studies 196

List of Figures

Chapter I Introduction

Figure 1.1: Solution NMR structure of full-length mammalian PrP 2
Figure 1.2: Crystal structure of PrP^{C} (residues 119-126) showing the dimer form 3
Figure 1.3: Solution NMR structure of PrP-octarepeat peptide according to Yoshida et al. (2000) 8
Figure 1.4: Copper-binding modes in PrP-octarepeats peptide according to Jackson et al. (2001) 9
Figure 1.5: Copper-binding mode in PrP-octarepeats peptide according to Stockel et al. (1998) 18
Figure 1.6: Copper-binding mode in PrP-octarepeats peptide according to Viles et al. (1999) 19
Figure 1.7: Two tautomeric forms of the imidazole side chain of His in its copper-free and copper-complex form 20
Figure 1.8: Copper-binding mode in PrP-octarepeat peptide according to Miura et al. (1999) 21
Figure 1.9: Copper-binding mode in PrP-octarepeat peptide according to Aronoff-Spencer et al. (2000) 22
Figure 1.10: Copper-binding mode in PrP-octarepeat peptide according to Burns et al. (2002) 23
Figure 1.11: Copper-binding mode in PrP-octarepeat peptide according to Bonomo et al. (2000) 24
Figure 1.12: Copper-binding mode in PrP-octarepeat peptide according to Luczkowski et al. (2002) 25

Chapter III Fourier Transform Infrared Spectroscopy

Figure 3.1: FTIR normalized absorbance spectra of Msp1 and copper complex of Msp1 44
Figure 3.2: FTIR second derivative spectra of Msp1 and copper complex of Msp1 44
Figure 3.3: FTIR normalized absorbance spectra of Msp1capC and copper complex of Msp1capC 45
Figure 3.4: FTIR second derivative spectra of Msp1capC and copper complex of Msp1capC 45
Figure 3.5: FTIR normalized absorbance spectra of Msp1capNC and copper complex of Msp1capNC 46
Figure 3.6: FTIR second derivative spectra of Msp1capNC and copper complex of Msp1capNC 46
Figure 3.7: Copper binding to some mutant and modified Msp1 Peptides 49
Figure 3.8: FTIR absorption difference spectra for the peptide end groups and side chain residues 50
Figure 3.9: Effect of copper addition on the FTIR spectrum of the di-histidine peptide 53
Figure 3.10: Structures of the two tautomeric forms of copper-free His (upper) and copper-bound Msp1 peptide (lower) 54
Figure 3.11: Copper binding to Msp1His(1Me)capC peptide 56
Figure 3.12: Copper binding to Msp1His(3Me)capC peptide 57
Figure 3.13: Copper binding to Msp1P3GcapNC peptide 61
Figure 3.14: Copper binding to Msp_1strepcapNC peptide 63
Figure 3.15: Copper binding to Msp_4threpcapNC peptide 65
Figure 3.16: Copper binding to Hu1capNC peptide 67
Figure 3.17: FTIR normalized absorbance spectra of Msp2 and copper complex of Msp2 70
Figure 3.18: FTIR second derivative spectra of Msp2 and copper complex of Msp2 70
Figure 3.19: FTIR normalized absorbance spectra of Msp2capC and copper complex of Msp2capC 71
Figure 3.20: FTIR second derivative spectra of Msp2capC and copper complex of Msp2capC 71

Figure 3.21: FTIR normalized absorbance spectra of Msp2capNC and copper complex of Msp2capNC 72
Figure 3.22: FTIR second derivative spectra of Msp2capNC and copper complex of Msp2capNC 72
Figure 3.23: FTIR normalized absorbance spectra of Msp3 and copper complex of Msp3 74
Figure 3.24: FTIR second derivative spectra of Msp3 and copper complex of Msp3 74
Figure 3.25: FTIR normalized absorbance spectra of Msp3capC and copper complex of Msp3capC 75
Figure 3.26: FTIR second derivative spectra of Msp3capC and copper complex of Msp3capC 75
Figure 3.27: FTIR normalized absorbance spectra of Msp3capNC and copper complex of Msp3capNC 76
Figure 3.28: FTIR second derivative spectra of Msp3capNC and copper complex of Msp3capNC 76
Figure 3.29: FTIR second derivative spectra of Msp4 and copper complex of Msp4 79
Figure 3.30: FTIR second derivative spectra of Msp4 and copper complex of Msp4 79
Figure 3.31: FTIR second derivative spectra of Msp4capC and copper complex of Msp4capC 80
Figure 3.32: FTIR second derivative spectra of Msp4capC and copper complex of Msp4capC 80
Figure 3.33: FTIR normalized absorbance spectra of Msp4capNC and copper complex of Msp4capNC. 81
Figure 3.34: FTIR second derivative spectra of Msp4capNC and copper complex of Msp4capNC. 81
Figure 3.35: Copper titration of Msp1 at pH 8.0 84
Figure 3.36: Binding of other metals to Msp1 peptide 86
Figure 3.37: Binding of other metals to Msp4 peptide 87

Chapter IV Fluorescence Titration Spectrophotometry

Figure 4.1: Jablonski diagram illustrating the processes involved in the creation of fluorescence 91
Figure 4.2: Typical fluorescence emission spectra (excitation at 280 nm) of Msp peptides during copper ion titration 97
Figure 4.3: Fluorescence titration curves for copper (II) binding to Msp1 100
Figure 4.4: Fluorescence titration curves (in duplicate) for copper (II) binding to Msp1capC 101
Figure 4.5: Fluorescence titration curves for copper (II) binding to Msp2 102
Figure 4.6: Fluorescence titration curves (in duplicate) for copper (II) binding to Msp2capC 103
Figure 4.7: Fluorescence titration curves for copper (II) binding to Msp3 104
Figure 4.8: Fluorescence titration curves (in duplicate) for copper (II) binding to Msp3capC 105
Figure 4.9: Fluorescence titration curves for copper (II) binding to Msp4 106
Figure 4.10: Fluorescence titration curves (in duplicate) for copper (II) binding to Msp4capC 107
Figure 4.11: Fluorescence titration curves for copper binding to Msp1capC 112
Figure 4.12: Fluorescence titration curves for copper binding to Msp4capC 113
Figure 4.13: Copper binding to Msp1 and its mutant peptides 115
Figure 4.14: Fluorescence titration curves for copper binding to Msp1 and its mutant peptides 116
Figure 4.15: Fluorescence titration curves for copper binding to Msp1His(1Me)capC 118

Chapter V Fluorescence Resonance Energy Transfer

Figure 5.1: Spectral overlap between the Trp and dansyl, and typical data from FRET experiments 127
Figure 5.2: CD spectra of dansylated and nondansylated peptides 128
Figure 5.3: Fluorescence emission intensity of dansyl upon energy transfer from Trp 129

Figure 5.4: pH effect on fluorescence emission intensity of dansylated and nondansylated peptides 130
Figure 5.5: Temperature dependence of FRET distances at pH 7.2 136
Figure 5.6: A comparison of experimental FRET distances and MD simulation results 139

Chapter VI Electrospray Ionisation Mass Spectrometry

Figure 6.1: Schematic diagram of ESI MS process 144
Figure 6.2: ESI MS data of copper binding to Msp peptides presented as mass/charge spectra 148
Figure 6.3: ESI MS data of copper binding to Msp peptides presented as transformed spectra 149
Figure 6.4: ESI MS data of binding of other metal ions to Msp2 peptide presented as mass/charge spectra 154
Figure 6.5: ESI MS data of binding of other metal ions to Msp2 peptide presented as transformed spectra 155
Figure 6.6: ESI MS data of copper ion distribution in copper Msp4 complex presented as transformed spectra 158
Figure 6.7: ESI MS data of copper ion distribution in copper Msp4 complex presented as detailed transformed spectra and saturation curves 159
Figure 6.8: Mass/charge spectra of copper binding to Msp1 and its modified peptides 161

Chapter VII Other approaches: equilibrium dialysis, circular dichroism, and visible absorption spectroscopy

Figure 7.1: Illustration of equilibrium dialysis process 167
Figure 7.2: Design of dialysis chambers 169
Figure 7.3: Effect of chamber design on copper diffusion 170
Figure 7.4: Time for copper diffusion across the dialysis membrane of MWCO 500 and MWCO 1000 171
Figure 7.5: Binding of $Cu(Gly)_2$ to Msp peptides measured by equilibrium dialysis experiments 172
Figure 7.6: CD spectra of copper binding to Msp peptides 176

Chapter VIII Concluding essay: biophysical properties of marsupial PrP repeats

Figure 8.1: Copper binding mode in $(PHPGGSNWGQ)_nG$ peptide at neutral pH 191
Figure 8.2: Copper binding mode in Ac-$(PHPGGSNWGQ)_nG$ peptide at basic pH 192
Figure 8.3: Copper binding mode in Msp1P3GcapNC (Ac-PHGGGSNWGQG-NH_2) peptide at neutral and slightly basic pH 194
Figure 8.4: Copper binding mode in Hu1capNC (Ac-PHGGGWGQG-NH_2) peptide at neutral and slightly basic pH 196

List of Tables

Chapter I Introduction

Table 1.1: Sequence of the N-terminal tandem repeats of PrP 5
Table 1.2: Structure of PrP repeats in the presence and absence of copper 8
Table 1.3: Dissociation constants of copper binding to PrP repeats 12
Table 1.4: Stoichiometry of copper binding to PrP repeats 15

Chapter II Materials and Methods

Table 2.1: Synthetic peptides used in the experiments 32
Table 2.2: Preparation of 10 x phosphate buffer 35

Chapter III Fourier Transform Infrared Spectroscopy

Table 3.1: General classification of amide I vibration of polypeptides in ^2H_2O 36
Table 3.2: Synthetic peptides used in the experiments 38

Chapter IV Fluorescence Titration Spectrophotometry

Table 4.1: Synthetic peptides used in the experiments 94
Table 4.2: Effect of pH on K_d values of copper binding to Msp and MspcapC peptides 108
Table 4.3: Effect of peptide concentration on K_d values of copper binding to Msp1capC and Msp4capC peptides at pH 7.4 113
Table 4.4: K_d values of copper binding to Msp1 and its mutant peptides at pH 7.4 115
Table 4.5: K_d values of copper binding to Msp1 His-methylated peptides 119

Chapter V Fluorescence Resonance Energy Transfer

Table 5.1: Pairs of peptides for measuring FRET distances 125
Table 5.2: FRET distance between Trp^8 and dansyl in Msp1, Msp1capN, and Msp1capNC peptides 132
Table 5.3: Effect of pH on FRET distances of Msp and Hu PrP-repeat peptides 132
Table 5.4: Preliminary data on the effect of temperature on FRET distances 135
Table 5.5: Temperature dependence of the FRET distances, and the geometry of the possible cation-π interactions in Msp and Hu PrP-repeat peptides 138

Chapter VI Electrospray Ionisation Mass Spectrometry

Table 6.1: Synthetic peptides used in the experiments 146
Table 6.2: Mass assignment for Msp peptides 150
Table 6.3: Molecular mass assignment for Msp peptides (Msp2, Msp3, and Msp4) and their copper-complexes observed by ESI MS 152
Table 6.4: Molecular mass assignment for Msp2 and Msp2-metal complexes observed by ESI MS 156
Table 6.5: Molecular mass assignment for modified Msp1 peptides and their copper complexes observed by ESI MS 162

Chapter VII Other approaches : equilibrium dialysis, circular dichroism, and visible absorption spectroscopy

Table 7.1: Synthetic peptides used in the experiments 168
Table 7.2: Visible absorption spectroscopic data for copper binding to PrP-octarepeat peptides 180
Table 7.3: Visible absorption spectroscopic data for copper complexes of Msp3 peptide .. 182

Chapter VIII Concluding essay: biophysical properties of marsupial PrP repeats

Table 8.1: Effect of peptide concentration on the stoichiometry of binding between copper and Msp4 188

List of Abbreviations

3D	Three dimension
capC	Peptides are capped at the C-terminus with an amide group
capN	Peptides are capped at the N-terminus with an acetyl group
capNC	Peptides are capped at both C- and N-termini
CD	Circular dichroism
ED	Equilibrium dialysis
EPR	Electron paramagnetic resonance
ESI MS	Electrospray ionization mass spectrometry
ESR	Electron spin resonance
FRET	Fluorescence resonance energy transfer
FTIR	Fourier transform infrared
HPLC	High-pressure liquid chromatography
Hu	Human PrP repeats
ICP OES	Inductively coupled plasma optical emission spectrometer
K_d	Dissociation constant
MD	Molecular dynamics
Msp	Marsupial PrP repeats
MW	Molecular weight
MWCO	Molecular weight cut off
NEM	N-ethylmorpholine
NMR	Nuclear magnetic resonance
PBS	Phosphate buffered saline
PrP	Prion protein
PrP^C	Cellular form of PrP
PrP^{Sc}	Scrapie form of PrP
TFA	Trifluoroacetic acid
UV/Vis	Ultra violet/Visible
XRD	X-ray diffraction

Chapter I

Introduction

Prion protein (PrP) is a cell surface glycoprotein, tethered to the membrane via a GPI anchor at the C-terminus, which is normally present in a soluble form (PrP^C). It is expressed primarily in the central nervous system (Prusiner, 1998), or in nervous tissues in peripheral organs (Ford et al., 2002). Although the physiological function of PrP^C is currently unclear, its pathogenic form has been associated with several neurodegenerative disorders that affect humans and other mammals. The diseases are characterized by an accumulation of an amyloid aggregate in the brain, in which an alternative conformer of PrP (PrP^{Sc}) is observed to be the major component (Prusiner, 1998). The difference between the two isoforms resides in their secondary structural content; PrP^C is rich in α-helix whereas PrP^{Sc} has a high β-sheet content (Pan et al., 1993). The formation of infectious "prion" has been ascribed to a conformational change in which the helix-rich structure rearranges into a high β-sheet form, which then aggregates. The relationship between the conformational change and the development of the diseases themselves is still debated. Nonetheless, the PrP phenomenon has been classified as one of the conformational diseases (Cohen and Prusiner, 1998; Sunde and Blake, 1998), and its properties have been intensively investigated using structural (Donne et al., 1997; Riek et al., 1997; Lopez Garcia et al., 2000; Zahn et al., 2000) and biophysical approaches (Baldwin et al., 1995; Cohen and Prusiner, 1998).

1.1. 3-D structure of PrP

Solution NMR structures. Although relatively short (~253 residues, mammalian), the sequence of PrP is unusual because it contains a number of regions with quite different amino acid compositions (Wopfner et al., 1999) and apparent structure. Figure 1.1 shows NMR structures of several full-length mammalians PrPs.

The figure shows that the C-terminal region (residues 126-231) adopts a loosely folded structure containing three α-helices and two short β-strands, while the N-terminal region (residues 23-125), including the PGH-rich tandem repeats region (residues 51-91), is largely unstructured (Donne et al., 1997; Riek et al., 1997; Lopez Garcia et al., 2000; Zahn et al., 2000) with a high degree of backbone flexibility (Viles et al., 2001).

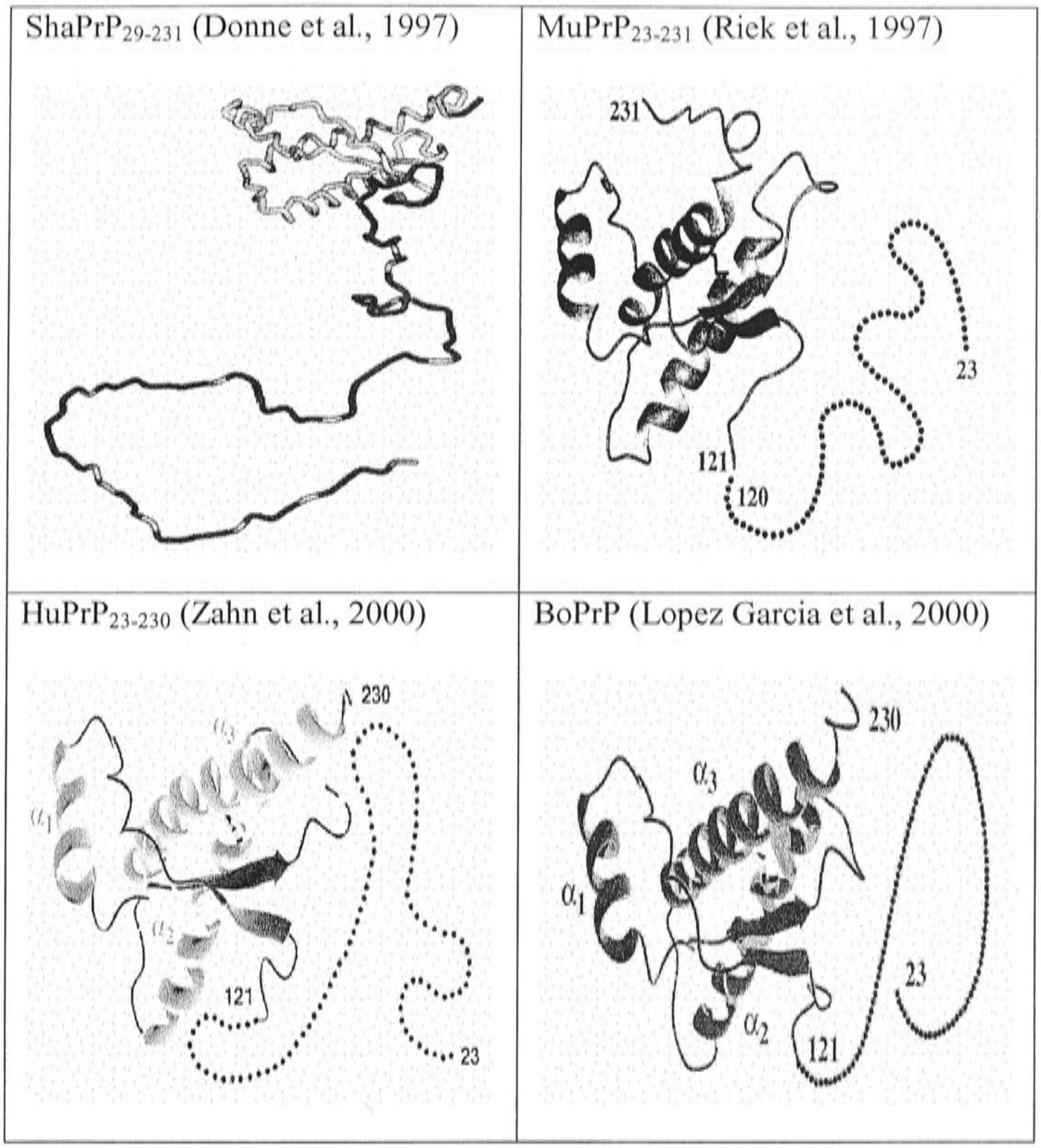

Figure 1.1: Solution NMR structure of full-length mammalian PrP. The NMR structure of syrian hamster (ShaPrP), murine (MuPrP), human (HuPrP), and bovine (BoPrP) show three helices (α_1, α_2, and α_3) and two stretches of β-strands within the C-terminal region (126-231), while the N-terminal region (23-125) is unstructured. These figures are taken from the sources stated above with some modification in size and colour.

XRD structure. A crystal structure of PrP^C (Figure 1.2) in dimer form has also been published. The dimer results from the three-dimensional swapping of the monomeric forms involving the C-terminal helix 3 and rearrangement of the disulfide bond. As many familial prion disease mutations map to the regions directly involved in helix swapping, it has been suggested that oligomerization through 3-D domain-swapping may constitute an important step on the pathway of the PrP^C – PrP^{Sc} conversion (Knaus et al., 2001).

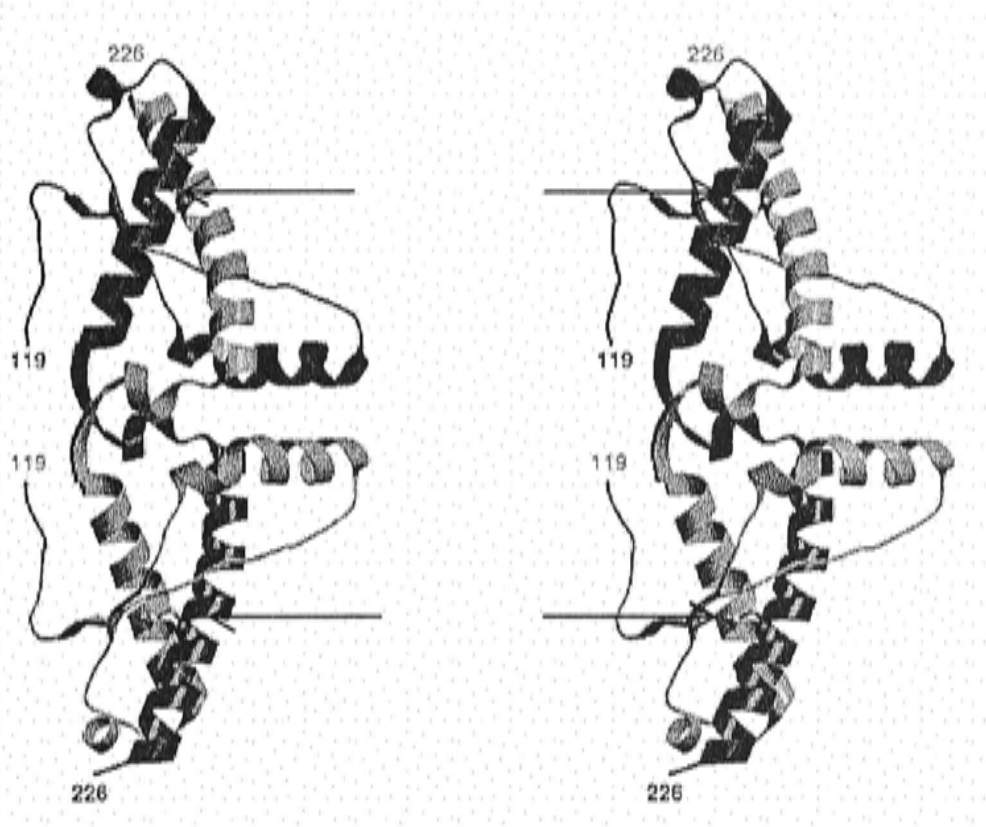

Figure source: Knaus et al. (2001)

Figure 1.2: Crystal structure of PrP^C (residues 119-126) showing the dimer form. The stereo figure is taken from Knaus et al. (2001) with some changes in size and colour so that the two peptide chains are in black and grey. The position of ball-and-stick structures, representing the interchain disulfide bridges, are not clear in the figure, so they are marked with arrows.

1.2. Copper binding and the proposed functions of PrP

Although the function of PrP is still a matter of debate, recent work has shown the ability of the protein to bind copper ions through its PGH-rich tandem repeats region (Hornshaw et al., 1995a; Viles et al., 1999; Aronoff-Spencer et al., 2000; Bonomo et al., 2000; Whittal et al., 2000; Burns et al., 2002; Luczkowski et al., 2002; Qin et al., 2002). Endocytosis of PrP^C from the cell surface has been shown to be rapidly and reversibly stimulated by copper ions (Pauly and Harris, 1998). This suggests that PrP is a recycling receptor for uptake of copper ions from the extracellular milieu. Other evidence that supports this hypothesis is that substitution and deletion mutation in the octarepeat region, which resulted in diminution of copper-binding ability, abolished the endocytosis, while a disease-associated mutation, addition of nine octarepeats, resulted in PrP failing to undergo copper-mediated endocytosis (Sumudhu et al., 2001).

Different lines of evidence suggest PrP^C has a role in regulating the activity of the enzyme Cu,Zn-SOD activity by influencing copper incorporation into the enzyme molecule (Brown and Besinger, 1998). PrP^C itself may have an enzymic function, as it exhibited SOD activity in vivo (Wong et al., 2000), following the binding of copper to the octarepeat region of the molecule during protein folding (Brown et al., 1999). It was

also shown that the octarepeats region of PrP protects the cell against oxidative stress and copper toxicity (Wong et al., 2000). This supports the suggestion that the octarepeats region of PrP may represent a functional domain of the native protein (Brown et al., 1998). It has also been suggested that PrP, through its octapeptide repeat region, can function to take away copper ions in the Cu(I) redox-inactive state and in so doing prevent the formation of copper-induced generation of reactive oxygen species (Shiraishi et al., 2000).

1.3. Repeats region of PrP

As noted above, some findings suggest a PrP role in copper metabolism (Brown and Besinger, 1998; Pauly and Harris, 1998; Brown et al., 1999; Wong et al., 2000) associated with binding to the N-terminal region, primarily the octapeptide tandem repeat region (Brown et al., 1997; Brown and Besinger, 1998; Brown et al., 1999; Shiraishi et al., 2000; Wong et al., 2000). Although the region comprising the octapeptide tandem repeat is not essential for mediating pathogenesis and prion replication, it modulates the extent of these events and of disease presentation (Flechsig et al., 2000). Copper ion itself has been suggested to have a role in the disease (Quaglio et al., 2001). Also, noting again, disease-associated mutation of the octarepeat region abolishes copper-induced endocytosis of PrP (Sumudhu et al., 2001). These findings make the repeats region another interesting part of PrP for separate study. In addition, the nature of the repeat sequence, which is known as a "low-complexity" sequence, makes this region very challenging for study.

1.4. PrP repeats as a segment with low-complexity sequence

The sequence of the repeats region of PrP is rich in Pro, Gly and His. This repetitive sequence is described as having low-complexity or non-random amino acid composition (Wootton, 1994). These types of sequence are abundant in natural proteins, and are often found in the unstructured domains of protein with unknown function. In fact they contribute 25% of the residues in the SwissProt database (Wootton, 1994). However, they have been little studied. This has been due to an assumption that they are less important than folded domains, and because methods to study them are not well established. Indeed, the tandem repeat region of PrP is located in the N-terminus that is unstructured as shown by NMR. However, the lack of intrinsic structure is often

relieved only when the protein binds to its target molecule (Wright and Dyson, 1999). In the case of the tandem repeats of PrP, the segment may take on more ordered structure when it binds to copper ions or sugars (the copper and sugar binding to PrP repeats will be discussed further in sections 1.5 and 1.6, respectively).

Table 1.1: Sequence of the N-terminal tandem repeats of PrP.

Species	Sequence
Human	[51]PQGGGGWGQ PHGGGWGQ PHGGGWGQ PHGGGWGQ PHGGGWGQ[91]
Chicken	[47]PRQPGY PHNPGY PHNPGY PHNPGY PHNPGY PHNPGY PQNPGY PHNPGY[94]
Possum	[61]PQGGGTNWGQ PHPGGSNWGQ PHPGGSSWGQ PHGGSNWGQ[99]
Wallaby	PQGGGTNWGQ PHPGGSSWGQ PHAGGSNWGQ PHGGSNWGQ

Table 1.1 shows that the human repeats region contains 5 tandemly repeated sequences. There are 2 variants: the major one is PHGGGWGQ (4 of 5), while the minor one is PQGGGGWGQ. The major one PHGGGWGQ is regarded as the consensus octarepeat sequence as it also dominates in similar repeats sequence in other mammals (Wopfner et al., 1999; Van Rheede et al., 2003).

The chicken repeats region contains 8 tandemly repeated sequences of 6 residues (Table 1.1). There are 3 variants: 6 of 8 are PHNPGY, one PQNPGY, and one PRQPGY. The sequence "PHNPGY" is the dominant one in other avian sequences, and is considered the prototype. Note that, similarly to mammalian, the second residue of the chicken prototype hexarepeat is His.

The PrP-repeats region of the brush-tailed possum, the only published marsupial sequence (Windl et al., 1995), contains 4 times tandemly repeated units of 10 or 9 residues (Table 1.1). There are 4 variants in the sequence: one PQGGGTNWGQ, one PHPGGSNWGQ, one PHPGGSSWGQ, and one PHGGSNWGQ. Recently, another marsupial PrP, which is from tammar wallaby (Premzl and Gready, 2003, personal communication; not yet published) has been sequenced. It revealed similarly to possum; wallaby also has 4 repeats of 10 or 9 residues (Table 1.1). The first and fourth repeats of wallaby are the same as those of possum. The second repeat is similar to the third repeat of possum. The third repeat of wallaby, PHAGGSNWGQ, is unusual because no other PrP repeat has an Ala.

The motif P[H/Q].GG.WGQ is conserved among the mammalian and marsupial sequences. The second residue in marsupial and mammalian is dominantly His. Marsupial has two additional residues, with polar amino acid side chains (Ser, Thr, or Asn). This is the feature that distinguishes marsupial from mammalian PrP repeats. Also, the segment of three Gly (GGG) following the His residue is dominant only in mammals. In marsupial, it is Pro (2 of 4 in possum and 1 of 4 in wallaby) or Ala (none in possum and 1 of 4 in wallaby) being the third residue following His, resulting in the presence of PGG or AGG instead of the GGG segment. Although the presence of Ala instead of Gly is unusual, a recent study indicates that a mutant peptide with tri-Ala instead of tri-Gly is still capable of binding of copper ions but with lower affinity (Luczkowski et al., 2003).

1.5. Copper binding to PrP repeats

Various biophysical methods have been applied to characterize peptides and proteins containing PrP repeats, in the presence and absence of copper. These include fluorescence spectroscopy (Hornshaw et al., 1995a; Smith et al., 1997; Stockel et al., 1998; Jackson et al., 2001; Kramer et al., 2001), circular dichroism (CD) (Hornshaw et al., 1995a; Smith et al., 1997; Stockel et al., 1998; Viles et al., 1999; Aronoff-Spencer et al., 2000; Bonomo et al., 2000; Whittal et al., 2000; Luczkowski et al., 2002; Garnett and Viles, 2003), electron paramagnetic resonance spectroscopy (EPR) (Viles et al., 1999; Aronoff-Spencer et al., 2000; Cereghetti et al., 2001; Luczkowski et al., 2002), electron spin resonance spectroscopy (ESR) (Bonomo et al., 2000), NMR spectroscopy (Viles et al., 1999; Yoshida et al., 2000; Janek et al., 2001; Luczkowski et al., 2002), mass spectrometry (Hornshaw et al., 1995b; Whittal et al., 2000; Kramer et al., 2001; Qin et al., 2002), voltammetry (Bonomo et al., 2000), potentiometry (Luczkowski et al., 2002), Raman spectroscopy (Miura et al., 1996; Miura et al., 1999), equilibrium dialysis (ED) (Miura et al., 1996; Brown et al., 1997; Stockel et al., 1998; Miura et al., 1999), infrared spectroscopy (FTIR) (Gustiananda et al., 2002), and x-ray difraction (Burns et al., 2002).

These have used a range of synthetic and cloned peptides containing different numbers of repeats with either consensus (Hornshaw et al., 1995a; Hornshaw et al., 1995b; Miura et al., 1996; Smith et al., 1997; Miura et al., 1999; Bonomo et al., 2000; Yoshida et al.,

2000; Burns et al., 2002; Gustiananda et al., 2002; Luczkowski et al., 2002) or actual sequences (Brown et al., 1997; Stockel et al., 1998; Viles et al., 1999; Aronoff-Spencer et al., 2000; Whittal et al., 2000; Cereghetti et al., 2001; Jackson et al., 2001; Kramer et al., 2001; Burns et al., 2002; Qin et al., 2002; Garnett and Viles, 2003) from mammals or chicken, or full-length mammalian protein (Stockel et al., 1998; Viles et al., 1999; Cereghetti et al., 2001; Kramer et al., 2001; Qin et al., 2002). There is also one publication using marsupial consensus-repeat peptide (Gustiananda et al., 2002).

1.5.1. Structure of PrP repeats in the absence and presence of copper ion

There are some discrepancies in the reported structure of repeat regions of PrP and the effect of copper ion addition on the structure, as summarized in Table 1.2. In the absence of copper, CD (Hornshaw et al., 1995a; Viles et al., 1999; Bonomo et al., 2000; Whittal et al., 2000), Raman (Hornshaw et al., 1995a; Miura et al., 1996; Viles et al., 1999; Bonomo et al., 2000; Whittal et al., 2000), and FTIR spectroscopy (Gustiananda et al., 2002) have shown that the repeat region is unstructured. This result is consistent with the NMR structure of full-length PrP (see previous section), which shows the repeat region is unstructured (Donne et al., 1997; Riek et al., 1997; Lopez Garcia et al., 2000; Zahn et al., 2000). However, another CD study reports the presence of non-random structure similar to the poly-L-proline type II left handed helix (Smith et al., 1997). An NMR study of cyclic and linear peptides containing a consensus octarepeat sequence suggests certain residues within the repeats adopt loop and β-turn structure (Figure 1.3) (Yoshida et al., 2000). It has been suggested that the inconsistency within the CD results is due to the high proportion of Trp, which can contribute to CD spectra in the far UV region (Whittal et al., 2000). However, the fact that peptides used in both CD experiments (Smith et al., 1997; Whittal et al., 2000) have similar number of Trps argues against this explanation.

Copper binding to octarepeat peptides has been reported to induce the formation of α-helix structure, as probed by Raman spectroscopy (Miura et al., 1996) and infrared spectroscopy (Gustiananda et al., 2002), in disagreement with one CD study which suggests no structural changes upon addition of copper (Hornshaw et al., 1995a). Yet, other CD experiments suggest the presence of turns and structured loop resulting from copper addition to repeat peptides (Hornshaw et al., 1995a; Viles et al., 1999; Bonomo et al., 2000; Whittal et al., 2000).

Table 1.2: Structure of PrP repeats in the presence and absence of copper.

Author	Peptide	Methods	No copper	Plus copper
Hornshaw et al., 1995a	Sc	CD	unstructured	unstructured
Smith et al., 1997	Sa	CD	PP II helix	Not done
Viles et al., 1999	Sa (capNC)	CD	unstructured	Turns & structured loop
Whittal et al., 2000	Sa	CD	unstructured	Turns & structured loop
Bonomo et al., 2000	Sc (capNC)	CD	unstructured	Turns & structured loop
Yoshida et al., 2000	Sc (cyclic)	NMR	Loop and β-turn	Not done
Miura et al., 1996	Sc	Raman	unstructured	α-helix

Sc: synthetic peptide of consensus sequence; Sa: synthetic peptide of actual sequence; capNC: peptides are blocked at the N-terminus with an acetyl group and at the C-terminus with an amide.

The discrepancy in CD results is suggested to be due to the type of buffer used in the experiments (Viles et al., 1999). It is suggested that the use of Tris HCl buffer in the experiment of Hornshaw (1995a) will prevent copper binding to the peptides, as buffer components will compete successfully for copper ion.

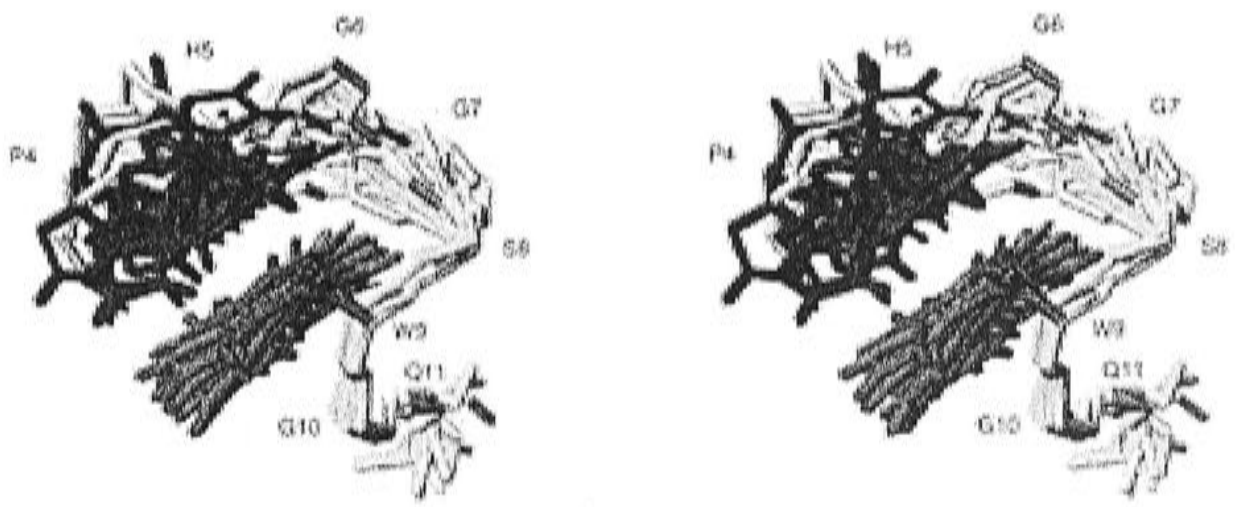

Figure source: Yoshida et al. (2000)

Figure 1.3: Solution NMR structure of PrP-octarepeat peptide according to Yoshida et al. (2000). Octarepeat peptide (^{1}PHGGGWGQ^{8}; note the numbering of residue is different from that in the figure) adopts a loop (^{2}HGGGW^{6} segment) and β-turn (^{5}GWGQ^{8} segment) conformation.

The discrepancy between CD and Raman (or FTIR) results may be due to several reasons such as peptide concentration and sample preparation method. In Raman and FTIR spectroscopy, peptide concentrations are in the mM range, while in CD spectroscopy they are in the μM range, i.e. 3 orders of magnitude lower. It may be that

in the presence of copper, there is a different copper-complex structure for different concentrations of peptide and copper. During sample preparation, in order to avoid copper precipitation as copper hydroxide at pH higher than 6.0 (Brown et al., 1997), samples for Raman (Miura et al., 1996) and FTIR (Gustiananda et al., 2002) study are prepared in the following way. The peptide solution is brought to pH around 9.0 (H.Takeuchi, personal communication) (Miura et al., 1996) or 12.0 (Gustiananda et al., 2002), copper solution is added, and then the pH of the solution is brought to the desired value by adding HCl. It is possible that complex prepared in this way will have different structure compared with complex where copper ion is added to neutral or slightly acidic peptide solution and the pH is increased by adding base solution later. The reason for this is probably due to differences in the copper-binding mode. High pH (basic) promotes more binding to the peptide backbone (pKa ≥ 15 (Creighton, 1983)) while low pH (neutral or slightly acidic) enables the binding only to the His residue (pKa 6.2 (Creighton, 1983)).

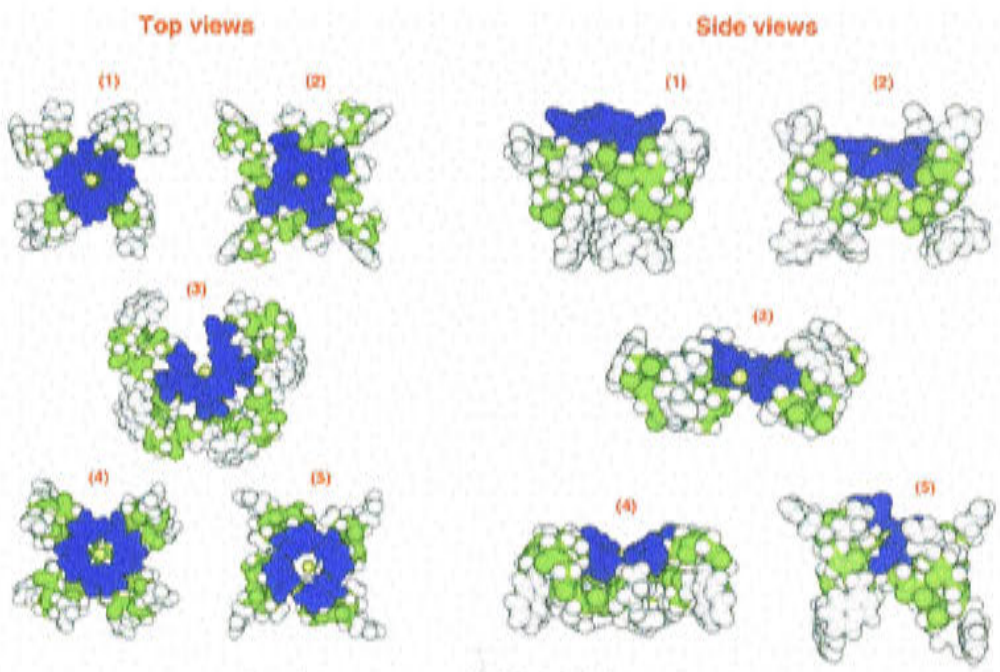

Figure source: Jackson et al.(2001)

Figure 1.4: Copper-binding modes in PrP-octarepeat peptide according to Jackson et al. (2001). Copper-binding modes presented as five energetically identical space-filled models in top and side views. In this model, copper ion (yellow, center) is proposed to coordinate four His side chains (blue), based on the assumption that the tight binding sites (femtomolar K_d) should be constructed from four imidazole ring side chains of His residues. Green and gray represent the backbone atoms and the remaining side chain, respectively. The diversity of the conformations suggests that copper binding will not induce one single fixed conformation although it does induce more compact structure.

Although most studies show copper binding induces some structural changes to become more compact, it does not force the peptide to adopt a single fixed conformation. A diversity of molecular models of the complex have been suggested (Figure 1.4) (Jackson et al., 2001). The formation of more ordered structure upon addition of copper

could be crucial for protection of the N-terminus of PrP against accidental proteolysis (Whittal et al., 2000). However, since the functions of the repeat region and the whole PrP protein itself are still unclear, it is not known whether the copper complex needs to have a defined conformation that will interact with some other molecule specifically, or have diverse conformations that will allow it to carry out different tasks and interact with several different molecular machineries inside and outside the cell. It is also unclear whether or not copper binding to the repeat region induces structural changes in the rest of the protein. So far results are available only from short synthetic peptides and it is difficult to apply them to full-length PrP. Stockel et al. (1998) observed Trp fluorescence quenching upon copper addition to $ShaPrP_{29-231}$. However, it is not possible to draw conclusions about changes in the tertiary structure environment of Trp residues in the folded domain as it is not possible to say whether only some or all the quenching is due to copper binding to the repeats.

1.5.2. Dissociation constant (K_d) of copper binding to PrP repeats

The reported K_d range for copper binding to synthetic or recombinant peptides, both consensus sequence (Hornshaw et al., 1995a) and actual sequence (Brown et al., 1997; Viles et al., 1999; Whittal et al., 2000; Kramer et al., 2001; Garnett and Viles, 2003) is in the μM range (Table 1.3). This is in good agreement with the binding to full-length protein (Stockel et al., 1998) but differs from one binding study, which reported a K_d value in the fM range (Jackson et al., 2001).

Jackson et al. (2001) argue that the μM range of K_d implies copper interaction with PrP repeats is extremely weak. They expect that given the octapeptide repeat region has five His side chains, its interaction with copper should be comparable with the interaction of copper with simple molecules such as four independent imidazole groups (K_d is 30 fM) or malonate (K_d is 10 nM). The femtomolar K_d value is obtained from Trp fluorescence quenching and Gly competition experiments. According to Jackson et al. (2001), the Gly competition will abolish weak binding and weaken tight binding between copper ion and the peptide, so that the K_d of the tight site, which is 10^{-14} M after the competitive buffering effect of Gly is taken into account, can be measured accurately (Jackson et al., 2001). This femtomolar K_d, however, should be contrasted with other findings.

It can be argued that the K_d for copper binding to the peptide should not be compared with the binding to simple molecules because the binding to simple molecules will not be hindered by steric effects, as likely for peptides. Thus, even though the PrP octarepeat peptides may have four or more His residues, it is unlikely that the affinity will be in the same order of magnitude as those with small ligands. Furthermore, the physiological concentration of total copper in plasma is 18.6 μM (quoted in Kramer et al., 2001). 65% is bound to ceruloplasmin in a nonexchangeable way and around 8.3 μM is bound in an exchangeable way to various proteins and amino acids. In the cerebrospinal fluid, copper concentration ranges from 0.5 to 2.5 μM, while in specialized areas such as synapses it is around 15 μM (Kramer et al., 2001). Thus, the fM copper-binding affinity is not necessary to be considered as physiologically relevant. Also, the use of Gly as a competitor to elucidate the tight binding site in copper binding study has been challenged (Garnett and Viles, 2003). The CD experiment shows that Gly competes strongly with copper ion, indicating that the affinity of the copper for PrP-repeat peptide is less than that of copper for Gly, for which the K_d is 12 nM. Together, these results suggest that the fM K_d value of copper binding to PrP-repeat peptides may be an error.

One speculation about the μM affinity for copper is that PrP may be similar to the glucose transporter whose K_d value is within glucose concentration in the blood and is exceptionally sensitive in that range. Thus, PrP may act as a cuprostat, which activates cellular machinery in response to changes in ambient copper concentration (Burns et al., 2002).

Although there is good general agreement (except Jackson et al. (2001)) among values measured for K_d's in the μM range, the precise values differ significantly. The disagreement in the K_d values (Table 1.3) is due not only to variation in the experimental conditions (pH, buffer component, and temperature), peptide sequence, and whether or not they are terminally capped (some peptides were N- and C-terminally capped (Viles et al., 1999; Garnett and Viles, 2003), while others remained uncapped), but also because copper binding to PrP repeats is not a simple system. A number of problems are encountered, originating from experimental (technical) factors as well as the nature of the repeat itself.

Table 1.3: Dissociation constants of copper binding to PrP repeats

Author	Methods	Peptide	Peptide Conc (μM)	pH	K_d (μM)
Hornshaw et al., 1995a	Fluorescence	Sc mammalian: $(PHGGGWGQ)_4$	0.215	PBS pH 7.4	6.7
		Sc avian: $(NPGYPH)_4$	1.148	PBS pH 7.4	4.5
Brown et al., 1997	ED	Ra $HuPrP_{23-98}$	2.7	NEM pH 7.4	5.9
Stockel et al., 1998	ED	Rfl $SHaPrP_{29-231}$	2.5	MES pH 6.0	14
	Fluorescence	Rfl $SHaPrP_{29-231}$	1.68	MES pH 6.0	14
Viles et al., 1999	CD	Sa (capNC) $SHaPrP_{51-75}$: $PQGGGTWGQ(PHGGGWGQ)_2$	34	No buffer pH 7.5	6.0
Whittal et al., 2000	ESI MS	Sa $ShaPrP_{73-91}$: $WGQ(PHGGGWGQ)_2$	10	Am OAc pH 6.0	2.2; 69
		Sa $ShaPrP_{57-91}$: $WGQ(PHGGGWGQ)_4$	10	Am OAc pH 6.0	0.7; 6.3; ~200
				Am OAc pH 7.4	0.2; 0.7; 2.5; 12
		Sa $ShaPrP_{57-98}$: $WGQ(PHGGGWGQ)_4GGGTHNQ$	10	Am OAc pH 6.0	1.0; 6.0; 70
				Am OAc pH 7.4	1.7; 0.5; <0.1; <0.1; 4.3
		Sa $ShaPrP_{23-98}$	10	Am OAc pH 6.0	1.5; 2.8; 55
				Am OAc pH 7.4	2.2; 0.5; <0.1; <0.1; ~5
Kramer et al., 2001	Fluorescence	Sa: $HuPrP_{60-91}$: $(PHGGGWGQ)_4$	0.17	MOPS pH 7.2	–d; [5.5]
		Sa: $HuPrP_{60-109}$: $(PHGGGWGQ)_4GGGTHSQWNKPSKPKTNM$	0.145	MOPS pH 7.2	8.8; [2.5]
		Ra: $HuPrP_{23-98}$	0.125	MOPS pH 7.2	1.4; [2.2]
		Ra: $HuPrP_{23-112}$	0.120	MOPS pH 7.2	2.4; [2.2]
		Rfl: $MurPrP_{23-231}$	0.085	MOPS pH 7.2	1.8; [2.2]
Jackson et al., 2001	Fluorescence	Sa $HuPrP_{52-98}$: $QG(GGGWGQPH)_4GGGWGQGGGTHSQ$	5	MOPS pH 8.0	3.2; 8 fM
Garnett & Viles, 2003	CD	Sa (capNC) $HuPrP_{58-91}$: $GQ(PHGGGWGQ)_4$	10	NEM pH 7.5	Between 10 and 0.01

Sc: synthetic peptide of consensus sequence; Sa: synthetic peptide of actual sequence; Ra: recombinant peptide of actual sequence; Rfl: recombinant of full-length protein; capNC: peptides are blocked at the N-terminus with an acetyl group and at the C-terminus with an amide. PBS: phosphate buffer saline, NEM: N-ethylmorpholine, MES: 2-(N-morpholino)ethanesulphonic acid, Am Oac: ammonium acetate, MOPS: 3-(N-morpholino)propanesulphonic acid. Values in brackets [ ] show dissociation constant for cooperative sites (Kramer et al., 2001). –d means that K_d values for individual sites are not available as all sites bind copper ion cooperatively. The sequence of K_d values reported by Whittal et al. (2000) is for the first, the second, the third, etc. copper binding to the peptide.

The experimental (technical) factors are described as follows. (1) The type of buffers used in the binding study. It is reported that some buffers such as Tris form complexes with copper ions and, thus, will compete very successfully for copper ions, while N-ethylmorpholine, phosphate, and acetate do not (Viles et al., 1999; Garnett and Viles, 2003). (2) Although apo-peptide is soluble, its copper complex may not be as soluble, espescially at high concentration. 3) Copper has a very low solubility at pH higher than 6.0, where it precipitates as copper hydroxide. In one experiment, copper ion was supplied as $Cu(Gly)_2$ to overcome this problem (Brown et al., 1997). 4) It is reported that the solubility of 5 mM octarepeat peptide reduces significantly upon addition of copper ion (Viles et al., 1999). However, 10 times dilution to <0.5 mM will re dissolve the precipitating material.

The influence of the nature of the repeat itself is illustrated as follows. First, the repeats region of PrP is a dynamic system with high backbone flexibility (Viles et al., 2001). Inconsistency in the reported structure of repeats in the literature leads to the conclusion that it does not adopt only one conformation, but more likely has a range of conformations, which will be dictated by its environment. As noted in section 1.5.1 solution NMR structures of octarepeat show loop and β-turn structure, which, the authors suggested, is in rapid equilibrium with random coil (Yoshida et al., 2000). Therefore, the initial conformation of the peptide just before it binds copper ion could be different from one condition to another, which is the case for experiments done in different laboratories with different peptide concentration, buffer components, pH and temperature. Thus, the initial conformational distribution of the repeat peptide could dictate its copper-binding properties. Second, copper binding to PrP repeats is completely different from a folded metalloprotein, where the site for metal binding is preorganized and dictated by the compact protein conformation. As PrP repeats adopt a range of conformations, there are no single preorganized sites for the first copper ions to bind. The sites for copper binding will likely vary depending on the experimental conditions (the copper-binding sites will be discussed further in section 1.5.4). Thus, measured copper-binding affinities can be expected to vary.

1.5.3. Stoichiometry of copper binding to PrP repeats

To some extent there is good agreement in the literature regarding the stoichiometry and cooperativity of copper-ion binding to the N-terminal segment of PrP, while results for binding to full-length protein still show apparent inconsistencies (Table 1.4). The reported stoichiometry for octarepeat peptide is 1:1 copper per octarepeat at pH above 7.0 (Hornshaw et al., 1995b; Brown et al., 1997; Miura et al., 1999; Viles et al., 1999; Aronoff-Spencer et al., 2000; Whittal et al., 2000; Kramer et al., 2001; Garnett and Viles, 2003) with some exceptions: Viles et al. (1999) reported stoichiometry of 1:2, while NMR Jackson et al. (2001) reported 1:4 copper per octarepeat. However, recently Viles, now working independently, confirmed that the stoichiometry is indeed 1:1 (Garnett and Viles, 2003).

Table 1.4 shows that the octapeptide region appears to bind up to five copper ions cooperatively. The Hill cooperative coefficient was reported to be 3.4 in PrP_{23-98} (Brown et al., 1997). A similar number was noted for PrP_{58-91} (3.3 copper ions bound cooperatively) (Viles et al., 1999; Garnett and Viles, 2003). Also, Whittal et al. (2000) reported results from ESI MS indicating the positive cooperativity of the binding of the second, third, and fourth copper ion to $ShaPrP_{57-98}$ and $ShaPrP_{23-98}$. Another ESI MS study revealed 3.7, 3.6, and 3.7 copper ions bind cooperatively to $HuPrP_{60-109}$, $HuPrP_{23-98}$, and $HuPrP_{23-112}$ respectively (Kramer et al., 2001).

As mentioned, there is disagreement as to the stoichiometry of copper binding to full-length mammalian PrP. This could be due to differences in pH. $ShaPrP_{29-231}$ was reported to bind only two copper ions at pH 6.0 (Stockel et al., 1998), which suggests two octarepeats are necessary to bind a single copper ion. However, it is also possible that one copper ion bound at the post-repeat region (Cereghetti et al., 2001; Hasnain et al., 2001; Jackson et al., 2001; Jobling et al., 2001). Full-length mammalian PrP from a different species ($MurPrP_{23-231}$) binds up to 5 copper ions at pH 7.4 (Kramer et al., 2001), which suggests each octarepeat binds one copper ion. The pH dependency of the copper-binding stoichiometry was confirmed by ESI MS (Whittal et al., 2000). It is reported that a peptide containing four octarepeats binds two copper ions at pH 6.0 but four at pH 7.4.

Table 1.4: Stoichiometry of copper binding to PrP repeats

Author	Methods	Peptide	Peptide Conc (μM)	pH	Number of Copper bound	Cooperativity
Hornshaw et al., 1995b	MALDI TOF MS	Sc mammalian: $(PHGGGWGQ)_3$	10	Not specified	3 (1 Cu per repeat)	Not specified
		Sc mammalian: $(PHGGGWGQ)_4$	10	Not specified	4 (1 Cu per repeat)	Not specified
		Sc avian: $(NPGYPH)_3$	10	Not specified	3 (1 Cu per repeat)	Not specified
		Sc avian: $(NPGYPH)_4$	10	Not specified	4 (1 Cu per repeat)	Not specified
Brown et al., 1997	ED	Ra $HuPrP_{23-98}$	2.7	NEM pH 7.4	5.6 (1 Cu/repeat+1.6 Cu)	3.4
Stockel et al., 1998	ED	Rfl $SHaPrP_{29-231}$	2.5	MES pH 6.0	2 (1/2 Cu per repeat)	0
Viles et al., 1999	CD	Sa (capNC) $SHaPrP_{51-75}$: $PQGGGTWGQ(PHGGGWGQ)_2$	34	No buffer pH 7.5	1 (1/2 Cu per repeat)	0
		Sa (capNC) $ShaPrP_{66-91}$: $GQ(PHGGGWGQ)_3$	21	No buffer pH 7.5	3 (1 Cu per repeat)	2.4
		Sa (capNC) $ShaPrP_{58-91}$: $GQ(PHGGGWGQ)_4$	33	No buffer pH 7.5	4 (1 Cu per repeat)	3.3
Miura et al., 1999	Raman	Sf (capN): PHGGG	20 mM	No buffer pH 8.2	1	Not specified
		Sc (capN) mammalian: PHGGGWGQ	20 mM	No buffer pH 8.2	1 (1 Cu per repeat)	Not specified
		Sc (capN) mammalian: $(PHGGGWGQ)_2$	20 mM	No buffer pH 8.2	2 (1 Cu per repeat)	Not specified
		Sc (capN) mammalian: $(PHGGGWGQ)_4$	20 mM	No buffer pH 8.2	4 (1 Cu per repeat)	Not specified
Aronoff-Spencer et al., 2000	CD	Sc mammalian (capNC): PHGGGWGQ	398	NEM pH 7.4	1 (1 Cu per repeat)	Not specified
		Sa (capNC) $HuPrP_{23-28,\ 73-91}$: $KKRPKPWGQ(PHGGGWGQ)_2$	333	NEM pH 7.4	2 (1 Cu per repeat)	Not specified
		Sa (capNC) $HuPrP_{23-28,\ 57-91}$: $KKRPKPWGQ(PHGGGWGQ)_4$	51	NEM pH 7.4	4 (1 Cu per repeat)	Not specified
	EPR	Sc mammalian (capNC): PHGGGWGQ	1000	NEM pH 7.4	1 (1 Cu per repeat)	Not specified
		Sa (capNC) $HuPrP_{23-28,\ 73-91}$: $KKRPKPWGQ(PHGGGWGQ)_2$	500	NEM pH 7.4	2 (1 Cu per repeat)	Not specified
		Sa (capNC) $HuPrP_{23-28,\ 57-91}$: $KKRPKPWGQ(PHGGGWGQ)_4$	250	NEM pH 7.4	4 (1 Cu per repeat)	Not specified
Whittal et al., 2000	ESI MS	Sa $ShaPrP_{73-91}$: $WGQ(PHGGGWGQ)_2$	10	Am OAc pH 6.0	2 (1 Cu per repeat)	Not specified
		Sa $ShaPrP_{57-91}$: $WGQ(PHGGGWGQ)_4$	10	Am OAc pH 6.0	2 (1/2 Cu per repeat)	Not specified
				Am OAc pH 7.4	4 (1 Cu per repeat)	Not specified
		Sa $ShaPrP_{57-98}$: $WGQ(PHGGGWGQ)_4GGGTHNQ$	10	Am OAc pH 6.0	3 (3/4 Cu per repeat)	Not specified
				Am OAc pH 7.4	5 (1 Cu/repeat + 1 Cu)	3
		Sa $ShaPrP_{23-98}$	10	Am OAc pH 6.0	3 (3/4 Cu per repeat)	Not specified
				Am OAc pH 7.4	5 (1 Cu/repeat + 1 Cu)	3

Kramer et al., 2001	ESI MS	Sa: $HuPrP_{60-91}$: $(PHGGGWGQ)_4$	20	NEM pH 7.4	4 (1 Cu per repeat	2.4
		Sa: $HuPrP_{60-109}$: $(PHGGGWGQ)_4GGGTHSQWNKPSKPKTNM$	10	NEM pH 7.4	5 (1 Cu/repeat + 1 Cu)	3.7
		Ra: $HuPrP_{23-98}$	10	NEM pH 7.4	6 (1 Cu/repeat + 2 Cu)	3.6
		Ra: $HuPrP_{23-112}$	10	NEM pH 7.4	5 (1 Cu/repeat + 1 Cu)	3.7
		Ra: $MurPrP_{121-231}$	13	NEM pH 7.4	1	Not specified
		Rfl: $MurPrP_{23-231}$	10	NEM pH 7.4	5 (1 Cu/repeat + 1 Cu)	4.2
Garnett & Viles, 2003	CD	Sf (capNC): HGG	50	NEM pH 7.5	0.5	None
		Sf (capNC): HGGG	50	NEM pH 7.5	1	None
		Sf (capNC): HGGGW	50	NEM pH 7.5	1	None
		Sa (capNC) $HuPrP_{83-91}$: QPHGGGWGQ	50	NEM pH 7.5	1 (1 Cu per repeat)	None
		Sa (capNC) $HuPrP_{70-83}$: GGGWGQPHGGGWGQP	50	NEM pH 7.5	1 (1 Cu per repeat)	None
		Sa (capNC) $HuPrP_{73-91}$: $WGQ(PHGGGWGQ)_2$	50	NEM pH 7.5	2 (1 Cu per repeat)	Slight coop
		Sa (capNC) $HuPrP_{66-91}$: $GQ(PHGGGWGQ)_3$	50	NEM pH 7.5	3 (1 Cu per repeat)	2.4
		Sa (capNC) $HuPrP_{58-91}$: $GQ(PHGGGWGQ)_4$	50	NEM pH 7.5	4 (1 Cu per repeat)	3.3

Sc: synthetic peptide of consensus sequence; Sa: synthetic peptide of actual sequence; Sf: synthetic peptide of fragment octarepeat; Ra: recombinant peptide of actual sequence; Rfl: recombinant full-length protein; capNC: peptides that are blocked at the N-terminus with an acetyl group and at the C-terminus with an amide group; capN: peptides that are blocked at the N-terminus with an acetyl group.

The pH dependency of the copper-binding stoichiometry is strongly linked to its binding sites. There is now much evidence to suggest that the imidazole side chain of the His residues is a major binding site for the copper ions (Viles et al., 1999; Bonomo et al., 2000; Qin et al., 2002). As protonation of the imidazole ring will inhibit copper binding to His, the stoichiometry of the binding will be pH-dependent. Raman spectroscopy provides one line of evidence for the differences in binding modes that eventually lead to differences in stoichiometry (Miura et al., 1999). It is reported that at pH 6.0, the copper-binding site of His switches from the nitrogen N_π to the N_τ to share a single copper ion between two His residues of different peptide chains. A review of copper-binding sites will be given in the following section.

1.5.4. Copper coordination in PrP repeats

How ligands coordinate in the complex is the key issue of all binding studies, as the coordination mode underpins the other properties of the complex such as the K_d and stoichiometry. Copper coordination in PrP repeats has been studied either directly or indirectly, or by a combination of both. Indirect study may be carried out by several approaches: measuring the effect of specific protein side chain modifications on metal binding, titrimetric determination of the pK_as of the ligand groups involved, and correlation of protein-metal ion spectra with those of appropriate model systems. Direct study includes direct observation of the complex by X-ray crystallography, and NMR studies (Breslow, 1973). It is also possible to combine the experimental data with computational and molecular dynamics simulations to search for possible models of the complex.

Several models of PrP repeats copper complexes has been reported in the literature. All models were deduced from spectroscopic properties of complexes in solution, sometimes combined with homology modelling using other protein with copper-binding sites (Stockel et al., 1998), with one exception where the model was from X-ray crystallography data (Burns et al., 2002). All models agree that the imidazole side chain of the His residues is the major binding site for copper ions. However, the other binding sites for a given copper ion may vary, and this could be due to differences in the peptide fragments used (Luczkowski et al., 2002).

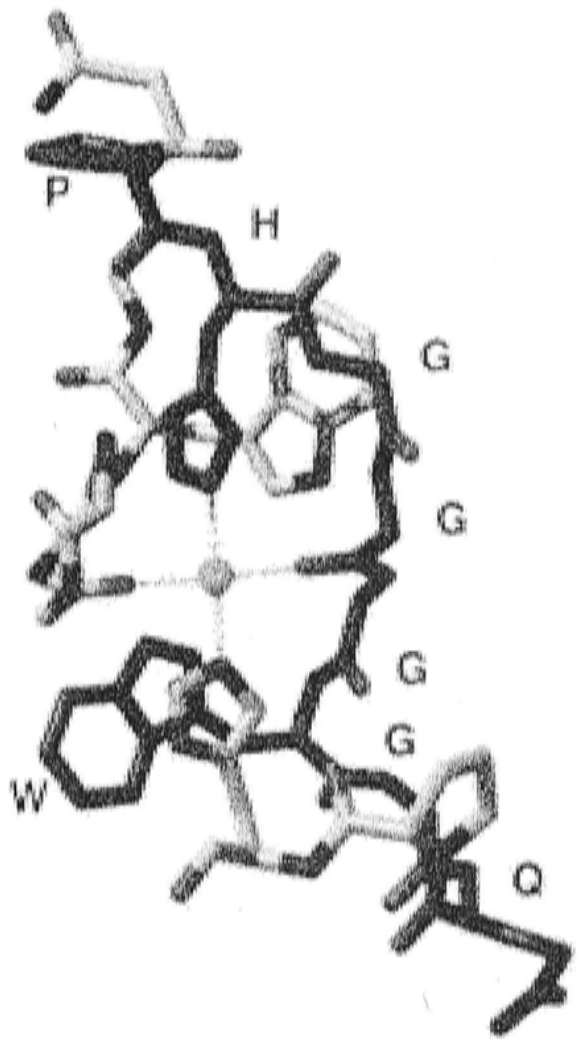

Figure source: Stockel et al. (1998)

Figure 1.5: Copper-binding mode in PrP-octarepeat peptide according to Stockel et al. (1998). One copper ion coordinates two N_τ atoms of the imidazole ring of His^2 residues and two oxygen atoms of the Gly^4 carbonyl of the peptide backbone (note the numbering of residue: ^{1}PHGGGWGQ^8). Figure was taken from Stockel et al., 1998, with some changes in size and colour.

To account for stoichiometry of 2 copper ions bound in $ShaPrP_{29\text{-}231}$ at pH 6.0, a model with square planar geometry was proposed (Figure 1.5). Copper ion is coordinated by two His residues and two oxygen main chain Gly carbonyl group, with each His and Gly coming from different repeats (Stockel et al., 1998). While His involvement is inferred from pH titration experiments, the involvement of Gly amide oxygens is not based on any spectroscopic evidence but rather on the proposed structure, which is based on sequence homology with sialidase enzyme, in which homologous residues form a loop structure. Hence, this suggestion has been contested and it may not be correct for pH > 4.0 or at physiological pH where backbone amide coordination is suggested to dominate (Viles et al., 1999). Although it comes from a different residue, the involvement of the oxygen amide from the Trp residue is indicated by EPR spectra at pH 7.45 (Aronoff-Spencer et al., 2000). Furthermore, the XRD structure of the copper PrP octarepeats complex clearly indicates the copper ion coordinates the oxygen amide of the Gly located on the C-terminal side of His (Burns et al., 2002).

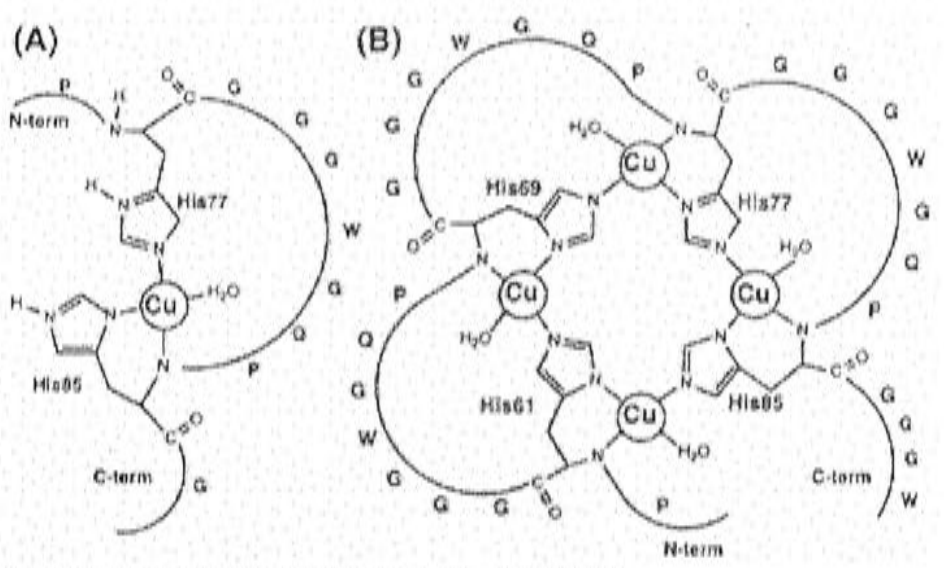

Figure source: Viles et al. (1999)

Figure 1.6: Copper-binding mode in PrP-octarepeat peptide according to Viles et al. (1999). (A) In 2 His peptide (PrP_{76-86}), one copper ion coordinates N_τ atom of imidazole ring of His^{77}, N_π atom of His^{85}, nitrogen atom of His amide of peptide backbone, and water molecule. The complex geometry is square planar with all four ligands in equatorial position. (B) In 4 His peptide (PrP_{58-91}), similar copper-coordination sphere is adopted. Note that each copper ion binds 2 His residues and both N_τ and N_π atoms of the imidazole ring of His participates in the binding forming the copper-bridging imidazolate.

As noted earlier, Viles et al. (1999) argue for the involvement of the Gly carbonyl backbone in copper binding. A model is proposed based on ^1H NMR and copper ESR spectra of PrP_{76-86} (peptide has two His residues), which binds only one copper ion. In this model both His residues coordinate to the same copper ion along with nitrogen atoms from the backbone amide of the more C-terminal His residue. A water molecule is attached as a final ligand to make the four-coordinate square planar copper complex (Figure 1.6 (A)). A model (Figure 1.6 (B)) was also proposed for the copper complex of PrP_{58-91}, which contains four His residues and measured stoichiometry 1:1 copper/octarepeat. In this model, four His residues in successive octarepeats form a bridged-copper complex, with the N_π and N_τ atom of the imidazole nitrogens from each His coordinating two adjacent copper ions ($Cu–N_\pi[His]N_\tau–Cu$). The amide nitrogen of His residue and oxygen atoms from four water molecules also participate in the binding.

Viles et al. (1999) suggest the formation of a copper-bridging imidazolate in this structure (Figure 1.6.B) can also provide an explanation for the observed cooperativity of copper ion binding to PrP_{58-91}. It is suggested that chelation of the first copper ion to the N_π atom lowers the pK_a of the $N_\tau H$ enabling the coordination of a second copper ion to the same His residue. Further, Viles et al. (1999) suggest that as the first copper ion coordinates two imidazoles, only two further imidazoles are needed to bind the next three copper ions. After the third copper binds, the fourth copper will have an entirely

preorganized site. However, it should be noted that this copper-bridging imidazolate in the copper complex of peptide containing 4-tandemly octarepeats failed to be detected by EPR (Aronoff-Spencer et al., 2000) and was only weakly observed by Raman spectra (Miura et al., 1999).

There are also some weaknesses in the model of Viles et al. (1999). Copper binding to a His side chain will induce the ionization of a nearby amide group (Miura et al., 1999). It is less likely that copper will bind to the imidazole ring of His, which is the primary ligation site, and then to an amide nitrogen of the His residue located at the more C-terminal side. This mode of binding results in a less compact arrangement of the primary ligation site (imidazole ring of His) and amide nitrogens, whereas, as Miura et al. (1999) suggest, metal chelation requires a compact arrangement (Miura et al., 1999). Viles et al. proposed this model to take account of the 1:2 copper/octarepeat stoichiometry, which later on has been revised (Garnett and Viles, 2003).

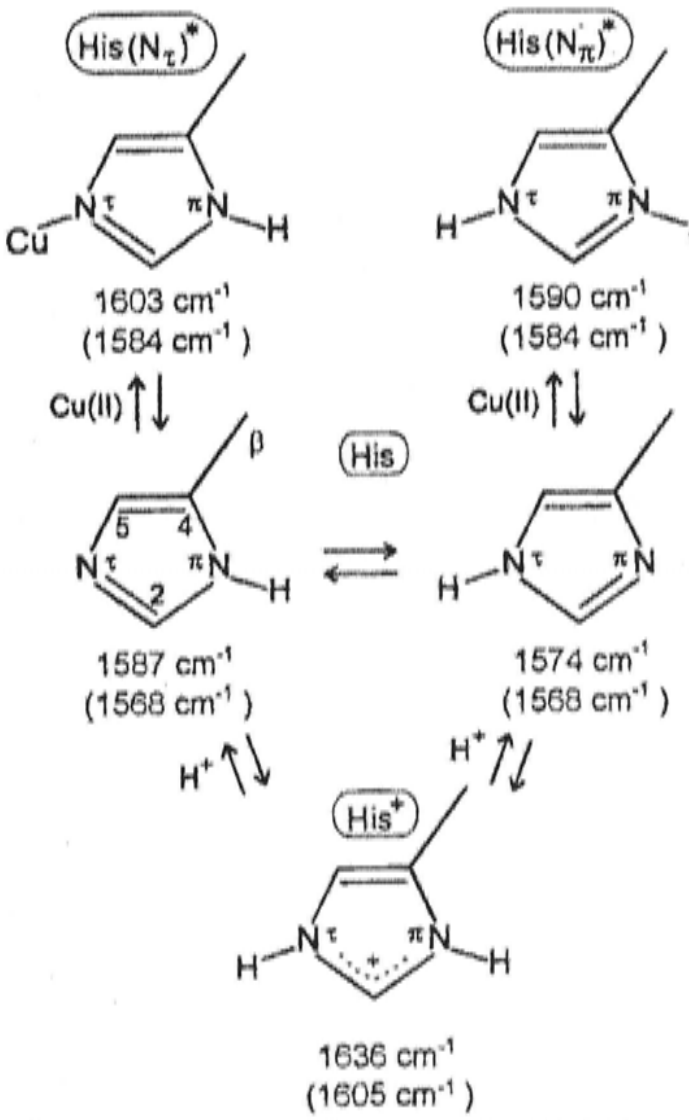

Figure source: Miura et al. (1999)

Figure 1.7: Two tautomeric forms of the imidazole side chain of His in its copper-free and copper-complex form. The band frequency is for the C4=C5 bond vibration of the imidazole ring of His in copper-free and complex form (see figures). The values in brackets ( ) represent the same band frequency in $^{2}H_2O$ solvent.

Although there is enough experimental evidence to support His as a major copper-binding site, the nitrogen atom that participates in the binding of copper ions is identified experimentally only by Raman spectroscopy. Note that the imidazole side chain has two tautomeric forms, dependent on which nitrogen atom binds the hydrogen. The tautomerism of the imidazole ring and its corresponding Raman frequency is shown in Figure 1.7. Apart from His coordination, Raman spectroscopy also shows that nitrogen atoms of deprotonated main-chain amides, rather than oxygen atoms of the HGGG segment, are the copper-binding sites (Figure 1.8) (Miura et al., 1996; Miura et al., 1999). This is in good agreement with the previous model of Viles et al. (Viles et al., 1999).

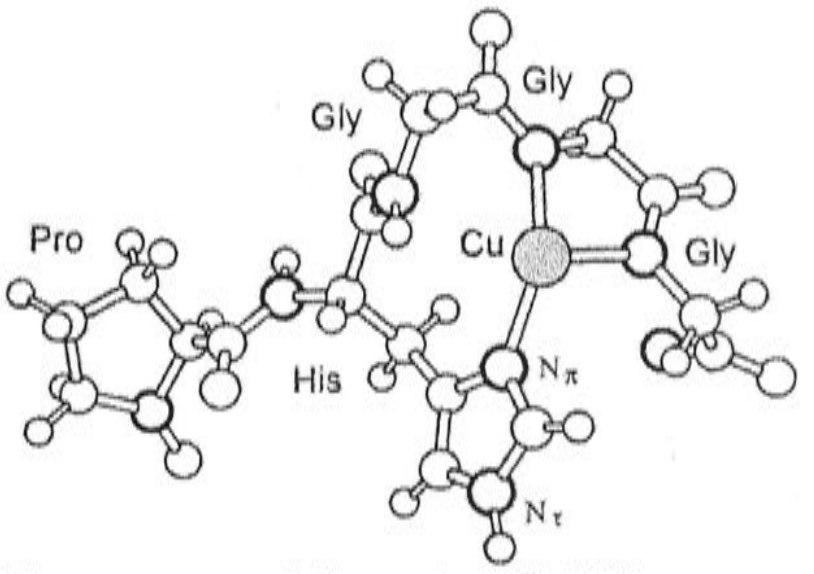

Figure source: Miura et al. (1999)

Figure 1.8: Copper-binding mode in PrP-octarepeat peptide according to Miura et al. (1999). At neutral and basic pH the ^{1}PHGGG^{5} segment binds copper ion via the N_π atom of the imidazole ring of His^{2}, two nitrogen atoms of the amide backbone of Gly^{4} and Gly^{5}, which occupy three out of four tetragonal ligand positions. A water molecule (not shown) occupies the fourth position.

As noted earlier, binding properties such as stoichiometry and ligand binding sites depend on the pH of the solution. Raman spectroscopy shows that at pH $\geq$ 6.4, one copper ion binds to the imidazole N_π atom of the His residue together with two deprotonated main chain amide nitrogens from the second and third Gly residues in the triglycine segment. At pH 6.0, one copper ion binds two imidazole N_τ atoms where each comes from different peptide chains (Miura et al., 1999).

Also as mentioned previously, Raman spectroscopy detected the presence of a weak band due to a copper-bridging imidazolate in the copper complex of a 4-octapeptide repeat. This band suggested that some of the His residues are coordinating to copper ions via both N_τ and N_π atoms. This result leads to the suggestion for two forms of

copper complex of 4-octapeptide tandem repeat at neutral and basic pH: the extended and the folded forms. In the extended form, copper ion binds the His N_π atom and deprotonated amide nitrogens of the second and third Gly residue, and the fourth ligand may be a water molecule. Copper complexes of 1-octarepeat and 2-octarepeat peptides also adopt this mode of binding. In the folded form, the fourth ligand may be a His N_τ atom of another octapeptide unit to produce the Cu-N_τ(His)N_π-Cu (copper-bridging imidazolate) structure.

The next model (Figure 1.9) was proposed by Aronoff-Spencer et al. (2000). It includes the nitrogen atom of His and two amide nitrogens from the first and second Gly after the His residue, while the fourth ligand is the amide carbonyl oxygen of the Trp residue more C-terminal in the repeat (Figure 1.9). The involvement of the amide nitrogen of the first Gly residue is in contrast to the three models previously proposed by Stocket et al. (1998), Viles et al. (1999) and Miura et al. (1999) (see section above), but in good agreement with the XRD structure of the PrP copper-repeats complex (Burns et al., 2002). However, the XRD structure indicates carbonyl oxygen comes from the second Gly residue rather than from Trp residue.

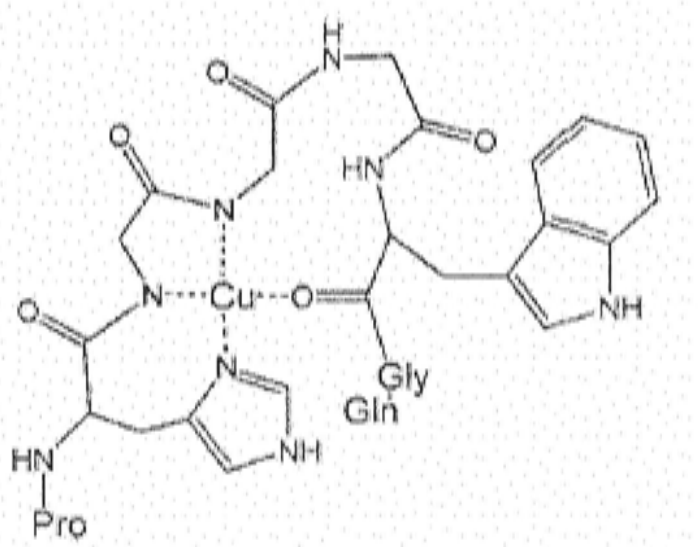

Figure source: Aronoff-Spencer et al., (2000)

Figure 1.9: Copper-binding mode in PrP-octarepeat peptide according to Aronoff-Spencer et al. (2000). The dominant EPR-active binding modes of octarepeat (^{1}PHGGGWGQ^8) at pH > 7.0 shows that coordination in the equatorial plane arises from the N_π atom of the imidazole ring of His^2, two nitrogen atoms each from the peptide backbone of Gly^3 and Gly^4 amides, and an oxygen atom from backbone carbonyl of the Trp^6 residue.

The crystal structure (Figure 1.10) also revealed that copper is coordinated by the His imidazoles, deprotonated amides from the next two Gly residues within the HGGGW segment, and one peptidic oxygen from Gly^3, all in the equatorial position. The Trp

indole also participates through a hydrogen bond to the axially coordinated water molecule. This structure is consistent with the EPR signals. It is also suggested that the HGGGW segment provides a five-ligand coordination (pentacoordination) environment as often found for copper complexes. Therefore, with regard to the binding to multiple octarepeats, EPR demonstrates that the identified structure is maintained in the full PrP 4-octarepeat domain (Burns et al., 2002). Thus, consistent with the previous study of Aronoff-Spencer et al. (2000) this study also does not detect the formation of a copper-bridging imidazolate in multiple octarepeat peptides, but rather each individual octarepeat binds a single copper ion within the HGGGW unit.

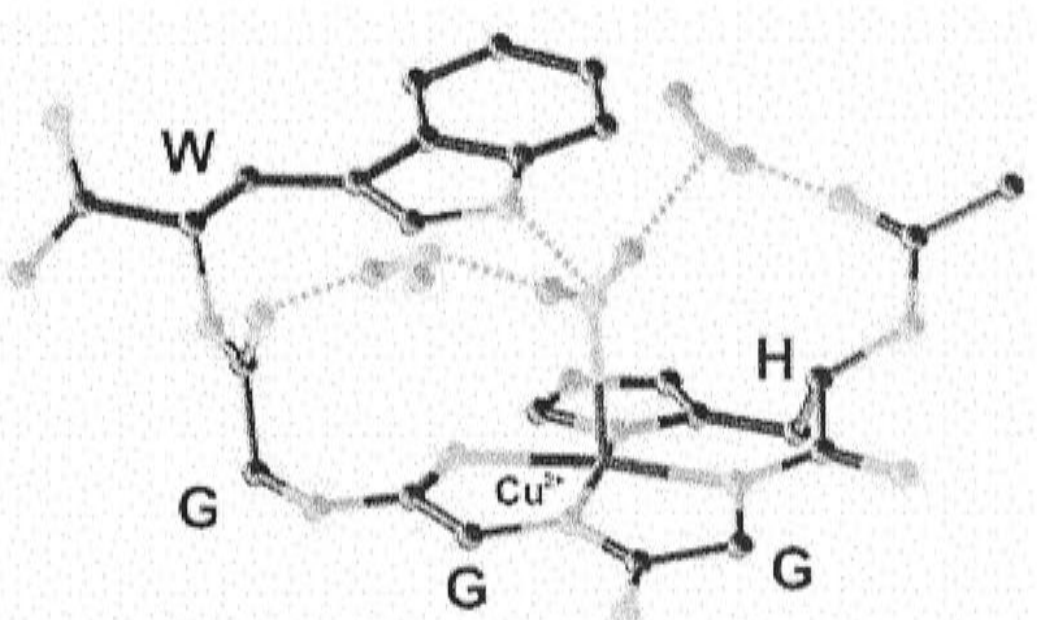

Figure source: Burns et al. (2002)

Figure 1.10: Copper-binding mode in PrP-octarepeat peptide according to Burns et al. (2002). The crystal structure of the copper-complex of ^{1}HGGGW^{5} segment of octarepeat shows copper pentacoordination in which 4 ligands are equatorially ligated and one water molecule is attached in the axial position. Four equatorial ligands are: N_{π} atom of the imidazole ring of His^{1}, two peptidic nitrogen atoms each from Gly^{2} and Gly^{3}, and one peptidic oxygen from Gly^{3}. This model also shows that an axially-bound water molecule is hydrogen bonded to the nitrogen atom of the indole ring side chain of the ^{5}Trp residue. This figure was taken from Burns et al. with some changes in size and colour.

Another type of pentacoordination is reported to allow copper complexes of octarepeat peptide to adopt a β-turn conformation (Bonomo et al., 2000). In this model, at neutral pH (Figure 1.11 a and c) the copper complex forms a square pyramid with one copper ion coordinating a water molecule, two peptidic nitrogen and one imidazole nitrogen all in equatorial position, while another peptidic nitrogen donor is linked at the apical position. At basic pH (Figure 1.11 b and d), the complex geometry is octahedral with hexacoordination from three peptidic nitrogens and one imidazole nitrogen, all

occupying the equatorial plane, while the two apical positions are filled with a water molecule and another peptidic nitrogen.

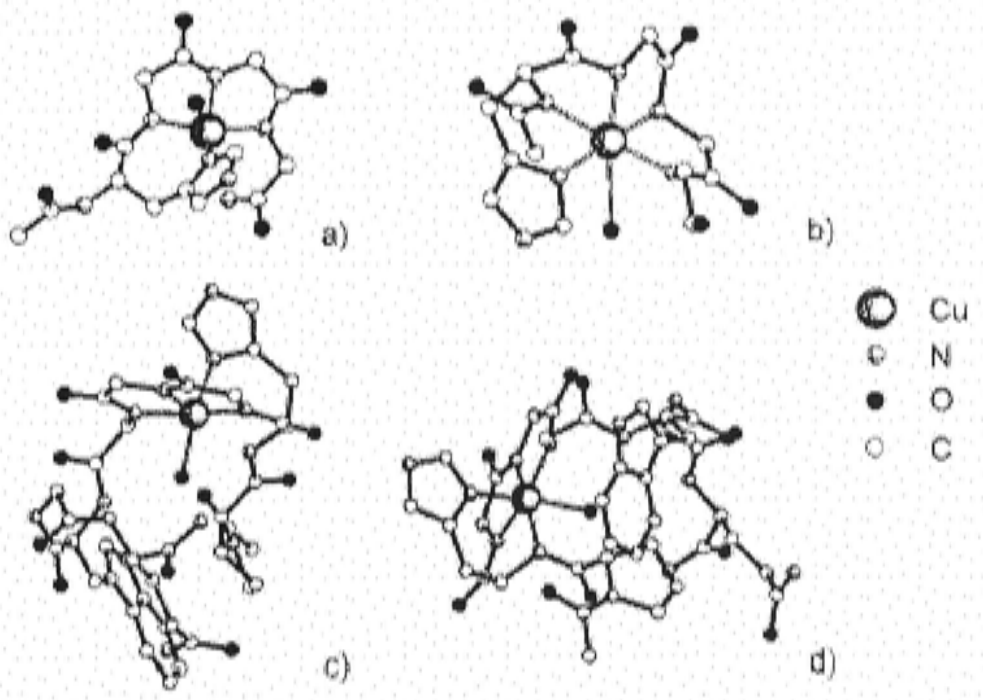

Figure source: Bonomo et al. (2000)

Figure 1.11: Copper-binding mode in PrP-octarepeat peptide according to Bonomo et al. (2000). a) and b) represent the binding mode in Ac-HGGG-NH_2 peptide at neutral and basic pH, respectively. c) and d) represent copper-binding mode in Ac-PHGGGWGQ-NH_2 at neutral and basic pH, respectively.

The involvement of the amine terminal group in copper binding has been indicated earlier in ESI MS experiments of Whittal et al. (2000). The role of this group in determining the copper-binding mode in octarepeat peptide was further investigated using potentiometry, NMR, and EPR methods (Luczkowski et al., 2002). Different binding modes were observed for the peptide with and without the free imino terminal group. In the absence of the imino terminal group of Pro due to acetylation, at pH ≈ 7.0, the copper ion binds 3 nitrogen ligands: the imidazole side chain of His^2, the amide nitrogen of Gly^3 and Gly^4 (note the residue numbering: ^{1}PHGGGWGQ^8) (Figure 1.12) (Luczkowski et al., 2002). In the presence of imino Pro, the copper ion binds to the nitrogen atom of the imidazole ring of His^2, the imino groups of Pro^1 at the N-terminus, and the amide nitrogen of the Gly^3 residue. The involvement of the amide nitrogen of the Gly^4 is detected only at higher pH. Protection of the N-terminal Pro nitrogen forces the copper ion to coordinate with the amide nitrogen on the C-terminal side of the His residue (i.e. third Gly) (Luczkowski et al., 2002).

The specificity of the HGGGW segment in binding of copper ions has been demonstrated (Garnett and Viles, 2003; Luczkowski et al., 2003). The replacement of the GGG segment with AAA (in peptide HAAAW) reduces the copper-binding

stoichiometry, as found by CD, the complex formed is $Cu(HAAAW)_2$ because of the reduction of potential for backbone coordination (Garnett and Viles, 2003). However, this result disagrees with EPR and potentiometry experiments of Luczkowski et al. (2003), which show that replacement of GGG with AAA or KKK does not change the coordination geometry or stoichiometry, but only reduces the stability of the complex. The formation of a $Cu(HAAAW)_2$ complex with such stoichiometry implies that there is at least one amide coordination besides the imidazole coordination because, otherwise, the stoichiometry would be 1:4, unless all other coordination is from water molecules.

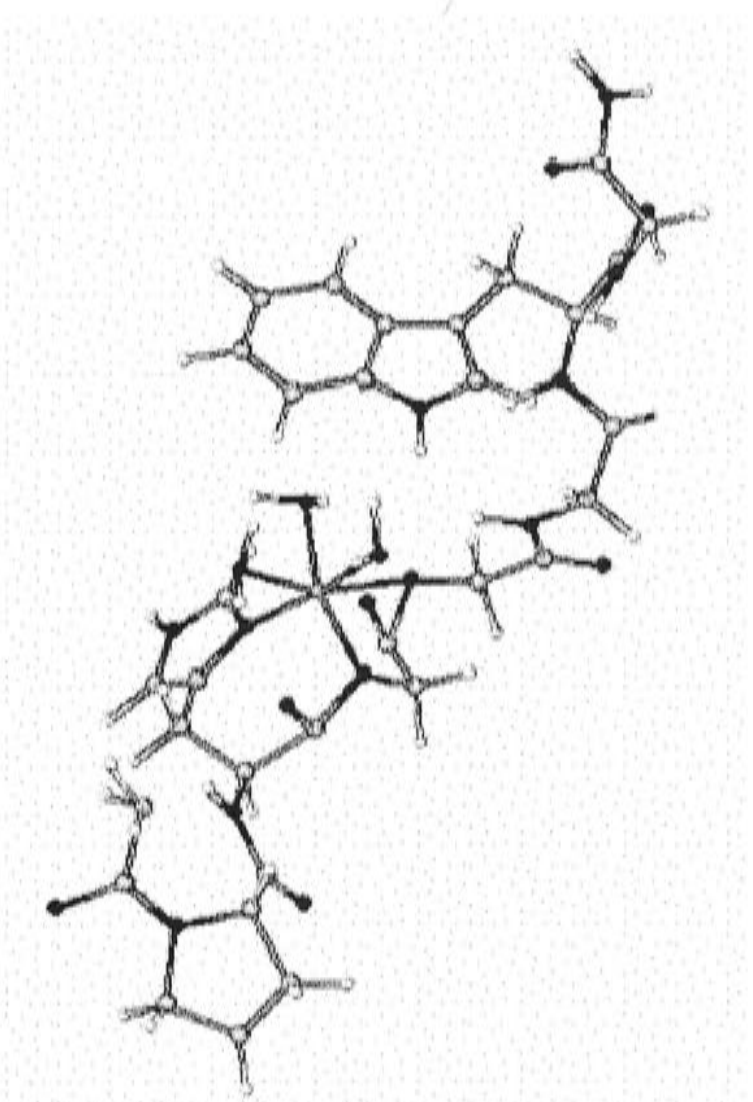

Figure source: Luczkowski et al. (2002)

Figure 1.12: Copper-binding mode in PrP-octarepeat peptide according to Luczkowski et al. (2002). Copper-complex of octarepeat (Ac-^{1}PHGGGWGQ^{8}-NH_2) has a distorted tetragonal geometry of coordination in which the N_π atom of the imidazole ring of His^2 bound apically to the copper ion, along with subsequent peptidic nitrogens of Gly^3 and Gly^4, which bound in the equatorial position. The copper ion bound three water molecules to complete the hexacoordinate complex.

Which Gly residues are essential for a 1:1 complex formation is the next question raised. The results with several segments of octarepeat peptides show that the stoichiometry is 1:1 for Cu:HGGG but 1:2 for HGG (Garnett and Viles, 2003). These data imply that the fourth Gly (note the numbering of the residue: ^{1}HGGG^{4}) is essential to maintain 1:1 stoichiometry. The result of Garnett and Viles (2003), however, is

different from the X-ray crystallography data, which demonstrated copper can bind the HGG segment with 1:1 stoichiometry, and that this segment is enough to make tetra coordination to copper (Burns et al., 2002).

The large variation in copper coordination reported in the literature indicates that there is more than one stable copper-complex form that is feasible for octarepeat PrP. Thus, NMR structure studies would not be useful even if they could be done in the presence of the copper ion, and X-ray crystallography shows just one isolated form. As stated earlier, the nature of the repeat region is such that it does not provide one single fixed set of copper-binding sites. The sites and their relative affinities are easily modified by the environment of the peptide, such as pH and the concentration ratio of copper and peptide.

The effect of pH on possible binding sites in the octarepeat peptide has been investigated by potentiometric titration. The results show that the more basic the solution, the more amide bond nitrogens participate in the binding (Luczkowski et al., 2002). Higher ratios of copper ions over peptide (>1) induce additional amide deprotonation and increase the number of amide bonds that participate in the binding, as demonstrated by Raman and visible absorption spectra (Miura et al., 1999). However, other experiments which varied the copper to peptide ratios at neutral pH, show that excess copper will not induce coordination from segments of octarepeat outside the HGGG segment. This implies the selectivity of the HGGG site (Bonomo et al., 2000).

1.5.5. Copper binding to post-repeat region

In addition to the N-terminal region of PrP, regions further towards the C-terminus have also been shown to interact with copper. Up to five copper ions bind to recombinant $MuPrP_{23\text{-}231}$ (Kramer et al., 2001). It is proposed that 4 copper ions bind to the repeat region (there are 4 repeats) and 1 copper ion binds to the C-terminal side of the octarepeat (see Table 1.4). The C-terminal site is identified around His^{96} and possibly His^{111} by NMR and fluorescence in the presence of Gly (Jackson et al., 2001). This is confirmed by mass spectrometric foot printing (Qin et al., 2002) and XAFS (Hasnain et al., 2001). Cereghetti et al. (2001) also found a copper-binding site in the C-terminal folded region by EPR (Cereghetti et al., 2001).

1.6. Sugar binding to PrP repeats

Several experimental results pointed to glycosaminoglycans (GAGs) being physiological ligands of PrP (Shyng et al., 1995; Brimacombe et al., 1999; Wong et al., 2001) and being likely to play a role in the cellular metabolism of both PrP^{C} and PrP^{Sc} (Shyng et al., 1995). The binding site in recombinant hamster PrP^{C} for GAGs, in the form of low molecular weight heparin and heparan sulfate, has been identified and has recently been shown to encompass the N-terminal region, the pre-repeat region (residues 23-52), the central, hydrophobic, amyloidogenic sequence (residues 110-128) and the octapeptide-repeat region (residues 53-93) (Warner et al., 2002).

As the octapeptide-repeat region is known to have both copper and GAG-binding capacities, the possibilities of concerted interaction between PrP, copper ions and heparin has also been investigated (Gonzalez-Iglesias et al., 2002; Warner et al., 2002). Warner et al. (2002) showed that copper ions enhanced the interaction between the octapeptide-repeat region and heparin and, furthermore, stabilized the oligomeric complexes resulting from PrP interaction with GAGs. In these complexes, PrP binds GAGs through His-bound copper in forming PrP – Cu(II) – GAG assemblies (Gonzalez-Iglesias et al., 2002). Recently it was shown that rPrP binding to GAGs is enhanced in the presence of Cu^{2+} and Zn^{2+}, but not Ca^{2+} and Mn^{2+} (Pan et al., 2002).

1.7. Review of low-complexity proteins and methods in general to study them

Low-complexity sequences or non-random amino acid compositions such as that in octapeptide tandem repeats of PrP are common in natural proteins but have been little studied (Wootton, 1994; Wright and Dyson, 1999). This is partly because methods to study them are not well established. Difficulties with crystallization have meant that only a few X-ray diffraction (XRD) structures for these types of protein have been solved. These structures are also difficult to solve by NMR, because apart from structural disorder, the repetitive sequence, which lacks a unique nuclear Overhauser enhancement (NOE), makes the assignment ambiguous. This has required use of combinations of several low-resolution techniques, such as fluorescence titration spectrophotometry, CD, mass spectroscopy, UV/Visible absorption spectroscopy, ED, EPR, potentiometry and voltammetry, Fourier transform infrared spectroscopy (FTIR), and fluorescence resonance energy transfer (FRET), to make studies of these proteins

feasible. Except EPR, potentiometry and voltammetry, this study has employed all the methods mentioned above to study the repeat system in marsupial PrP. Unlike the rest of the methods, the last two (FTIR and FRET) have not previously been used in PrP-repeat studies, hence, their use in this thesis is novel.

However, FTIR has long been used to probe conformation of proteins and peptides and conformational changes associated with ligand binding (Haris and Chapman, 1995; Jung, 2000; Torreggiani et al., 2000; Torreggiani et al., 2000). The technique generates a low-resolution secondary structure. Compared with the 3-D structures obtained from high-resolution XRD and NMR, FTIR is less informative, but nevertheless, there are situations where FTIR is preferred to XRD and NMR in elucidating the structure and function of peptides and proteins, especially when the peptide has high backbone flexibility and conformational dynamics.

FTIR is also more suitable than NMR for studying conformational changes upon binding of copper ions to proteins, such as in the case of copper binding to PrP repeats, because the copper ion is paramagnetic and this will interfere with the NMR signal. Furthermore, the interaction of copper with amino acid side chains can be detected. Thus, with thorough analysis of the spectrum, FTIR can be used to gain information about both conformational changes and ligand-binding sites in PrP-repeat peptides.

FRET has potential for elucidating inter residue distances in PrP-repeat peptides. The technique itself is well established in conformational study of peptides and proteins (Stryer, 1978; Wu and Brand, 1994; Selvin, 1995) and has been applied to investigate structural characteristics of small and highly flexible peptides such as galanin (Kulinski et al., 1997).

1.8. Copper-binding mode in PrP from species other than mammalian

The specific PrP sequence HGGGW is highly conserved across mammalian species of PrPs. However, this feature is absent from avian (Wopfner et al., 1999), reptile (turtle) (Simonic et al., 2000), and marsupial (brush-tailed possum (Windl et al., 1995) and tammar wallaby (Premzl and Gready, personal communication)) PrPs (see Table 1.1 above).

A study with chicken hexarepeat peptide revealed that it does bind copper ion (Hornshaw et al., 1995a; Hornshaw et al., 1995b). Recently, it has been confirmed that chicken hexarepeat peptide binds copper ion but with different stoichiometry, and certainly different mode of binding, to that of mammalian octarepeat (Garnett and Viles, 2003). Garnett and Viles (2003) suggest the stoichiometry is 1 copper ion per two hexarepeats (PHNPGY), which suggests two His residues from different peptide chains bind a single copper ion, as the amide nitrogen of Pro (the second residue after His) is not available for coordination to copper ion.

The studies reported in this thesis are based on investigation of the properties of repeats from a marsupial PrP (brush-tailed possum). As shown in Table 1.1, marsupial repeats do not have the HGGGW segment, which is a feature of mammalian PrP repeats. It is suspected that marsupial repeats may have a different copper-binding mode and mechanism. Although the motif P[H/Q].GG.WGQ is conserved among the mammalian and marsupial sequences, the marsupial repeat has a Pro inserted as its third residue (after H/Q), which cannot coordinate copper ion through its amide nitrogen. It is the aim of this study to characterize marsupial PrP repeats and their copper-binding properties.

Chapter II

Materials and Methods

2.1. Instrumentation

Instruments that were used in these experiments are located in various departments and research schools within the Australian National University (ANU).

2.1.1. UV/Vis spectrophotometer

A Varian Cary 1 Bio UV/Vis spectrophotometer located at the John Curtin School of Medical Research (JCSMR) ANU was used to measure the concentration of peptides based on Trp absorption at 280 nm [ε_{280} = 5500 (Pace and Schmid, 1997)].

2.1.2. High-pressure liquid chromatography (HPLC)

A Waters HPLC located at JCSMR ANU was used to check the purity of the peptides. The instrument was equipped with Waters 2487 dual λ absorbance detector, Waters 515 pump and Waters reverse phase C_{18} analytical column.

2.1.3. Chromatography column

A Biorad Econo Column (size of 0.5 x 5 cm) chromatography column was used to remove residual TFA from the peptides. The column was filled with Amberlite IR 45 anion exchange resin (Muga et al., 1990).

2.1.4. Fluorescence spectrophotometer

A Perkin Elmer LS 50B Fluorescence spectrophotometer located in JCSMR was used in the fluorescence titration experiments to determine the dissociation constant of copper–Msp-peptide complexes as well as in the fluorescence resonance energy transfer (FRET) experiments to determine the distance between residues in the peptides.

2.1.5. Electrospray ionization mass spectrophotometer (ESI MS)

A VG Quattro II triple quadrupole ESI MS from Fisons Instruments located in the Research School of Chemistry (RSC) ANU was used in experiments to determine the stoichiometry of copper binding to Msp peptides and to initially assess the binding of other metals.

2.1.6. Fourier transform infrared spectrophotometer (FTIR)

A Perkin Elmer Spectrum One FTIR spectrophotometer located in RSC ANU was used to probe the conformation and conformational changes of the peptide backbone upon copper binding and to determine the copper-binding sites.

2.1.7. Circular dichroism spectrophotometer (CD)

A Jobin-Yvon Model CD6 CD spectrophotometer located in RSC ANU was used to determine the conformation of the peptide backbone under particular conditions, such as in the presence of copper ions at different pHs.

2.1.8. Equilibrium dialysis (ED) apparatus

Forty dialysis chambers and a rotation device made in the JCSMR workshop were used in experiments to study copper binding to Msp peptides.

2.1.9. Inductively coupled plasma optical emission spectrophotometer (ICP OES)

A Varian Vista Pro ICP OES located in the Geology Department, Faculty of Science ANU was used to determine the concentration of metals from equilibrium dialysis experiments.

2.2. Materials

2.2.1. Synthetic peptides

Synthetic peptides were supplied by the Biomolecular Resources Facility (BRF) JCSMR, ANU.

Table 2.1: Synthetic peptides used in the experiments. All peptides were terminated at the C-terminus with a Gly residue.

Group	Peptide	Sequence	Size
Msp4 group	Msp4	$(PHPGGSNWGQ)_4G$	41
	Msp4capC	$(PHPGGSNWGQ)_4G\text{-}NH_2$	41
	Msp4capNC	$Ac\text{-}(PHPGGSNWGQ)_4G\text{-}NH_2$	41
Msp3 group	Msp3	$(PHPGGSNWGQ)_3G$	31
	Msp3capC	$(PHPGGSNWGQ)_3G\text{-}NH_2$	31
	Msp3capNC	$Ac\text{-}(PHPGGSNWGQ)_3G\text{-}NH_2$	31
Msp2 group	Msp2	$(PHPGGSNWGQ)_2G$	21
	Msp2capC	$(PHPGGSNWGQ)_2G\text{-}NH_2$	21
	Msp2capNC	$Ac\text{-}(PHPGGSNWGQ)_2G\text{-}NH_2$	21
Msp1 group	Msp1	PHPGGSNWGQG	11
	Msp1capC	$PHPGGSNWGQG\text{-}NH_2$	11
	Msp1capNC	$Ac\text{-}PHPGGSNWGQG\text{-}NH_2$	11
Msp1 variant and mutant	Msp1capN	Ac-PHPGGSNWGQG	11
	Msp1H2A	PAPGGSNWGQG	11
	Msp1N7A	PHPGGSAWGQG	11
	Msp1Q10A	PHPGGSNWGAG	11
Msp1 His-methylated	Msp1His(1Me)capC	$PH[\tau Me]PGGSNWGQG\text{-}NH_2$	11
	Msp1His(3Me)capC	$PH[\pi Me]PGGSNWGQG\text{-}NH_2$	11
Modified repeat sequences	Msp1P3GcapNC	$Ac\text{-}PHGGGSNWGQG\text{-}NH_2$	11
	Msp_1strepcapNC	$Ac\text{-}PQGGGTNWGQG\text{-}NH_2$	11
	Msp_4threpcapNC	$Ac\text{-}PHGGSNWGQG\text{-}NH_2$	10
	Hu1capNC	$Ac\text{-}PHGGGWGQG\text{-}NH_2$	9
	Msp2F8capNC	$Ac\text{-}PHPGGSNFGQPHPGGSNWGQG\text{-}NH_2$	21
	Msp2F18capNC	$Ac\text{-}PHPGGSNWGQPHPGGSNFGQG\text{-}NH_2$	21
	Msp3F8F18capC	$Ac\text{-}(PHPGGSNFGQ)_2PHPGGSNWGQG\text{-}NH_2$	31
	Hu2F6capC	$Ac\text{-}PHGGGFGQPHGGGWGQG\text{-}NH_2$	17
	Hu2F14capC	$Ac\text{-}PHGGGWGQPHGGGFGQG\text{-}NH_2$	17
Dansylated peptides	DansMsp1	Dans-PHPGGSNWGQG	11
	DansMsp1capC	$Dans\text{-}PHPGGSNWGQG\text{-}NH_2$	11
	DansMsp2F8capC	$Dans\text{-}PHPGGSNFGQPHPGGSNWGQG\text{-}NH_2$	21
	DansMsp2F18capC	$Dans\text{-}PHPGGSNWGQPHPGGSNFGQG\text{-}NH_2$	21
	DansMsp3F8F18capC	$Dans\text{-}(PHPGGSNFGQ)_2PHPGGSNWGQG\text{-}NH_2$	31
	DansHu1capC	$Dans\text{-}PHGGGWGQG\text{-}NH_2$	9
	DansHu2F6capC	$Dans\text{-}PHGGGFGQPHGGGWGQG\text{-}NH_2$	17
	DansHu2F14capC	$Dans\text{-}PHGGGWGQPHGGGFGQG\text{-}NH_2$	17

capC is peptide with the terminal COO^- group protected with an amide group; capN is peptide with the terminal NH group protected with an acetyl group; capNC is peptide with both terminal groups protected; Msp1H2A is Msp1 with His^2 replaced by Ala^2; Msp1N7A is Msp1 with Asn^7 replaced by Ala^7, Msp1Q10A is Msp1 with Gln^{10} replaced by Ala^{10}; Msp2F18capC is Msp2capC where Trp^{18} is replaced with Phe^{18}; Dans is the peptide with a dansyl group attached to the terminal imino group.

2.2.1.1. Peptide synthesis

Peptide synthesis was carried out using two instruments. In the initial stage of the research, the peptides were synthesized using the Applied Biosystems 430A Peptide Synthesizer and in the final stage the synthesis was carried out using the SYMPHONY/MULTIPLEX Multiple Peptide Synthesizer. Peptide syntheses on both instruments were performed using FMOC chemistry and the solid-phase peptide

synthesis technique. Cleavage of the peptide from the resin was performed in a mixture of 10 mL trifluoroacetic acid (TFA), 0.5 mL H_2O, 0.75 g phenol, 0.5 mL thioanisole, and 0.25 mL ethaneditiol. The crude peptide was purified by Bio-Rad HPLC on a C_{18} column, using a 4-40% linear gradient of acetonitrile in 0.09% (v/v) TFA. The peptide was then freeze dried. When required, the N-or C-terminus or both N- and C-termini were protected by means of acetylation and amidation, respectively.

For dansylated peptide, the dansyl group was attached to the imino end of the peptide before the oligomer was released from the resin. About 0.5 gram of deprotected resin was removed from the reaction vessel, reacted for 10 hr with 250 mg of dansyl chloride in methylene chloride containing 1 mL of triethylamine, and then washed thoroughly with methylene chloride and ethanol. The dansylated peptide was released from the resin by stirring for 20 hr with 20 mL of ethanol containing 4 mL of anhydrous (97 %) hydrazine. Purification was carried out using HPLC. The peptide was then freeze dried.

2.2.1.2. Peptide purification: the removal of residual trifluoroacetic acid (TFA)

Synthetic peptides (Table 2.1) contained a small amount of TFA (the buffer used in HPLC purification). The removal of residual TFA is important for peptides to be used in the FTIR experiment because it has IR absorption overlapping the peptide spectrum. Thus, the peptide was additionally purified either by anion exchange resin (amberlite IR-45) mini column chromatography (Muga et al., 1990) or by repeated lyophilization (after addition of sufficient amount of HCl). In the anion exchange method, the column was pre-equilibrated with Milli-Q water. The peptide was dissolved in 1 mL of Milli-Q water, transferred to the column, and eluted with Milli-Q water. Collected fractions were then freeze dried.

2.2.1.3. Preparation of stock peptide solutions

Typically, 1-5 mg of peptide was weighed out on an analytical balance into a 1.5 mL Eppendorf tube. The peptide was dissolved in Milli-Q water. The concentration of peptide was determined by measuring the Trp absorbance of peptide in the solution at 280 nm, using UV/Vis spectrophotometer. The concentration of the stock solution was then calculated using the Beer-Lambert relation

$$A = \varepsilon \times c \times l \qquad \text{(Equation 2.1)}$$

in which ε = molar absorbance coefficient, c = concentration of peptide, l = the cell length, A = absorbance. The molar absorbance coefficient (ε) at 280 nm for each peptide was calculated using the equation (Pace and Schmid, 1997):

$$\varepsilon_{280}\ [M^{-1}\ cm^{-1}] = 5500 \times n_{Trp} \qquad \text{(Equation 2.2)}$$

in which n_{Trp} is the number of Trp residue in the peptide.

2.2.2. General buffer and reagent solution

Amberlite IR-45, anion exchange resin analytical grade, was manufactured by Rohm Haas company. Buffer components, NaCl, $Na_2HPO_4.2H_2O$, $NaH_2PO_4.H_2O$, NaOH, HCl, KCl, KOH, NEM (N-ethylmorpholine), ammonia, ammonium formate, KH_2PO_4, sodium tetraborate, Tris, and formic acid were all analytical grade and purchased from Analar BDH. Metal salts; $CuSO_4.5H_2O$, $CaCl_2.2H_2O$, $ZnCl_2$, $MgSO_4$, and $MnSO_4.4H_2O$ were all analytical grade and purchased from Analar BDH. $CuCl_2.2H_2O$ were analytical grade and purchased from Sigma. Amino acids Glycine and Tryptophan were both analytical grade and purchased from Analar BDH. Deuterium Oxide was purchased from Sigma. Milli-Q water was used as a solvent in all buffer and reagent solutions. The buffer and all reagent solutions were filtered prior to use, using the 0.45 μm Whatman filter paper.

2.2.2.1. Preparation of stock PBS (phosphate buffered saline) buffer

100 mL PBS buffer (10 x) was prepared by dissolving 8 g NaCl, 1.25 g $Na_2HPO_4.2H_2O$, and 0.3535 gram $NaH_2PO_4.H_2O$ in Milli-Q water. The pH was adjusted to 7.4 by addition of dilute HCl or NaOH solution.

2.2.2.2. Preparation of stock NEM (N-ethylmorpholine) buffer

100 mL of stock (10 x) NEM buffer was prepared by dissolving 3.2 mL NEM (MW = 115.2; d = 0.91 gram /mL) and 11.175 gram KCl in Milli-Q water. The solution was adjusted to pH 7.4 by addition of dilute HCl or KOH. The concentration of NEM in the working solution (1 x solution) was 25 mM and KCl was 150 mM.

2.2.2.3. Preparation of stock phosphate buffer solutions at pH 6.0, 7.4 and 8.0

50 mL of stock (10 x) phosphate buffer was prepared according to Table 2.2. The concentration of phosphate in working solution (1 x solution) is 25 mM and ionic strength is 0.1 M.

Table 2.2: Preparation of 10 x phosphate buffer

pH	2 M Na_2HPO_4	2 M NaH_2PO_4	5 M NaCl	Milli-Q water	Total Volume
6.0	0.769 mL	5.481 mL	6.885 mL	36.865 mL	50 mL
7.4	5.062 mL	1.188 mL	4.450 mL	39.300 mL	50 mL
8.0	5.919 mL	0.331 mL	2.765 mL	40.985 mL	50 mL

2.2.2.4. Preparation of stock universal buffer solution pH 3.0-8.0

Stock I universal buffer was prepared by dissolving 21.014 g of citric acid, 13.609 g of KH_2PO_4, 38.136 g of sodium tetraborate, 12.114 g of Tris, and 7.455 g of KCl in Milli-Q water and made up to 400 mL. 5 x stock buffer solutions (pH 3.0, 5.0, 6.5, 7.4, and 8.0), were prepared by taking 25 mL stock I, adjusting to desired pH by adding 5 M NaOH or 5 M HCl, and adding Milli-Q water to 50 mL. The concentration of each component in the working solution (1 x solution) is 25 mM.

2.2.2.5. Preparation of stock solutions of metal salts

100 mL of 0.2 M of stocks of metal salts ($CuSO_4$, $CaCl_2$, $ZnCl_2$, $MgSO_4$, and $MnSO_4$) were made in Milli-Q water. The following amounts of metal salts were weighed out using an analytical balance (4.994 g $CuSO_4.5H_2O$, 2.940 g $CaCl_2.2H_2O$, 2.726 g $ZnCl_2$, 4.461 g $MnSO_4.4H_2O$ and 2.407 g $MgSO_4$). The sample was transferred to a 100 mL of volumetric flask, and made up with Milli-Q water.

Chapter III

Fourier Transform Infrared Spectroscopy

Fourier transform infrared spectroscopy (FTIR) was used to probe the conformation of PrP-repeat peptides and follow their conformational changes associated with copper binding. The interaction of copper with amino acid side chains was also detected by FTIR. Thus, with thorough analysis of the FTIR spectrum, both conformational changes and copper-binding sites in PrP-repeat peptides can be revealed.

3.1. Introduction

Fourier transform infrared spectroscopy (FTIR) is an extremely useful tool to probe protein and peptide conformation in a wide range of environments (Haris and Chapman, 1992; Haris and Chapman, 1995; Jung, 2000). The most useful band for infrared analysis of the protein secondary structure is the amide I band, which appears in the region between 1600-1700 cm^{-1} (Byler and Susi, 1986; Surewitz and Mantsch, 1988; Haris and Chapman, 1992; Haris and Chapman, 1995; Jung, 2000). This band arises primarily from the C=O stretching vibration of the amide backbone coupled weakly to the in plane NH bending, CCN deformation and CN stretching modes.

in-plane

Table 3.1. General classification of amide I vibration of polypeptides in ^2H_2O.

Wavenumber (cm^{-1})	Assignment	Reference
1649-1658	α-Helix	(Byler and Susi, 1986; Surewitz and Mantsch, 1988; Haris and Chapman, 1995; Arrondo and Goni, 1999; Heimburg et al., 1999; Jung, 2000)
1640-1648	Random coil	
1620-1635 and 1672 (weak)	Intramolecular β-sheets	
1665-1690	Turns	
1614-1624 and 1684 (weak)	Intermolecular antiparallel β-sheets in aggregated proteins	(Ismail et al., 1992; Jackson et al., 1992; Panick et al., 1999)

The frequency region of the amide I band is characteristic for each type of secondary structure. The correlation between the positions of the amide I band and the type of secondary structure adopted by the polypeptide chain in solution has been extensively reported in the literature (Byler and Susi, 1986; Surewitz and Mantsch, 1988; Haris and

Chapman, 1995; Arrondo and Goni, 1999; Heimburg et al., 1999; Jung, 2000). For the purpose of spectral assignment in this chapter, the amide I band and its corresponding structure of peptides and proteins in ^2H_2O is presented in Table 3.1. However, there are some exceptions to this general assignment, especially the one related to α-helical structure.

The absorption of α-helical structures is sensitive to their environment. The position of the amide I band of α-helical structure in a membrane protein can be different from α-helix in a soluble protein, or in a homopolypeptide or a short highly solvent-exposed peptide (Haris and Chapman, 1995). In membrane proteins the α-helix absorption occurs between 1656-1658 cm^{-1} while in a soluble protein it occurs between 1649-1658 cm^{-1} (see Table 1). In a homopolypeptide, such as poly-L-lysine, α-helix absorption is located at 1638 cm^{-1}. For a short solvent-exposed peptide, the band frequency of α-helical structure occurs at 1644 cm^{-1} (Haris and Chapman, 1995). It should also be noted that the position of the amide I band of polypeptides in ^2H_2O is 2-9 cm^{-1} lower than its value for protein in ^1H_2O.

3.2. Aims

The aims of this work are to probe the conformational changes in marsupial PrP-repeat peptides (Msp), as a function of copper binding at different pHs and for different numbers of repeats. As shown in Table 3.2, much of this copper-binding study has used the synthetic peptide containing 1-4 copies of the second-repeat sequence (PHPGGSNWGQ) of marsupial (brush-tailed possum) PrP (Windl et al., 1995). However, the first-repeat sequence (PQGGGTNWGQ), where QG replaces HP, and the fourth-repeat sequence (PHGGSNWGQ), where P is deleted, were also studied for their copper-binding properties. The study also compares the copper-binding properties of marsupial PrP repeats with those of human PrP octarepeat (PHGGGWGQ). Experiments using some mutant peptides of the second-repeat sequence, where the third Pro is replaced with Gly (PHGGGSNWGQ), the second His is replaced with Ala (PAPGGSNWGQ), the seventh Asn is replaced with Ala (PHPGGSAWGQ), and the tenth Gln is replaced with Ala (PHPGGSNWGA), were carried out to obtain information about the copper-binding sites. Copper binding to peptides with the His ring methylated (PH[1Me]PGGSNWGQ and PH[3Me]PGGSNWGQ) was studied to determine which tautomeric form (nitrogen atom of the imidazole ring of His) binds the

copper ion. Copper titration of Msp1 monitored by FTIR was used to obtain information about the number of copper ions bound in a single marsupial repeat. The possibility of other metal (calcium, zinc, manganese, and magnesium) ions binding to Msp peptides was also investigated.

3.3. Materials and methods

3.3.1. Sample preparation

The peptide (see Table 3.2) was additionally purified either by anion exchange resin, amberlite IR-45, mini column chromatography (Muga et al., 1990) or repeated lyophilization (after addition of sufficient amount of HCl) to remove residual TFA. In anion exchange method, the column was pre-equilibrated with Milli-Q water. The peptide was dissolved in 1 mL of Milli-Q water, transferred to the column, and eluted with Milli-Q water. Collected fractions were then freeze dried. UV/Vis spectrometry was used to check the peptide concentration based on the Trp absorption at 280 nm (ε_{280} = 5500) (Pace and Schmid, 1997).

Table 3.2: Synthetic peptides used in the experiments.

Group	Peptide	Sequence	Size
Msp4 group	Msp4	$(PHPGGSNWGQ)_4G$	41
	Msp4capC	$(PHPGGSNWGQ)_4G\text{-}NH_2$	41
	Msp4capNC	$Ac\text{-}(PHPGGSNWGQ)_4G\text{-}NH_2$	41
Msp3 group	Msp3	$(PHPGGSNWGQ)_3G$	31
	Msp3capC	$(PHPGGSNWGQ)_3G\text{-}NH_2$	31
	Msp3capNC	$Ac\text{-}(PHPGGSNWGQ)_3G\text{-}NH_2$	31
Msp2 group	Msp2	$(PHPGGSNWGQ)_2G$	21
	Msp2capC	$(PHPGGSNWGQ)_2G\text{-}NH_2$	21
	Msp2capNC	$Ac\text{-}(PHPGGSNWGQ)_2G\text{-}NH_2$	21
Msp1 group	Msp1	PHPGGSNWGQG	11
	Msp1capC	$PHPGGSNWGQG\text{-}NH_2$	11
	Msp1capNC	$Ac\text{-}PHPGGSNWGQG\text{-}NH_2$	11
Msp1 variant and mutant	Msp1capN	Ac-PHPGGSNWGQG	11
	Msp1H2A	PAPGGSNWGQG	11
	Msp1N7A	PHPGGSAWGQG	11
	Msp1Q10A	PHPGGSNWGAG	11
Msp1 His-methylated	Msp1His(1Me)capC	$PH[\tau Me]PGGSNWGQG\text{-}NH_2$	11
	Msp1His(3Me)capC	$PH[\pi Me]PGGSNWGQG\text{-}NH_2$	11
Modified repeat sequences	Msp1P3GcapNC	$Ac\text{-}PHGGGSNWGQG\text{-}NH_2$	11
	Msp_1strepcapNC	$Ac\text{-}PQGGGTNWGQG\text{-}NH_2$	11
	Msp_4threpcapNC	$Ac\text{-}PHGGSNWGQG\text{-}NH_2$	10
	Hu1capNC	$Ac\text{-}PHGGGWGQG\text{-}NH_2$	9

Copper ion binding to Msp peptides. In order to avoid copper precipitation as copper hydroxide at pH higher than 6.0, the sample was prepared according to the Takeuchi procedure (personal communication), with some modifications. The Msp peptide solution was brought to pH around 12.0 (by addition of NaOH), and then $CuCl_2$ solution was added. The pH was adjusted to the desired pH by addition of HCl. The solution was freeze dried and redissolved in ^2H_2O. In the final solution, the concentration of Msp peptide is 2.5 mM and $CuCl_2$ is 10 mM, unless otherwise stated.

Other metal ions (Zn, Ca, Mn, Mg) binding to Msp peptides. The metal salts ($ZnCl_2$, $CaCl_2$, $MnSO_4$, and $MgCl_2$) solution were added into the peptide solution and then, by adding HCl or NaOH solution, the mixture was brought to the desired pH. The solution was freeze dried and redissolved in ^2H_2O. In the final solution, the concentration of Msp peptide is 2.5 mM and metal ion is 10 mM, unless otherwise stated.

3.3.2. Infrared spectroscopic measurement and analysis

In these experiments, the FTIR spectra were recorded in ^2H_2O to avoid the overlapping band of the HOH bending motion of water in the amide I band region. The use of ^2H_2O also enabled use a longer path-length cell, which meant that the noise can be minimized and the signal to noise ratio increased, while using low concentration of peptides.

Infrared spectra were recorded on a Perkin Elmer Spectrum One Fourier Transform Infrared Spectrometer. Samples were placed in a micro cell fitted with CaF_2 windows and a 50 μm Teflon spacer. 200 scans were taken and signal averaged at a resolution of 4 cm^{-1}. Spectra were recorded at room temperature (25 °C) and the sample compartment was continuously purged with nitrogen gas to suppress water vapour absorbance in the spectral region of interest. Data were analysed using the Spectrum v.3.0 software from Perkin Elmer. Subtraction of the ^2H_2O spectrum from the sample spectrum was carried out digitally to give a straight baseline in the region 2000 - 1800 cm^{-1} (Haris et al., 1986). The resulting absorbance spectrum of the peptide was analyzed using the second derivative procedure with 19 data point Savitzky-Golay smoothing window (Haris et al., 1986). In the second derivative spectrum, the height of the bands is proportional to the square of the height of the original peak, but with

opposite sign (Susi and Byler, 1983; Susi and Byler, 1986). Thus, the original intensity or absorbance of particular peaks after the spectrum has undergone the second derivative procedure can be calculated. This method was used to quantify the intensity or absorbance of some peaks (1650 cm^{-1}, 1593 cm^{-1}, and 1563 cm^{-1}) which occur in the spectra of Msp1 and Msp1 titrated with copper ions. Difference spectra were also generated, after normalization of the amide I band region to absorbance = 1. Normalized spectra were also used to monitor the increase and decrease of some peaks upon addition of copper at different pHs.

3.4. Results and discussion

In order to investigate the effect of pH and copper binding on the structure of the peptides, FTIR spectra were recorded at different pH values, ranging from pH 6.0-9.0, in the presence and absence of copper ions. Msp peptides with various numbers of repeats were used to investigate the effect of peptide length on its conformation and copper-binding properties. Experiments with Msp peptides where the C-terminus was capped, or both C- and N-termini were capped, were also carried out to investigate the effect of free N- and C-termini on copper binding. Copper binding to some mutant peptides was studied to identify binding sites in Msp peptides. The first and fourth-repeat sequence of marsupial PrP, as well as human repeat sequence, were also investigated to identify the repeat segments and sequence most important for copper binding.

3.4.1. FTIR spectra of Msp1 group in the absence and the presence of copper ions

3.4.1.1. Conformational analysis – amide I band at ~1650 cm^{-1}

The amide I band of Msp1 at pH 6.0–9.0 appears at 1650-1644 cm^{-1} in the absorbance spectra (see Figure 3.1, left panel), and 1652-1648 cm^{-1} in the second derivative spectra (Figure 3.2, left panel). Both spectra show a gradual down shift of the position of the band with increasing pH. It is quite plausible that this downshift is due to pH-dependent conformational changes, as Msp1 is a small peptide whose structure could be easily modified by pH.

Msp1. According to the general assignment (see Table 3.1), the amide I band frequency of Msp1 peptide falls within the range of frequency for α-helix structure. However, the fact that the amide II band* completely disappears immediately upon dissolution of sample in ^2H_2O supports the spectral assignment for random-coil structure. This assignment is in good agreement with other spectroscopy measurements undertaken during these studies, such as CD, fluorescence spectroscopy, and FRET. Furthermore, it also fits conclusions from the literature that suggested the structure of PrP-repeat peptides is random coil or disordered (Hornshaw et al., 1995a; Miura et al., 1996; Miura et al., 1999; Viles et al., 1999; Bonomo et al., 2000; Whittal et al., 2000).

Msp1capC. Protection of the C-terminus in Msp1capC peptide does not change the structure. The amide I band at pH 6.0-9.0 is observed at 1651-1646 cm^{-1} in absorbance spectra (Figure 3.3, left panel), and at 1655-1649 cm^{-1} in second derivative spectra (Figure 3.4, left panel); as above, this indicates the presence of random-coil structure. The gradual downshift of the peak upon increasing pH from 6.0 to 9.0 is also observed in the Msp1capC spectra.

Msp1capNC. Msp1capNC peptides, where both C- and N-termini are protected, adopted a random coil structure throughout pH 6.0-9.0: this is suggested by the amide I band at 1650-1646 cm^{-1} in the absorbance spectra (Figure 3.5, left panel), and 1653-1646 cm^{-1} in the second derivative spectra (Figure 3.6, left panel). As also observed in the spectra of Msp1 and Msp1capC, there is a gradual red shift in the spectra of Msp1capNC upon increasing pH from 6.0 to 9.0.

---

*The amide II band arises from the NH bending of the peptide backbone coupled with CN stretching. In ^1H_2O this band is located at 1550 cm^{-1}. Upon dissolution of protein in ^2H_2O, the amide II band is observed at 1450 cm^{-1} as a result of ^1H-^2H exchanges where the N-^1H group of the amide backbone becomes N-^2H. Polypeptides with highly solvent-exposed amide groups or having weak hydrogen bonding, such as random-coil structure, undergo ^1H-^2H exchange more rapidly than polypeptide with defined conformation where the NH backbone is usually buried inside the globular folded protein core. Therefore, the amide II band of random-coil structure disappears almost instantly upon dissolution of polypeptide in ^2H_2O, while the more ordered protein requires a longer time (Haris and Chapman, 1995).

The Msp1 group is a small peptide, with only 11 residues (PHPGGSNWGQG). The large red shift (4-7 cm^{-1}), observed in these three peptides, indicates that the peptides are very flexible, and their structure can easily be modified by pH. However, pH variation does not result in a compact structure of the peptide as the amide I band position still indicates they are unstructured throughout pH 6.0-9.0. Nonetheless, the increase in intensity of the band at 1360 cm^{-1} upon increasing pH from 6.0 to 9.0 (Figure 3.2, 3.4, 3.6; left panel), supports the suggestion that the structure of Msp1 peptide is slightly modified by pH. This 1360 cm^{-1} band is the high-frequency component of the doublet 1360 and 1340 cm^{-1}, which is assigned as arising from Trp, and can be used as a marker of the environment around the Trp residue (Harada et al., 1986). The 1360 cm^{-1} band would increase in intensity when the Trp is in a more hydrophobic environment or surrounded by more aliphatic side chains. The noticeable increase of the 1360 cm^{-1} band intensity upon increasing pH from 6.0 to 9.0 suggests that the Trp residue has moved into a more hydrophobic environment, probably getting closer to the Pro side chain or to the N-terminal part of the peptide. This suggestion would be in good agreement with FRET experiments (see Chapter V), where the distance between Trp and the N-terminal residue is slightly closer at pH 9.0 than at lower pH.

Msp1+Cu. Addition of copper modified the IR spectra of Msp1, with the most striking change being the appearance of a new band at ~1560 cm^{-1}. This band assignment will be made in a later section. However, with regard to the amide I band at pH 6.0-8.0, addition of copper does not change the band position as shown in the absorbance spectra (Figure 3.1, right panel). At pH 9.0, there is a 3 cm^{-1} shift toward lower frequency upon addition of copper; now the amide I absorption is at 1641 cm^{-1}. The shift toward lower frequency is also reported in Raman spectra for copper interaction with human PrP octarepeat. This shift has been assigned as arising from an increase in helix content (Miura et al., 1996; Miura et al., 1999). However, in this FTIR spectrum the frequency of the amide I band in the range of 1651-1641 cm^{-1} more likely indicates the presence of random-coil structure.

Msp1capC+Cu. Copper ion also forms a complex with Msp1capC, as suggested by the appearance of the new band at ~1560 cm^{-1} (Figure 3.3 right panel). Concerning the amide I band, addition of copper to Msp1capC at pH 9.0 results in a 3 cm^{-1} shift from 1646 cm^{-1} to 1643 cm^{-1} in absorbance spectra, while at pH range 6.0-8.0, the frequency

of the amide I band is unchanged. The position of amide I band of copper complex of Msp1capC at 1651-1643 cm^{-1} throughout pH 6.0-9.0 suggests the random-coil structure.

Msp1capNC+Cu. Addition of copper ion to Msp1capNC peptide produces smaller spectral changes (Figures 3.5 and 3.6, right panels) compared with those for Msp1 and Msp1capC. Regarding the amide I band, at pH 9.0, the position shifts from 1646 cm^{-1} in free peptide to 1641 cm^{-1} in the copper complex. Second derivative spectra (Figure 3.6 right panel) show the amide I band of the copper complex of Msp1capNC at pH 6.0-8.0 is around 1653-1650 cm^{-1} and at pH 9.0 it is at 1646 cm^{-1}. Although the exact position of the amide I band in second derivative and absorbance spectra is slightly different, the same trend, which is a red shift upon increasing pH from 6.0 to 9.0, is observed. These data suggest that copper ion induces the formation of a more hydrogen-bonded structure in Msp1capNC at pH 9.0. However, the position of the amide I band suggests that the copper complex of Mp1capNC peptide adopts a random-coil structure. The smaller spectral changes in Msp1capNC upon addition of copper could indicate that the binding of copper to the peptide is not so effective, and suggest a role for the imino group of Pro at the N-terminus in copper binding.

As copper can coordinate 6 atoms to form a complex, a thorough analysis of the FTIR spectrum may reveal the other copper-binding sites in Msp peptides. The spectral regions where changes mostly occur are analyzed below.

3.4.1.2. Assignment of the band at 1611-1617 cm^{-1}

Msp1 and Msp1capC. Second derivative spectra of Msp1 (Figure 3.2 right panel) and Msp1capC (Figure 3.4 right panel) show the appearance of a new shoulder at 1611 cm^{-1} upon addition of copper ions at pH 6.0. This shoulder gets stronger and becomes a discrete individual band at 1617 cm^{-1} as the pH increases from 6.0 to 8.0. A discrete band is not observed at pH 9.0. However, there is a very weak shoulder around 1620 cm^{-1}, which overlaps with the major amide I band that also shifts but toward lower frequency. As a result, the overlapping band cannot be fully resolved by the second derivative procedure.

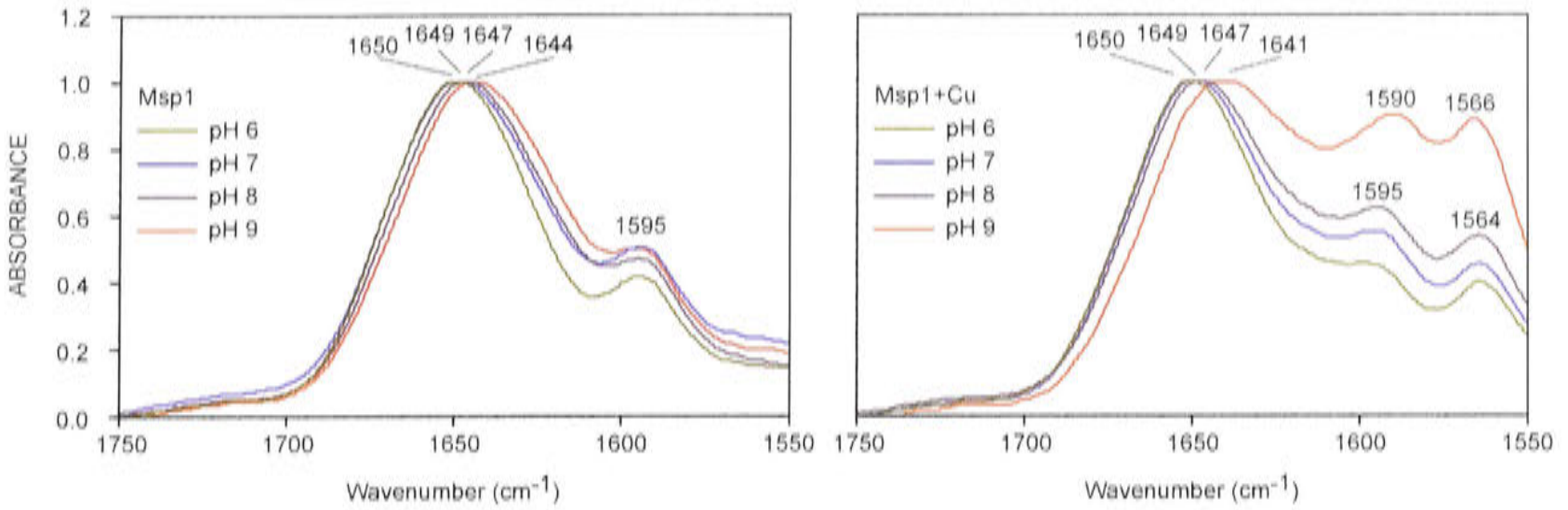

Figure 3.1: FTIR normalized absorbance spectra of Msp1 and copper complex of Msp1. The spectra of Msp1 in ^2H_2O at 2.5 mM peptide concentration, in the absence (left) and the presence (right) of 10 mM $CuCl_2$ at pH 6.0, 7.0, 8.0, and 9.0.

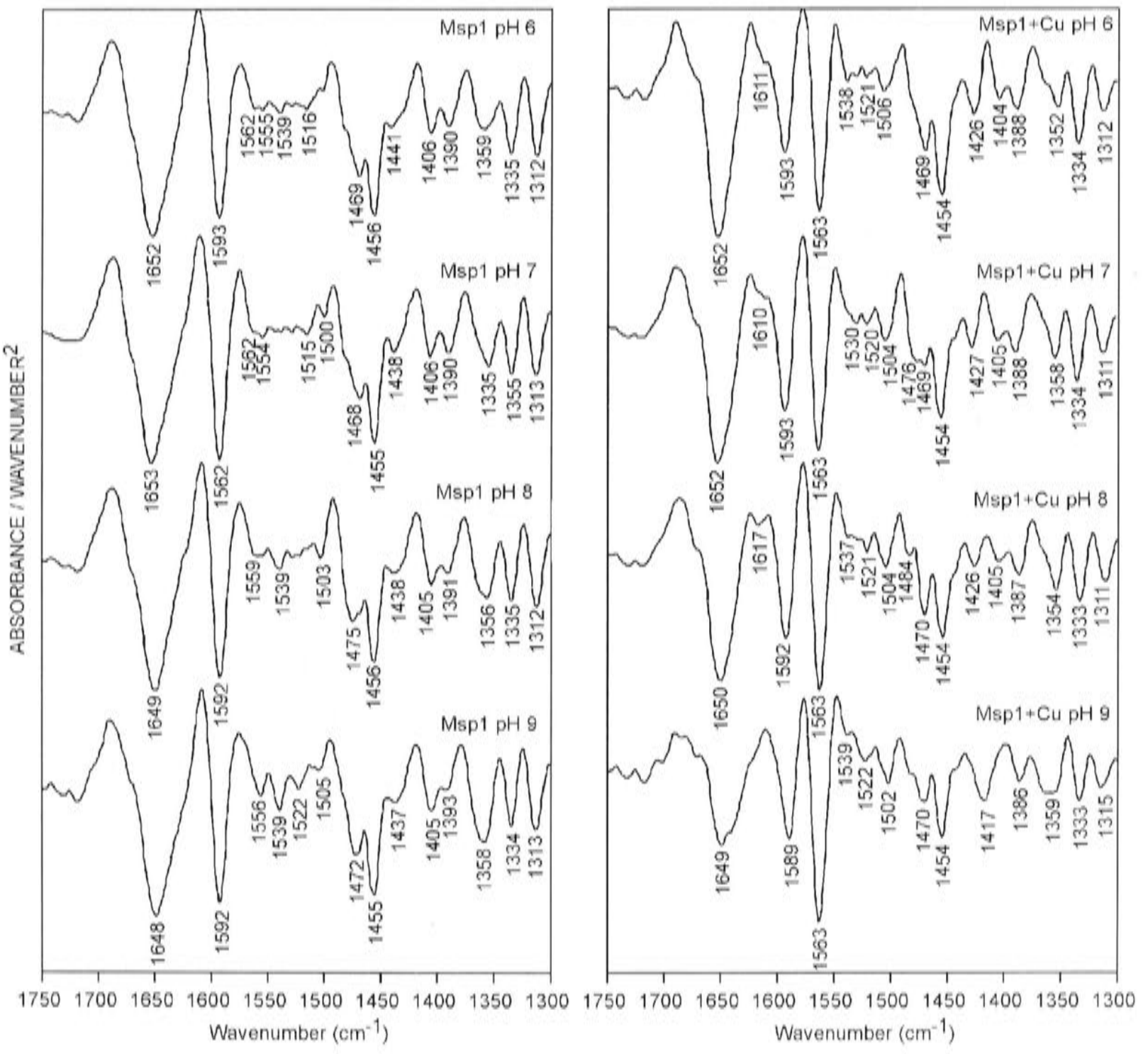

Figure 3.2: FTIR second derivative spectra of Msp1 and copper complex of Msp1. The spectra of Msp1 in ^2H_2O at 2.5 mM peptide concentration in the absence (left) and the presence (right) of 10 mM $CuCl_2$, at pH 6.0, 7.0, 8.0, and 9.0.

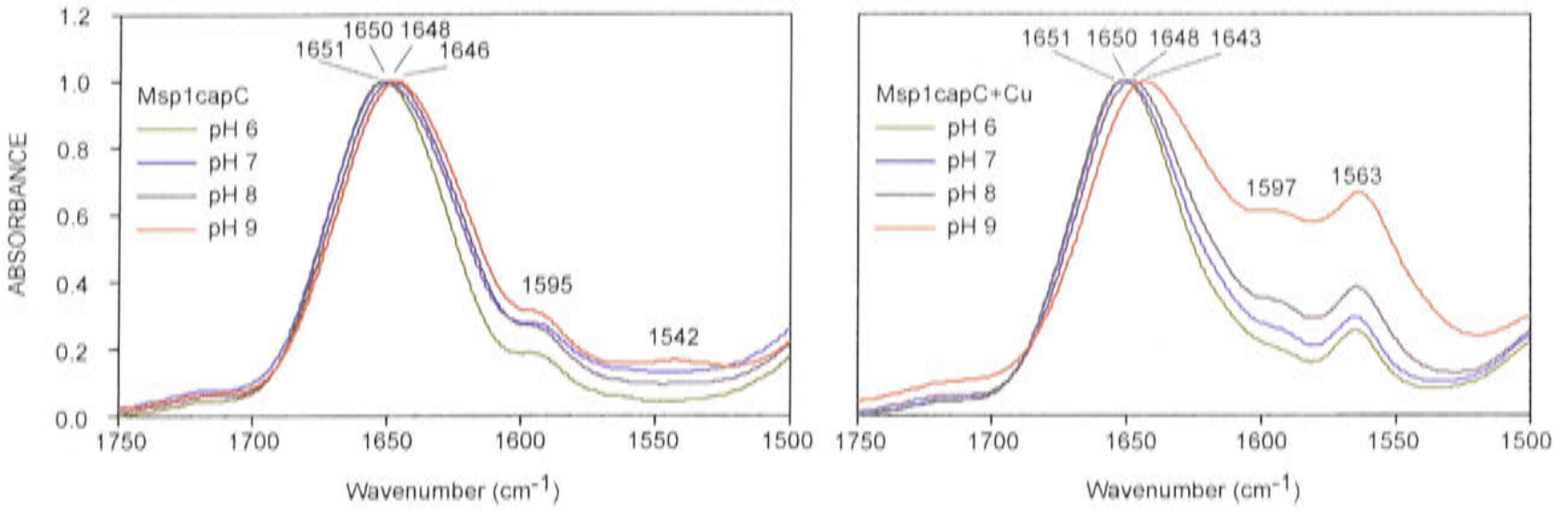

Figure 3.3: FTIR normalized absorbance spectra of Msp1capC and copper complex of Msp1capC. The spectra of Msp1capC in $^{2}H_2O$ at 2.5 mM peptide concentration, in the absence (left) and the presence (right) of 10 mM $CuCl_2$ at pH 6.0, 7.0, 8.0, and 9.0.

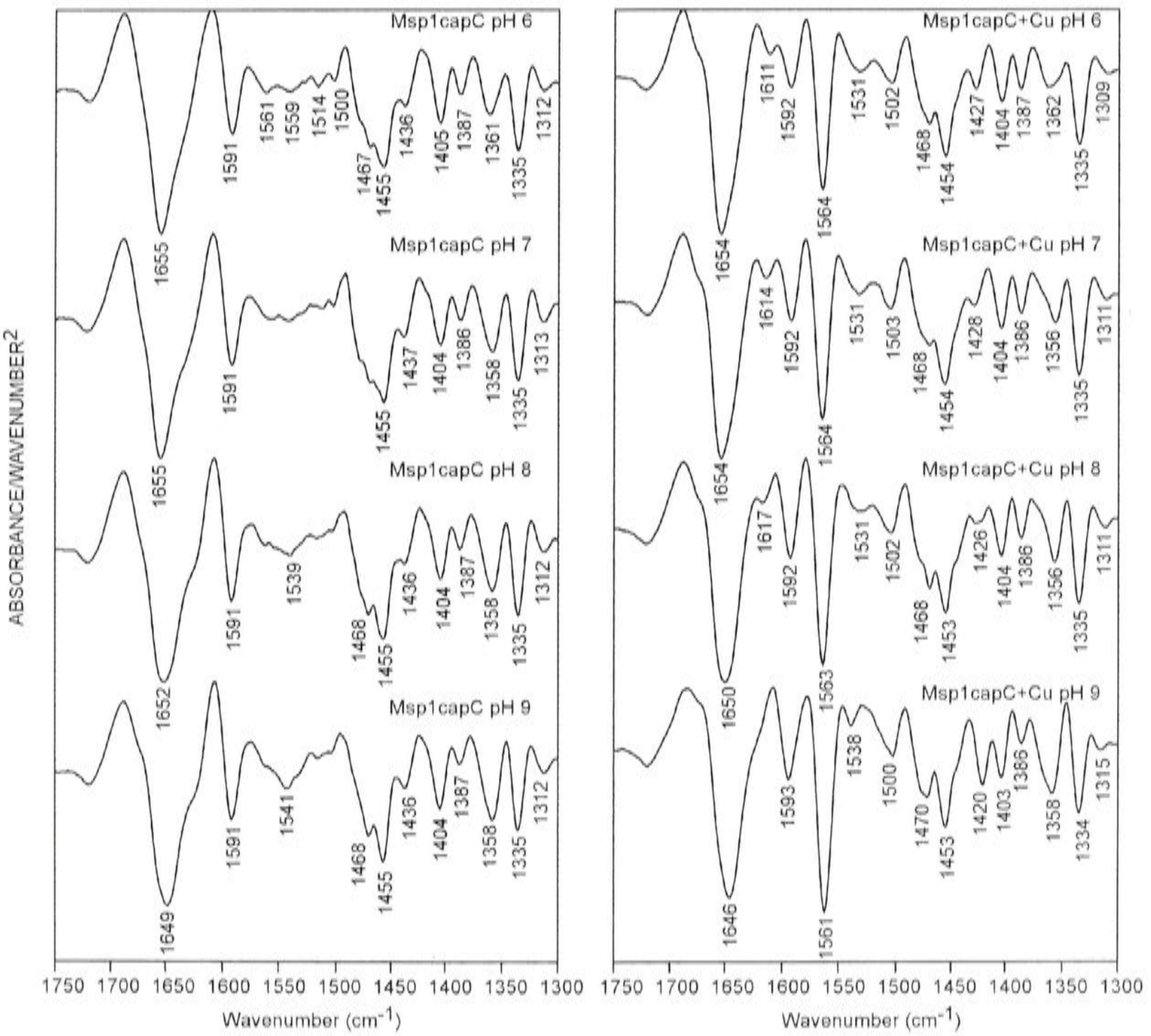

Figure 3.4: FTIR second derivative spectra of Msp1capC and copper complex of Msp1capC. The spectra of Msp1capC in $^{2}H_2O$ at 2.5 mM peptide concentration, in the absence (left) and the presence (right) of 10 mM $CuCl_2$ at pH 6.0, 7.0, 8.0 and 9.0.

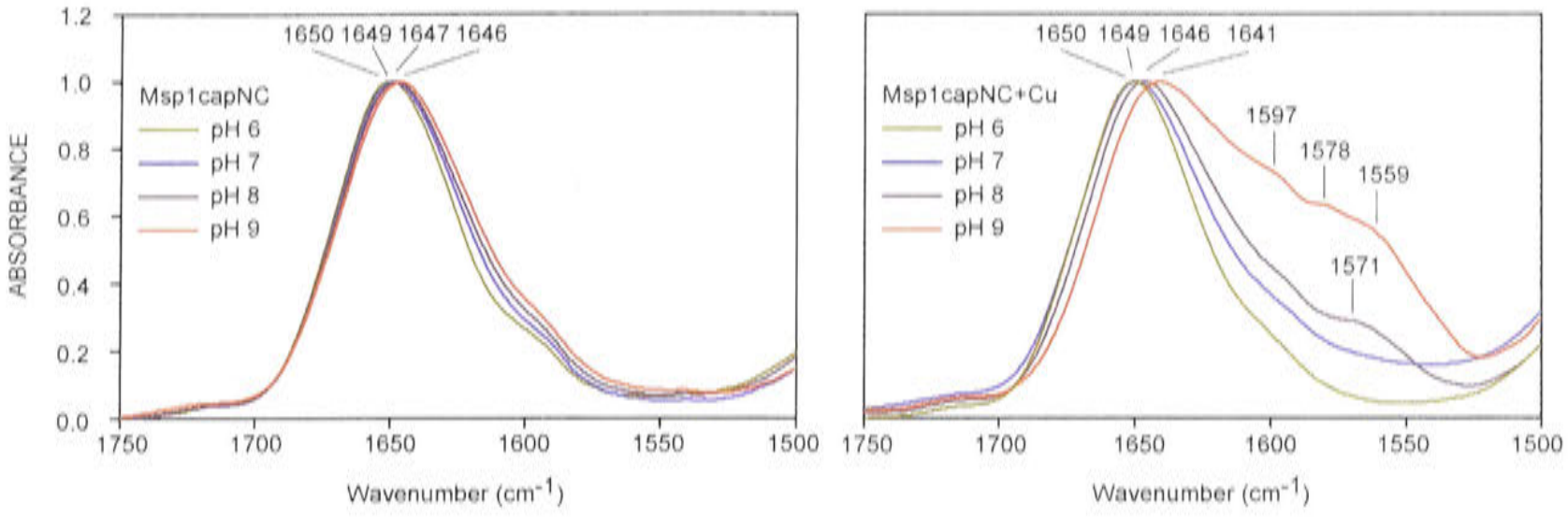

Figure 3.5: FTIR normalized absorbance spectra of Msp1capNC and copper complex of Msp1capNC. The spectra of Msp1capNC in $^{2}H_2O$ at 2.5 mM peptide concentration, in the absence (left) and the presence (right) of 10 mM $CuCl_2$ at pH 6.0, 7.0, 8.0, and 9.0.

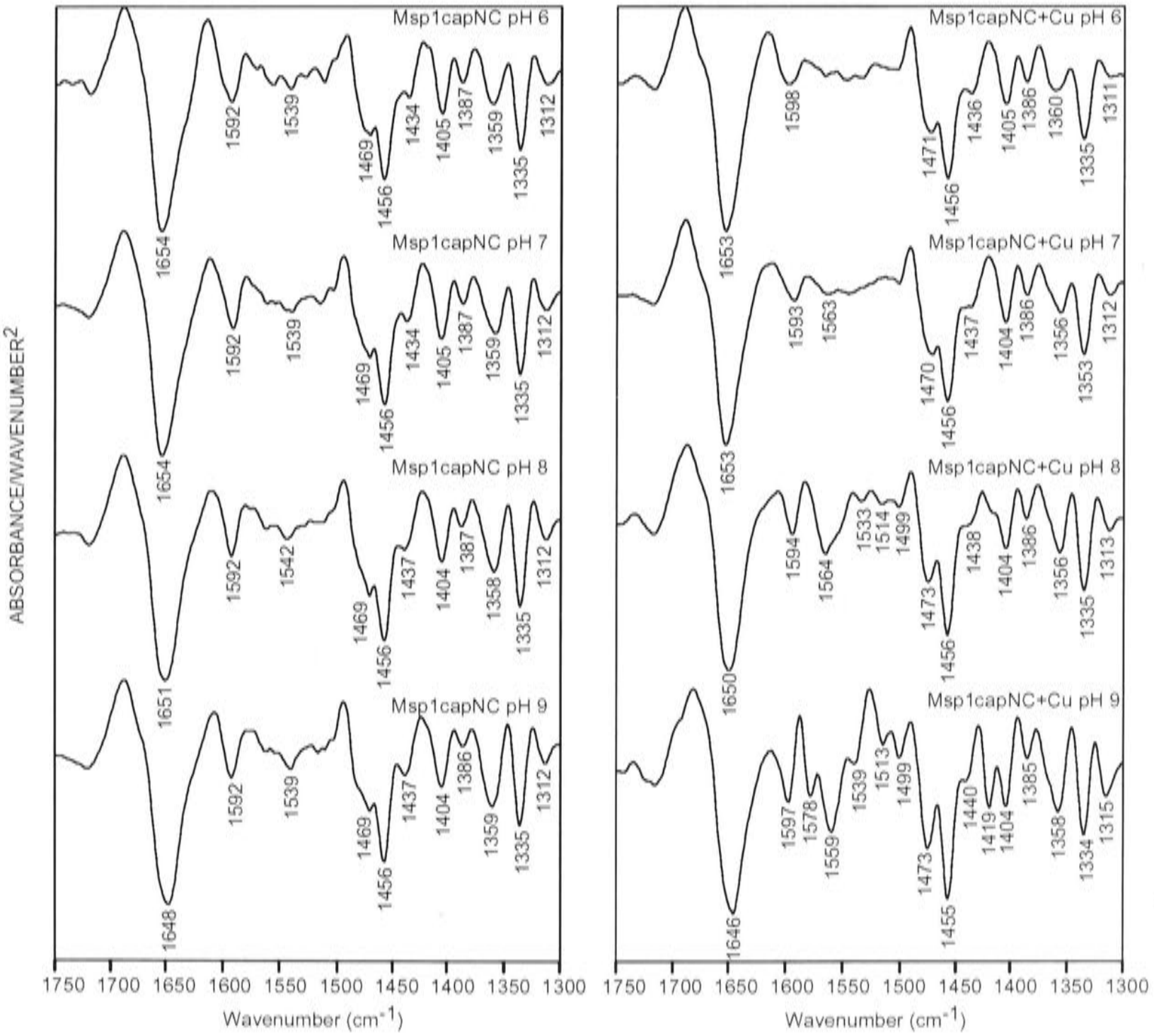

Figure 3.6: FTIR second derivative spectra of Msp1capNC and copper complex of Msp1capNC. The spectra of Msp1capNC in $^{2}H_2O$ at 2.5 mM peptide concentration, in the absence (left) and the presence (right) of 10 mM $CuCl_2$ at pH 6.0, 7.0, 8.0 and 9.0.

Msp1capNC. The small band around 1611-1617 cm^{-1} observed in copper complexes of Msp1 and Msp1capC appears less obvious in second derivative spectra of Msp1capNC (Figure 3.6 right panel). This is consistent with the smaller spectral changes in general for copper addition to Msp1capNC peptide, compared with those for Msp1 and Msp1capC. However, curvature at the base of the amide I band around 1611-1617 cm^{-1} indicates the presence of a very weak shoulder: this is observed most clearly at pH 7.0 and 8.0.

The assignment of the weak band at 1611-1617 cm^{-1} is not straightforward: there are several possible origins as discussed below.

Possible assignment – antiparallel β-sheet. The appearance of the band at 1611-1617 cm^{-1} could reflect peptide aggregation or self-association related to the formation of an intermolecular antiparallel β-sheet structure (Ismail et al., 1992; Panick et al., 1999) (see Table 3.1). The weak component band that usually appears at 1684 cm^{-1} cannot be detected in the spectrum probably because the proportion of this type of structure is much smaller than the random-coil structure that is predominantly present. Msp1 group is a relatively small peptide (11 residues), and it is very common for a small peptide to aggregate to form an intermolecular antiparallel β-sheet structure.

Possible assignment – Trp ring. According to the literature, a band at 1618 cm^{-1} could arise from the vibration of the C-C bond of benzene and the C=C bond of pyrole in the Trp ring (Barth, 2000). In the absence of copper, this Trp band is observed with relatively high intensity, in the Raman spectra of human PrP repeats (Miura et al., 1999). However, addition of copper does not change this Trp band (Miura et al., 1999) suggesting that the origin of this band is less likely due to the Trp residue.

Possible assignment – deprotonated amide backbone. The band at 1611-1617 cm^{-1} could also arise from the out-of-phase (antisymmetrically coupled) component of the $C{=}O/C{-}N^{-}$ stretching vibration of the deprotonated amide backbone. This band appears at 1610 cm^{-1} in the copper complex of glycylglycine at pH > 5.0 (Tasumi, 1979). In that complex, the in-phase (symmetrically coupled) component appeared at 1428 cm^{-1}. In the copper complex of Msp1 and Msp1capC peptide at pH 6.0-8.0, the symmetric

component of C=O/C-N$^-$ vibration is observed at 1426-1427 cm^{-1}. As mentioned earlier, the band at 1611-1617 cm^{-1} shifts to 1620 cm^{-1} at pH 9.0. The shifted phenomenon is also observed for the 1426-1427 cm^{-1} band, which is at pH 9.0 located at 1417-1420 cm^{-1}. The band at 1419 cm^{-1} is also observed in the copper complex of Msp1capNC at pH 9.0. The fact that there are two bands, one at 1611-1617 cm^{-1} and the other at 1426-1427 cm^{-1}, that behave similarly (shift at pH 9.0) strongly suggests the presence of a deprotonated peptide group as a result of copper interaction with the peptide. This suggestion is in good agreement with the literature, where copper is reported to coordinate via the NH of the amide backbone (Miura et al., 1996; Miura et al., 1999; Aronoff-Spencer et al., 2000; Burns et al., 2002; Luczkowski et al., 2002).

Thus, overall, the 1611-1617 cm^{-1} band could have more than one origin. Firstly, it could reflect an intermolecular antiparallel β-sheet structure, which is associated with peptide aggregation. Secondly, it could originate from the C=O/C-N$^-$ stretching vibration of deprotonated amide backbone.

3.4.1.3. Assignment of the ~1590 cm^{-1} and ~1560 cm^{-1} band

The band at 1590 cm^{-1} is visible in the spectra of copper-free as well as copper-complexed forms of Msp1 peptide (see Figures 3.1 and 3.2). Some possible origins of this band are outlined below.

Possible assignment – from terminal COO$^-$. The band at 1590 cm^{-1} could arise from the antisymmetric vibration of COO$^-$. This assignment is based on the second derivative spectra, which show that the intensity of the 1590 cm^{-1} band in Msp1 is higher than that in Msp1capC peptide (see Figure 3.7), and also the difference spectra, which show a strong positive peak at 1590 cm^{-1} emerging as a result of Msp1-Msp1capC subtraction (Figure 3.8).

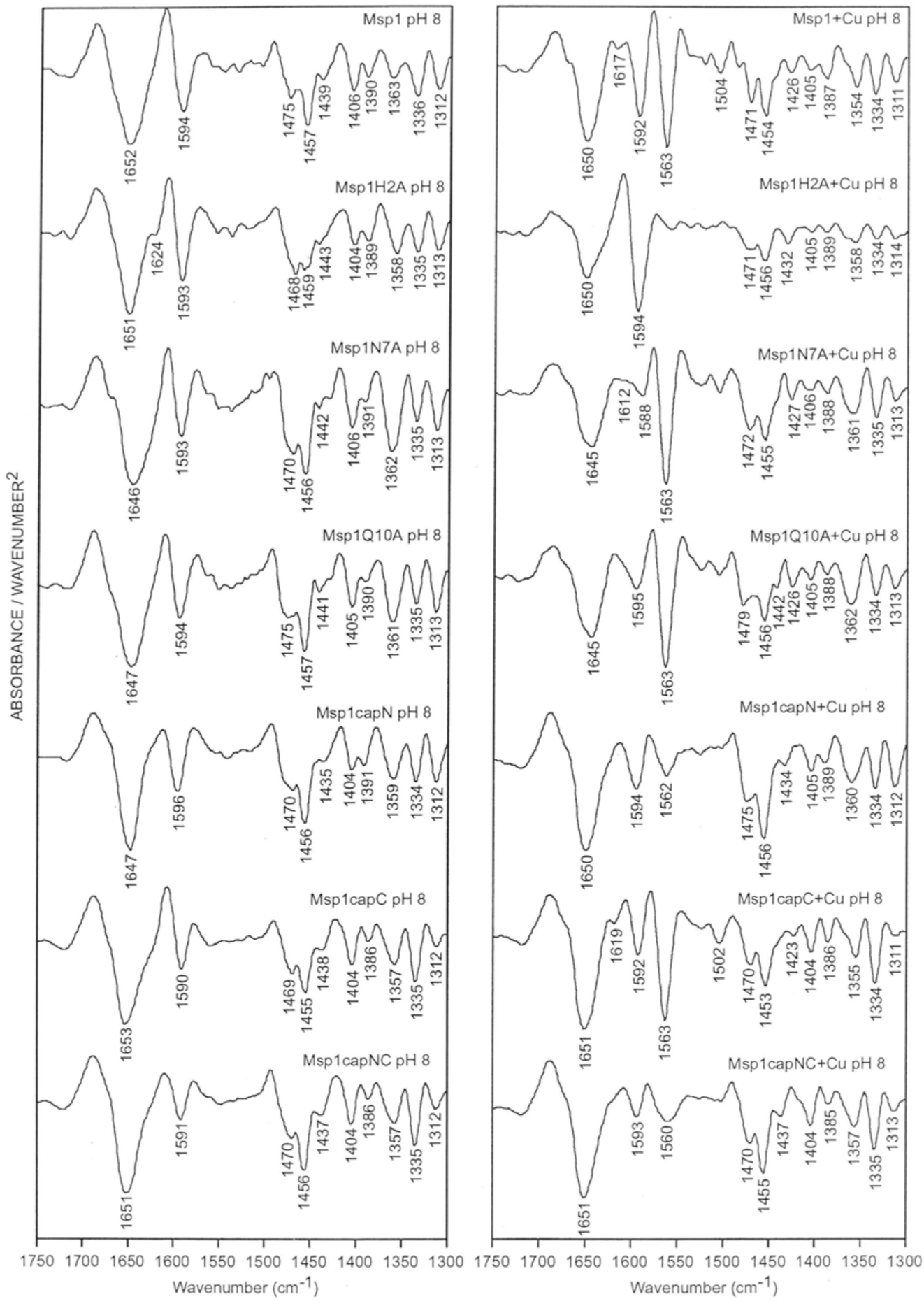

Figure 3.7: Copper binding to some mutant and modified Msp1 peptides. FTIR second derivative spectra of various Msp1 peptides (from top to bottom: Msp1, Msp1H2A, Msp1N7A, Msp1Q10A, Msp1capN, Msp1capC, and Msp1capNC) in ^2H_2O at 2.5 mM peptide concentration, in the absence (left) and the presence (right) of 10 mM $CuCl_2$, at pH 8.0.

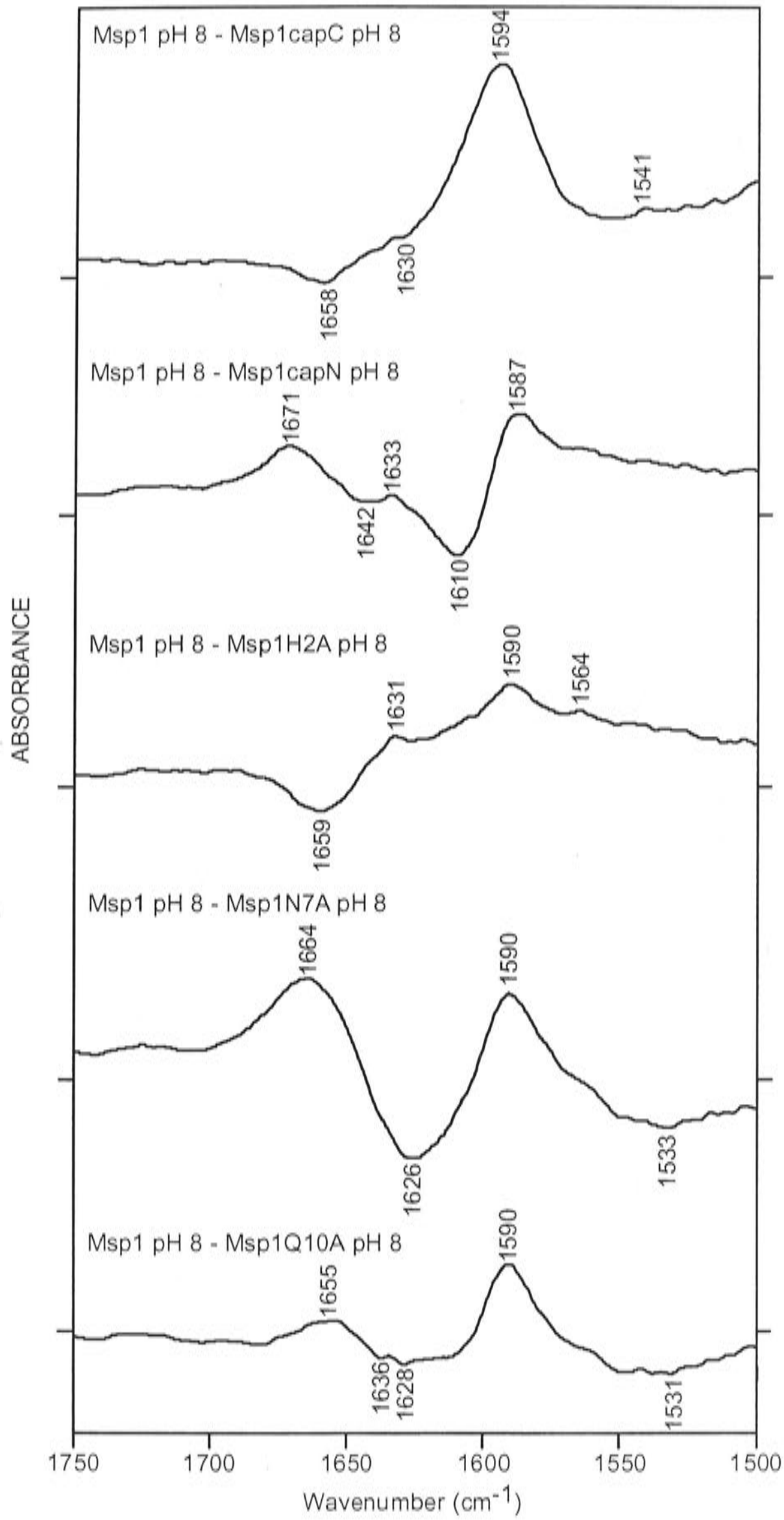

Figure 3.8: FTIR absorption difference spectra for the peptide end groups and side chain residues. The spectra were normalized to absorbance = 1 before the subtraction procedure was carried out. A positive peak reflects the absorption of the first spectrum while a negative peak belongs to the second spectrum. The difference spectra show the positive peak at 1590 cm^{-1} is strongest in the difference spectra of Msp1-Msp1capC, suggesting it arises mainly from the COO^- vibration of the C-terminus of the peptide.

The assignment of the 1590 cm^{-1} band for the COO^- vibration is supported by data from the literature. It has been reported that the ionized carboxyl group in ^2H_2O has strong absorption with the maximum at 1590 cm^{-1}, and that this band results from the antisymmetric stretching of the COO^- group (Chirgadze et al., 1975). The antisymmetric stretching of the COO^- vibration of polylysine peptide was also observed at 1590 cm^{-1}; the intensity of this band decreases as the chain length of polylysine increases (Jackson et al., 1989).

The chain length phenomenon is also observed in Msp peptides. The FTIR absorbance and second derivative spectra of the Msp2 group (21 residues) (Figures 3.17-3.22), Msp3 group (31 residues) (Figures 3.23-3.28), and Msp4 group (41 residues) (Figures 3.29-3.34) peptides show that the intensity of the 1590 cm^{-1} band is not as prominent as in the Msp1 group (11 residues) (Figures 3.1-3.6). This supports the assignment of the 1590 cm^{-1} band in Msp1 peptide as originating partly from the COO^- vibration. However, it seems obvious that the band has at least 2 origins as it is still observed in the spectra of Msp1capC (other origins of this band will be discussed in later sections).

Addition of copper resulted in increase of the intensity of the band at 1590 cm^{-1} (see Figure 3.1), which, partly, indicates interaction between copper ions and the COO^- group. In this case, copper ion binds to only one of the oxygen atoms; therefore, the antisymmetric stretching vibration of COO^- group could be expected to increase in intensity. The interaction of copper with the COO^- group at the C-terminus of the peptide was reported for the copper complex of glycylglycine. The FTIR absorbance of this complex revealed bands at 1596 cm^{-1} (antisymmetric stretching) and 1385 cm^{-1} (symmetric stretching) (Tasumi, 1979). In the spectra of the copper complex of Msp1 peptide, the symmetric component of the COO^- stretching vibration is probably located at 1390 cm^{-1}. Thus, the data suggest the possibility of the COO^- group at the C-terminus of Msp1 being one of copper-binding sites. However, binding to the COO^- group is not essential because in its absence binding still occurs as shown in fluorescence quenching experiments (Chapter III) and FTIR spectra of Msp1capC (Figures 3.3-3.4 and 3.7).

As already mentioned, amidation of the COO^- group (in Msp1capC) does not abolish the 1590 cm^{-1} band but only decreases its intensity. This suggests that other vibrations

also contribute to the absorbance in this region. In order to identify other groups that absorb at 1590 cm^{-1} and interact with copper ion, some mutant peptides were investigated and analyzed using FTIR difference spectra; these are discussed in the section below.

Possible assignment – imino group of Pro. The difference spectrum of Msp1 and Msp1capN (Figure 3.8) shows a positive peak at 1587 cm^{-1}, suggesting the imino nitrogen of Pro at the N-terminus absorbs in this region. As has been shown in the previous section, addition of copper to Msp1capN does not produce as great spectral changes as for Msp1 and Msp1capC. The smaller changes suggest the free imino group of Pro has a significant role in copper binding. The possibility that the imino nitrogen participates in copper binding has also been investigated using fluorescence titration spectrophotometry (see Chapter IV). It was found that upon addition of copper to Msp1capN peptide no quenching occurred, while addition of copper to Msp1 and Msp1capC peptides resulted in large quenching. Together these data suggest the imino group of Pro is a copper-binding site in Msp1 peptide. This suggestion fits data from the literature which suggest the amino group of the N-terminal residue facilitates the binding of copper ion to the human PrP octarepeat (Whittal et al., 2000; Luczkowski et al., 2002). It was reported that protection of the N-terminus by acetylation caused some reduction in the stoichiometry of binding (Whittal et al., 2000). The unprotected N-terminal Pro-His segment is a quite specific sequence for interaction with copper ions (Luczkowski et al., 2002). The interaction of copper with the imino terminal Pro, however, would be physiologically irrelevant as this group is not present in the real protein.

Possible assignment – imidazole ring of His. It is clear that the band at 1590 cm^{-1} has more than one origin. Apart from the COO^- and imino groups, another possibility is the imidazole ring of His. This suggestion follows from the difference spectrum of Msp1-Msp1H2A, which shows a positive band at 1590 cm^{-1} (Figure 3.8). It is also supported by the literature, which shows that the C4=C5 stretching vibration of the imidazole ring of His can contribute to absorption in this region, as observed in the FTIR spectra of carnosine in a KBR pellet (Torreggiani et al., 2000a; Torreggiani et al., 2000b). Besides the band at 1590 cm^{-1}, the difference spectrum of Msp1-Msp1H2A also shows a small positive peak at 1564 cm^{-1}, which might originate from the His residue.

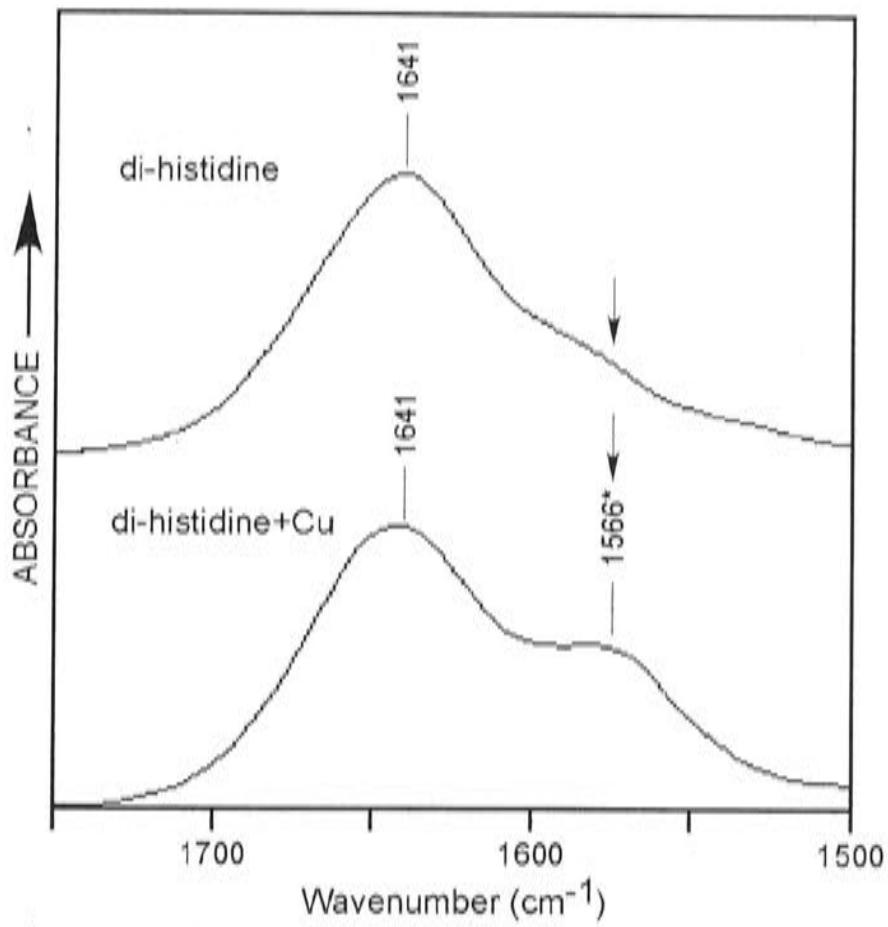

Figure 3.9: Effect of copper addition on the FTIR spectrum of the di-histidine peptide. Absorbance spectra of di-histidine at 40 mM peptide concentration recorded at pH 8.0, in the absence (top) and the presence (bottom) of 10 mM $CuCl_2$.

The band at 1564 cm^{-1} deserves further comment as this band becomes quite strong in the spectra of copper complexes of Msp1 group peptides (Figures 3.1-3.6, right panels), which most probably results from copper interaction with the His residue. This band is also observed in the spectrum of the copper complex of di-His peptide (Figure 3.9), which strongly supports the assignment for copper-bound His. Other evidence that this band is due to the His residue is its absence from the spectra of the copper complex of Msp1H2A (Figure 3.7). This assignment is in good agreement with reports in the literature which suggest that the His residue is a copper-binding site in human PrP octarepeat (Miura et al., 1996; Miura et al., 1999; Aronoff-Spencer et al., 2000).

3.4.1.4. Tautomeric forms of His ring

As has been pointed out earlier, the band at 1590 cm^{-1} could also arise from the His residue. The presence of two bands associated with His clearly indicates the presence of two tautomeric forms of His. Literature reports indicate that between pH 6.0-11.0 in ^2H_2O, free His would have IR absorbance at 1569 and 1575 cm^{-1} (Barth, 2000; Hasegawa et al., 2000), which is the C4=C5 stretching vibration of the imidazole ring of His. These two bands appear as a doublet, representing the two tautomeric forms: these differ depending on which N atom the proton is bound to (see Figure 3.10). In tautomer I, N_τ is protonated, while in tautomer II the proton is attached to N_π. The 1569 cm^{-1} and

1575 cm^{-1} bands represent tautomer I and II, respectively. It is possible that the two bands, 1564 cm^{-1} and 1590 cm^{-1}, observed in the difference spectrum of Msp1-Msp1H2A (see Figure 3.8) represent these two tautomeric forms of His.

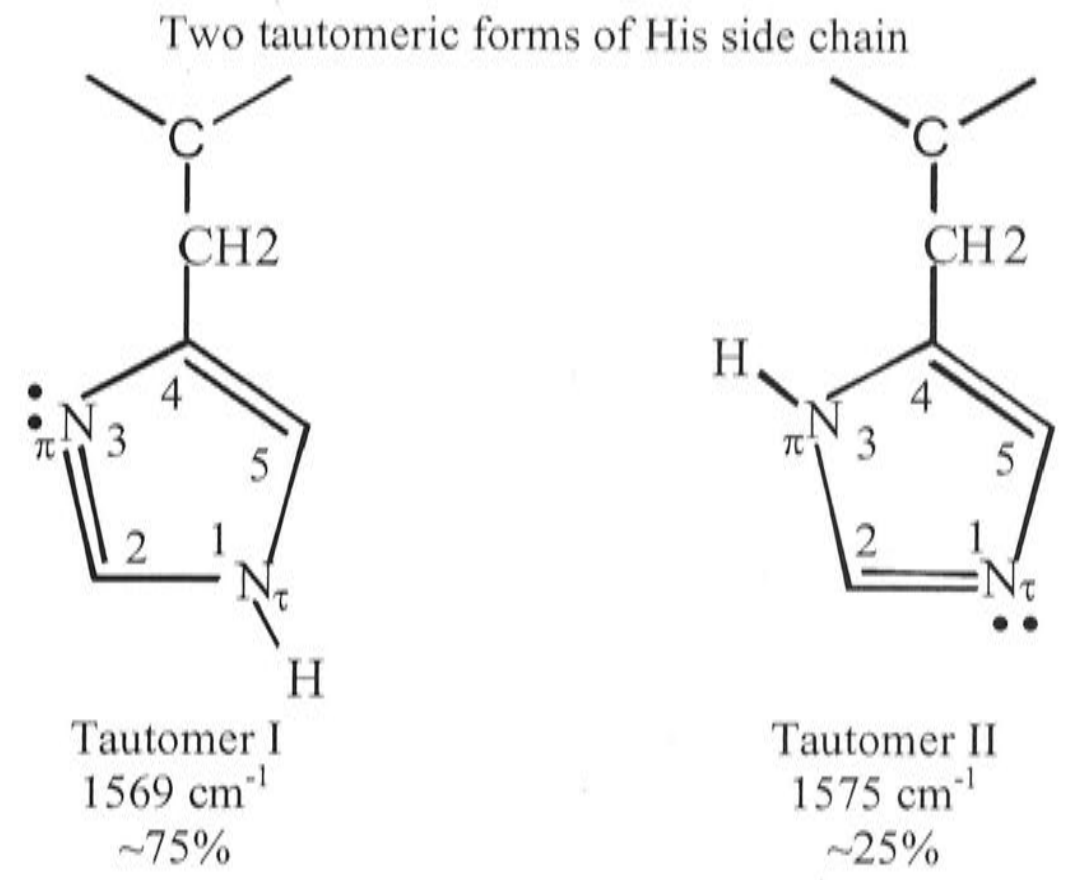

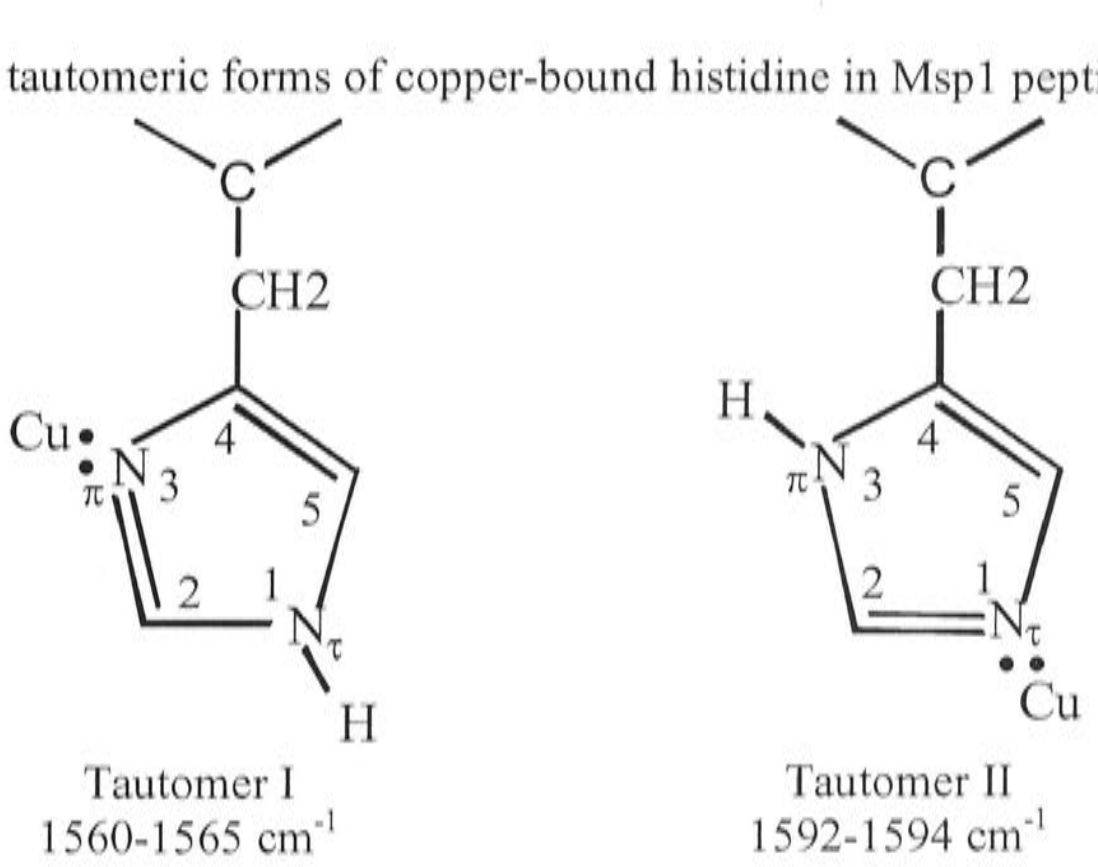

Figure 3.10: Structures of the two tautomeric forms of copper-free His (upper) and copper-bound Msp1 peptide (lower). In the copper-free form, the reported IR frequency for the C4=C5 bond vibration of His in ^2H_2O is 1569 cm^{-1} (tautomer I) and 1575 cm^{-1} (tautomer II) (Barth, 2000). According to the difference spectrum (Msp1-Msp1H2A), the copper-free tautomer I in Msp1 peptide could be located at 1564 cm^{-1} and tautomer II at 1590 cm^{-1}. In the copper-bound form of Msp1 peptides, the IR frequency for the C4=C5 vibration of tautomer I appears in the range between 1560-1565 cm^{-1} and tautomer II in the range 1592-1594 cm^{-1}. However, the frequency of these two tautomeric forms may vary. It appears that the frequency of tautomer I has been downshifted and tautomer II upshifted as a result of copper interaction.

It has also been reported in the literature that in ^2H_2O the two tautomeric forms are difficult to detect by Raman spectra (Miura et al., 1999). The proton attached to the N_τ or N_π atoms of His undergoes ^1H-^2H exchanges readily in ^2H_2O solution. As a result, a singlet Raman band around 1570 cm^{-1} is observed for the C4=C5 stretching vibration that is now insensitive to tautomerism. Upon metal chelation the frequency up shift of the C4=C5 vibration still occurs in ^2H_2O solution. Thus, in the copper complex, the C4=C5 vibration was observed at 1584 cm^{-1}. In H_2O, the copper-free His is observed as a doublet at 1587 and 1574 cm^{-1}, while in the copper complex it is observed at 1603 and 1590 cm^{-1} (Miura et al., 1999).

Methylated His peptides. In order to investigate further the two tautomeric forms of His, Msp1 peptides with either N_τ or N_π methylated were synthesized. These peptides, Msp1His(1Me)capC (N_τ methylated) and Msp1His(3Me)capC (N_π methylated), were C-terminally capped to eliminate the strong absorption of COO^- at ~1590 cm^{-1}, which would complicate the spectral assignment. The N-terminus of the peptides was left uncapped to facilitate copper binding to the peptide.

Copper complex of τMe-His peptide – ~1560 cm^{-1} (Tautomer I). Copper addition to Msp1His(1Me)capC resulted in an increase in intensity of the band at 1564 cm^{-1} (see Figure 3.11). This result strongly supports the suggestion that tautomer I with copper bound to the N_π atom of the imidazole ring will absorb at ~1560 cm^{-1}.

In the copper-free form of all Msp1 peptides, the intensity of the 1560 cm^{-1} band is very weak and not clearly visible in the spectrum (Figures 3.1-3.6, left panels). However, copper binding to N_π has altered the environment around C4=C5 bond leading to an increase in band intensity. In FTIR only vibrations that produce changes in dipole moment can be detected. During the vibration, the absorption coefficient increases with the change of dipole moment. The change in dipole moment is often correlated with the polarity of the vibrating bonds. Thus, a change in environment that results in an altered bond polarity will lead to a change in band intensities (Barth, 2000). It is proposed that copper binding to N_π has increased the polarity of the C4=C5 bond, so that the bond vibration produces larger changes in dipole moment, and consequently the IR intensity of the absorption is increased.

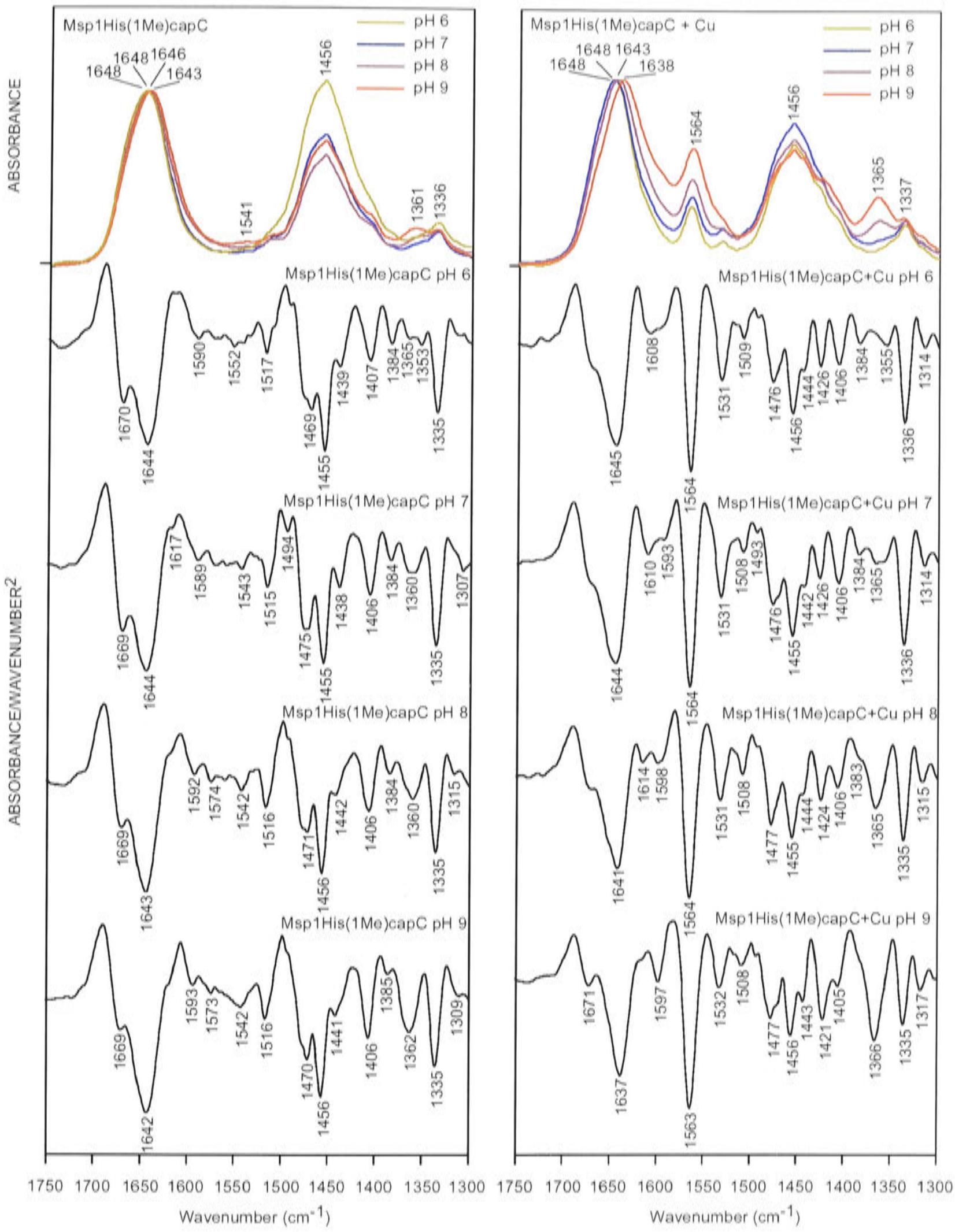

Figure 3.11: Copper binding to Msp1His(1Me)capC peptide. FTIR Absorbance (upper panel) and second derivative (lower panel) spectra of Msp1His(1Me)capC in ^2H_2O at 2.5 mM peptide concentration, in the absence (left) and the presence (right) of 10 mM $CuCl_2$, at pH 6.0, 7.0, 8.0 and 9.0. The spectra clearly show the band at 1563 cm^{-1} appears upon addition of copper, which indicates the formation of a Cu-N_π bond (tautomer I).

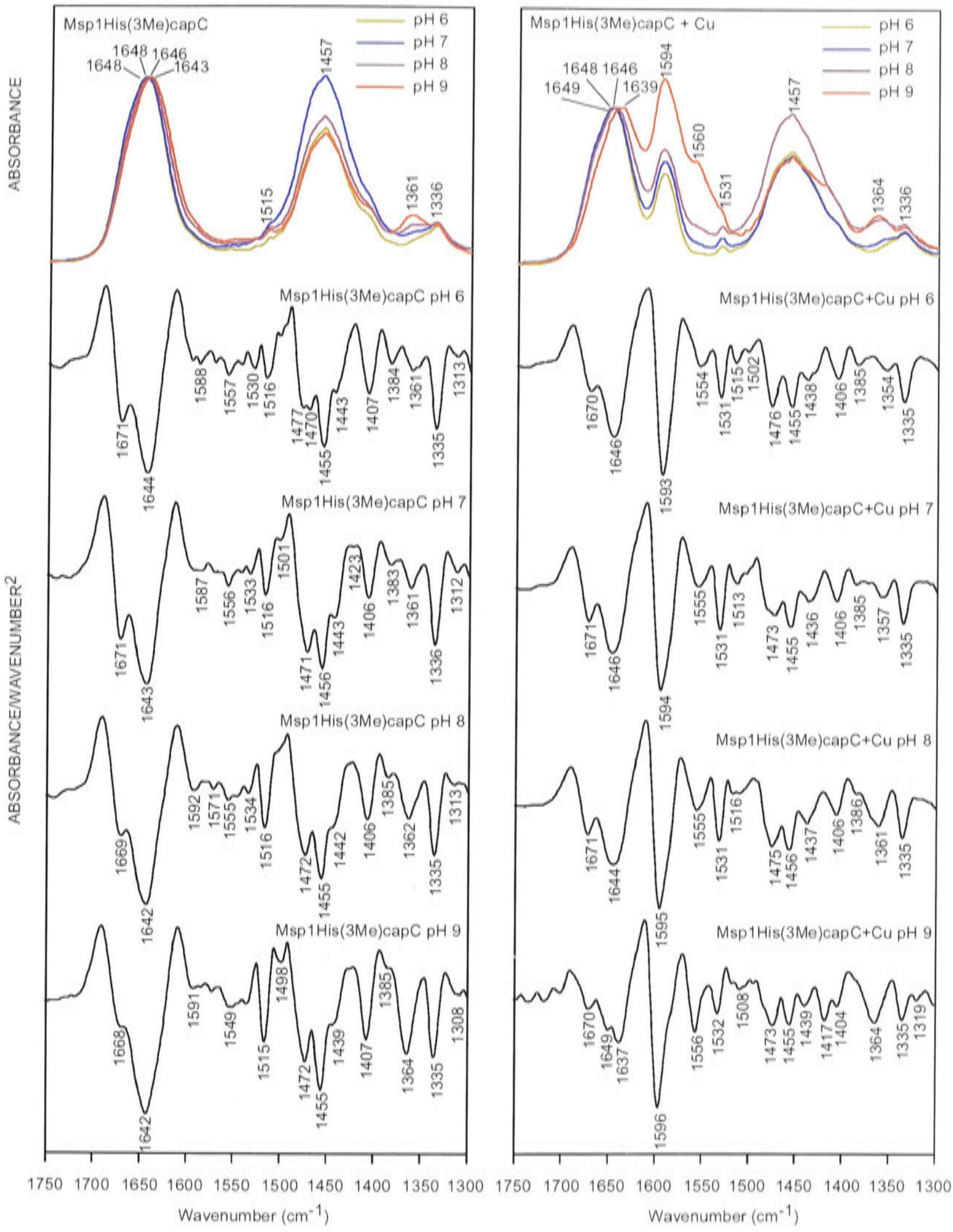

Figure 3.12: Copper binding to Msp1His(3Me)capC peptide. FTIR Absorbance (upper panel) and second derivative (lower panel) spectra of Msp1His(3Me)capC in $^{2}H_2O$ at 2.5 mM peptide concentration, in the absence (left) and the presence (right) of 10 mM $CuCl_2$, at pH 6.0, 7.0, 8.0 and 9.0. The prominent band at 1595 cm^{-1} appears upon addition of copper, which indicates the formation of a Cu-N_τ bond (tautomer II).

Copper complex of πMe-His peptide – ~1590 cm^{-1} (Tautomer II). The FTIR spectrum of the copper complex of Msp1His(3Me)capC shows a very strong band at ~1590 cm^{-1} (see Figure 3.12). The appearance of this band suggests that copper binding to the N_τ atom of imidazole will produce an IR band at ~1590 cm^{-1}. However, as even in the absence of a His residue, this band is still observed in the copper complex of Msp1H2A (see Figure 3.7), one could argue that the band at 1590 cm^{-1}, which appears upon copper addition to Msp1His(3Me)capC, is in fact due to the imino group of Pro that absorbs at this region. Furthermore, fluorescence spectroscopy experiments (Chapter IV) showed copper binding to Msp1His(3Me)capC occurs only at pH ≥ 8.0 with affinity much lower than the binding to Msp1His(1Me)capC and close to that for Msp1H2A, where His is replaced by Ala.

However, the appearance of a band at 1602-1603 cm^{-1} in the copper complexes of some C- and N-terminally capped peptides: Msp1P3GcapNC (PHGGGSNWGQG) (Figure 3.13), Msp_4threpcapNC (PHGGSNWGQG) (Figure 3.15) and Hu1capNC (PHGGGWGQG) (Figure 3.16) supports the assignment of the 1590 cm^{-1} band as originating from tautomer II of His. Although the frequency of this band is slightly higher than that observed in Msp1 peptide (1590 cm^{-1}), the appearance of this band in these capNC peptides suggests that it is not only copper-bound imino or COO^- groups but also His. The absence of changes in intensity of this band in the copper complex of Msp_1strepcapNC (Ac-PQGGGTNWGQ-NH_2) also suggests that the origin of intensity changes of this band is copper interaction with the His residue. Together, these data suggest that the band in the region of 1590-1600 cm^{-1} is a copper-bound form of tautomer II of His.

3.4.1.5. Assignment of the band at 1500-1506 cm^{-1}

Msp1+Cu – His tautomer I. Another band appearing in the second derivative spectra of copper complexes of Msp1 group peptides that can be attributed to binding sites of copper is at 1500-1506 cm^{-1} (Figures 3.2 and 3.4). It is suggested this band arises from N_τ-protonated/N_π-copper-ligated histidine. The same band is observed in the Raman spectra of copper complexes of human PrP octarepeats (Miura et al., 1999): these authors suggested that the band originates from copper ion binding to the N_π atom of the imidazole ring of His. However, the vibration that produces the 1503 cm^{-1} band is not yet clarified (Miura et al., 1998).

Msp1His(1Me)capC +Cu. This band is also observed at 1508-1509 cm^{-1} in second derivative spectra of copper complexes of Msp1His(1Me)capC (Figure 3.11), where copper is forced to bind to the N_π atom. This band is not observed in copper complexes of Msp1His(3Me)capC (Figure 3.12) where the N_π atom is methylated and copper binds to the N_τ atom. It is also evident from the spectra of Msp1P3GcapNC (Figure 3.13) and Hu1capNC (Figure 3.16) that increase in intensity of the band at 1560 cm^{-1} (1570-1577 cm^{-1} for Hu1capNC) is concomitantly followed by increase of the band intensity at 1503-1499 cm^{-1}. These data may be compared with the spectra of Msp_4threpcapNC (Figure 3.15) where the bands at 1560 cm^{-1} and 1495 cm^{-1} are both weak. Overall these data strongly support the assignment of the band at 1502 cm^{-1} as originating from copper ion binding to the N_π atom of the imidazole ring of His.

3.4.1.6. Copper-binding sites in Msp1 group peptides (PHPGGSNWGQG)

The above FTIR assignments identified three nitrogen atoms as copper-binding sites in Msp1 peptides: the nitrogen atom from the imino group of Pro at the N-terminus, the N_π atom of the imidazole ring of His, and the nitrogen atom of the deprotonated amide backbone (the data do not indicate how many deprotonated amides). In Msp1 peptide (PHPGGSNWGQG), the role of the free terminal imino group of Pro in binding copper ion is very significant, especially at pH 6.0 and 7.0; the absence of it results in effectively no binding. However, binding to this group has no physiological relevance, as in the real protein this group does not exist.

The literature suggests that in the absence of the imino group, copper can bind to two nitrogen atoms from the deprotonated amide backbone of the third and fourth Gly residue, in addition to the His side chain (Luczkowski et al., 2002) in the sequence of ^{1}PHGGG^{5} found naturally in human PrP repeat (see Figure 1.10 in Chapter I). This report may explain why there is no binding between copper and Msp1capNC peptide (Ac-PHPGGSNWGQG-NH_2), as the third residue in this peptide is Pro, which lacks on amide that can be deprotonated. The fourth residue in Msp1 peptides that is capable of binding copper through its deprotonated amide is Gly: however, the deprotonation probably appears to require a rather high pH, so that copper binding in Msp1capNC occurs only at pH 8.0 and higher.

An X-ray diffraction report of a copper complex of a PHGGG fragment of human PrP repeat generated a model where copper ion coordinates via 3 nitrogen atoms and two oxygen atoms (see Figure 1.12 in Chapter I): one nitrogen atom of His, two nitrogen atoms of the deprotonated amide backbone of the third and fourth Gly residues, one oxygen atom from the amide carbonyl group of the fifth Gly, and the oxygen atom of a water molecule that forms a bridge with the Trp indole ring (Burns et al., 2002). Another model suggested one nitrogen atom of His and two nitrogen atoms of the amide backbone of the third and fourth Gly as copper-binding sites in PrP octarepeat (Aronoff-Spencer et al., 2000) (see Figure 1.9 in Chapter I). These three models do not agree with the model proposed by Miura et al. (1999), where copper ion binds to the fourth and fifth Gly amides rather than the third and fourth Glys (Miura et al., 1999) (see Figure 1.8 in Chapter I). A model of copper complex of Msp1 peptide is presented in Chapter VIII. In terms of which Gly residues are the copper-binding sites in Msp1 peptide, this model follows the model proposed by Luczkowski et al. (2002), Burns et al. (2002), and Aronoff-Spencer et al. (2000), rather than Miura et al. (1999), as these models can explain the lack of binding between copper ion and the N-terminally capped Msp1 peptide at pH lower than 8.0. At pH 8.0 and higher, maybe the amide of Gly^4 and Gly^5 participate or backbone amides further along. It is also possible the amide side chains of Asn or Gln, which require higher pH for deprotonation, participate in copper binding. In order to check whether or not the presence of Gly as the third residue replacing Pro can facilitate copper binding, the peptide Msp1P3GcapNC, where the third Pro is replaced with Gly, was analyzed. Several other marsupial PrP-repeat peptides with capNC and human PrP repeat capNC were also investigated.

3.4.2. FTIR spectra of Msp1P3GcapNC (Ac-PHGGGSNWGQG-NH_2)

FTIR spectra show that upon addition of copper to Msp1P3GcapNC at pH 8.0, large changes occur in the amide I band region as well as other parts of the spectrum (Figure 3.13). The amide I band shifts from 1645 cm^{-1} to 1641 cm^{-1} (4 cm^{-1} red shift), this position indicates random coil structure.

A new band with relatively strong intensity is observed at 1621 cm^{-1} upon interaction of the peptide with copper ion. Concomitantly a 1419 cm^{-1} band also appears. These two bands have been attributed (see section 3.4.1.2) to the out-of-phase and in-phase stretching of the C=O/C-N^- of the deprotonated amide group. Similar band frequencies

with relatively weak intensity were observed in the second derivative spectra of copper complexes of Msp1 group (see Figures 3.2, 3.4, 3.6, right panels). The reason for the weak intensity is probably because the number of deprotonated main-chain amide groups in Msp1 is less than in Msp1P3GcapNC, as a result of the sequence difference. It is likely that in Msp1P3GcapNC, the nitrogen of the amide backbone of the third Gly residue is deprotonated and coordinated to a copper ion. In Msp1, the Pro residue does not have a deprotonated NH amide.

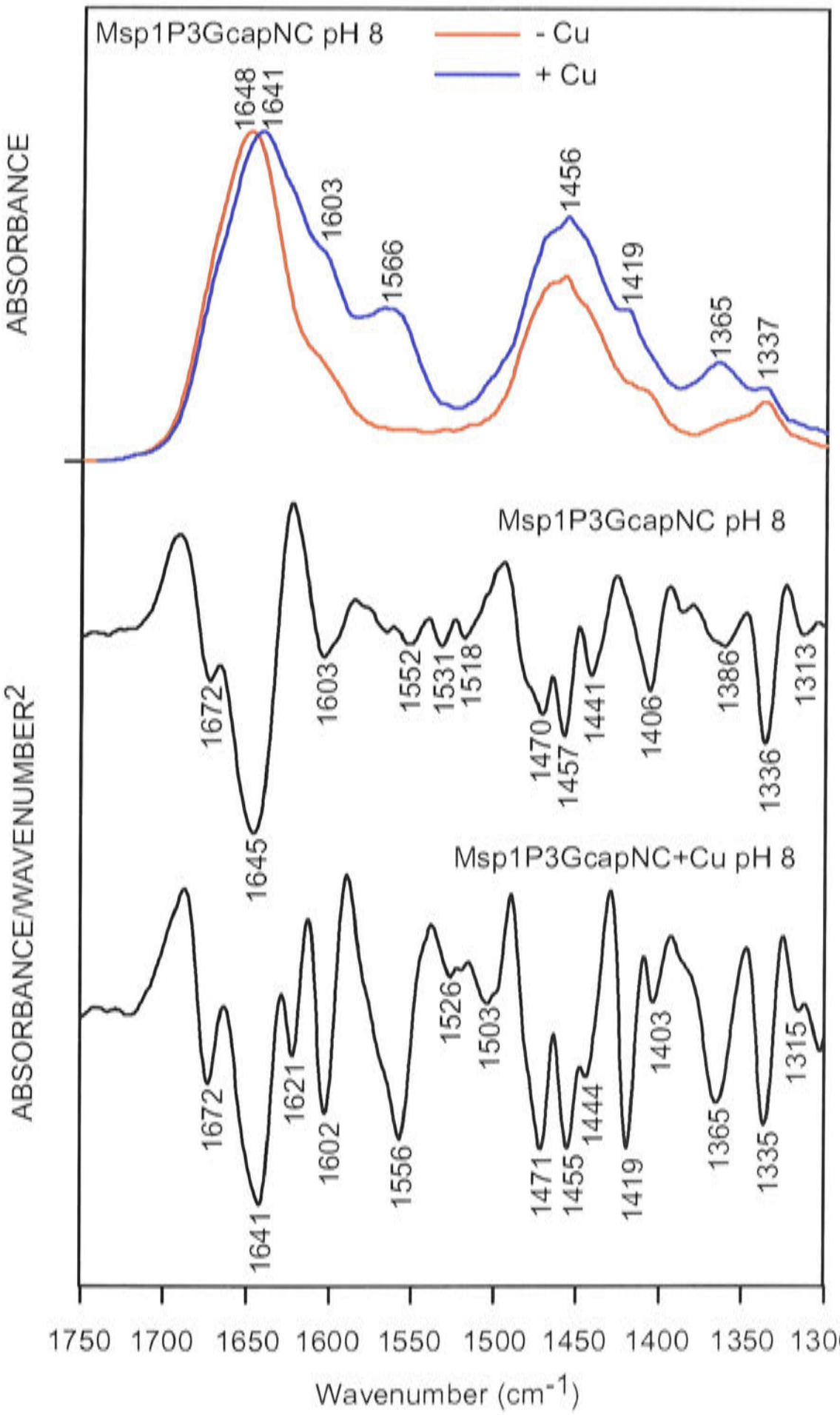

Figure 3.13: Copper binding to Msp1P3GcapNC peptide. The normalized absorbance (upper panel) and second derivative (middle and bottom) spectra in $^{2}H_2O$ of 2.5 mM Msp1P3GcapNC peptide (Ac-PHGGGSNWGQG-NH_2) in the absence and presence of 10 mM $CuCl_2$ at pH 8.0.

Together these data suggest that in the absence of the NH-deprotonated amide backbone from the third residue, the N-terminal imino group of Pro is required to form the complex with copper. If the amide NH of the third residue is available, then copper can form the complex with the peptide without requiring the imino group. This suggestion fits the model proposed in the literature (Luczkowski et al., 2002).

However, the fluorescence titration experiment (see Chapter IV) does not confirm the binding of copper to Msp1P3GcapNC peptide. Fluorescence quenching is not observed upon addition of copper to these capNC peptides, even when the third residue is Gly. One reason may be that addition of copper to the capNC peptides does not perturb the microenvironment around the Trp residue, even though copper is being bound. Another possible reason is the concentration difference between the FTIR and fluorimetry experiments. In FTIR, the peptide and copper concentrations are in the mM range, while in fluorimetry, they are in the μM range. Fluorescence experiments also do not confirm the FTIR observation of copper binding to Hu1capNC, although in this peptide, the Trp residue is 2 residues closer to His (anchoring site for copper). Furthermore, the XRD structure of copper-octarepeat complex shows the involvement of the indole ring of Trp in constructing the complex structure (Burns et al., 2002) (see Chapter I Figure 1.10).

The observed frequency of the copper complex of tautomer I in Msp1P3GcapNC is relatively low (1556 cm^{-1}) compared with the same vibration in Msp1 peptide (1565 cm^{-1}), while the frequency of the copper-bound tautomer II appears at higher frequency (1602 cm^{-1}) compared with this vibration in Msp1 (1595 cm^{-1}). The width of the 1556 cm^{-1} band is also larger than for the 1565 cm^{-1} band. Application of the deconvolution procedure revealed three component bands at 1556, 1568, and 1586 cm^{-1} (data not shown). While the origin of the bands at 1568 and 1586 cm^{-1} is currently unclear, the appearance of the band at 1556 and 1602 cm^{-1} in copper complexes of Msp1P3GcapNC suggests the formation of complex via both the N_π and N_τ atoms of the imidazole ring of His. In summary, these data suggest that the copper-binding sites in Msp1P3GcapNC are: the nitrogen atom, which could be N_π and N_τ of the imidazole ring of His, the deprotonated amide backbone of the third Gly, and probably the fourth and fifth Gly residues.

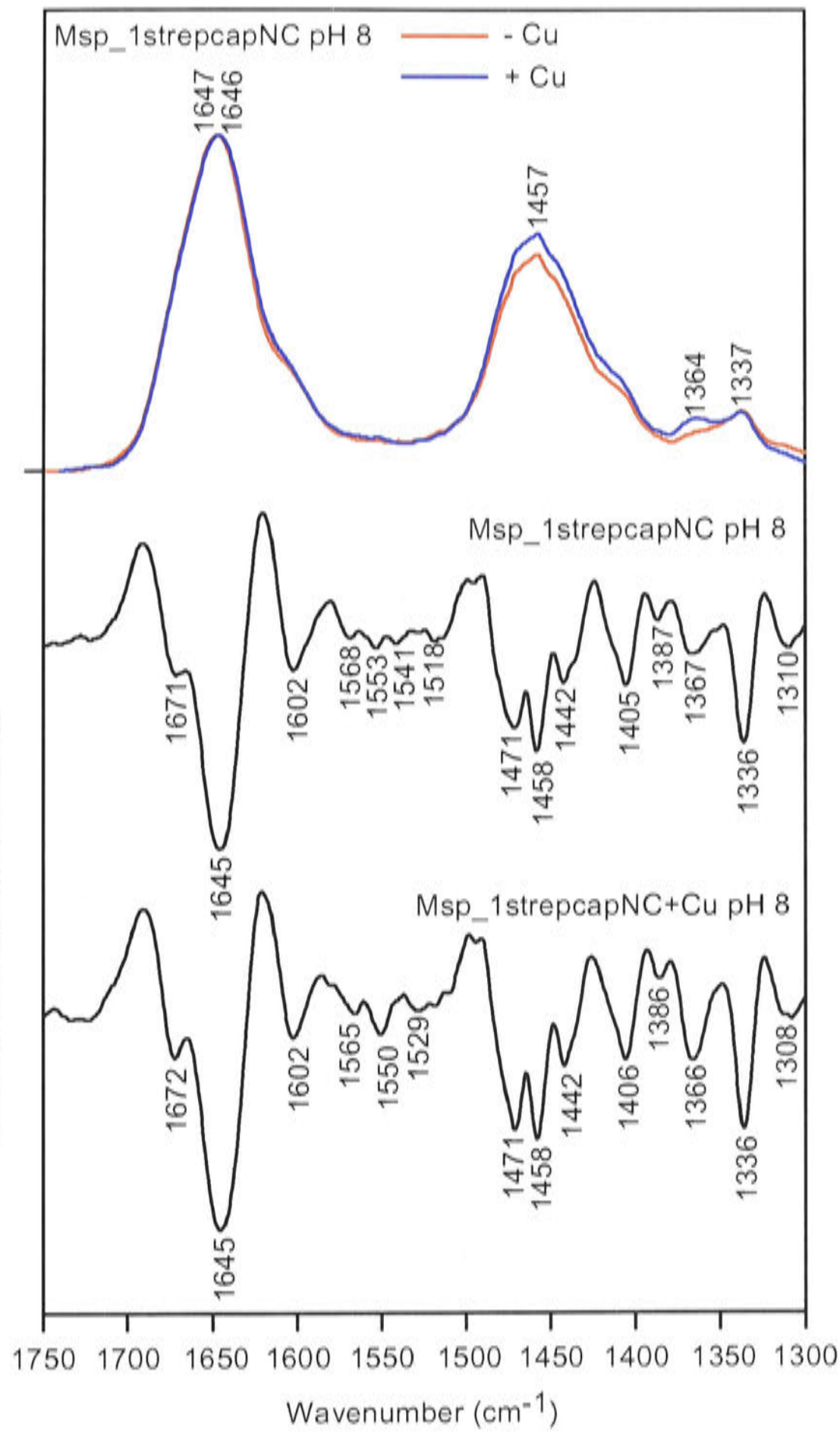

Figure 3.14: Copper binding to Msp_1strepcapNC peptide. The normalized absorbance (upper panel) and second derivative (middle and bottom) spectra in ^2H_2O of 2.5 mM Msp_1strepcapNC peptide (Ac-PQGGGTNWGQG-NH_2) in the absence and presence of 10 mM $CuCl_2$ at pH 8.0.

3.4.3. FTIR spectra of Msp_1strepcapNC (Ac-PQGGGTNWGQG-NH_2)

The first-repeat sequence of marsupial PrP was investigated. It was found that the peptide does not bind copper ion, as indicated by the lack of changes in the FTIR spectrum upon addition of copper (see Figure 3.14). During the sample preparation, the color of the peptide solution in the presence of copper at pH higher than 9.0 is violet with some blue precipitate. Upon addition of HCl to pH 8.5 the solution becomes colourless with some blue pale precipitate. It is possible that at pH higher than 9.0, the

peptide forms a complex with copper through the nitrogen atoms of the deprotonated amide backbone, such as the formation of the biuret complex (Creighton, 1983). It appears that the lack of a His residue prevents the peptide from binding copper at neutral and slightly basic pH, even though the GGG segment is available. This experiment suggests that the His residue is an important copper-binding site: the GGG segment alone cannot bind a copper ion and the Gln residue seems unable to substitute for His in binding copper.

The PQGGGTNWGQ repeat is found naturally as the first-repeat sequence of marsupial PrP (brush-tailed possum (Windl et al., 1995) and tammar wallaby (Premzl and Gready, 2003, personal communication)). Its lack of binding with copper indicates that this part of the repeat region does not participate in copper binding.

3.4.4. FTIR spectra of Msp_4threpcapNC (Ac-PHGGSNWGQG-NH_2)

The fourth repeat of the marsupial PrP-repeats region was analyzed for its ability to bind copper ions. The peptide was both N- and C-terminally protected. The spectra (Figure 3.15) show that upon addition of copper, the amide I band does not change, suggesting the structure of the copper-complexed and copper-free forms of Msp_4threpcapNC is random coil.

Upon addition of copper, the band at 1601 cm^{-1} increases in intensity and the band at 1566 cm^{-1} emerges. The intensity of the 1601 cm^{-1} band is higher than the 1566 cm^{-1} band: this indicates that the copper complex forms mainly via the N_τ atom, rather than the N_π atom, of the imidazole ring of His. This is also suggested by the fact that the band at 1502 cm^{-1}, which is a marker for copper binding to the N_π atom, appears only very weakly.

The band at 1421 cm^{-1}, which is assigned as the in-phase stretching of $C{=}O/C{-}N^-$ of the deprotonated amide backbone, emerges. However, its intensity is not as strong as that observed in the copper complex of Msp1P3GcapNC. Furthermore, the out-of-phase component at 1615 cm^{-1} appears only weakly as a shoulder. This result suggests that, in Msp_4threpcapNC, participation of the NH of the amide backbone in copper binding is much less than that in Msp1P3GcapNC. The difference between these two peptides is

the absence of the fifth residue Gly in Msp_4threpcapNC: this likely reduces the number of the amide backbone groups that participate in copper binding.

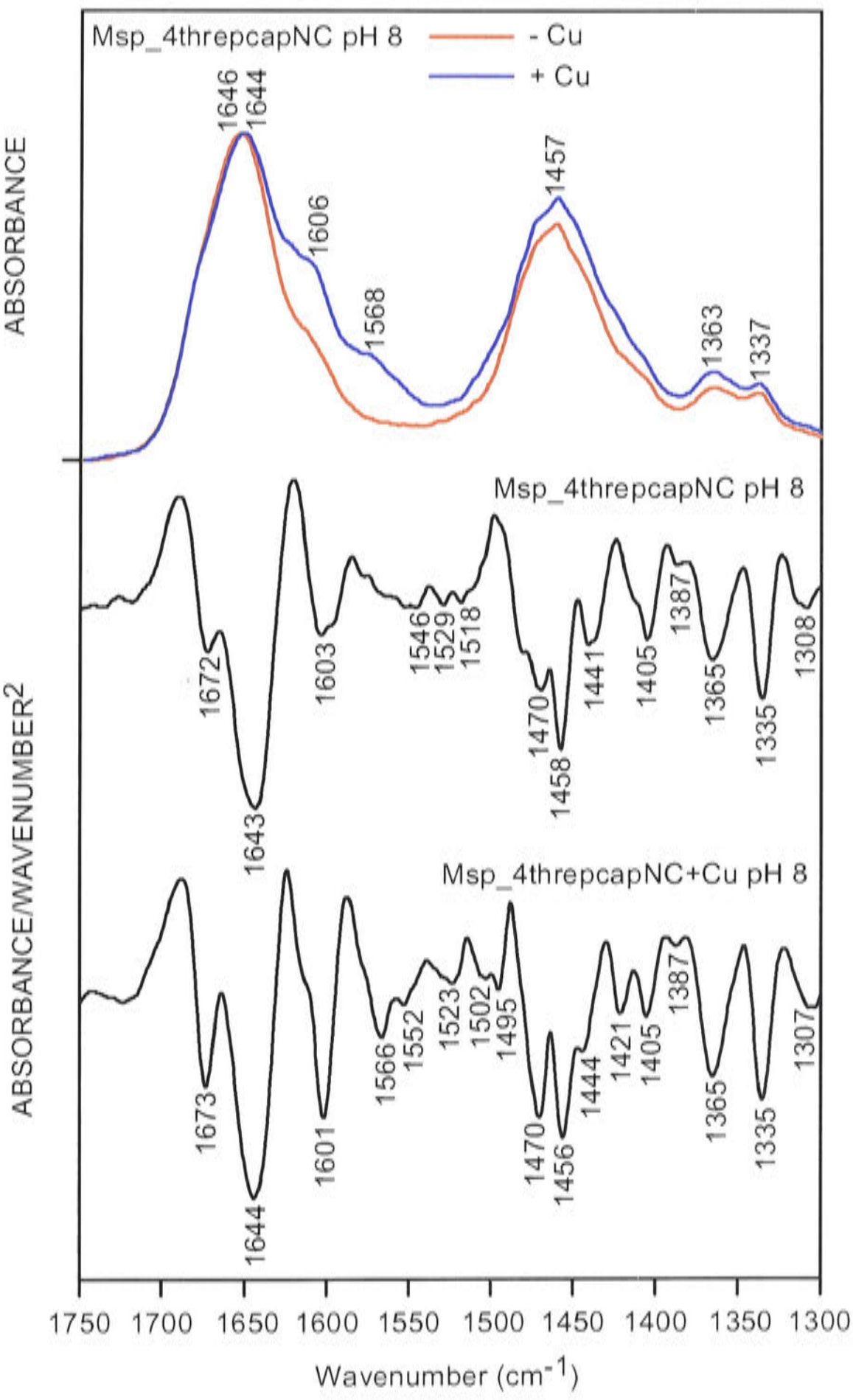

Figure 3.15: Copper binding to Msp_4threpcapNC peptide. The normalized absorbance (upper panel) and second derivative (middle and bottom) spectra in ^2H_2O of 2.5 mM Msp_4threpcapNC peptide (Ac-PHGGSNWGQG-NH_2) in the absence and presence of 10 mM $CuCl_2$ at pH 8.0.

These results suggest that copper-binding sites in Msp_4threpcapNC involve: the nitrogen atom of the imidazole ring of His, predominantly the N_τ atom and only a small proportion of N_π atom, and the nitrogen atom of the deprotonated amide backbone from the third and fourth Gly residues. The nitrogen atom of the amide backbone of the fifth

Ser residue probably does not participate in binding. These data emphasize the role of the GGG segment in copper binding.

The sequence of PHGGSNWGQ is found naturally as the fourth repeat in the marsupial PrP-repeat region. In the absence of the free imino group of Pro at the N-terminal end, this sequence is still capable of binding of copper ion strongly, suggesting that this part of the marsupial PrP repeats could naturally bind copper ion.

3.4.5. FTIR spectra of Hu1capNC (PHGGGWGQG)

Addition of copper to Hu1capNC peptide does not induce formation of more hydrogen-bonded structure as suggested by the amide I band position at 1644-1645 cm^{-1} (Figure 3.16), which indicates a random-coil structure. However, the other parts of the spectrum show significant changes.

Bands at 1619 and 1419 cm^{-1} emerge upon interaction with copper ion, reflecting copper binding to the deprotonated amide backbone. The suggestion that this band arises from the deprotonated amide backbone is supported by the literature, which reported that the group participates in copper binding (Miura et al., 1996; Miura et al., 1999; Aronoff-Spencer et al., 2000; Burns et al., 2002; Luczkowski et al., 2002). It is possible that the NH amide groups of the third, fourth and fifth Gly residues participate in copper binding as the peak intensities of the 1619 and 1419 cm^{-1} bands are quite high. The involvement of the third Gly residue in copper binding is in good agreement with some molecular models proposed in the literature (Aronoff-Spencer et al., 2000; Burns et al., 2002; Luczkowski et al., 2002). But it differs from model of Miura et al. (1999) in which the NH amide of the third Gly residue does not participate in copper binding (Miura et al., 1999).

The FTIR spectra show a strong band at 1603 cm^{-1}, suggesting the formation of a Cu-N_τ bond, and a medium intensity band at 1570 cm^{-1}, suggesting the formation of a Cu-N_π bond. These data indicate that the copper complex of Hu1capNC at pH 8.0 forms mainly through the formation of a Cu-N_τ bond, with His, with only a small proportion with a Cu-N_π bond. This result disagrees with the Raman results of Miura et al. (1999), who reported that the N_π atom, rather than the N_τ atom, of the imidazole ring of His

coordinates mainly with copper ion at pH 8.0. Miura et al. reported the binding of copper mainly to the N_τ atom occurs at pH 6.0. At this pH, Miura et al. reported the amide backbone does not participate in the binding, so that copper coordinated to two N_τ atoms from two different peptide chains. However, FTIR data of copper binding at pH 6.0 is not available for comparison with Raman results of Miura et al.

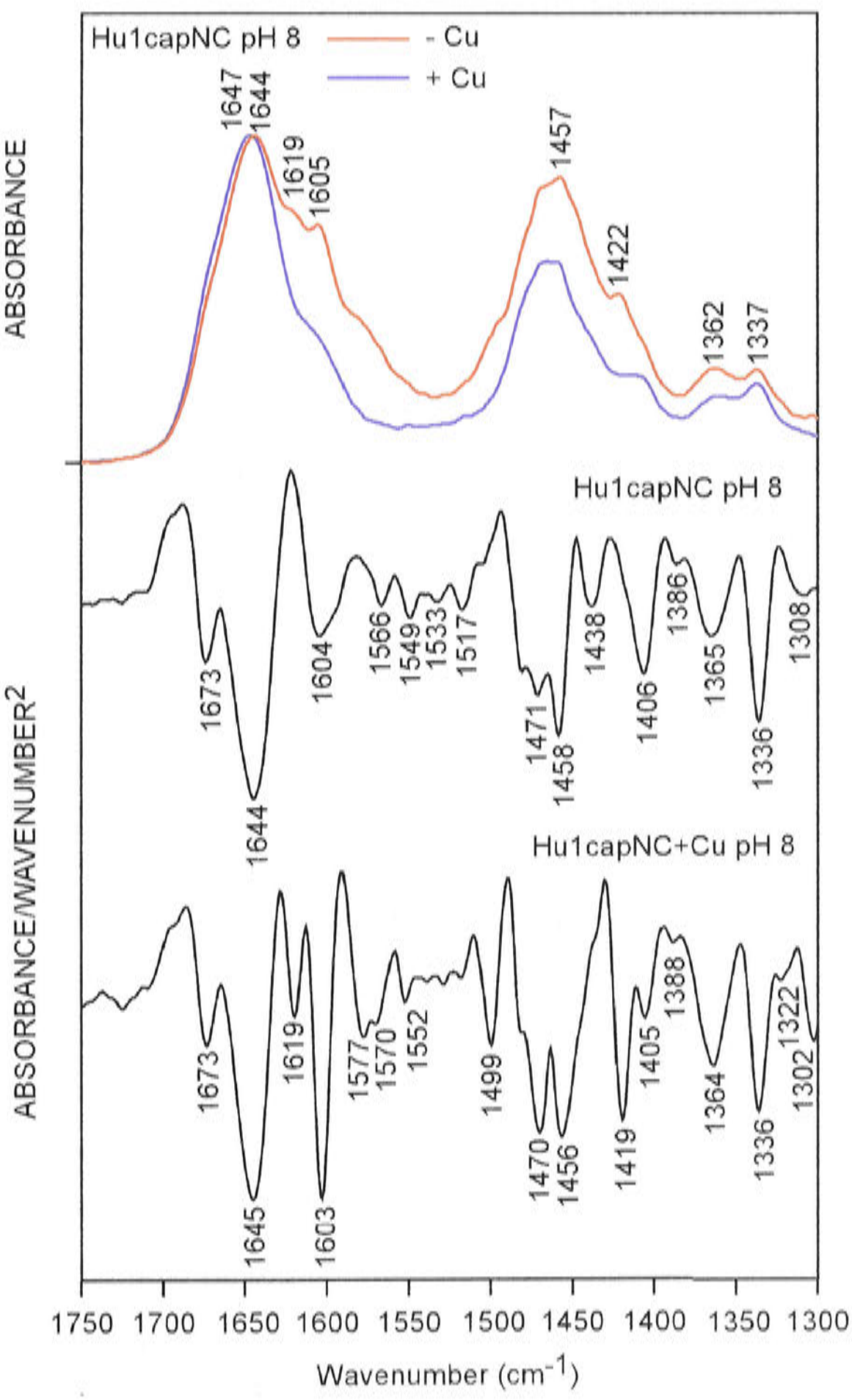

Figure 3.16: Copper binding to Hu1capNC peptide. The normalized absorbance (upper panel) and second derivative (middle and bottom) spectra in ^2H_2O of 2.5 mM Hu1capNC peptide (Ac-PHGGGWGQG-NH_2) in the absence and presence of 10 mM $CuCl_2$ at pH 8.0

The difference between the FTIR result here and the Raman results of Miura et al. (1999) is probably due to the amount of copper ions in the solution. In the latter, the ratio of copper to peptide was 1:1, while in this experiment the ratio is 4:1. It is suggested that at high concentration, copper ion would mainly bind to the N_τ atom of the imidazole ring of His, while at lower concentration it binds to the N_π atom. However, due to time constraints of this thesis, experiments to obtain the spectra of the Hu1capNC peptide as a function of copper-ion concentration could not be done.

3.4.6. Conformational analysis of multi-repeat peptides (Msp2 group, Msp3 group, and Msp4 group) in the absence and presence of copper ions

Compared with that of Msp1, the spectra of longer peptides are more complex. This has allowed the interpretation possible only for the amide I band. The greater possibility of conformational heterogeneity within the complexes of longer peptides depending on stoichiometry of binding, and the fact that complex precipitates, are factors that complicate the spectrum. The latter is apparent for several peptides where residual TFA has not been removed completely, by the intensity ratio of the amide I/TFA band (~1672 cm^{-1}), which is lower for a less soluble complex.

3.4.6.1. Msp2 group peptides

Amide I band analysis of the Msp2 group peptides reveals that on going from pH 6.0 to 9.0 the maximum shifts from 1647 to 1645 cm^{-1} (Msp2 peptide, Figure 3.17, left panel), 1647 to 1644 cm^{-1} (Msp2capC, Figure 3.19, left panel) and 1646 to 1645 cm^{-1} (Msp2capNC, Figure 3.21, left panel). Other than the appearance of a peak at 1670 cm^{-1}, which is due to residual TFA, the second-derivative analysis (Figures 3.18, 3.20, and 3.22, right panels) confirms what can be seen from the absorbance spectra. The amide I maximum at 1647-1644 cm^{-1} for the copper-free form of the peptide in ^2H_2O can be attributed to random-coil structure.

Msp2+Cu. Addition of copper to Msp2 at pH 6.0 and 7.0 results in no shift of the amide I band position as shown in the second derivative spectra (Figure 3.18, right panel). At pH 8.0, there is only a 1 cm^{-1} shift toward lower frequency upon addition of copper. The amide I band of the copper complex at pH 6.0-8.0, which is in the region

of 1644-1643 cm^{-1}, is assigned to random-coil structure. A larger shift, reflecting an increase in hydrogen bonding, is evidenced at pH 9.0 (9 cm^{-1}), where the amide I band is now at 1635 cm^{-1}. The assignment of the 1635 cm^{-1} band is complicated because absorbance in this region can arise from β-sheet and β-turn structure, as well as from solvent-exposed α-helices (Haris and Chapman, 1995). However, the fact that the amide I band is shifted toward lower frequency indicates an increase in ordered secondary structure, which could possibly be solvent-exposed α-helical structure, although the assignment of the 1635 cm^{-1} band is not straightforward. This assignment would be in good agreement with the Raman studies of Miura et al. (Miura et al., 1996; Miura et al., 1999), who detected an increase in helix content upon interaction of copper ions with a human PrP-octarepeat peptide (single and multi octarepeat: $[PHGGGWGQ]_{n=1, 2, 4}$). The difference between results of Miura et al. and this FTIR result is that in these FTIR experiments helix structure is detected only in multi-repeat and not in single-repeat peptides, while Miura et al. detected it in both repeats.

Msp2capC+Cu. The second derivative spectra of copper complexes of Msp2capC (see Figure 3.20, right panel) shows that at pH 6.0-8.0 the complex adopts a random-coil structure, as shown by the amide I band at 1645-1640 cm^{-1}. At pH 9.0, the amide I band of the complex is located at 1634 cm^{-1}, again suggestive of solvent exposed α-helical structure.

Msp2capNC+Cu. Addition of copper to Msp2capNC peptide at pH 6.0 produces only small changes in the second derivative spectra (Figure 3.22, right panel): the amide I band maximum of the copper complex is at 1645 cm^{-1}. This indicates a random-coil structure. Addition of copper to Msp2capNC at pH 7.0 results in the appearance of two components of the amide I band: 1647 and 1639 cm^{-1}. Two components of the amide I band are also observed at pH 8.0 (1649 and 1635 cm^{-1}) and 9.0 (1649 and 1634 cm^{-1}). At pH 7.0, the intensities of the two components are comparable, while at pH 8.0, the intensity of the lower-frequency component is higher. At pH 9.0, the higher-frequency component appears merely as a shoulder. The lower-frequency component of the amide I band, at ~1636 cm^{-1}, could be attributed to solvent exposed α-helical structure, as proposed above for the copper complex of Msp2 peptide.

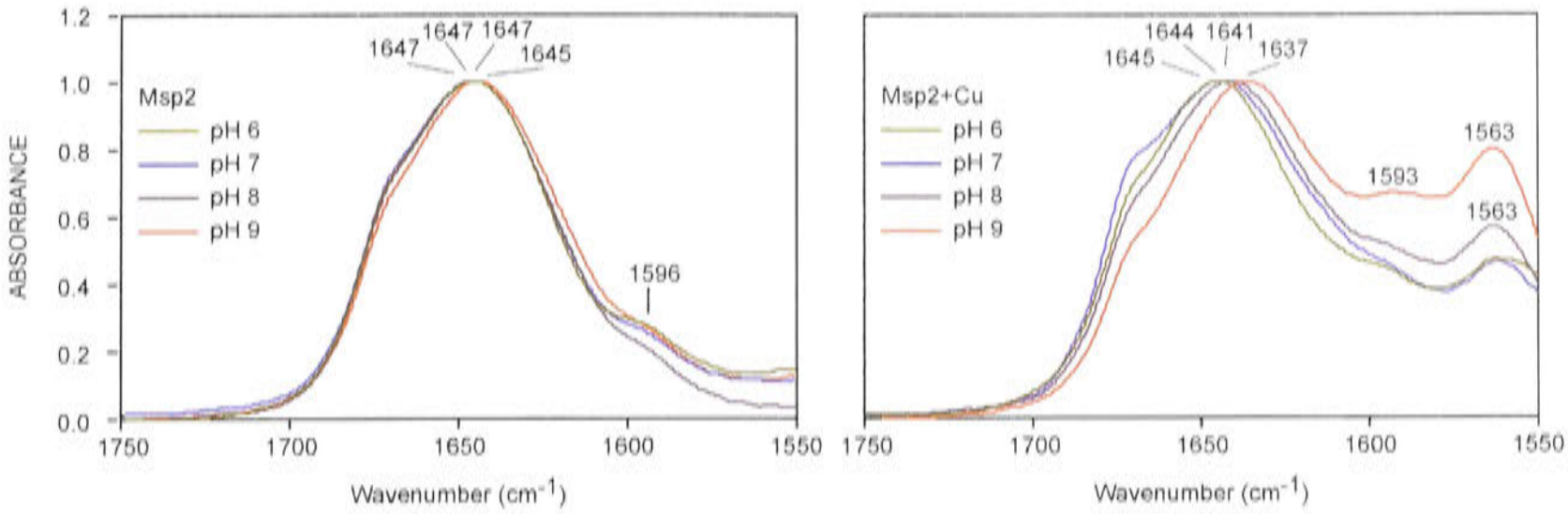

Figure 3.17: FTIR normalized absorbance spectra of Msp2 and copper complex of Msp2. The spectra of Msp2 in $^{2}H_2O$ at 2.5 mM peptide concentration, in the absence (left) and presence (right) of 10 mM $CuCl_2$, at pH 6.0, 7.0, 8.0, and 9.0.

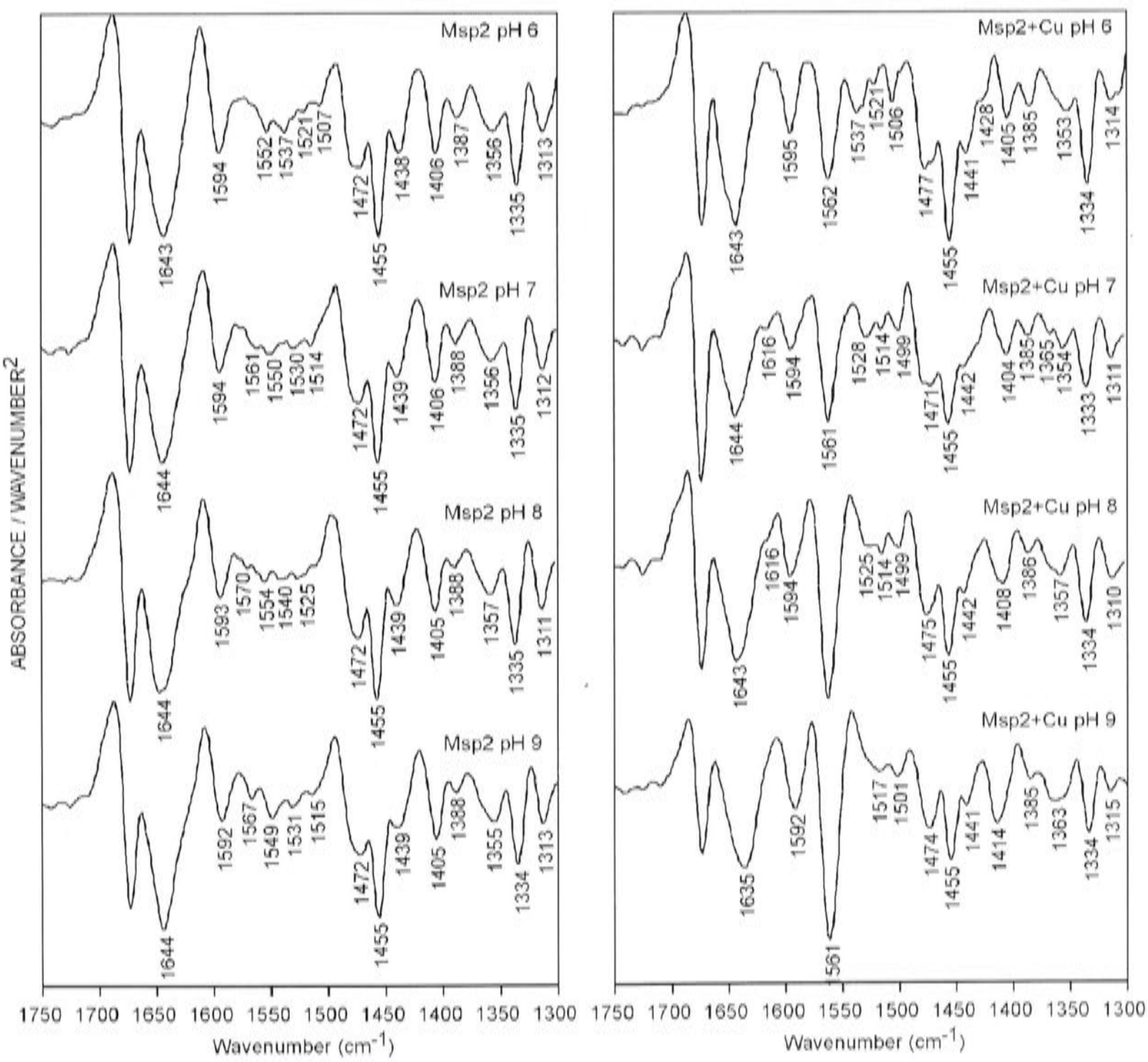

Figure 3.18: FTIR second derivative spectra of Msp2 and copper complex of Msp2. The spectra of Msp2 in $^{2}H_2O$ at 2.5 mM peptide concentration, in the absence (left) and presence (right) of 10 mM $CuCl_2$, at pH 6.0, 7.0, 8.0, and 9.0.

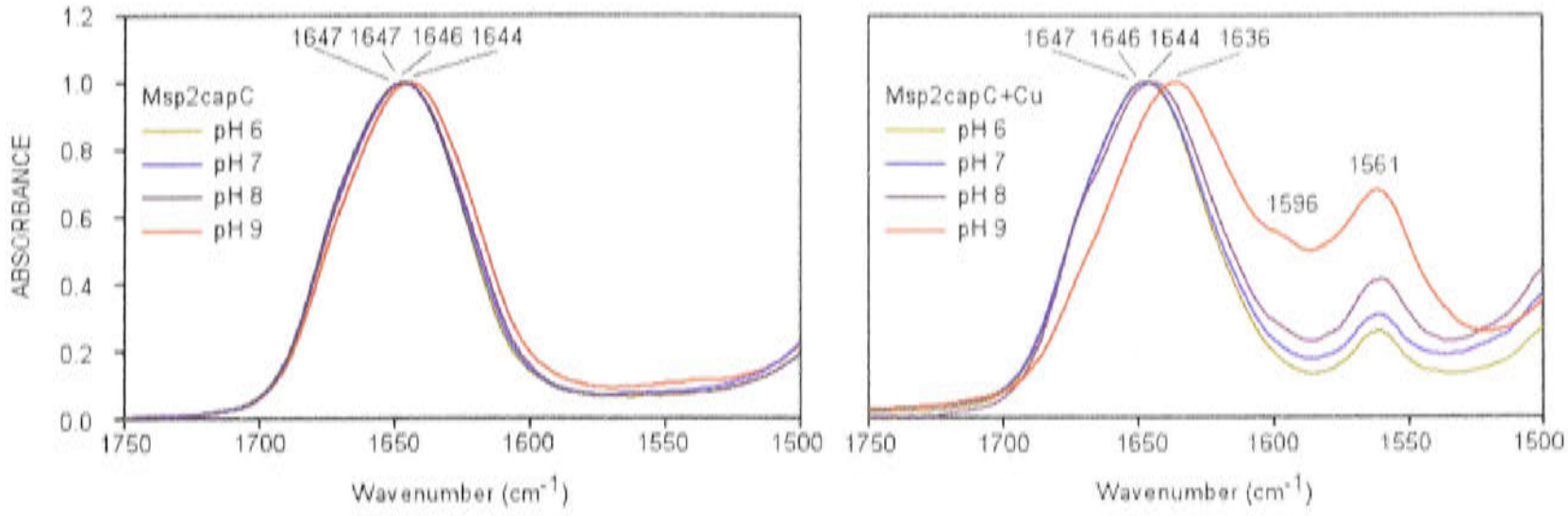

Figure 3.19: FTIR normalized absorbance spectra of Msp2capC and copper complex of Msp2capC. The spectra of Msp2capC in $^{2}H_2O$ at 2.5 mM peptide concentration, in the absence (left) and presence (right) of 10 mM $CuCl_2$, at pH 6.0, 7.0, 8.0, and 9.0.

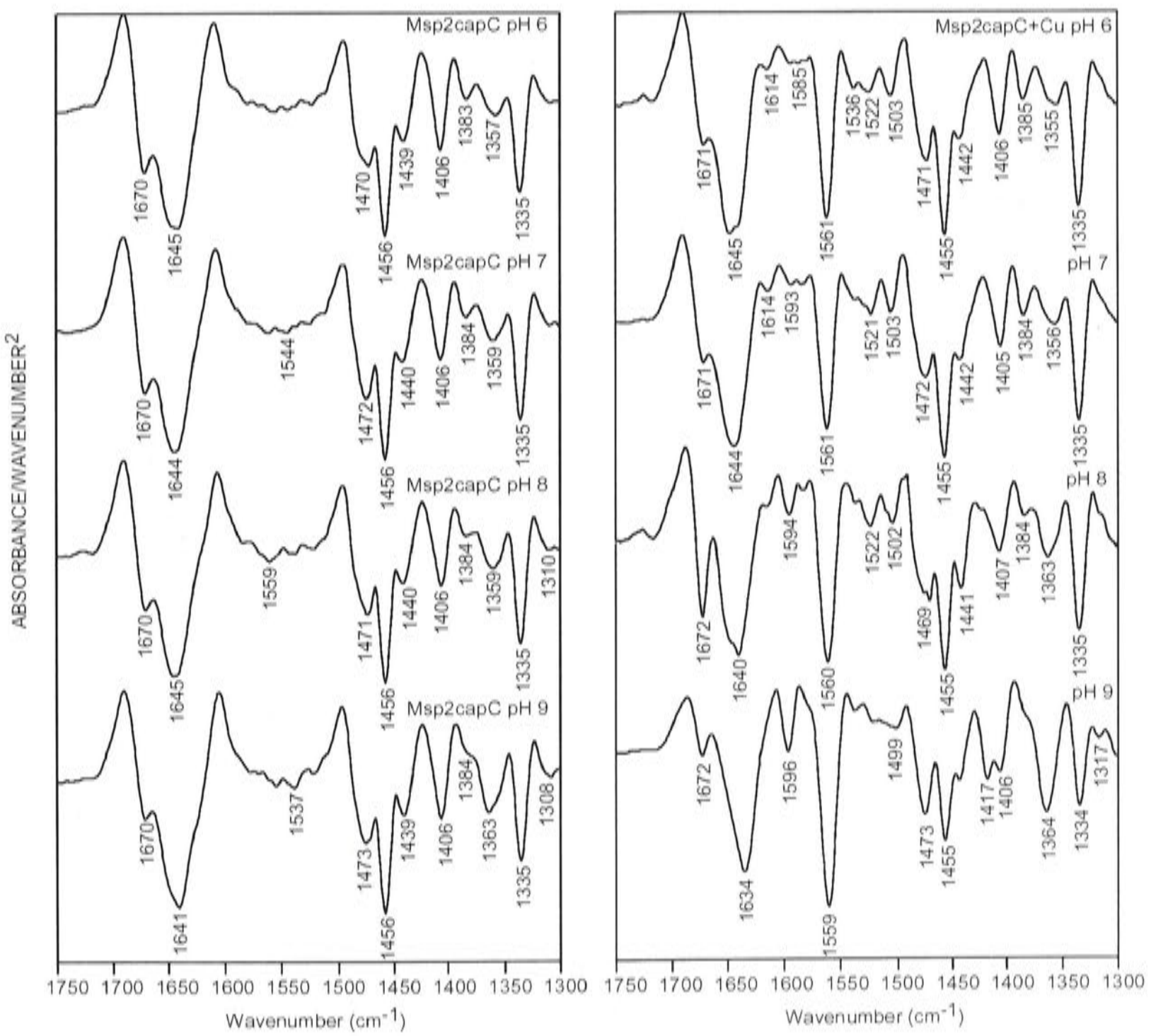

Figure 3.20: FTIR second derivative spectra of Msp2capC and copper complex of Msp2capC. The spectra of Msp2capC in $^{2}H_2O$ at 2.5 mM peptide concentration, in the absence (left) and presence (right) of 10 mM $CuCl_2$, at pH 6.0, 7.0, 8.0, and 9.0.

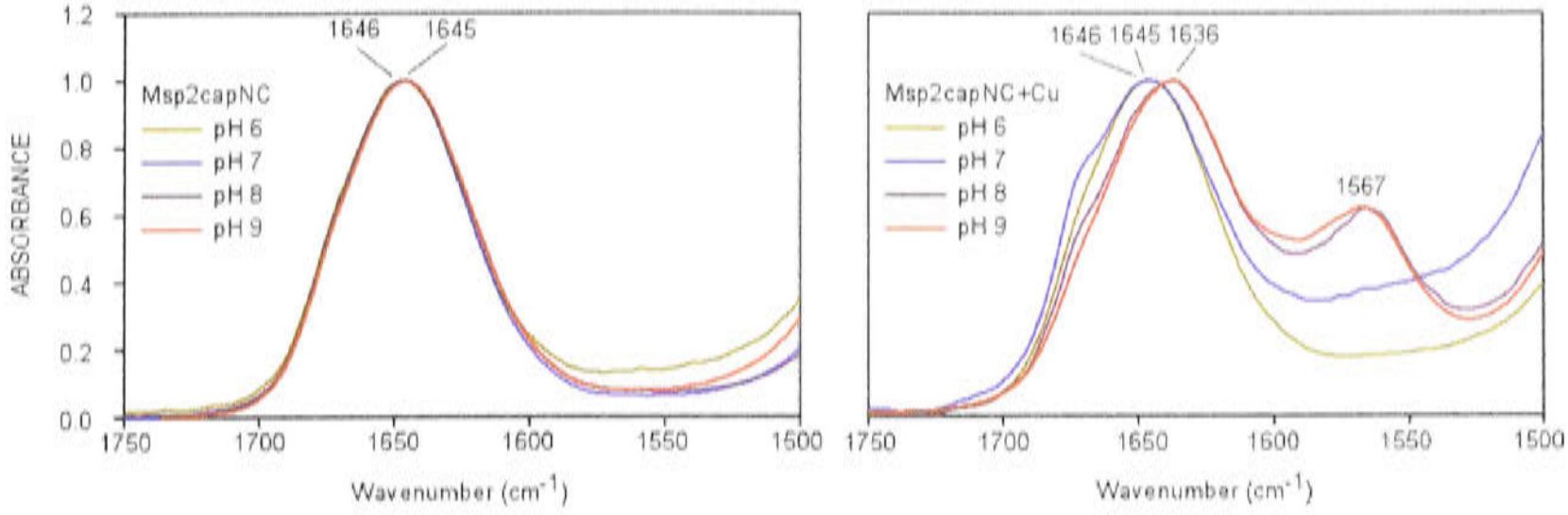

Figure 3.21: FTIR normalized absorbance spectra of Msp2capNC and copper complex of Msp2capNC. The spectra of Msp2capNC in $^{2}H_2O$ at 2.5 mM peptide concentration, in the absence (left) and presence (right) of 10 mM $CuCl_2$, at pH 6.0, 7.0, 8.0, and 9.0.

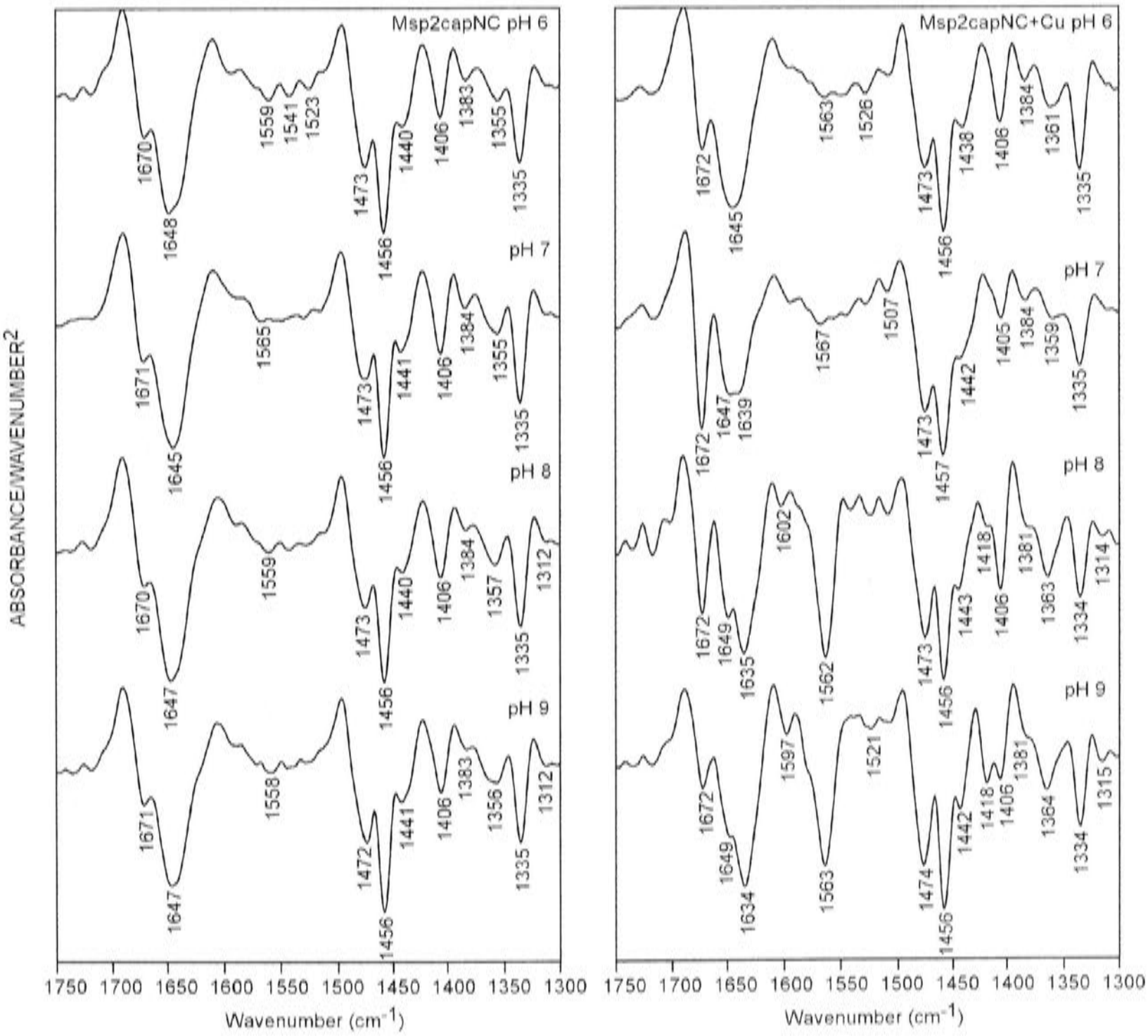

Figure 3.22: FTIR second derivative spectra of Msp2capNC and copper complex of Msp2capNC. The spectra of Msp2capNC in $^{2}H_2O$ at 2.5 mM peptide concentration, in the absence (left) and presence (right) of 10 mM $CuCl_2$, at pH 6.0, 7.0, 8.0, and 9.0.

Preliminary conclusion. In general, copper complexes of Msp2 group peptides are less soluble than the copper-free peptides. Although the appearance of the TFA band in the IR spectra is unfortunate, the intensity of this band can give indirect information about the complex solubility. The intensity ratio of the amide I/TFA band suggests that the copper complex of Msp2 group peptides is less soluble at pH 7.0-8.0 than at the other pHs (pH 6.0 and 9.0), as the intensity ratio is higher at these latter pHs.

The peaks of the amide I band of copper complex of Msp2 group peptide splits into two components, each typical of random-coil and α-helix structure. Two explanations are possible for this peak splitting. The first one is that the FTIR spectra represent a distribution of complexed (~1636 cm-1) and uncomplexed (~1645 cm-) Msp2 molecules, with the relative concentration of the former depleted by precipitation. This issue would be resolved by copper titration experiments. The second explanation is that there are two conformations of complexed peptide, on different regions of the Msp2 molecule adopting mostly either random-coil or helical conformation. Interpretation of other regions of the spectra, as done for Msp1 peptides, might allow discrimination of the two explanations, but unfortunately the other spectral regions are much more complicated in the multi-repeat peptides and it is difficult to draw conclusions.

3.4.6.2. Msp3 group peptides

There are no significant pH-induced changes in the structure of Msp3 group peptides in the absence of copper. In Msp3, the amide I band frequency between 1646-1643 cm^{-1} throughout the pH range studied suggests the presence of a random-coil structure (see Figures 3.23 and 3.24, left panel: note that the concentration of the peptide is 5 mM, which is twice that of the other peptides). This assignment is further supported by the fact that the amide II band disappears very rapidly upon dissolution of peptide in ^2H_2O. Amidation of the C-terminus of Msp3 (Msp3capC) does not change the structure of the peptide: its structure is still random coil, as suggested by the position of the amide I band at 1646-1644 cm^{-1} (see Figures 3.25 and 3.26, left panel). The highest frequency belongs to the peptide at pH 6.0 and the lowest to the peptide at pH 9.0. Msp3capNC peptides also adopt a random-coil structure as suggested by the amide I band position at 1645-1644 cm^{-1}, which appears in the FTIR absorbance spectra (see Figures 3.27 and 3.28, left panel).

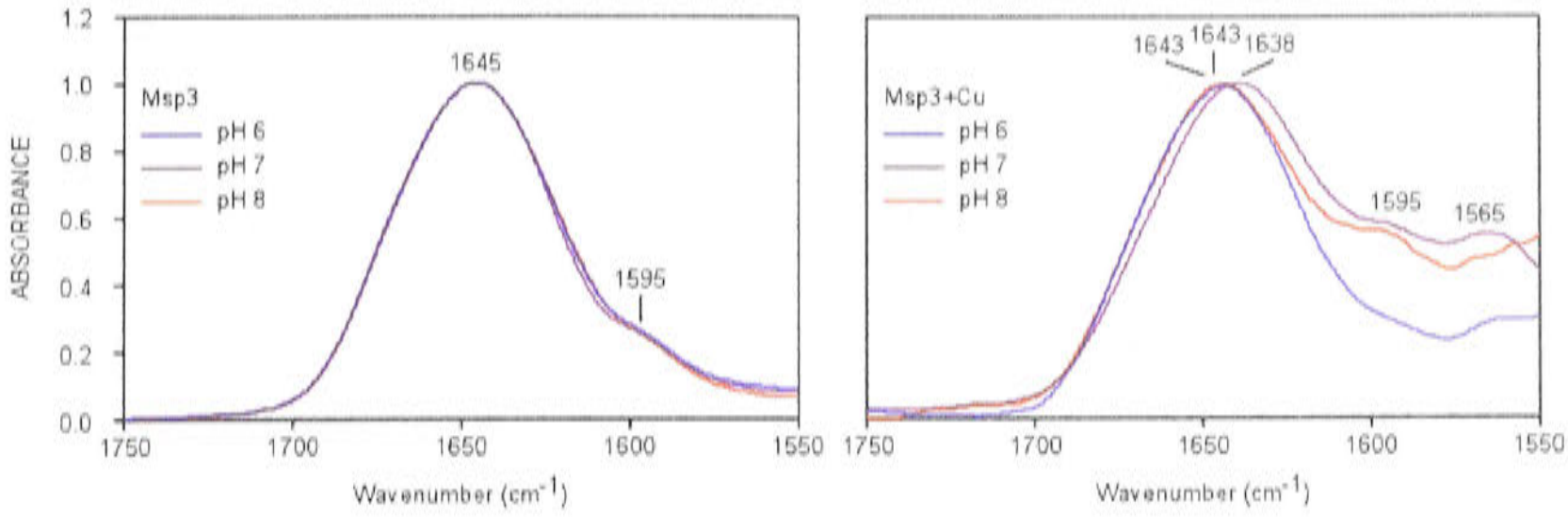

Figure 3.23: FTIR normalized absorbance spectra of Msp3 and copper complex of Msp3. The spectra of Msp3 in $^{2}H_2O$ at 5 mM peptide concentration, in the absence (left) and presence (right) of 20 mM $CuCl_2$, at pH 6.0, 7.0, and 8.0. The absorbance spectra at pH 9.0 are not shown.

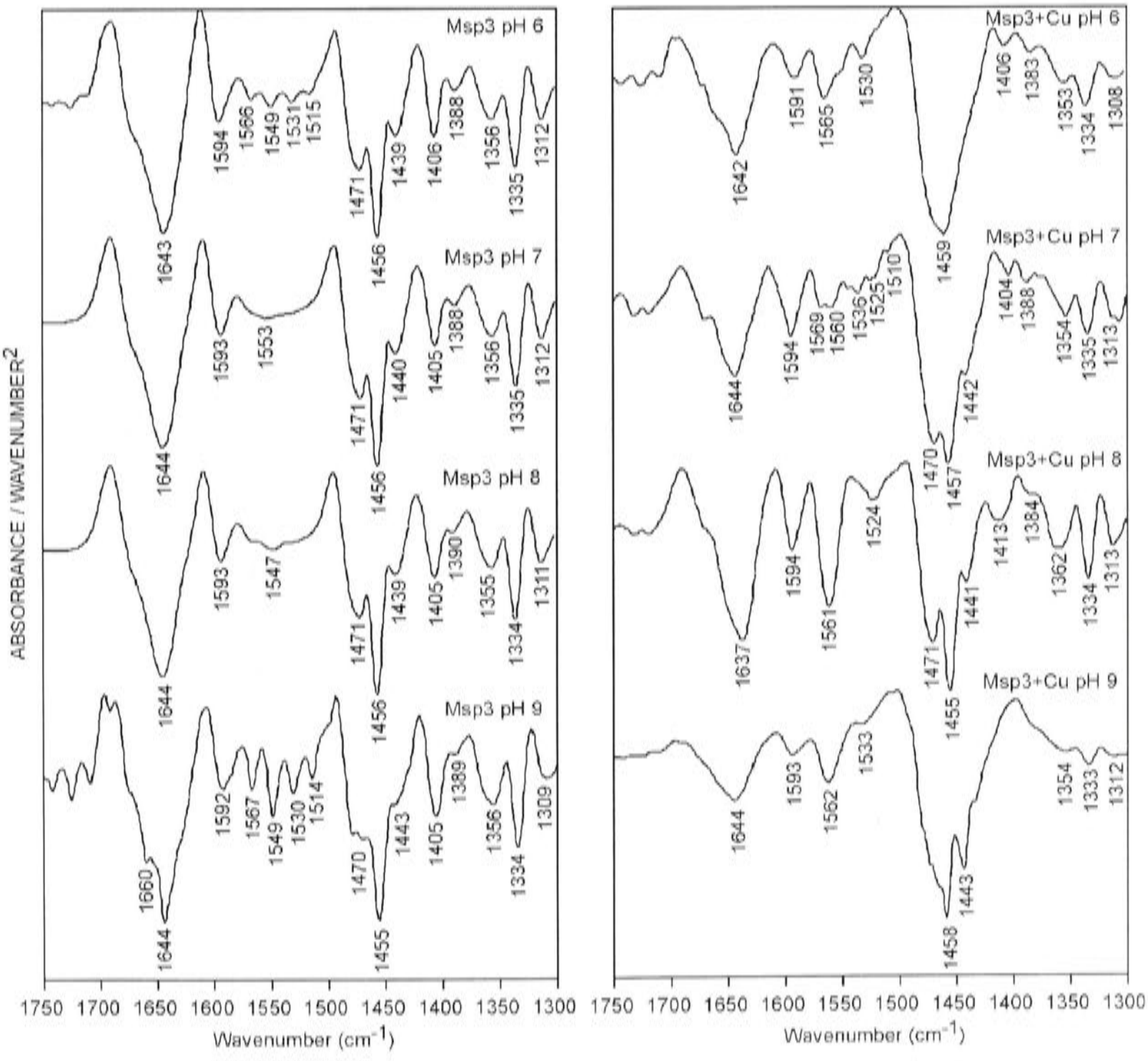

Figure 3.24: FTIR second derivative spectra of Msp3 and copper complex of Msp3. The spectra of Msp3 in $^{2}H_2O$ at 5 mM peptide concentration, in the absence (left) and presence (right) of 20 mM $CuCl_2$, at pH 6.0, 7.0, 8.0 and 9.0.

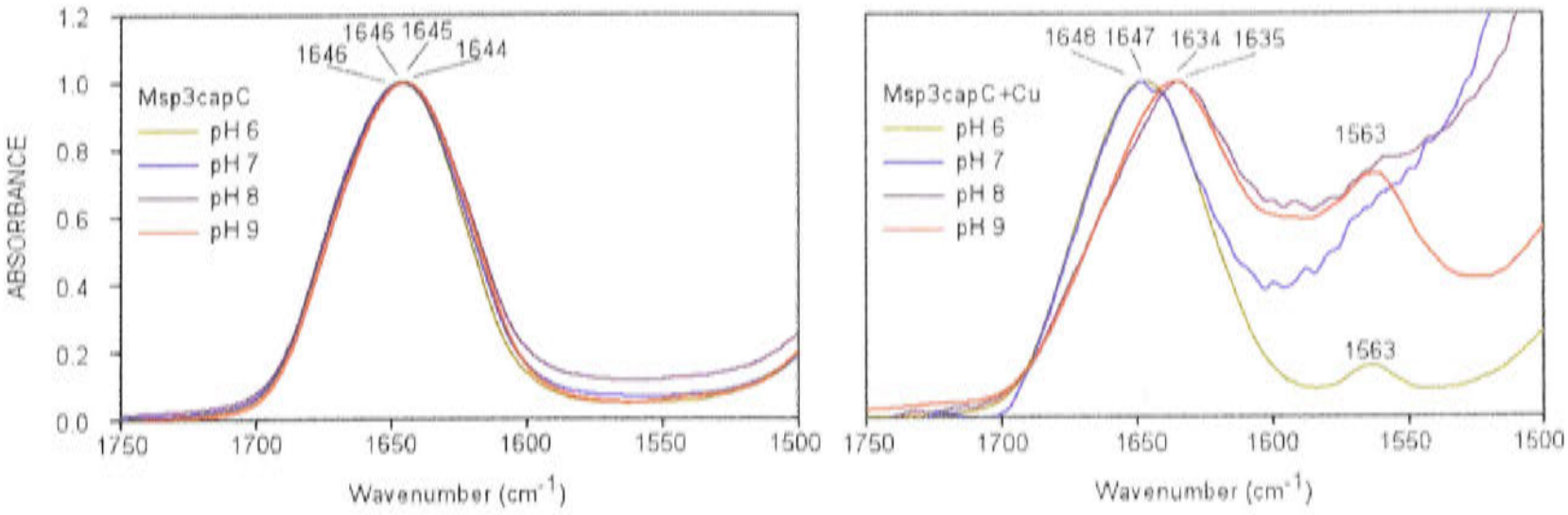

Figure 3.25: FTIR normalized absorbance spectra of Msp3capC and copper complex of Msp3capC. The spectra of Msp3capC in ^2H_2O at 2.5 mM peptide concentration, in the absence (left) and presence (right) of 10 mM $CuCl_2$, at pH 6.0, 7.0, 8.0, and 9.0. Large absorbance increases for pH 7.0 and 8.0 at lower wavenumber in right panel are due to HOD absorbance (wet ^2H_2O).

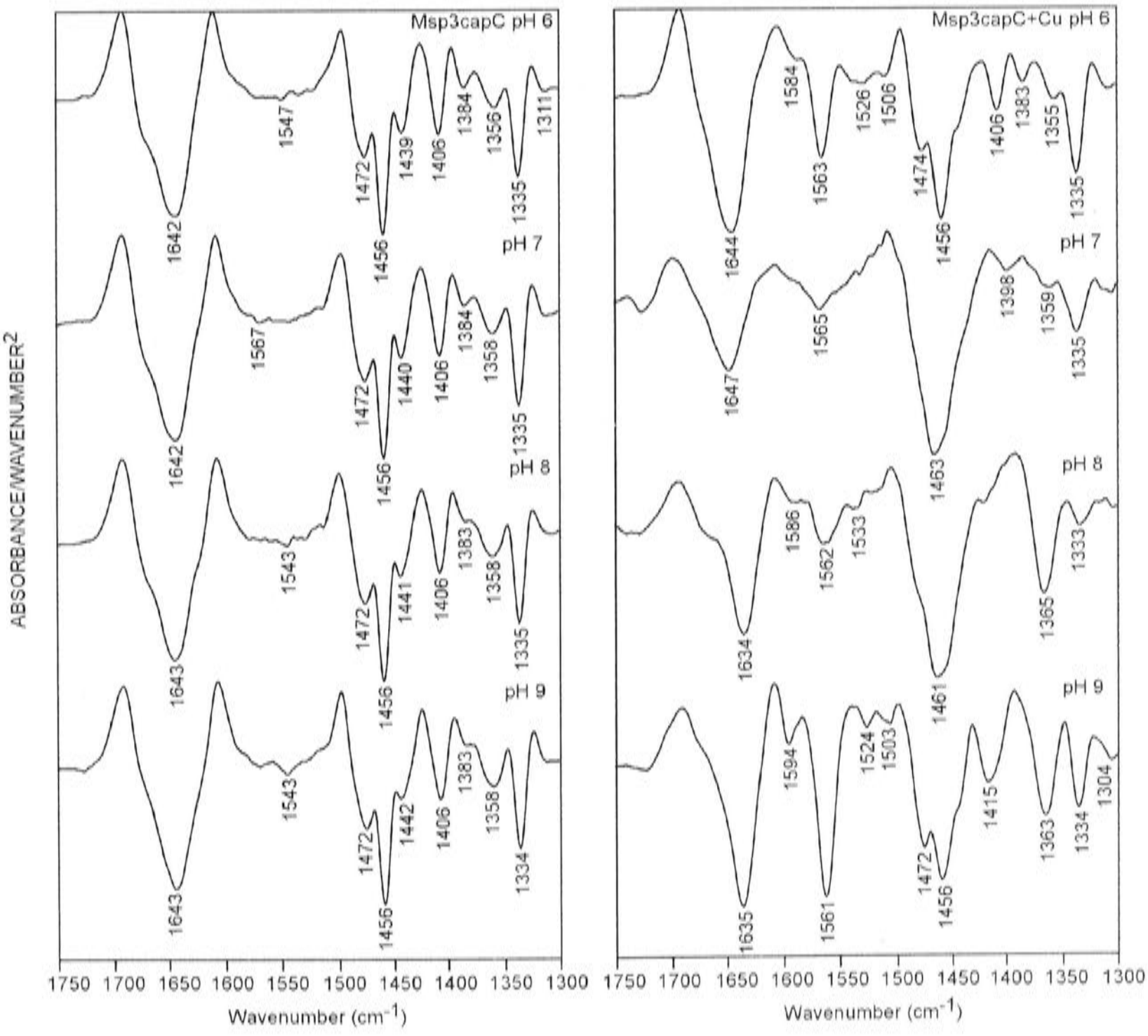

Figure 3.26: FTIR second derivative spectra of Msp3capC and copper complex of Msp3capC. The spectra of Msp3capC in ^2H_2O at 2.5 mM peptide concentration, in the absence (left) and presence (right) of 10 mM $CuCl_2$, at pH 6.0, 7.0, 8.0, and 9.0.

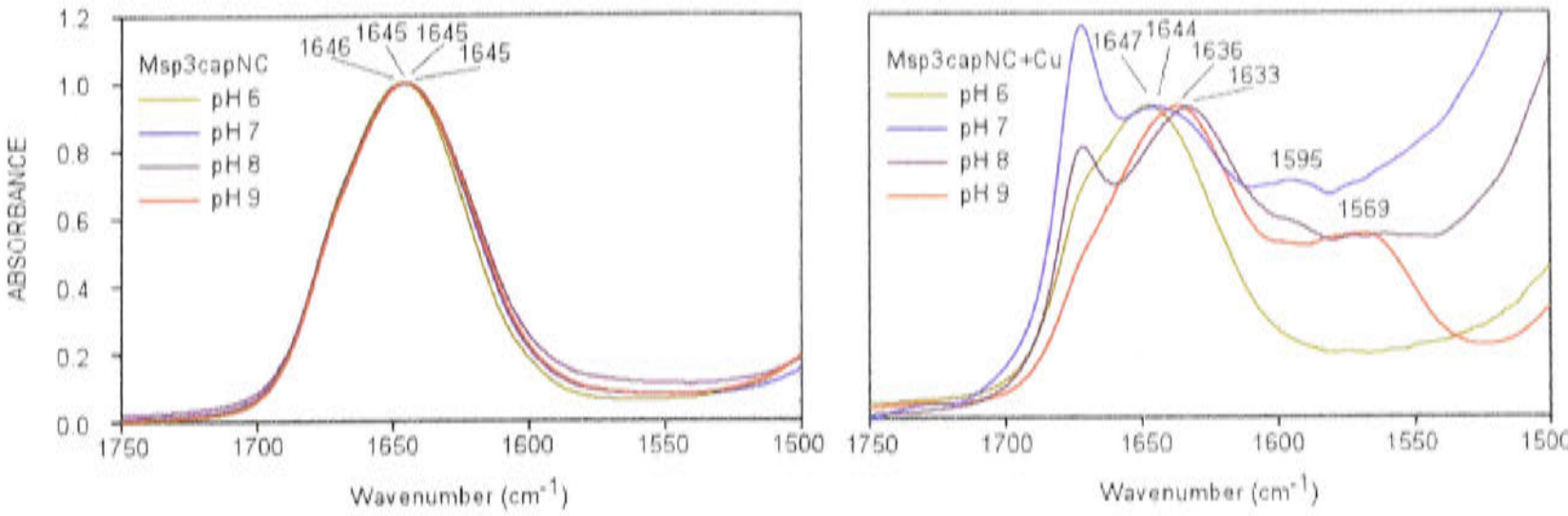

Figure 3.27: FTIR normalized absorbance spectra of Msp3capNC and copper complex of Msp3capNC. The spectra of Msp3capNC in ^2H_2O at 2.5 mM peptide concentration, in the absence (left) and presence (right) of 10 mM $CuCl_2$, at pH 6.0, 7.0, 8.0, and 9.0. Large absorbance increases for pH 7.0 and 8.0 at lower wavenumber in right panel are due to HOD absorbance (wet ^2H_2O).

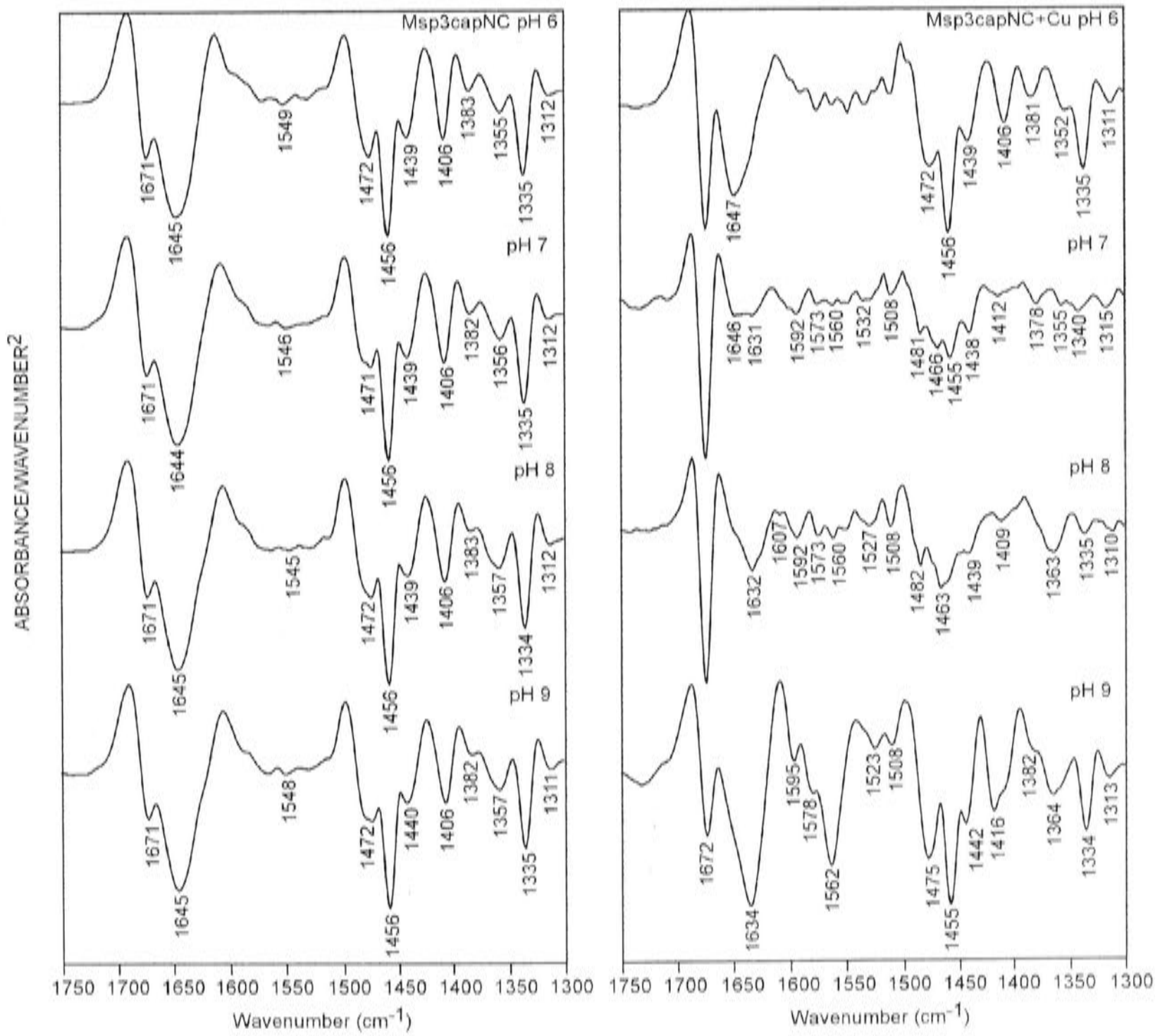

Figure 3.28: FTIR second derivative spectra of Msp3capNC and copper complex of Msp3capNC. The spectra of Msp3capNC in ^2H_2O at 2.5 mM peptide concentration, in the absence (left) and presence (right) of 10 mM $CuCl_2$, at pH 6.0, 7.0, 8.0, and 9.0.

In general, the copper complexes of Msp3 group peptides, as also the case for Msp2 (section 3.4.6.2) and Msp4 (see later in section 3.4.6.3), are less soluble than their copper-free forms, as indicated by the formation of precipitate. From observations during sample preparation and judging from the intensity ratio of the amide I/TFA band, it appears the complex is more soluble at pH 9.0 than at the other pHs. The lower solubility of the complexes resulted in low peptide concentration left in the supernatant, which in turn lead to the low-resolution spectra (see Figures 3.23-3.28, right panel). However, spectral assignment is still possible for the amide I band.

Msp3+Cu. Addition of copper ions at pH 6.0 and pH 7.0 to Msp3 peptide does not seem to change the position of the amide I band in second derivative spectra (Figure 3.24, right panel), although in the original absorbance spectra it changes the amide I band position slightly (3 cm^{-1} red shift) (see Figure 3.23, right panel). However, at pH 8.0 the amide I band frequency shifts significantly to lower frequency and now is located at 1637 cm^{-1}, reflecting solvent-exposed α-helical structure, similar to copper complex of Msp2 group peptides. The spectrum of the copper complex of Msp3 at pH 9.0 is poor because of wet ^2H_2O, which can absorb in the amide I region.

Msp3capC+Cu. Upon addition of copper to Msp3capC peptides at pH 6.0 and 7.0, the position of the amide I band is relatively unchanged (see Figures 3.25 and 3.26, right panel), suggesting the peptide is still random coil. Interaction of peptide with copper ion at pHs 8.0 and 9.0 produced a position for the amide I band at 1635 cm^{-1}, again, reflecting a solvent exposed α-helical structure.

Msp3capNC+Cu. Absorbance spectra show that addition of copper ions to Msp3capNC at pHs 6.0 and 7.0 does not change the position of the amide I band, which is at 1647-1644 cm^{-1} (Figure 3.27, right panel). However, the second derivative procedure applied to the copper-complex spectrum at pH 7.0 reveals two amide I components at 1646 cm^{-1} and 1631 cm^{1} (see Figure 3.28, right panel). The higher frequency is ascribed to a random-coil structure, while the lower frequency is assigned to a solvent-exposed α-helical structure. The complex at pH 8.0 and 9.0 also adopts this latter structure: the amide I band position is at 1634-1632 cm^{-1}.

Preliminary conclusion. The splitting of the amide I band is observed in the copper complex of Msp3 group peptides. As explained at the end of section 3.4.6.1, these two components could reflect either conformational heterogeneity within the same molecule or the presence of complexed and uncomplexed molecules.

3.4.6.3. Msp4 group peptides

Msp4+Cu. The structure of Msp4 throughout the pH range 6.0-9.0 is random-coil as suggested by the frequency of the amide I band at 1644-1641 cm^{-1} (Figures 3.29 and 3.30, left panel). Addition of copper at pH 6.0 and 7.0 changes the amide I band only slightly (Figure 3.29, right panel). However, the second derivative procedure reveals that in the copper complex at pH 6.0-7.0, the amide I band is composed of two component bands at 1650 cm^{-1} and 1637-1635 cm^{-1} (Figure 3.30, right panel). The band at 1650 cm^{-1} is attributed to a random-coil structure and the band at 1635-1639 cm^{-1} is assigned to a solvent-exposed α-helical structure, with the former being the major component. Two component bands (1650 cm^{-1} and 1634 cm^{-1}) are also observed in the second derivative spectrum of the copper complex at pH 8.0, but with the solvent-exposed α-helix now being the main structure. At pH 9.0, the structure of the copper complex is almost entirely α-helix as suggested by the band at 1634 cm^{-1}. These results suggest a shift in the equilibrium between random-coil and α-helix structure as a function of pH.

Large spectral changes that could also indicate a structural change upon copper binding to peptide are the intensity ratio of the 1360/1340 cm^{-1} doublet. As mentioned in section 3.4.1.1, the 1360/1340 cm^{-1} doublet is assigned as arising from Trp (Harada et al., 1986), and can be used as a marker of the environment around the Trp residue. Thus, in the copper complex of Msp4, the higher intensity ratio of the 1360/1340 cm^{-1} doublet indicates the formation of more folded structure, in which the Trp residue becomes more buried. Ratio is highest at pH 9.0 indicative of almost complete complexation.

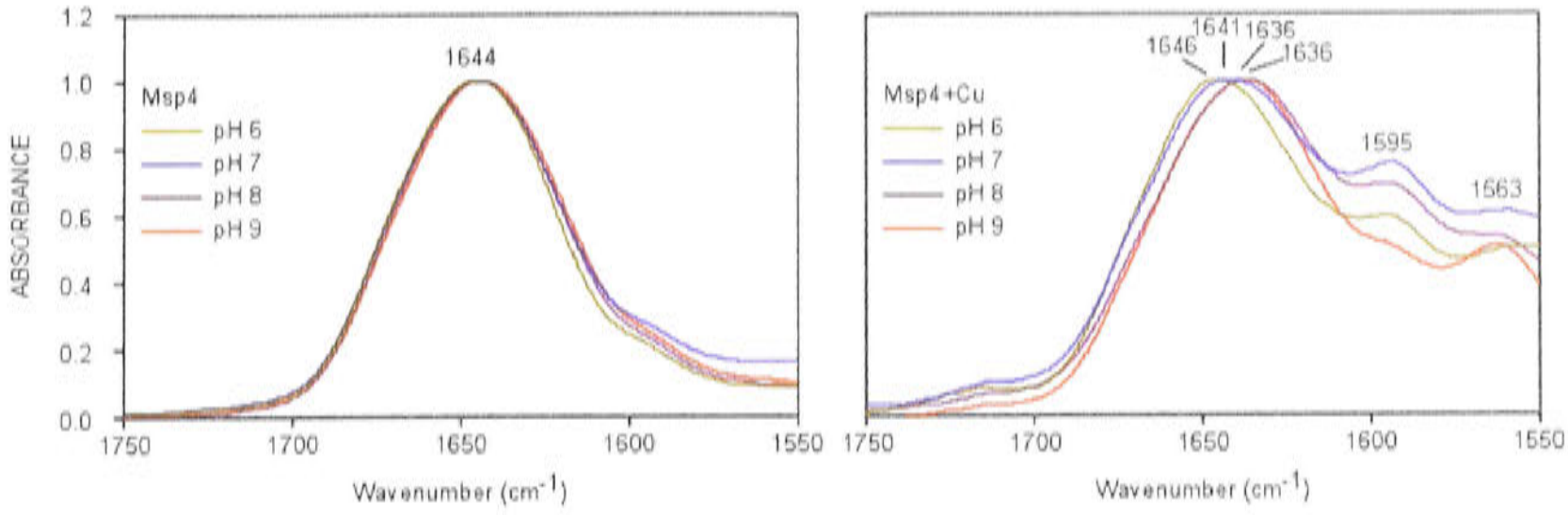

Figure 3.29: FTIR normalized absorbance spectra of Msp4 and copper complex of Msp4. The spectra of Msp4 in $^{2}H_2O$ at 2.5 mM peptide concentration, in the absence (left) and presence (right) of 10 mM $CuCl_2$, at pH 6.0, 7.0, 8.0, and 9.0.

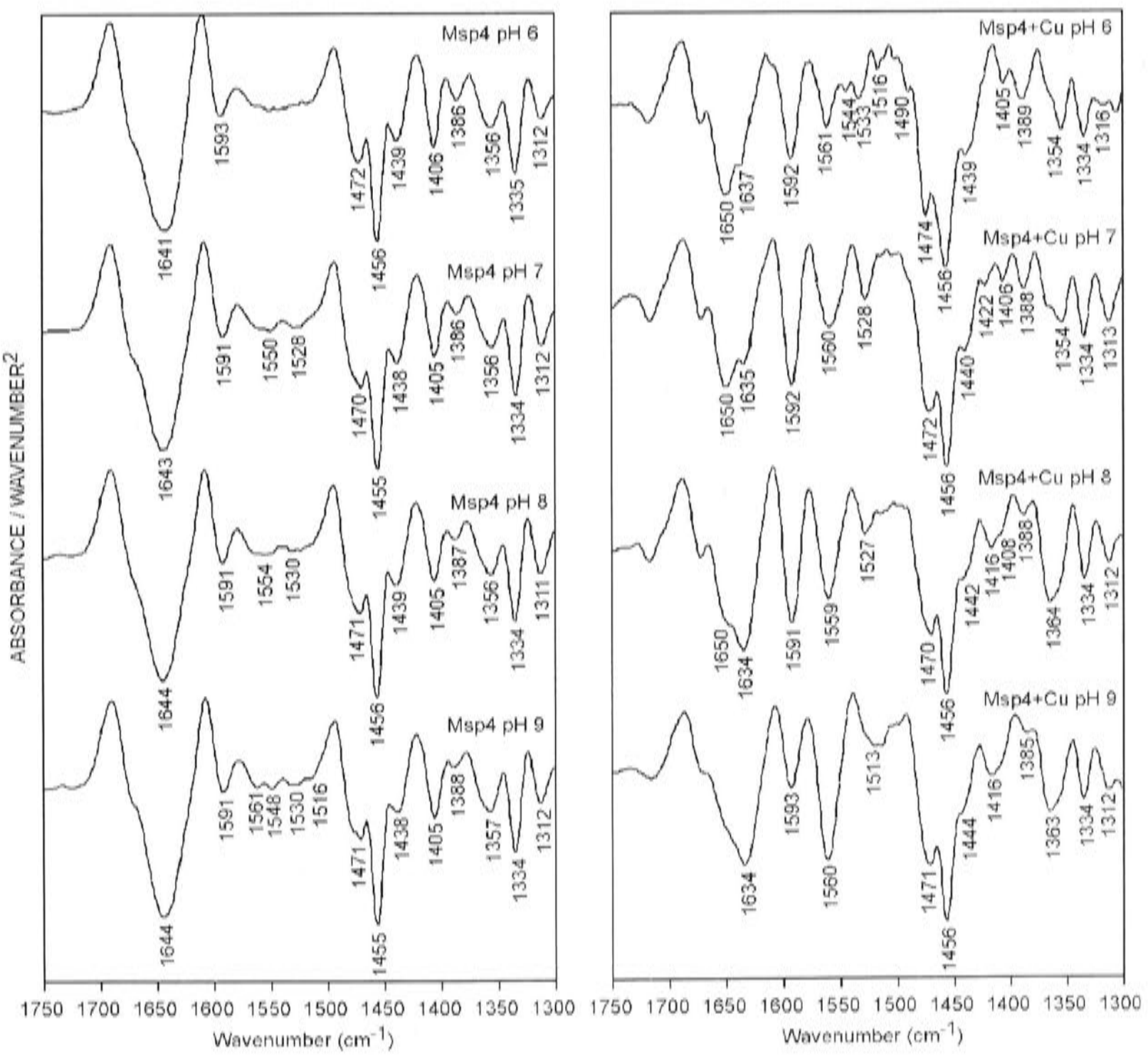

Figure 3.30: FTIR second derivative spectra of Msp4 and copper complex of Msp4. The spectra of Msp4 in $^{2}H_2O$ at 2.5 mM peptide concentration, in the absence (left) and presence (right) of 10 mM $CuCl_2$, at pH 6.0, 7.0, 8.0, and 9.0.

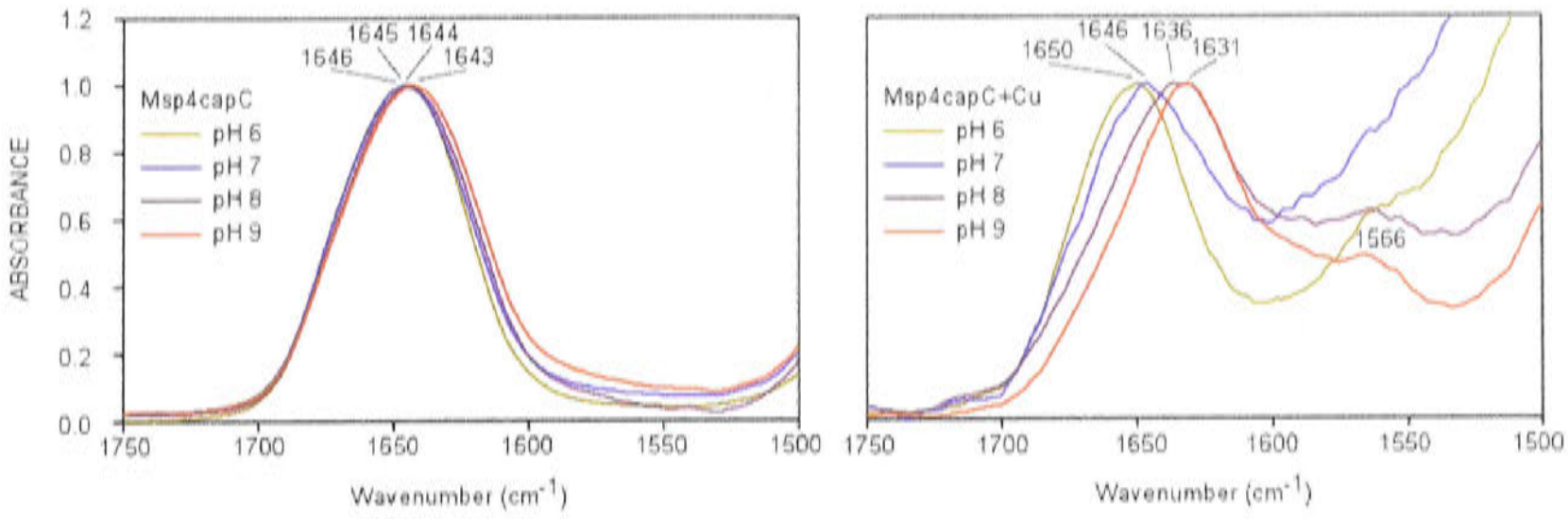

Figure 3.31: FTIR normalized absorbance spectra of Msp4capC and copper complex of Msp4capC. The spectra of Msp4capC in ^2H_2O at 2.5 mM peptide concentration, in the absence (left) and presence (right) of 10 mM $CuCl_2$, at pH 6.0, 7.0, 8.0, and 9.0. Large absorbance increases for pH 6.0 and 7.0 at lower wavenumber in right panel are due to HOD absorbance (wet ^2H_2O).

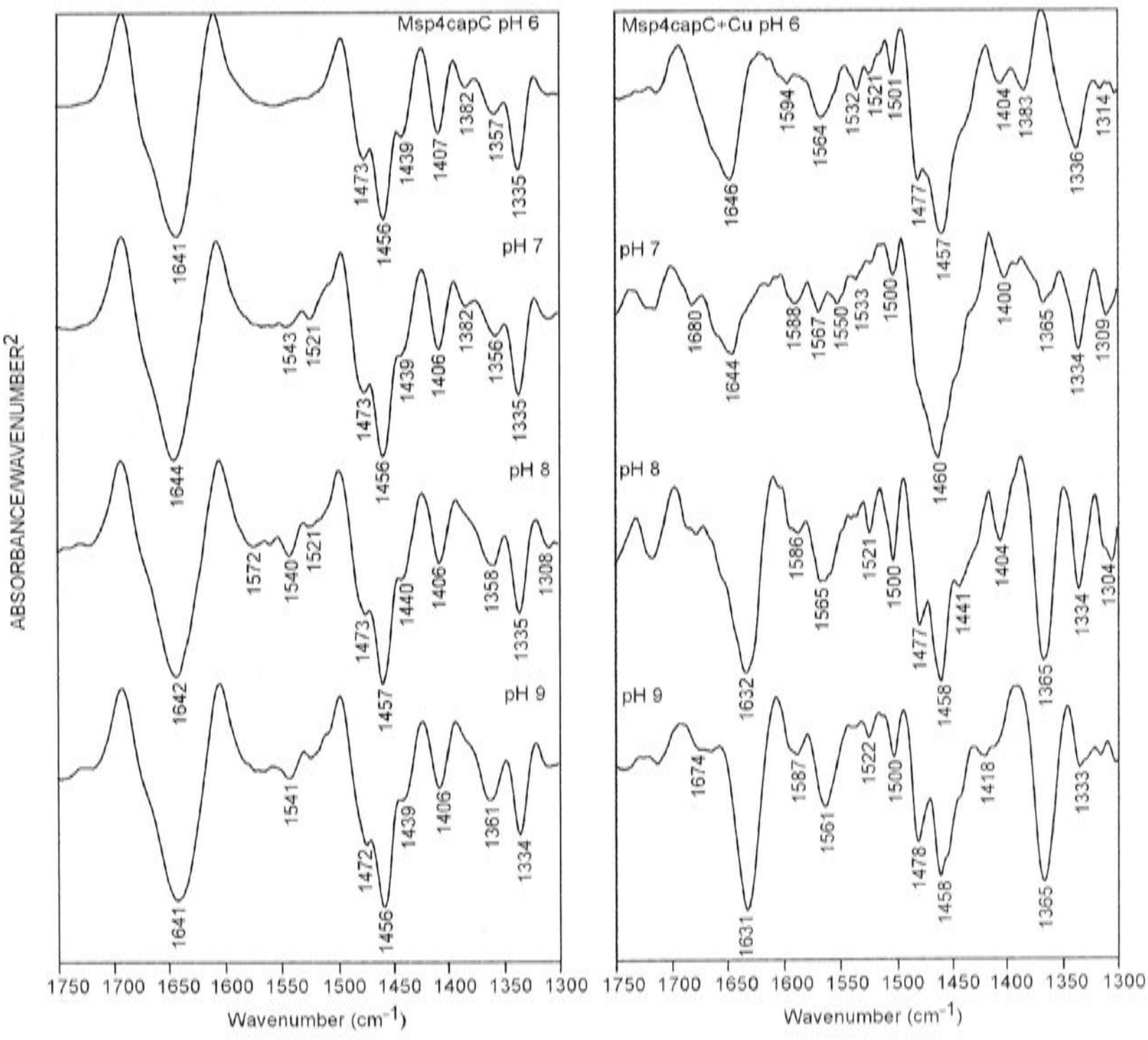

Figure 3.32: FTIR second derivative spectra of Msp4capC and copper complex of Msp4capC. The spectra of Msp4capC in ^2H_2O at 2.5 mM peptide concentration, in the absence (left) and presence (right) of 10 mM $CuCl_2$, at pH 6.0, 7.0, 8.0, and 9.0.

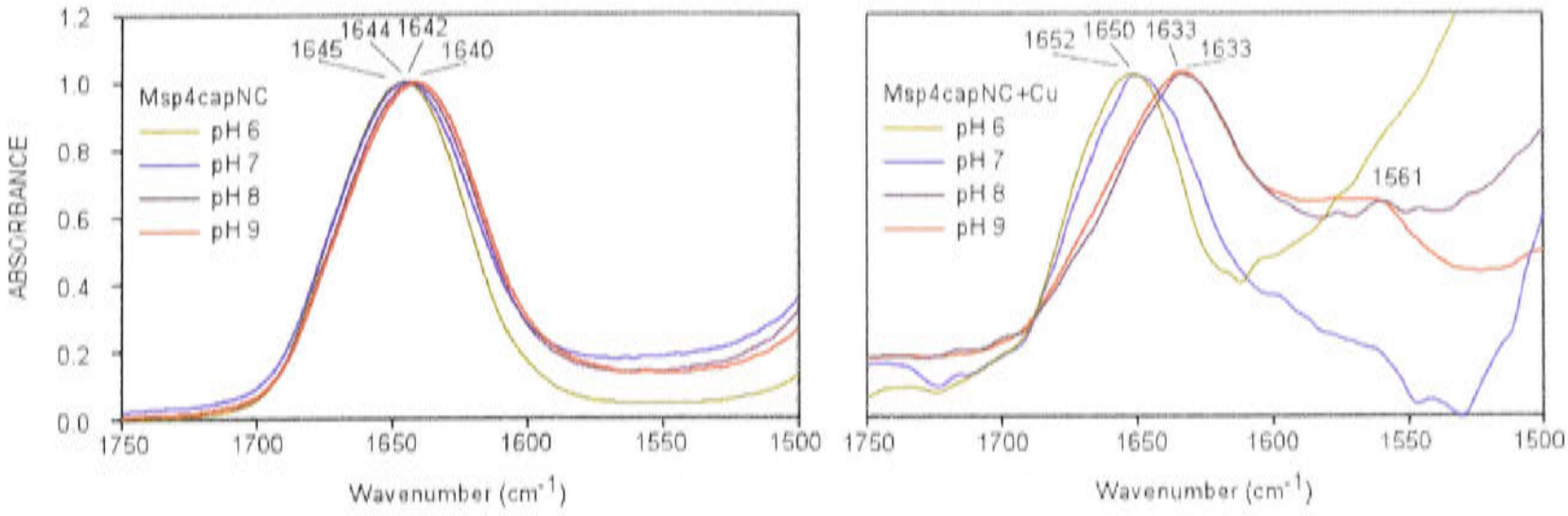

Figure 3.33: FTIR normalized absorbance spectra of Msp4capNC and copper complex of Msp4capNC. The spectra of Msp4capNC in ^2H_2O at 2.5 mM peptide concentration, in the absence (left) and presence (right) of 10 mM $CuCl_2$, at pH 6.0, 7.0, 8.0, and 9.0. Large absorbance increases for pH 6.0 and 7.0 at lower wavenumber in right panel are due to HOD absorbance (wet ^2H_2O).

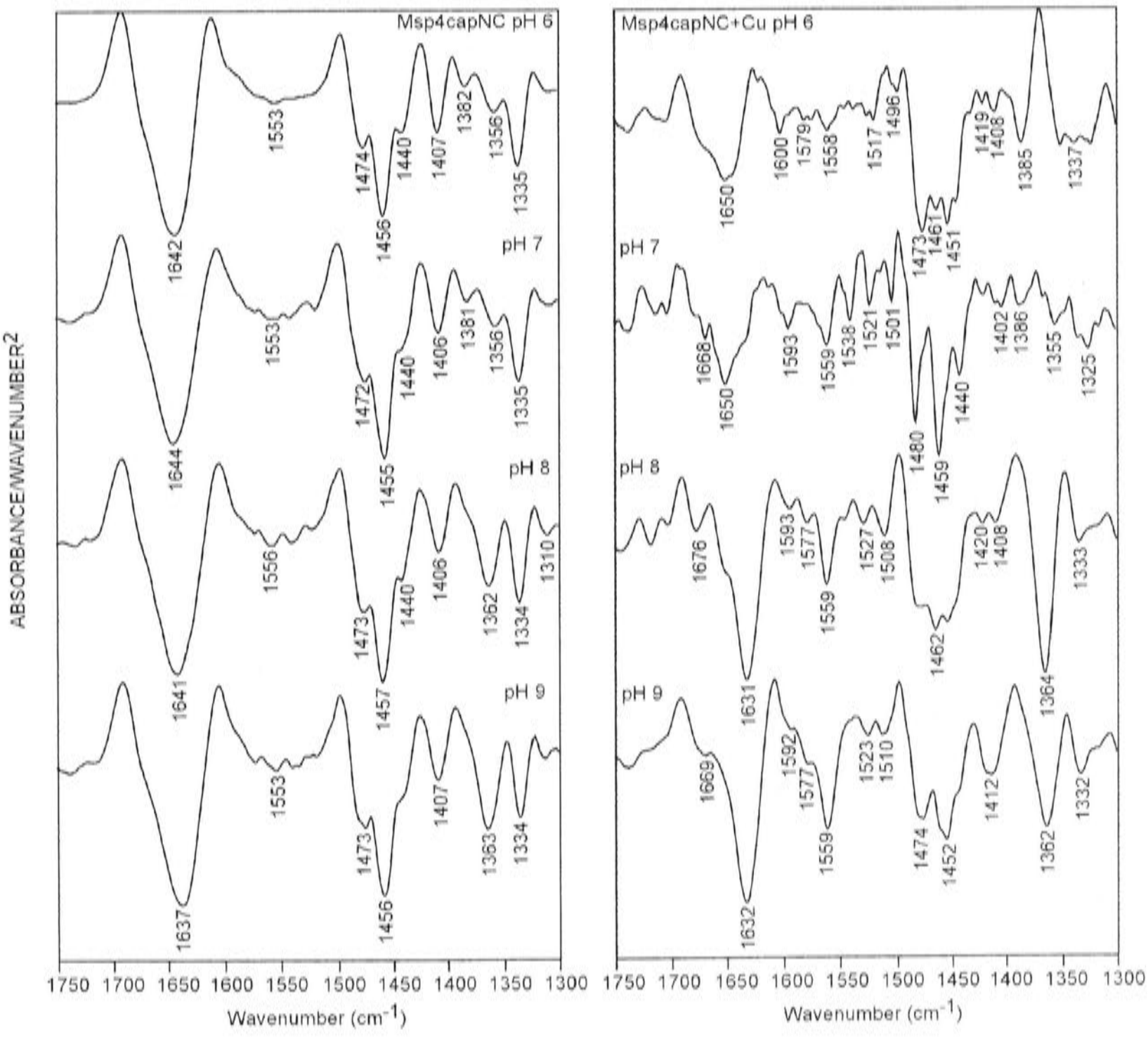

Figure 3.34: FTIR second derivative spectra of Msp4capNC and copper complex of Msp4capNC. The spectra of Msp4capNC in ^2H_2O at 2.5 mM peptide concentration, in the absence (left) and presence (right) of 10 mM $CuCl_2$, at pH 6.0, 7.0, 8.0, and 9.0.

Msp4capC+Cu. Absorbance and second derivative spectra (Figures 3.31 and 3.32, left panel, respectively) show that at pH 6.0-9.0 Msp4capC peptide adopts random-coil structure (the amide I band position at 1644-1641 cm^{-1}). Copper addition at pH 6.0 and 7.0 does not induce the formation of solvent-exposed α-helical structure as it does at pH 8.0 and 9.0. The high intensity ratio of the 1360/1340 cm^{-1} doublet also indicates the formation of more folded structure at pH 8.0 and 9.0, compared with pH 6.0 and 7.0.

Msp4capNC+Cu. The amide I band position of Msp4capNC at pH 6.0-9.0 (see Figures 3.33 and 3.34, left panel) suggests that the peptide adopts random-coil structure. Copper ion induces the formation of solvent-exposed α-helical structure in Msp4capNC at pH 8.0 and 9.0 as indicated by the position of the amide I band at 1633 cm^{-1} in the absorbance (Figure 3.33, right panel) and second derivative spectra (Figure 3.34, right panel). The high intensity ratio of the 1360/1340 cm^{-1} doublets suggests the formation of a much more folded structure in the copper complex at pH 8.0-9.0. The absorbance spectra of Msp4capNC at pH 6.0 and 7.0 in the presence of copper are very poor and much noisier. However, the position of the amide I band (1652-1650 cm^{-1}) and the low intensity ratio of the 1360/1340 cm^{-1} doublet indicate random-coil structure.

Preliminary conclusion. As observed in the spectra of the previous two peptides, the spectra of the copper complex of Msp4 peptides also show two components of the amide I band (random-coil and α-helix structure), which reflect either the conformational heterogeneity within the same molecule or the presence of complexed and uncomplexed molecules.

3.4.7. Copper-binding sites in multi-repeat (Msp2, Msp3, and Msp4 group) peptides.

In the absence of stoichiometry data under similar experimental conditions, copper-binding modes in multi-repeat peptides are difficult to predict. The role of the free imino group of Pro on binding of copper ion in multi-repeat peptides is evident from the lack of changes in the spectra of all capNC peptides, particularly at neutral pH and below. The appearance of the 1564 cm^{-1} band in copper-complex peptides indicates the coordination of the His side chain. The small shoulder at 1418 cm^{-1}, which is the $C{=}O/C{-}N^-$ stretching of the deprotonated amide backbone, is also observed. Generally,

upon increasing pH to 9.0, this 1418 cm^{-1} band becomes stronger and appears as a discrete band. Overall, these data suggest that the possible copper-binding sites in the N-terminally uncapped multi-decarepeat peptides at neutral pH are the terminal imino group of Pro, the N_π atom of the His side chain, and the nitrogen atom of the peptide backbone. The fact that the free imino terminal group of Pro is so important for copper binding indirectly suggests that the binding occurs only in the first repeat, where the imino group is the anchoring site. Therefore, in this case and assuming the stoichiometry is one copper ion per peptide molecule, the copper-coordination sphere in multi-repeat peptides will be the same as that for single-repeat peptide. However, we cannot eliminate the possibility that the subsequent repeat(s) would also bind copper ion, probably through the His side chain (as an anchoring site) and amide nitrogen. Nonetheless, this binding will only occur at high pH, where copper coordination to the His side chain can be supported by the deprotonated amide nitrogen of the fourth and fifth Gly residues.

The proposed binding mode described above could explain the phenomenon of the amide I band splitting reflecting the presence of conformational heterogeneity within the same peptide molecule. As copper binding in the multi-repeat peptides only occurs in the first repeat at low pH, this part of the peptide is likely α-helical but the C-terminal end still random coil. At higher pH, the complexes contain more α-helical content because subsequent repeat(s) bind copper ion via His and the amide backbone.

3.4.8. Copper titration of Msp1 at pH 8.0

Figure 3.35 (A) shows the second derivative spectra obtained from copper-ion titration of Msp1, while (B) shows the plot of band intensity as a function of copper concentration.

At 2.5 mM copper (1:1 ratio of copper to Msp1 concentration), the band at ~1617 cm^{-1} starts to emerge. Addition of more copper increases the intensity of the ~1617 cm^{-1} band, which, as discussed in section 3.4.1.2, has two origins: the intermolecular antiparallel β-sheet structure and the deprotonated amide backbone. Above 5.0 mM copper concentration, the intensity of this band plateaus.

(A)

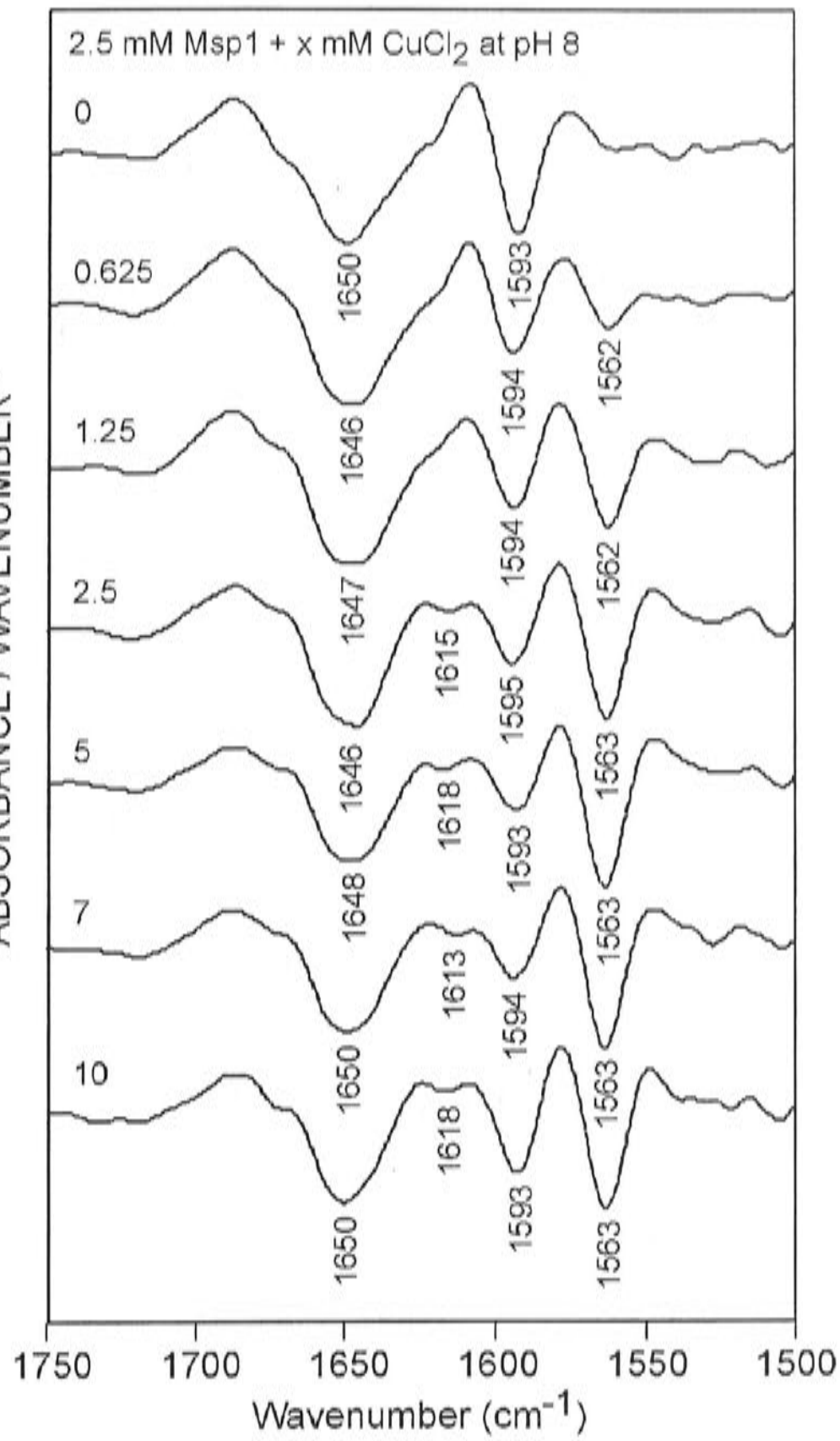

(B)

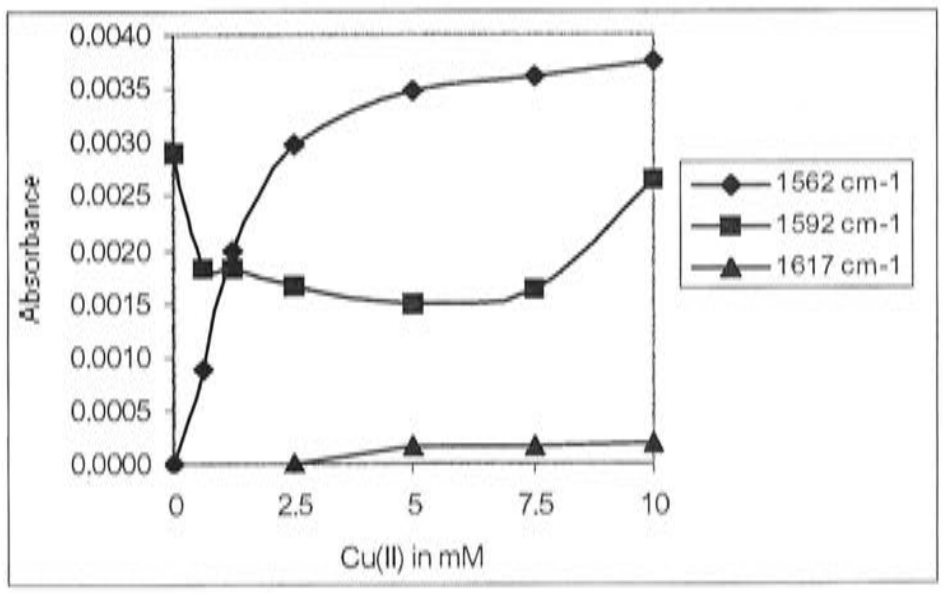

Figure 3.35: Copper titration of Msp1 at pH 8.0. (A). FTIR second derivative spectra of Msp1 in ^2H_2O at 2.5 mM peptide concentration, in the absence and presence of various amounts of $CuCl_2$, at pH 8.0. (B). Plot of absorbance versus copper concentration. The half height of the curve of absorbance at 1562 cm^{-1} versus copper concentration indicates a K_d of 1.7 mM.

The intensity of the 1562 cm^{-1} band increases upon addition of copper and then starts to level out, while the intensity of the ~1592 cm^{-1} band decreases, reaching its lowest value at 5 mM copper concentration, and then increases as more copper is added. The decrease of the band at ~1592 cm^{-1} could reflect a shift of the tautomeric form from II to I upon interaction with copper ion, while the increase indicates that this band has more than one vibrational origin.

The band at 1562 cm^{-1} was taken as a marker band for copper binding to Msp1 peptide. The intensity of this band was plot against the copper concentration. The shape of the curve (Figure 3.35 (B)) shows the binding is under equilibrium conditions, rather than stoichiometric conditions, from which we can only extract accurate information about the K_d but not stoichiometry. The half height of the maximum indicates a K_d value of 1.7 mM. This K_d value is 6 orders of magnitude greater than the value obtained from fluorescence titration spectroscopy (Chapter IV), which is in the nM range. The peptide concentrations employed in each method differ greatly: FTIR requires peptide in the mM range, while fluorescence measurements are made in the μM range. The result indicates the dependence of the K_d value on peptide concentration.

3.4.9. Binding of other metals to Msp1 and Msp4

The possibility that other metals bind to Msp1 and Msp4 has been investigated. As shown in Figure 3.36, addition of other metal ions (Zn^{2+}, Ca^{2+}, Mn^{2+}, and Mg^{2+}) at pH 8.0 does not change the conformation of Msp1, as suggested by the frequency of the amide I band at ~1652 cm^{-1}, and lack of the 1617 cm^{-1} band. The possibility that Msp1 binds Zn^{2+} without inducing structural changes is suggested by changes in some bands. Upon addition of Zn^{2+}, a weak band appears at 1572 cm^{-1}, suggesting binding to the nitrogen atom of the imidazole ring of His, most likely the N_π atom.

Addition of Zn^{2+} to Msp4 resulted in a dramatic change in the amide I band (see Figure 3.37). A weak component band appears at 1684 cm^{-1} and a shoulder appears at 1630 cm^{-1}. The appearance of these two weak bands probably reflects the formation of an intramolecular β-sheet structure in the zinc-bound form of Msp4. Upon addition of Ca^{2+} and Mg^{2+} to Msp4, the amide I band becomes broader, suggesting the possibility of metal binding to the C=O group of the amide backbone and to the terminal COO^- group.

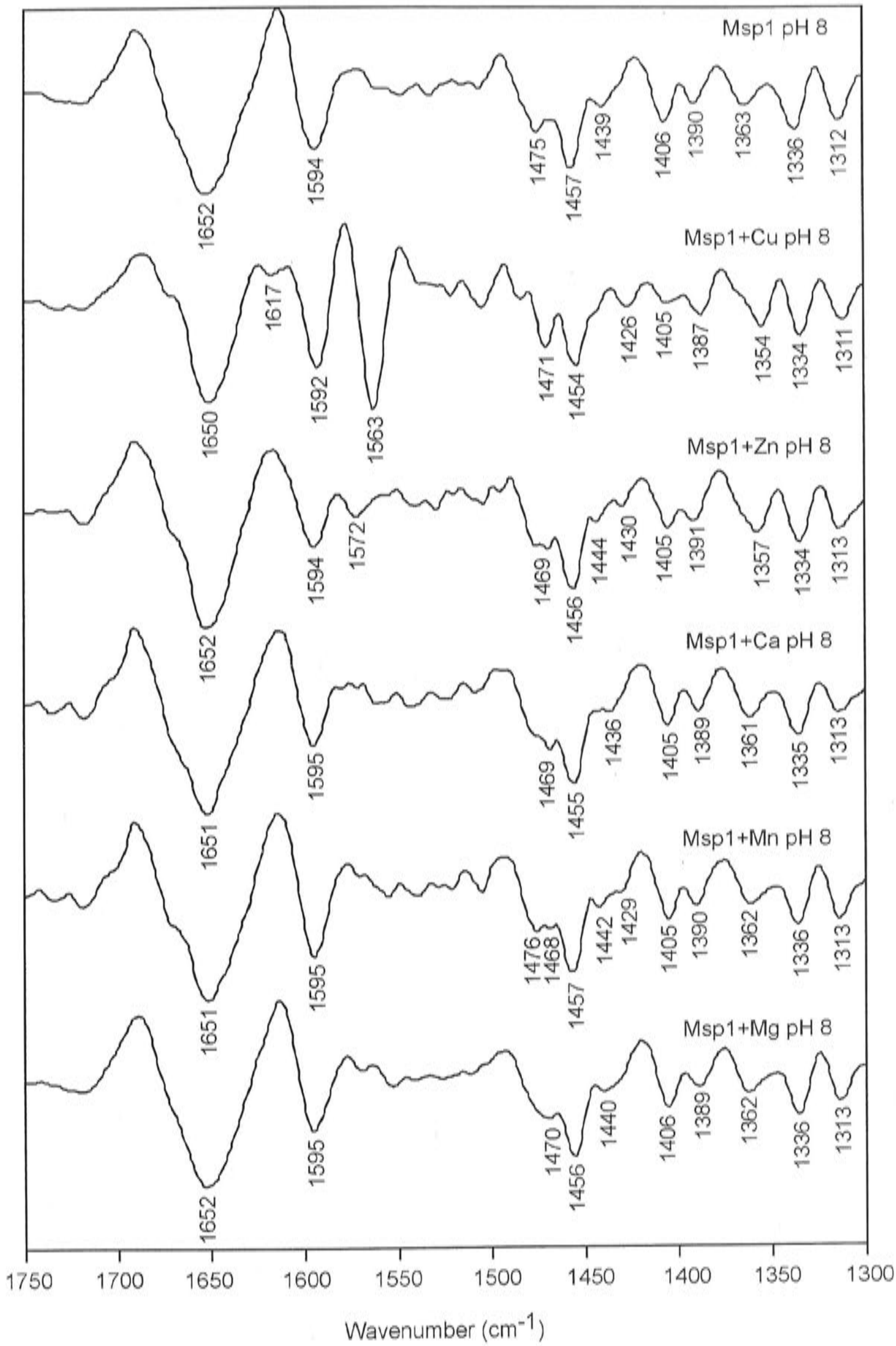

Figure 3.36: Binding of other metals to Msp1 peptide. FTIR second derivative spectra of Msp1 in ^2H_2O at 2.5 mM peptide concentration, in the absence and presence of 10 mM metal salts ($CuCl_2$, $ZnCl_2$, $CaCl_2$, $MnCl_2$, and $MgCl_2$), at pH 8.0.

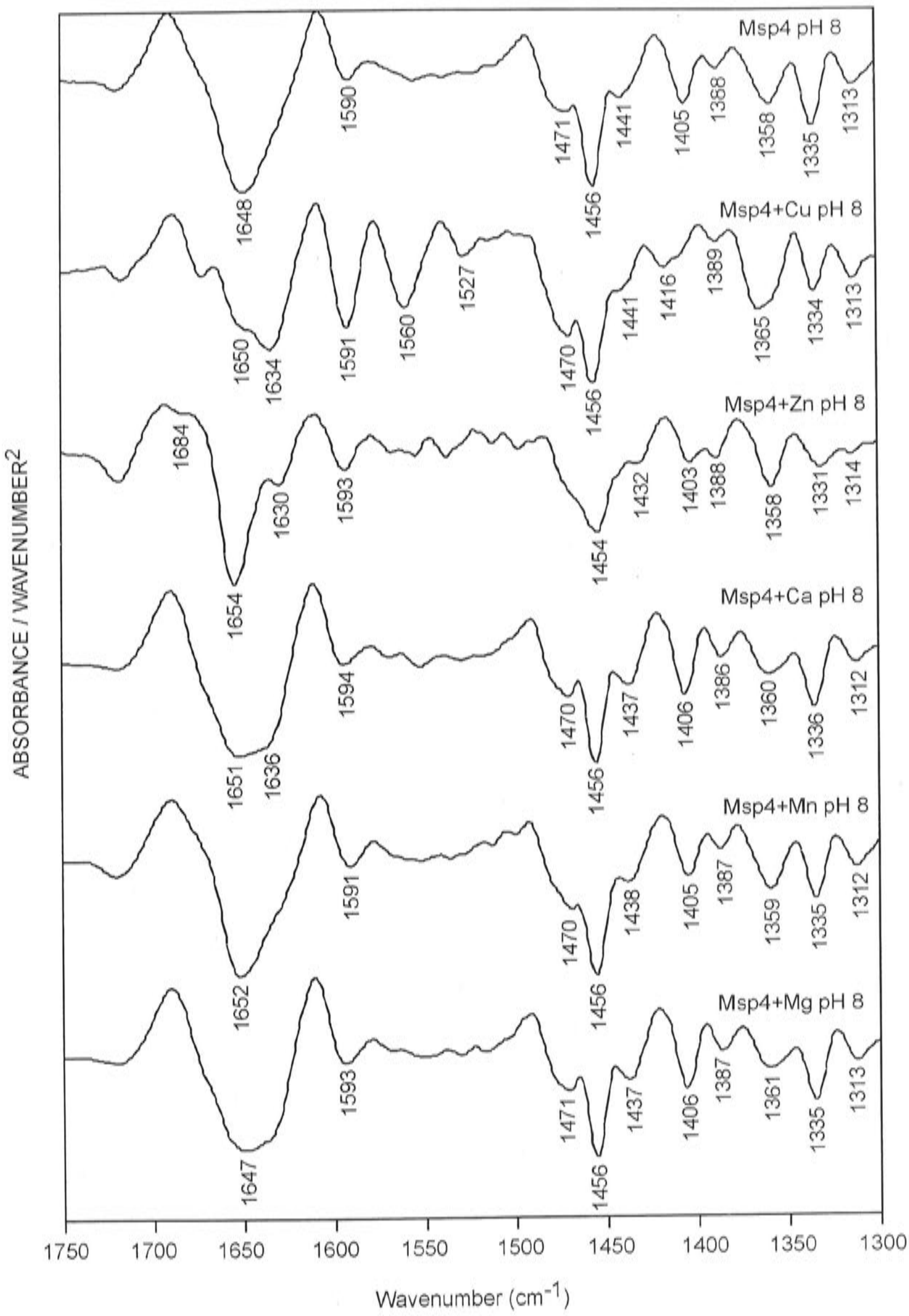

Figure 3.37: Binding of other metals to Msp4 peptide. FTIR second derivative spectra of Msp4 in ^2H_2O at 2.5 mM peptide concentration, in the absence and presence of 10 mM metal salts ($CuCl_2$, $ZnCl_2$, $CaCl_2$, $MnCl_2$, and $MgCl_2$), at pH 8.0.

3.5. Conclusions

Information on the conformation of PrP-repeat peptides of marsupial origin has been obtained. In the absence of copper, the structure of the repeat peptides is random coil, as suggested by the position of the amide I band. Interaction with copper ion induces the formation of more hydrogen-bonded structure. Although short repeats (Msp1, 11 residues and Msp2, 21 residues) show some structural modification towards more ordered structure upon interaction with copper, the major increase in helical content occurs in the long-repeat (Msp3, 31 residues and Msp4, 41 residues) peptides.

Modes for copper binding in the marsupial PrP-repeat peptides have been proposed, based on their FTIR spectra. These binding modes differ from those proposed for human PrP repeats. Also as marsupial PrP has four repeats, each with slightly different sequence, the binding modes differ from each other. It is suggested that the first-repeat sequence (PQGGGTNWGQ) does not bind copper ions. The lack of a His residue prevents copper binding to this repeat, while the GGG segment does not appear sufficient to mediate the binding by itself. The second- and third-repeat sequences (PHPGGSNWGQ PHPGGSSWGQ) are deduced to bind copper ion at pH 8.0 and above, based on the assignment of the FTIR spectra of the Msp2capNC peptide (PHPGGSNWGQ PHPGGSNWGQ). The fourth-repeat sequence (PHGGSNWGQ) binds copper ion well at pH 8.0 and possibly also at lower pH. In this peptide copper ion binds predominantly to the N_τ atom of the second His and the nitrogen atoms of the third and fourth Gly amides. Thus overall, it is proposed that the marsupial PrP-repeats region binds only one copper ion below pH 8.0, while at pH 8.0 and above it will probably bind two copper ions. However, this stoichiometry still needs further clarification. A substantial literature implicates a role for mammalian PrP in regulating intracellular copper concentration (refer to Chapter I). The findings here support a similar mechanism for regulating intracellular copper concentration in marsupial brain.

Mutation of the third Pro residue into Gly in the second-repeat sequence (PHPGGSNWGQ into PHGGGSNWGQ) changes the binding pattern significantly. This peptide binds copper very effectively at pH 8.0 and below, via Cu-N_π and Cu-N_τ bonds of His and a Cu-N bond of the amide backbone of the third and fourth Gly residues. This mutated sequence is analogous to the mammalian PrP-repeat sequence in

the first half of the repeat: the results suggest that mammalian PrP-repeats are more effective at binding copper than the marsupial PrP-repeat region.

The experiments also showed copper complexes of multi-repeat peptides at pH 8.0 and below have very low solubility compared with the single-repeat peptide. This low solubility is associated with more folded structure in which the Trp environment is more shielded from solvent. The consequences of this for the solubility of the multi-repeat region of marsupial PrP when embedded in the complete protein are not predictable, but lead to a reduction in overall protein solubility. Copper-bound repeats may also be less available for proteolysis or may configure the protein for enhanced binding with other ligands, such as sugar.

Chapter IV

Fluorescence Titration Spectrophotometry

Fluorescence spectrophotometry is a widely used technique in the study of protein-ligand interactions. Although it does not provide detailed structural information, the technique can be used to characterize functionality and biochemistry of a protein or peptide by studying the binding of particular compounds. In this project, fluorescence spectrophotometry has been used to characterize one proposed function of PrP, namely the binding of copper ions to synthetic peptides of the N-terminal tandem repeat region of a marsupial PrP (Msp).

4.1. Introduction

Fluorescence is the process that occurs when a molecule absorbs light at a particular wavelength and then quickly re-emits the energy at a slightly longer wavelength. Fluorescence occurs in certain molecules, which are called fluorophores. The fluorescence properties of these molecules arise from delocalized electrons formally present in conjugated double bonds. The fluorescence process is illustrated in Figure 4.1, which is the energy level diagram also known as a Jablonski diagram. The diagram shows that absorbing light will excite the electron of the fluorophore from the lowest energy level, S_0 (singlet ground state), to a higher energy level of either S_1 (first singlet state) or S_2 (second singlet state). The fluorescence radiation occurs when the paired electron returns from the first excited state to the ground state (Lakowicz, 1983 p.4).

The fluorescence of proteins originates from Phe, Tyr, and Trp residues. In most proteins the fluorescence of Tyr and Phe residues is greatly exceeded by that of Trp residues: the extinction coefficient at the wavelength of excitation and the quantum yield of emission of Trp are considerably greater than the respective values for Tyr and Phe. The fluorescence sensitivity, which is the quantum yield multiplied by the extinction coefficient, is 730 for Trp, 200 for Tyr and 4 for Phe (Schmid, 1997).

The emission maximum of Trp is highly sensitive to solvent polarity, as well as to specific interactions between the solvent and the indole ring. As a result, the emission maximum of proteins is dependent upon these factors, which affect the exposure of the

Trp residues to the aqueous phase (Lakowicz, 1983 p.354). The sensitivity of Trp fluorescence to the surrounding environment thus makes it a very useful probe to study the binding of protein to ligand. The association of a ligand with a protein to form a complex is sometimes accompanied by a change in the fluorescence spectrum of the protein, due to changes in protein conformation. The emission maximum of Trp in the protein will be blue shifted if the binding of ligand results in Trp being more buried in the interior of the protein and shielded from contact with the solvent water. When binding causes Trp to be more exposed to water, a red shift will occur (Lakowicz, 1983 p.358-359). Such shifts of the emission maximum, resulting from conformational changes, are often accompanied by a decrease in the emission intensity. These properties of Trp fluorescence provide considerable potential for quantification of association reactions between proteins and other molecules.

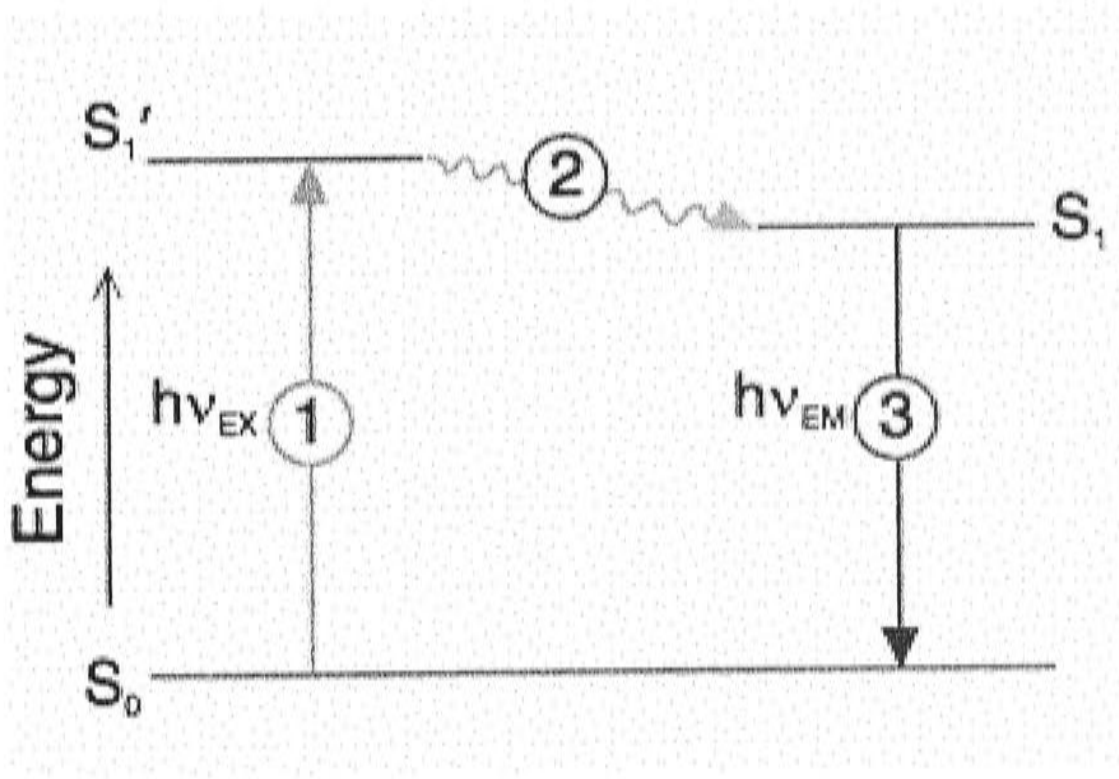

Figure 4.1: Jablonski diagram illustrating the processes involved in the creation of fluorescence. Excitation (1), a molecule is initiated with a photon of energy $h\nu_{EX}$ creating an excited electronic singlet state (S_1') from the ground state (S_o); excited state lifetime (2), typically 1–10 nanoseconds, during this time, the fluorophore loses part of its energy due to its interaction with the environment resulting in a relaxed singlet excited state (S_1); fluorescence emission (3), the fluorophore returns to its ground state by emitting a photon of energy $h\nu_{EM}$ (Haughland, 2001).

Besides the presence of intrinsic fluorophores such as Trp, the quantification of the binding process between protein and ligand using the fluorescence method must meet several other conditions. According to Pesce (1971), first, the changes in fluorescence should be rapid relative to the binding process, so that the only time-dependent processes are the actual binding processes. The second condition is the dissociation constant, which should be about 10^{-8} M or more in order to be able to detect changes

due to ligand binding, given the lowest protein concentration that can be managed (Pesce, 1971 p.212).

All of the above requirements are fulfilled in the copper-binding PrP-repeats system. Fluorescence spectrophotometry has previously been used to study copper binding to the repeats (Hornshaw et al., 1995a; Jackson et al., 2001; Kramer et al., 2001). In this case, the measurable parameter is the fluorescence quenching of the intrinsic Trp (or Tyr for avian repeats) upon binding of copper. The fluorescence results reported in the literature are included in Table 1.3 of Chapter I.

Table 1.3 indicates that binding of copper to synthetic peptides containing four tandemly repeated units of the consensus sequence of the human PrP octarepeats ($[PHGGGWGQ]_4$) (Octa4) showed a measured K_d of 6.7 μM, while for the chicken PrP hexarepeat ($[NPGYPH]_4$) (Hexa4) the value was 4.5 μM (Hornshaw et al., 1995a). A similar binding affinity of 5.5 μM was reported for synthetic peptide spanning residues 60-91 of the N-terminal human PrP (Kramer et al., 2001), which contains the sequence of 4 consensus octarepeats ($[PHGGGWGQ]_4$), exactly the same as Octa4 reported by Hornshaw et al. (1995a). The affinity and cooperativity were increased if the octarepeat region was C- and N-terminally extended. Thus, the affinity for copper binding to human PrP_{60-109} was reported as 2.5 μM, and to human PrP_{23-98}, human PrP_{23-112}, and human PrP_{23-231} all as 2.2 μM (Kramer et al., 2001). Copper ions also bind to the C-terminal structured part of murine $PrP_{121-231}$ with a dissociation constant of 8 μM (Kramer et al., 2001).

As mentioned in Chapter I, the K_d values in the micromolar range obtained from fluorimetry experiments of Hornshaw et al. (1995a) and Kramer et al. (2001) are in good agreement with those from other methods, but in contrast to one fluorimetry study by Jackson et al. (2001). Jackson et al. (2001) measured the copper-binding affinity of PrP_{52-98} in the presence of a weak chelator, Gly (500 μM), and obtained an apparent K_d of 3.2 μM, that when back calculated from the competitive buffering effect of Gly resulted in a real K_d of 8 fM. Jackson et al. (2001) argued that incorporation of Gly in the system abolished the weak binding, and weakened the apparent binding affinity of the tight sites, to a level that is measurable by fluorescence. In the absence of Gly, the

only measurable signal observed represents binding to the weak site, while the tight site has already been saturated in the early states of titration. Jackson et al. (2001) also show that the real K_d was unaffected by the Gly concentration. This suggested Gly as a suitable chelating agent to weaken the affinity of the tight sites (Jackson et al., 2001). However, this idea has been challenged by recent CD experiments of Garnett and Viles (2003), which show that Gly, for which the affinity for copper is 12 nM, completely abolishes the binding between copper and the human repeat peptide (PrP_{58-91}). Thus, Garnett and Viles (2003) suggest that the affinity of copper binding to PrP-repeat peptide should be less than the affinity of copper binding to the amino acid Gly, or the K_d value should be higher than 12 nM (Garnett and Viles, 2003).

To measure binding equilibria, it is necessary that experimental conditions be such that free peptide, free ligand, and protein complex are all present in detectable concentrations (in equilibrium). To achieve this condition, the concentration of peptide must be less than or about equal to K_d, and certainly not greater than a factor of 10 different (Pesce, 1971 p.211; Bagshaw and Harris, 1987). So to be able to identify the tight binding sites for copper in PrP in the absence of a weak chelator, the peptide concentration would need to be of the same order as the K_d. This requirement sometimes cannot be fulfilled, especially if the intrinsic Trp is used as a fluorophore, as it can only be detected down to about 100 nM in the best of cases; this is a drawback of using Trp as a fluorescence probe. Hence, the method of using a weak chelating agent to elucidate the tight copper-binding site in PrP, such that has been developed by Jackson et al. (2001), could be an alternative way of elucidating the tight binding site. However, it would be good to confirm this method by using a different type of chelator with different copper-binding affinity. If the method is valid, then by varying the type of chelator, the real K_d of copper binding to PrP should remain the same.

4.2. Aims

Fluorescence spectrophotometry experiments were performed to measure the K_d of complexes between Msp peptides (see Table 4.1) and copper ions at various pHs. Experiments using mutant Msp1 peptides, His-methylated peptides, and peptides with modified repeat sequence were carried out to gain information on the possible roles of some residue groups in copper binding.

4.3. Materials and methods

4.3.1. Sample preparation

Table 4.1: Synthetic peptides used in the experiments.

Group	Peptide	Sequence	Size
Msp4 group	Msp4	$(PHPGGSNWGQ)_4G$	41
	Msp4capC	$(PHPGGSNWGQ)_4G\text{-}NH_2$	41
	Msp4capNC	$Ac\text{-}(PHPGGSNWGQ)_4G\text{-}NH_2$	41
Msp3 group	Msp3	$(PHPGGSNWGQ)_3G$	31
	Msp3capC	$(PHPGGSNWGQ)_3G\text{-}NH_2$	31
	Msp3capNC	$Ac\text{-}(PHPGGSNWGQ)_3G\text{-}NH_2$	31
Msp2 group	Msp2	$(PHPGGSNWGQ)_2G$	21
	Msp2capC	$(PHPGGSNWGQ)_2G\text{-}NH_2$	21
	Msp2capNC	$Ac\text{-}(PHPGGSNWGQ)_2G\text{-}NH_2$	21
Msp1 group	Msp1	PHPGGSNWGQG	11
	Msp1capC	$PHPGGSNWGQG\text{-}NH_2$	11
	Msp1capNC	$Ac\text{-}PHPGGSNWGQG\text{-}NH_2$	11
Msp1 variant and mutant	Msp1capN	Ac-PHPGGSNWGQG	11
	Msp1H2A	PAPGGSNWGQG	11
	Msp1N7A	PHPGGSAWGQG	11
	Msp1Q10A	PHPGGSNWGAG	11
Msp1 His-methylated	Msp1His(1Me)capC	$PH[\tau Me]PGGSNWGQG\text{-}NH_2$	11
	Msp1His(3Me)capC	$PH[\pi Me]PGGSNWGQG\text{-}NH_2$	11
Modified repeat sequences	Msp1P3GcapNC	$Ac\text{-}PHGGGSNWGQG\text{-}NH_2$	11
	Msp_1strepcapNC	$Ac\text{-}PQGGGTNWGQG\text{-}NH_2$	11
	Msp_4threpcapNC	$Ac\text{-}PHGGSNWGQG\text{-}NH_2$	10
	Hu1capNC	$Ac\text{-}PHGGGWGQG\text{-}NH_2$	9

Msp + Cu at different pHs. For the measurement of K_d at various pHs, 0.5 μM peptide (see Table 4.1) solution was prepared in 25 mM phosphate buffer pH 6.0, 7.4 and 8.0. The ionic strength of the solution was kept constant at 0.1 by incorporating 0.1 M NaCl in the buffer solution. The presence of 0.1 M NaCl also prevents nonspecific binding of copper to Msp peptides (Kramer et al., 2001). During the titration, incremental 1 μL aliquots of 100 μM $Cu(Gly)_2$ were added to the peptide solution in experiments at pH 6.0, 7.4, and 8.0. These experiments were performed before the Jackson et al. (2001) paper was published. The reason why copper ion was supplied as $Cu(Gly)_2$ was to prevent the precipitation of copper as copper hydroxide at the higher pH (Brown et al., 1997). The final concentration of Gly (2 x Cu) is much lower (0-2.5 μM) than in the experiments of Jackson et al. (500 μM). Also, the total concentration of copper ions added to the solution during the titration is very low, in most cases under 1 μM, so collisional quenching of Trp by copper ions and the inner filter effect of copper can be neglected.

Mutant Msp1 + Cu. The conditions for investigating copper binding to mutant Msp1 peptides were different: in each experiment 2 μM peptide (Msp1, Msp1capN, Msp1capNC, Msp1H2A, Msp1N7A, and Msp1Q10A) was used. During the titration, incremental 1 μL aliquots of 100 μM $CuSO_4$ were added to the peptide solution until the final concentration of $CuSO_4$ was 2.5 μM. The solution was maintained at pH 7.4 by PBS buffer (for concentrations of buffer components refer to section 2.2.2.1 of Chapter II).

4.3.2. Conditions of data acquisition and data analysis

The measurements were carried out using the LS 50B Perkin-Elmer Spectrofluorimeter. The temperature was regulated by means of a circulating water bath to be around 25 ± 0.2 ^{O}C. The sample, 3 mL Msp peptide (from 100 μM stock) solution in appropriate buffer, was placed in a 3 mL quartz cuvette with four-sided polished windows of path length 10 mm. The sample was excited at 280 nm with band slit width 5 nm. Emission spectra were recorded between 300 and 500 nm before and after addition of incremental 1 μL aliquots of copper ion solution.

To determine the K_d in conditions where the concentration of metal-binding sites was smaller than K_d (equilibrium binding conditions), quenching data were fitted to Equation 4.1 (Jackson et al., 2001). The fitting was carried out with non-linear least square methods using the computer program GraphPad Prism 3. However, most of the curves of fluorescence intensity (F) versus copper concentration [Cu] indicate that the experiments have been conducted under stoichiometric binding conditions where the peptide concentration is equal to or greater than K_d. Therefore, the binding data was fitted to the quadratically derived equation (Equation 4.2) (Jackson et al., 2001; Ozer and Tacal, 2001).

$$F=F_o-\{(F_o-F_s)[Cu]/(K_d+[Cu])\} \qquad \text{(Equation 4.1)}$$

$$F=F_o-\{(F_o-F_s)[(C_s+[Cu]+K_d)\pm\{(C_s+[Cu]+K_d)^2-4C_s[Cu]\}^{0.5}]/2C_s\} \qquad \text{(Equation 4.2)}$$

F_o F, and F_s are fluorescence at zero, sub-saturating and saturating copper concentration [Cu]. C_s is the concentration of copper-binding sites.

4.4. Results and discussion

4.4.1. The emission maximum of Msp peptides does not change upon copper addition

The wavelength of the emission maximum of Msp peptides is typically at 354-356 nm (see Figure 4.2). As this is the same as free amino acid Trp (Schmid, 1997), it indicates that Trp residues in the peptides are highly exposed to solvent. Upon copper binding the emission maximum does not change; this suggests that the Trp residues do not become more buried but are still exposed to water even though conformational changes take place. FTIR experiments (Chapter III) showed that the conformation of the Msp peptides in the absence of copper is random coil, while in the presence of copper it is a solvent-exposed α-helix. Both conformations would allow the Trp residues to be in contact with the solvent water, and are thus consistent with the unchanged emission maximum of the fluorescence spectra at 354-356 nm.

4.4.2. Titrations have been carried out under stoichiometric binding conditions

Copper-binding sites in Msp peptides, except in Msp1H2A, 0.1 μM Msp1capC, and 0.1 μM Msp4capC, are saturable as shown by the curves that reach a plateau at μM concentration (see Figures 4.3 - 4.10, and 4.12 – 4.15). The plot of fluorescence versus [Cu] is bi-phasic with no curved regions: most of the graphs except for copper binding to Msp1H2A (see Figure 4.12 D), 0.1 μM Msp1capC (Figure 4.14 E) and 0.1 μM Msp4capC (Figure 4.15 D) are composed simply of two linear segments. In the initial phase, increase in the copper ion concentration resulted in a linear decrease of fluorescence as long as there are sites available on the peptides. When all sites have been occupied the fluorescence no longer decreases; it reaches a saturation point, which occupies the second phase of the curve. The absence of a curvature region indicates the presence of extremely tight binding between copper and Msp peptides. This bi-phasic behavior also shows that the concentration of the peptides used in the experiment is far greater than the K_d. This condition is often referred to as stoichiometric binding in which either the peptide or ligand (or both) is fully bound (Pesce, 1971 p.208), and, therefore no free copper ions are left in the system. The binding curves that exhibit a sharp transition at the saturation point, indicating tight binding, were also observed for copper titration to segments of PrP octarepeat (HGGGW, HGGG, and HGG) (Garnett and Viles, 2003).

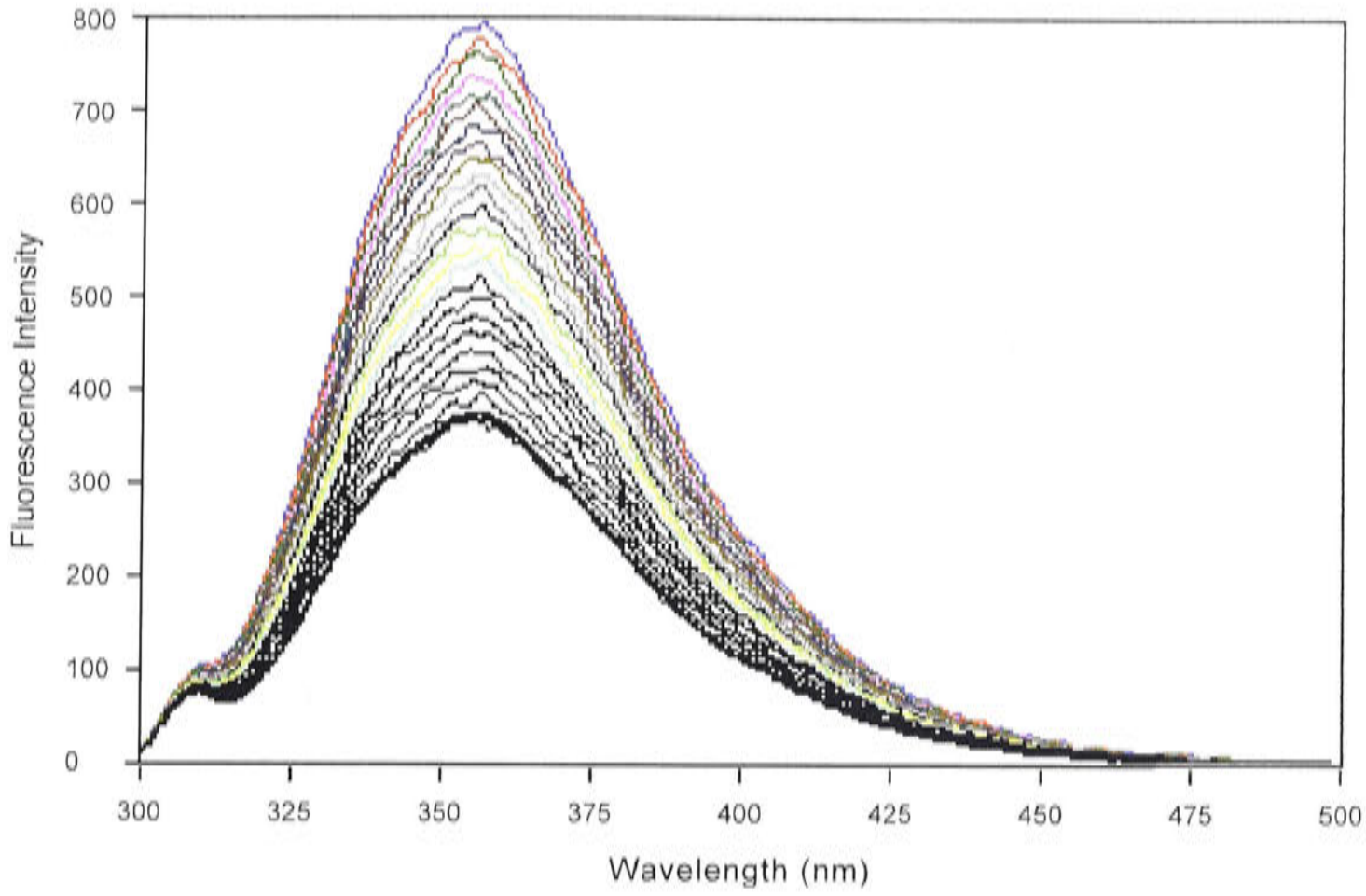

Figure 4.2: Typical fluorescence emission spectra (excitation at 280 nm) of Msp peptides during copper ion titration. Spectra of 2 μM Msp1N7A in PBS buffer pH 7.4 titrated with 1 μL aliquots of 300 μM $CuSO_4$.

4.4.3. Different equations used to describe different binding conditions

A straight line in the initial part of titration under stoichiometric binding conditions (Figures 4.3 – 4.10, and 4.12 – 4.15) shows a linear relationship between fluorescence intensity and the addition of copper ion solution. This is evidence for the validity of the assumption that the change in quantum yield of a protein or ligand is the same for each molecule of ligand bound (Pesce, 1971 p.220). This assumption is made for the validity of the usage of Equations 4.1 and 4.2.

From the fluorescence titration curves (see Figures 4.3 - 4.10, and 4.12 - 4.15), it is apparent that all titration experiments, except those with Msp1H2A (see Figure 4.12 D), 0.1 μM Msp1capC (Figure 4.14 E) and 0.1 μM Msp4capC (Figure 4.15 D), were conducted under stoichiometric binding conditions (Pesce, 1971 p.208). These data were best fitted by nonlinear regression analysis using Equation 4.2 (Jackson et al., 2001; Ozer and Tacal, 2001).

The graph of F versus [Cu] in Msp1H2A (see Figure 4.14 D), 0.1 μM Msp1capC (Figure 4.11 E) and 0.1 μM Msp4capC (Figure 4.12 D) shows the curvature region. This indicates that the binding between copper and these peptides is under equilibrium

conditions (Pesce, 1971 p.208). In this situation, free copper, free peptide, as well as the complex are present in the system. The K_d for copper binding to these peptides was calculated using Equation 4.1 (Jackson et al., 2001; Ozer and Tacal, 2001).

K_d values generated from analysis of the stoichiometric binding data that fit to Equation 4.2 are very approximate, even though the R^2 values in most cases are reasonably high. Under stoichiometric conditions, the binding parameter that can be determined with reasonable accuracy is the number of binding sites or the binding stoichiometry (in Equation 4.2 it is represented as C_s), while in the equilibrium binding conditions it is the K_d value that can be accurately determined.

4.4.4. Copper-binding properties of Mspn (n = 1, 2, 3, and 4) group peptides

4.4.4.1. The effect of N-terminal capping on copper binding to the peptides

The experiments show that copper addition to uncapped Msp1 and Msp1capC peptides resulted in quenching of Trp fluorescence intensity, which suggests binding occurs between the peptides and copper ions. Copper ion addition to the Msp1capNC peptide, on the other hand, does not result in quenching of Trp fluorescence intensity, indicating no binding between the peptide and copper ion, and suggesting that copper binding to the peptide requires the free imino group of Pro at the N-terminus. These data are in good agreement with FTIR results, which also show the importance of the imino group of Pro in copper binding.

4.4.4.2. The K_d values for copper binding to the peptides at pH 6.0, 7.4, and 8.0

Quantitative data in Table 4.2 show that pH has a significant influence on the K_d values for copper binding to Mspn group peptides. Several experiments at pH 7.4 and 8.0 result in K_d values that do not differ if the errors are taken into account. K_d values at pH 6.0 are generally much higher than values at pH 7.4 and 8.0, which indicates weaker binding, which is likely due to the His residue being protonated. Several points regarding the K_d values in Table 4.2 are discussed below.

The large error in the K_d value for copper binding to Msp1capC at pH 8.0 (0.2 ± 0.2 nM; see Figure 4.4.F and Table 4.2) indicates it is only approximately determined. As

has been pointed out in the above section, the binding conditions under which these data were acquired is stoichiometric binding conditions, where K_d determination is not accurate.

One K_d value for copper binding to Msp2capC at pH 7.4 is 1.1 nM with no standard error, as the data have been fitted to Equation 4.2 by incorporating this K_d value as a constant to get the best R^2 parameter.

K_d values for copper binding to Msp3capC and Msp4capC show large variation between duplicate experiments. The large variation suggests sensitivity to set up, and may also be due in part to fact that the experimental conditions (stoichiometric binding conditions) are not appropriate for the determination of K_d. Also, in Msp4capC, the differences in K_d as a function of pH are not so prominent.

The K_d values for copper binding to Mspn (n = 1, 2, 3, 4) group peptides (see Table 4.2) are in the nM range. This is significantly lower than values for copper binding to other PrP peptides reported in the literature (see Table 1.3 of Chapter I), where the measurements were conducted using the fluorimetry method, but in the absence of a chelator (Hornshaw et al., 1995a; Kramer et al., 2001). However, the difference between these K_d values and those of Hornshaw and Kramer probably arise mainly from the difference in the way the data have been analyzed. Hornshaw et al. (1995a) utilized linear regression analysis, which is the double reciprocal plot of the binding data, while Kramer et al. (2001) employed a modified Stern-Volmer equation to calculate the K_d. However, some differences will also result from the different repeat sequence (we have used marsupial PrP sequence) and other experimental conditions (pH, peptide concentration, etc.). K_d values here fall between the fM (Jackson et al., 2001) and μM ranges (Hornshaw et al., 1995a; Kramer et al., 2001) reported for copper binding to PrP-repeat peptides obtained from fluorimetry experiments. Garnett and Viles (2003) predict the K_d values for human repeats are between 10 nm – 10 μM (see Table 1.3 of Chapter I).

The effect of pH on the K_d value (lower pH resulted in higher K_d and vice versa) is consistent with a proposed function of PrP as a copper transport protein, which shuttles

copper ions from the extracellular milieu to endolysosomes (Pauly and Harris, 1998). As the pH of the extracellular space is neutral and the pH of the endolysosomes is slightly acidic, it can be predicted that copper will bind more tightly to PrP in the extracellular space and will dissociate in the endolysosomes.

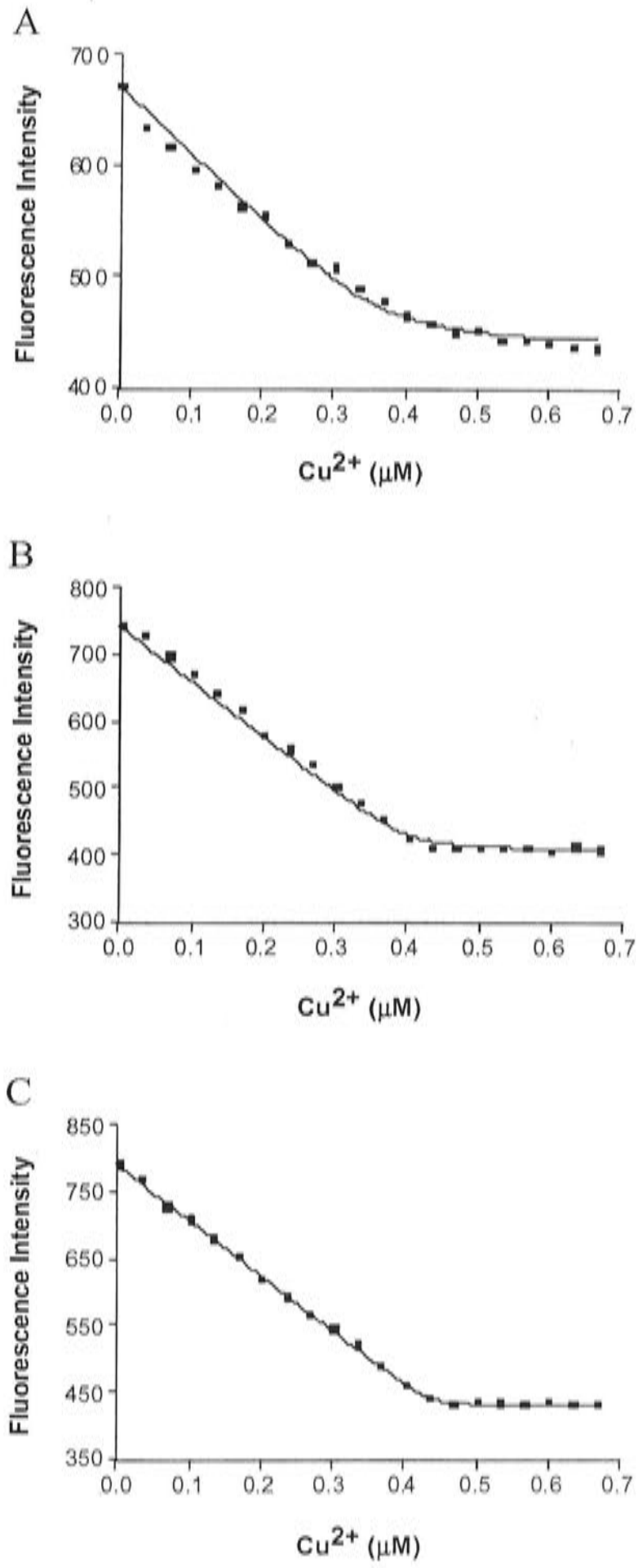

Figure 4.3: Fluorescence titration curves for copper (II) binding to Msp1. Experiments were carried out with 0.5 μM peptide titrated with 1 μL aliquots of 100 μM $Cu(Gly)_2$ in phosphate buffer pH 6.0 (A), pH 7.4 (B) and pH 8.0 (C). Squares represent the data points and the line results from nonlinear regression analysis according to Equation 4.2. The analysis generates K_d values of 10.4 ± 2.8 nM at pH 6.0 (A), 2.2 ± 0.7 nM at pH 7.4 (B), and 0.5 ± 0.3 nM at pH 8.0 (C).

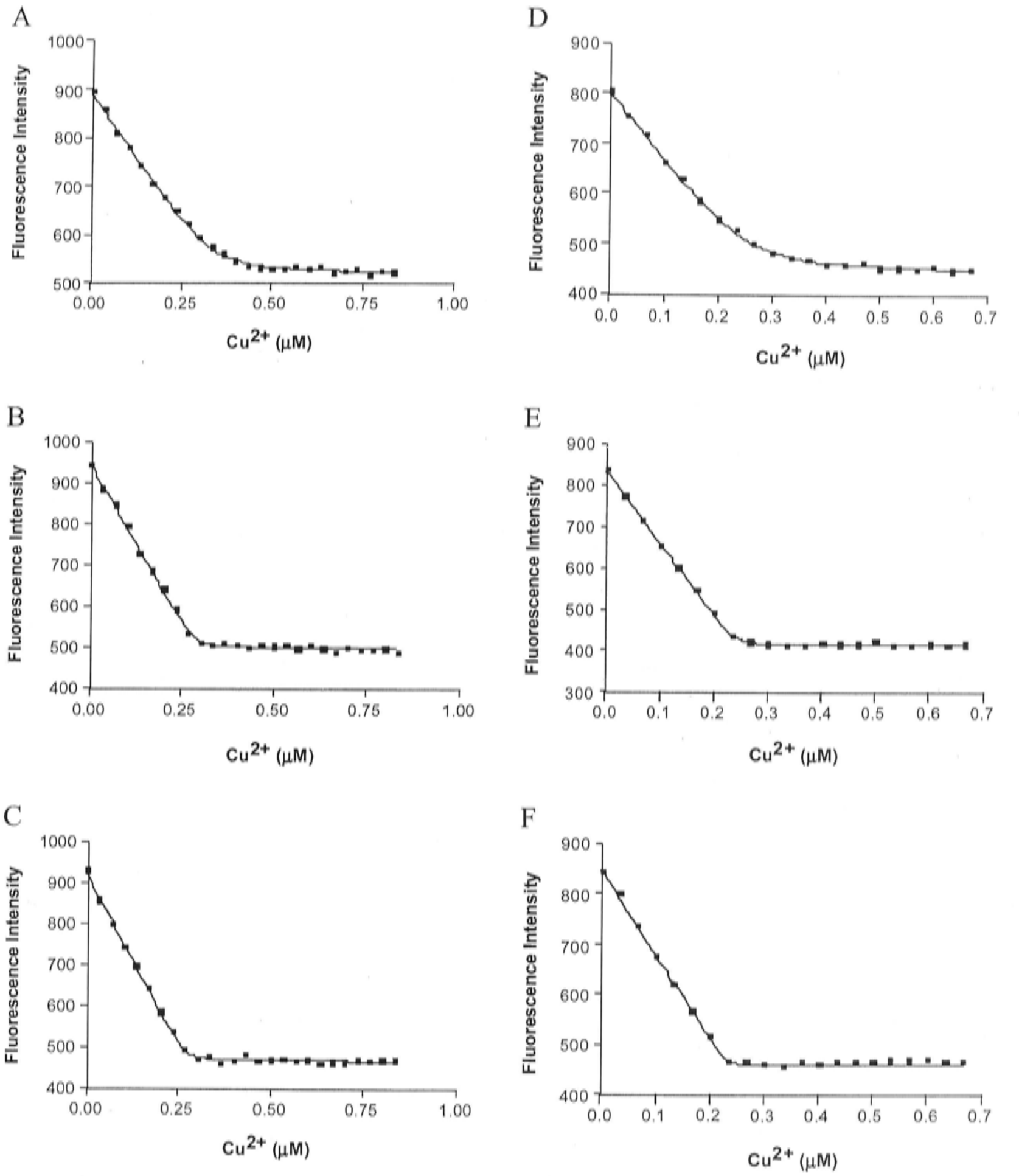

Figure 4.4: Fluorescence titration curves (in duplicate) for copper (II) binding to Msp1capC. Experiments were carried out with 0.5 μM peptide titrated with 1 μL aliquots of 100 μM $Cu(Gly)_2$ in phosphate buffer pH 6.0 (A & D), pH 7.4 (B & E) and pH 8.0 (C & F). Squares represent the data points and the line results from nonlinear regression analysis according to Equation 4.2. The analysis generates K_d values of 8.2 ± 1.6 nM (A) and 10.9 ± 1.7 nM (D) at pH 6.0, 1.0 ± 0.5 nM (B) and 0.5 ± 0.2 nM (E) at pH 7.4, and 0.9 ± 0.4 nM (C) and 0.2 ± 0.2 nM (F) at pH 8.0.

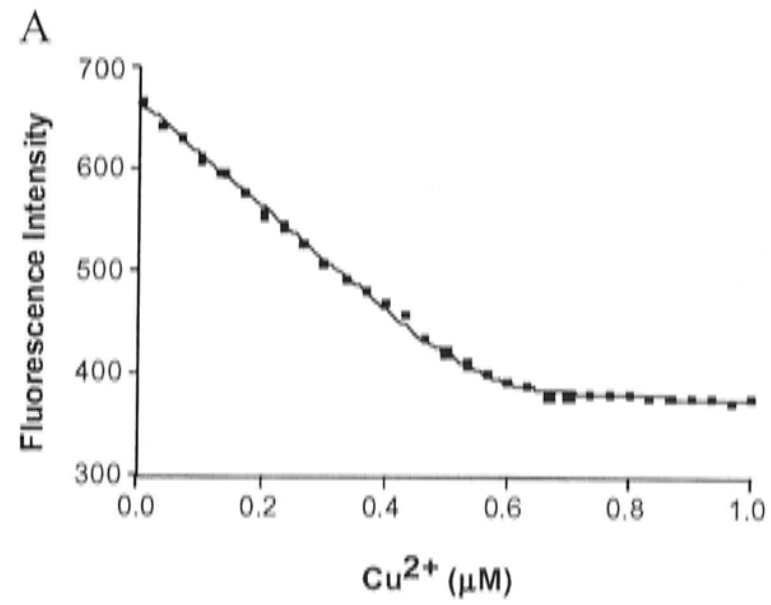

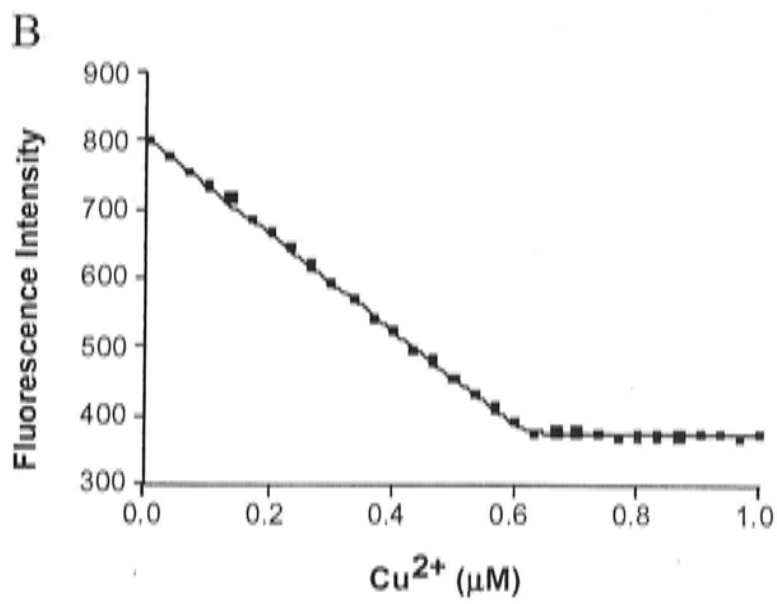

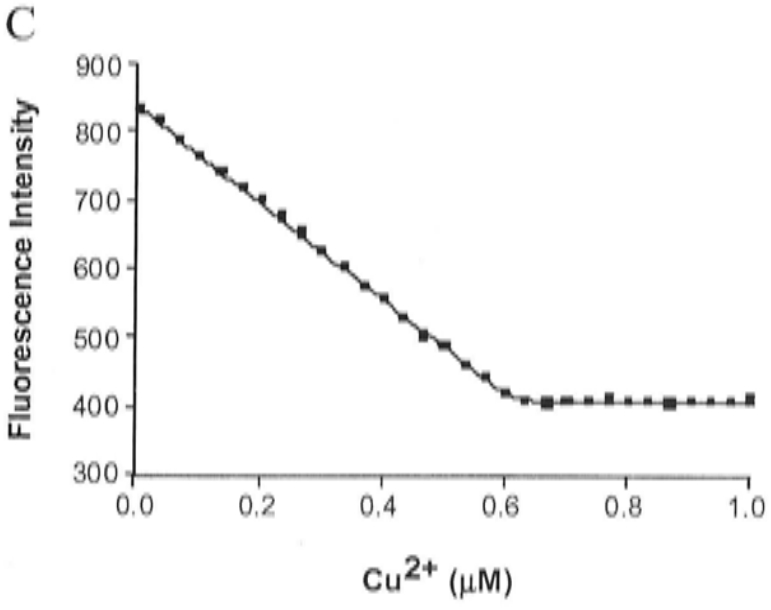

Figure 4.5: Fluorescence titration curves for copper (II) binding to Msp2. Experiments were carried out with 0.5 μM peptide titrated with 1 μL aliquots of 100 μM $Cu(Gly)_2$ in phosphate buffer pH 6.0 (A), pH 7.4 (B) and pH 8.0 (C). Squares represent the data points and the line results from nonlinear regression analysis according to Equation 4.2. The analysis generates K_d values of 4.9 ± 0.7 nM at pH 6.0 (A), 0.4 ± 0.2 nM at pH 7.4 (B), and 0.3 ± 0.2 nM at pH 8.0 (C).

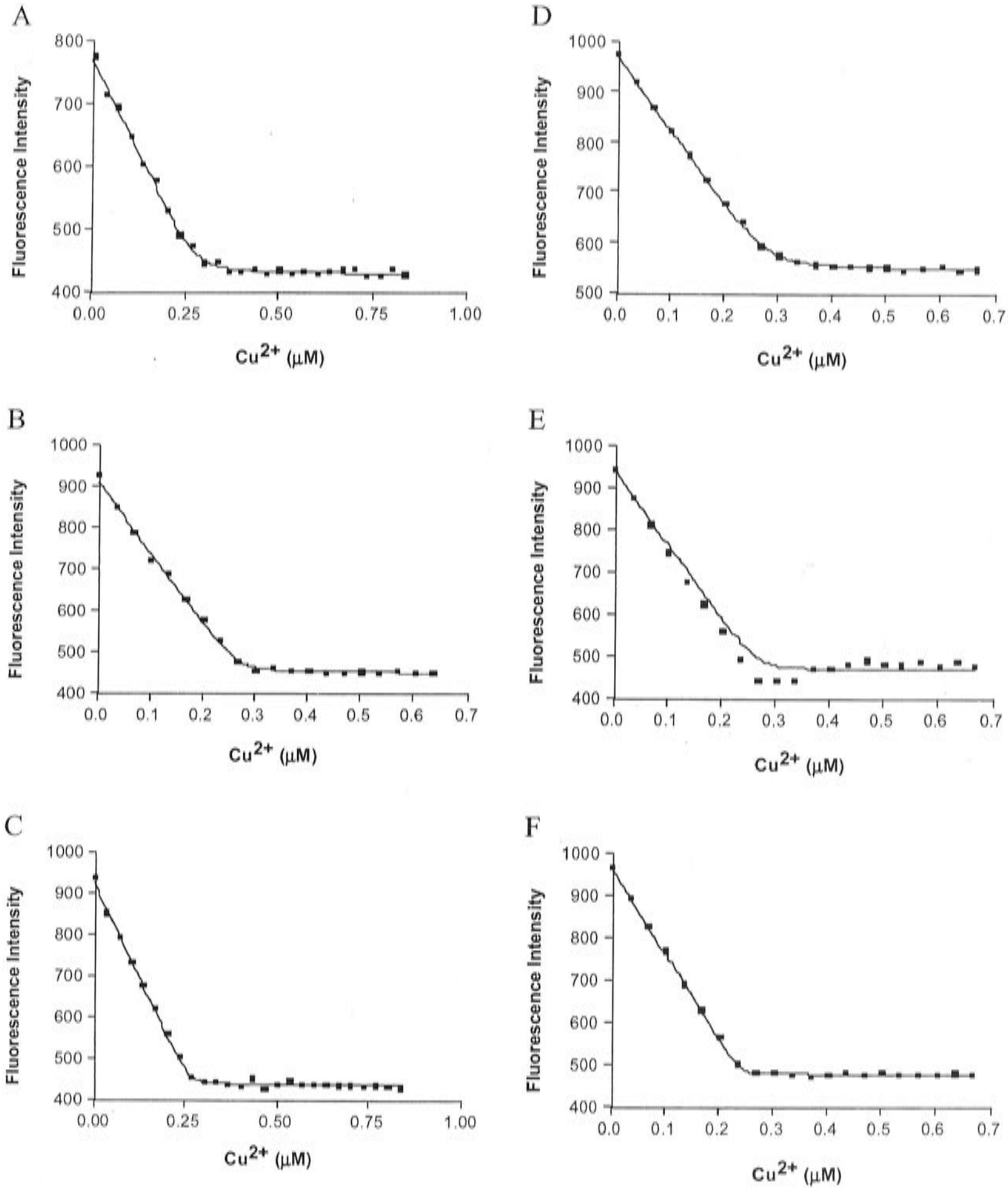

Figure 4.6: Fluorescence titration curves (in duplicate) for copper (II) binding to Msp2capC. Experiments were carried out with 0.5 μM peptide titrated with 1 μL aliquots of 100 μM $Cu(Gly)_2$ in phosphate buffer pH 6.0 (A & D), pH 7.4 (B & E), and pH 8.0 (C & F). Squares represent the data points and the line results from nonlinear regression analysis according to Equation 4.2. The analysis generates K_d values of 2.6 ± 1.1 nM (A) and 2.8 ± 0.5 nM (D) at pH 6.0, 1.2 ± 0.7 nM (B) and 1.1 nM (E) at pH 7.4, and 0.8 ± 0.5 nM (C) and 0.2 ± 0.1 nM (F) at pH 8.0.

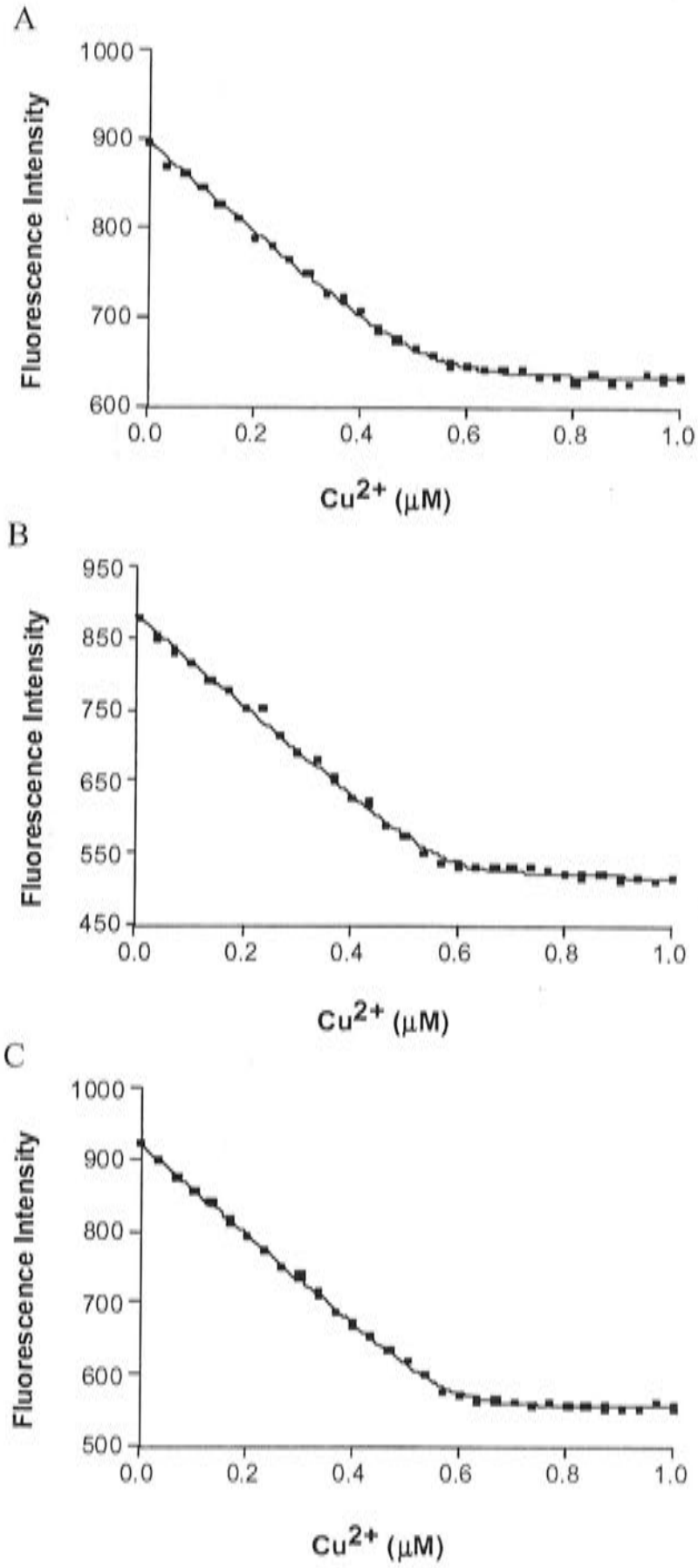

Figure 4.7: Fluorescence titration curves for copper (II) binding to Msp3. Experiments were carried out with 0.5 μM peptide titrated with 1 μL aliquots of 100 μM $Cu(Gly)_2$ in phosphate buffer pH 6.0 (A), pH 7.4 (B), and pH 8.0 (C). Squares represent the data points and the line results from nonlinear regression analysis according to Equation 4.2. The analysis generates K_d values of 7.7 ± 1.0 nM at pH 6.0 (A), 3.9 ± 0.9 nM at pH 7.4 (B), and 3.7 ± 0.5 nM at pH 8.0 (C).

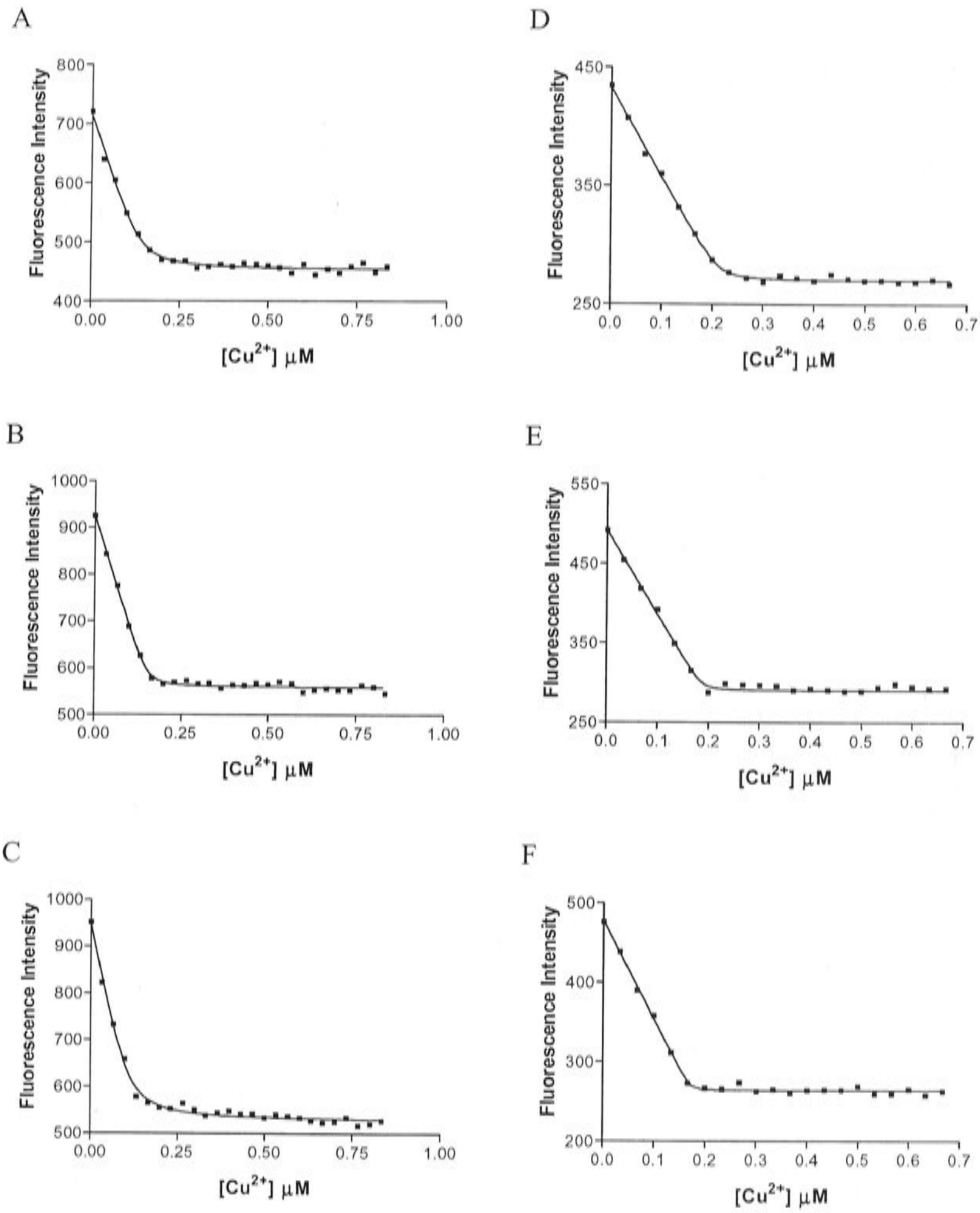

Figure 4.8: Fluorescence titration curves (in duplicate) for copper (II) binding to Msp3capC. Experiments were carried out with 0.5 µM peptide titrated with 1 µL aliquots of 100 µM $Cu(Gly)_2$ in phosphate buffer pH 6.0 (A & D), pH 7.4 (B & E), and pH 8.0 (C & F). Squares represent the data points and the line results from nonlinear regression analysis according to Equation 4.2. The analysis generates K_d values of 7.0 ± 2.3 nM (A) and 1.3 ± 0.7 nM (D) at pH 6.0, 1.7 ± 0.8 nM (B) and 0.5 ± 0.5 nM (E) at pH 7.4, and 8.4 ± 2.1 nM (C) and 0.3 ± 0.4 nM (F) at pH 8.0.

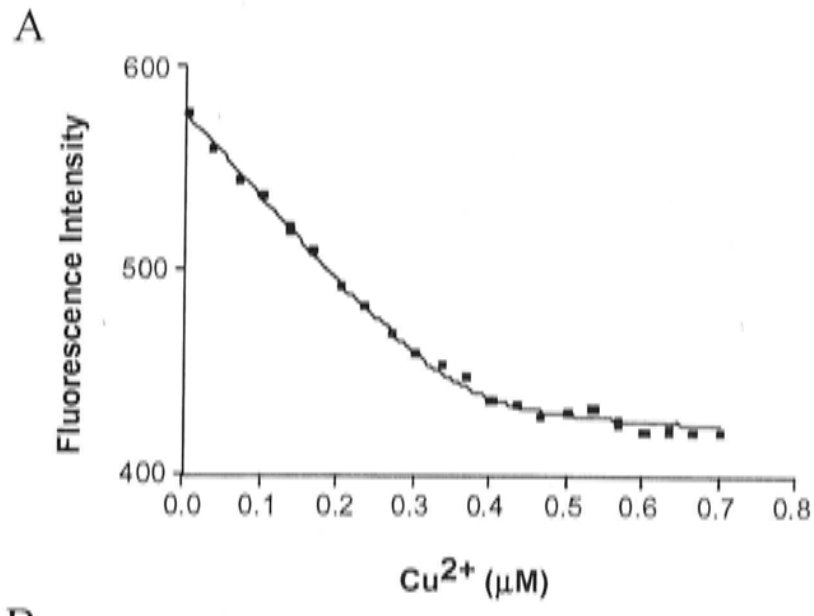

Figure 4.9: Fluorescence titration curves for copper (II) binding to Msp4. Experiments were carried out with 0.5 μM peptide titrated with 1 μL aliquots of 100 μM $Cu(Gly)_2$ in phosphate buffer pH 6.0 (A), pH 7.4 (B), and pH 8.0 (C). Squares represent the data points and the line results from nonlinear regression analysis according to Equation 4.2. The analysis generates K_d values of 9.3 ± 1.6 nM at pH 6.0 (A), 3.2 ± 1.0 nM at pH 7.4 (B), and 2.6 ± 1.0 nM at pH 8.0 (C).

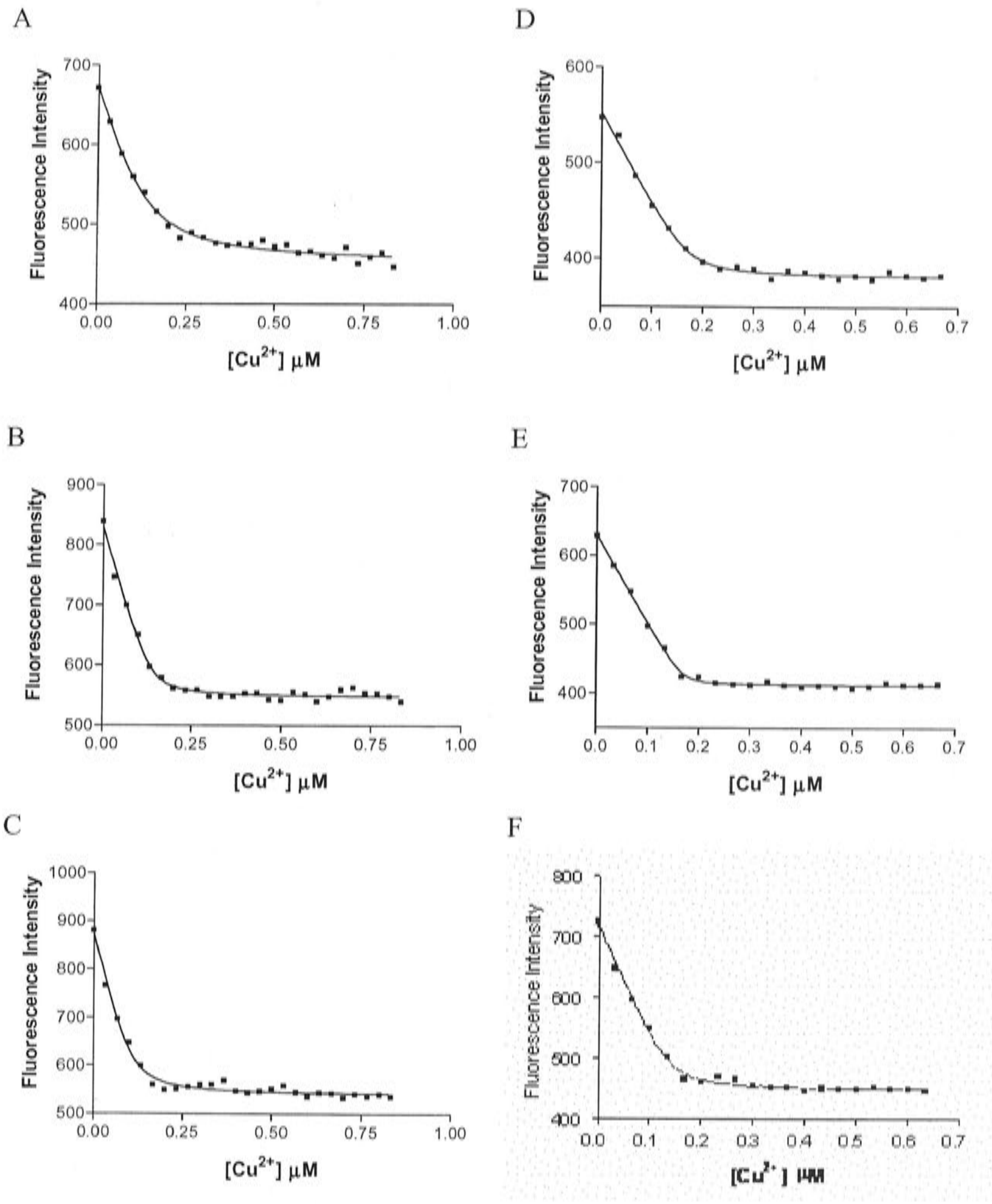

Figure 4.10: Fluorescence titration curves (in duplicate) for copper (II) binding to Msp4capC. Experiments were carried out with 0.5 µM peptide titrated with 1 µL aliquots of 100 µM $Cu(Gly)_2$ in phosphate buffer pH 6.0 (A & D), pH 7.4 (B & E), and pH 8.0 (C & F). Squares represent the data points and the line results from nonlinear regression analysis according to Equation 4.2. The analysis generates K_d values of 31.2 ± 8.5 nM (A) and 5.0 ± 2.0 nM (D) at pH 6.0, 5.1 ± 2.0 nM (B) and 1.2 ± 0.6 nM (E) at pH 7.4, and 9.1 ± 3.0 nM (C) and 4.8 ± 1.7 nM (F) at pH 8.0.

Table 4.2: Effect of pH on K_d values of copper binding to Msp and MspcapC peptides.

Experimental conditions			Results			Fig no.
Peptide	[peptide]	pH	K_d (nM)	C_s (μM)	R^2	
Msp1	0.5 μM	6.0	10.4 ± 2.8	0.366 ± 0.014	0.9895	4.3 A
		7.4	2.2 ± 0.7	0.400 (c)	0.9954	4.3 B
		8.0	0.5 ± 0.3	0.434 ± 0.003	0.9991	4.3 C
Msp1capC (a)	0.5 μM	6.0	8.2 ± 1.6	0.335 ± 0.006	0.9988	4.4.A
		7.4	1.0 ± 0.5	0.286 ± 0.004	0.9983	4.4.B
		8.0	0.9 ± 0.4	0.269 ± 0.003	0.9988	4.4 C
Msp1capC (b)	0.5 μM	6.0	10.9 ± 1.7	0.254 ± 0.005	0.9992	4.4 D
		7.4	0.5 ± 0.2	0.239 ± 0.002	0.9995	4.4 E
		8.0	0.2 ± 0.2	0.232 (c)	0.9976	4.4 F
Msp2	0.5 μM	6.0	4.9 ± 0.7	0.566 ± 0.005	0.9988	4.5 A
		7.4	0.4 ± 0.2	0.620 ± 0.002	0.9996	4.5 B
		8.0	0.3 ± 0.2	0.617 ± 0.003	0.9995	4.5 C
Msp2capC (a)	0.5 μM	6.0	2.6 ± 1.1	0.279 ± 0.006	0.9973	4.6 A
		7.4	1.2 ± 0.7	0.268 ± 0.005	0.9979	4.6 B
		8.0	0.8 ± 0.5	0.264 ± 0.004	0.9982	4.6 C
Msp2capC (b)	0.5 μM	6.0	2.8 ± 0.5	0.283 ± 0.002	0.9996	4.6 D
		7.4	1.1(c)	0.268 (c)	0.9738	4.6 E
		8.0	0.2 ± 0.1	0.242 ± 0.002	0.9997	4.6 F
Msp3	0.5 μM	6.0	7.7 ± 1.0	0.524 ± 0.006	0.9982	4.7 A
		7.4	3.9 ± 0.9	0.581 ± 0.007	0.9974	4.7 B
		8.0	3.7 ± 0.5	0.584 ± 0.004	0.9992	4.7 C
Msp3capC (a)	0.5 μM	6.0	7.0 ± 2.3	0.140 ± 0.009	0.9920	4.8 A
		7.4	1.7 ± 0.8	0.153 ± 0.005	0.9959	4.8 B
		8.0	8.4 ± 2.1	0.110 ± 0.008	0.9933	4.8 C
Msp3capC (b)	0.5 μM	6.0	1.3 ± 0.7	0.213 ± 0.004	0.9980	4.8 D
		7.4	0.5 ± 0.5	0.188 ± 0.004	0.9950	4.8 E
		8.0	0.3 ± 0.4	0.171 ± 0.004	0.9969	4.8 F
Msp4	0.5 μM	6.0	9.3 ± 1.6	0.364 ± 0.008	0.9964	4.9 A
		7.4	3.2 ± 1.0	0.376 ± 0.007	0.9967	4.9 B
		8.0	2.6 ± 1.0	0.370 ± 0.008	0.9953	4.9 C
Msp4capC (a)	0.5 μM	6.0	31.2 ± 8.5	0.131 ± 0.021	0.9891	4.10 A
		7.4	5.1 ± 2.0	0.136 ± 0.009	0.9904	4.10 B
		8.0	9.1 ± 3.0	0.107 ± 0.011	0.9880	4.10 C
Msp4capC (b)	0.5 μM	6.0	5.0 ± 2.0	0.172 ± 0.008	0.9951	4.10 D
		7.4	1.2 ± 0.6	0.168 ± 0.004	0.9977	4.10 E
		8.0	4.8 ± 1.7	0.141 ± 0.007	0.9956	4.10 F

(a) and (b) are duplicates, C_s is copper concentration at saturation point, which indicates the binding stoichiometry, (c) the data have been fitted to Equation 4.2 by incorporating this K_d or the C_s value as a constant to get the best R^2 parameter.

4.4.4.3. The stoichiometry of the binding (C_s)

As noted earlier, the binding data show that experiments were conducted under stoichiometric binding conditions. Under these conditions, the number of binding sites can be determined accurately: this is shown by the low standard errors for the C_s values. The C_s values indicate the concentration of copper ions bound to the peptide, or the concentration of the binding sites in the peptide that is occupied by copper.

The C_s values for copper binding to 0.5 μM Msp1 and Msp1capC (shown in Table 4.2) indicate the concentration of copper ion bound to peptide is lower than the peptide concentration. The C_s value suggests less than one copper ion bound per peptide molecule. This may mean that under these conditions one copper ion binds to two Msp1 molecules. However, except for these fluorimetry data, there is no evidence for the formation of Cu(II) – 2 Msp1 or Cu – 2 Msp1capC complexes.

The concentration of copper ion bound to 0.5 μM Msp2 (see Table 4.2) indicates that one copper ion binds per peptide molecule (Cu(II) – Msp2). Amidation of the C-terminus resulted in reduction of the number of copper ions bound. The C_s value for copper binding to 0.5 μM Msp2capC, shown in Table 4.2, is half that for Msp2, which may suggest, as above, that one copper ion binds to two Msp2capC molecules (Cu(II) – 2 Msp2capC). But again, except for these fluorimetry results, there is no evidence for the formation of these complexes.

The C_s values for the binding to 0.5 μM Msp3, shown in Table 4.2, suggest one copper ion bound per peptide molecule. The number of copper ions bound per peptide molecule is less than one in Msp3capC peptide, as shown by the C_s values in Table 4.2. In analogy to above, this might suggest one copper ion binds to 3 molecules of Msp3capC (Cu(II) – 3 Msp3capC). But again, there is no other evidence to support this suggestion.

0.5 μM Msp4 binds to 0.364 – 0.376 μM of copper ions. This result differs from those for Msp2 and Msp3, but is similar to that for Msp1, which also binds less than one copper ion per peptide molecule. As also happens for Msp2 and Msp3, there is a marked decrease in the copper-binding stoichiometry for the C-terminally capped

peptide. The concentration of copper ion bound to 0.5 μM Msp4capC, shown in Table 4.2, suggests formation of Cu(II) – 4 Msp4capC complexes, extension again of the analogy with the other C-capped peptides. These multi-peptide complexes seem increasingly unlikely.

The results show that in general the C_s values for C-terminally capped peptides are lower than for the uncapped peptides. This suggests the COO^- group at the C-terminus participates in the binding, and that the absence of this group reduces the stoichiometry. However, binding to the COO^- group is physiologically irrelevant, as this group does not exist in the real protein.

4.4.5. Effect of peptide concentration on K_d and C_s values

The effect of peptide concentration has been investigated using Msp1capC (Figure 4.11) and Msp4capC (Figure 4.12) peptides. At 5 μM Msp1capC concentration, the K_d value is 3.0 ± 2.4 nM (see Table 4.3 and Figure 4.11). Large standard error indicates inaccuracy of the calculation. Under these conditions, the C_s value is 5.511 ± 0.033 μM, suggesting one copper ion binds per peptide molecule or Cu(II) – Msp1capC. As shown in the previous experimental data (Table 4.2), copper binding to 0.5 μM Msp1capC is predicted to form a Cu(II) – 2 Msp1capC complex. Data in Table 4.3 confirms this form (0.277 ± 0.002 μM Cu(II) for 0.5 μM Msp1capC). K_d values for copper binding to 0.5 μM Msp1capC is 0.4 ± 0.2 nM. Although this value bears a large standard error, comparison with previous experimental data (Table 4.2) suggests the value is of the same order of magnitude as the previous results. A complex of Cu(II) – 2 Msp1capC is also observed at 0.25 μM peptide concentration (C_s values from duplicate experiments are 0.131 ± 0.003 μM and 0.125 ± 0.002 μM, see Table 4.3). The K_d values are now 2.6 ± 0.6 nM or 1.2 ± 0.3 nM, from duplicate experiments. The standard error of the K_d at 0.25 μM Msp1capC concentration is lower than at higher peptide concentrations. This suggests that the measurement may get more accurate as the peptide concentration is lowered. This is probably because the peptide concentration approaches the K_d value or moves toward the equilibrium binding conditions. At 0.10 μM Msp1capC, the shape of the curve (Figure 4.11) indicates equilibrium binding conditions, as there is a curvature region. The lack of a saturation point prevents determination of the binding stoichiometry. The data was best fitted

using Equation 4.1 and resulted in a K_d value of 37.1 ± 6.3 nM. Under these conditions, the K_d value also bears a reasonably low standard error.

The K_d value for copper binding to Msp4capC at 5 μM peptide concentration is 18.6 ± 11.8 nM. As just pointed out for Msp1capC, the large standard error indicates inaccuracy of the determination. Stoichiometry of the binding as shown by the C_s value is 3.125 ± 0.069 μM copper ions, or around 2 molecules of Msp4capC bind to one copper ion (Cu(II) – 2 Msp4capC). It may also mean part of the sample binds 1 Cu/Msp4capC and the other part 1 Cu/2 Msp4capC. At 0.5 μM peptide concentration, the K_d value (6.0 ± 1.4 nM) is of the same order of magnitude as the previous result (see Table 4.2). The stoichiometry of the binding (C_s value of 0.103 ± 0.005 μM) is also the same as the previous result (Table 4.2) only about a quarter of the 0.5 μM Msp4capC concentration. This indicates around 4 Msp4capC molecules bind to one copper ion (Cu(II) – 4 Msp4capC). At 0.25 μM Msp4capC, the stoichiometry of the binding is even lower (0.017 ± 0.002 μM). However, this value is clearly suspect, as it would indicate that more than 10 molecules of Msp4capC bind to one copper ion. The K_d at 0.25 μM Msp4capC is 5.8 ± 0.9 nM. The standard error of K_d for this binding condition is lower than for higher peptide concentrations. As noted earlier, the K_d measurement will be more accurate at lower peptide concentration, as the concentration of the peptide approaches the K_d value. As the peptide concentration was lowered to 0.10 μM, the binding curve showed a large curvature region (Figure 4.12). The data were best fitted using Equation 4.1 and resulted in a K_d of 4.3 ± 0.3 nM.

The data (Table 4.3) show both K_d and C_s values are affected by peptide concentration, which indicates that apart from the binding between copper and the peptide, the association between peptide molecules also occurs in the system. It is possible such association is mediated by copper ion, as the stoichiometry parameter (C_s) is always lower than the peptide concentration.

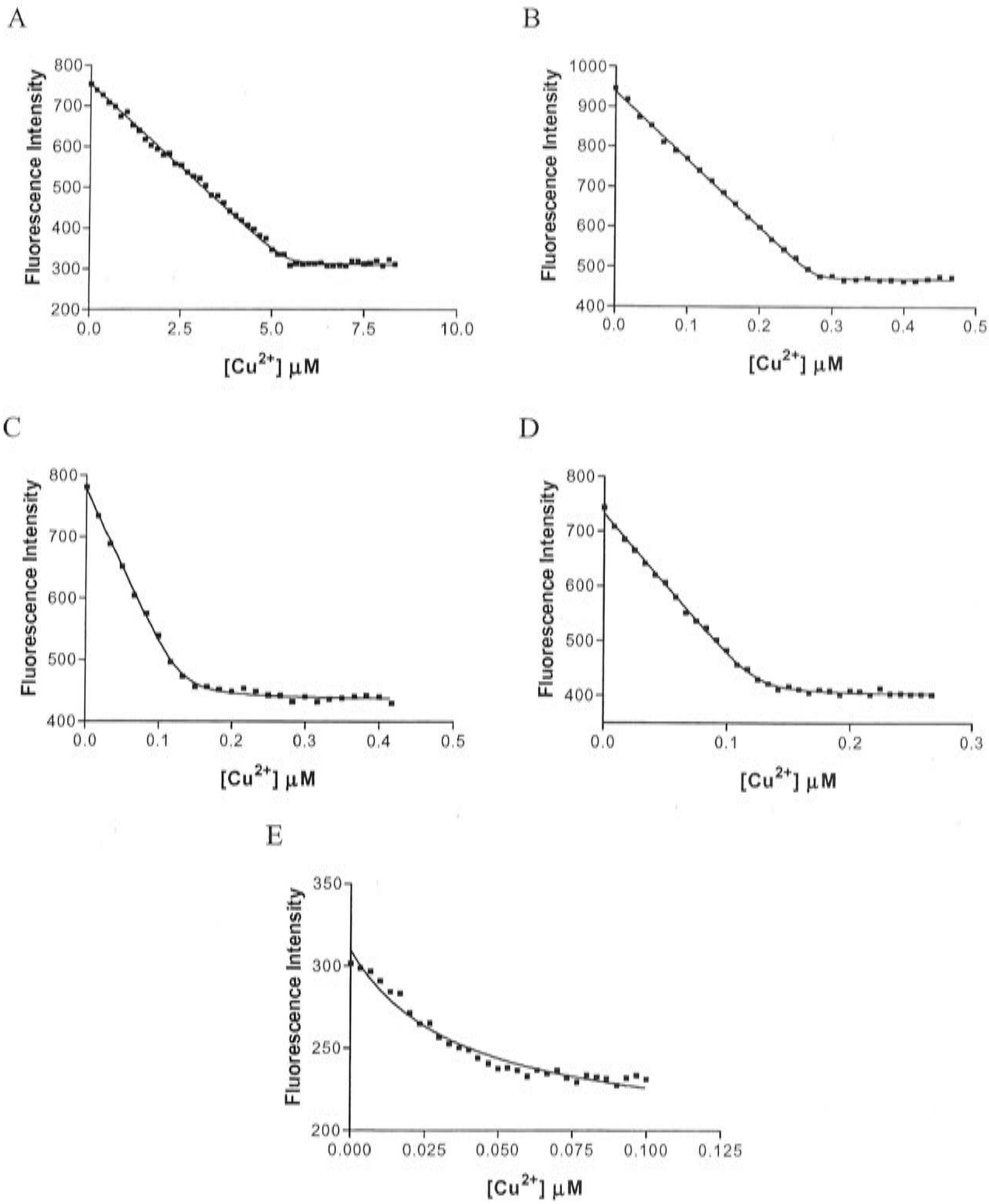

Figure 4.11: Fluorescence titration curves for copper binding to Msp1capC. Experiments were carried out at various concentrations of peptide: 5 µM (A), 0.5 µM (B), 0.25 µM (C and D) and 0.1 µM (E), titrated with 1 µL aliquots of 100 µM $Cu(Gly)_2$ in phosphate buffer pH 7.4. Squares represent the data points and the line results from nonlinear regression analysis according to Equation 4.2 (A, B, C, and D) and Equation 4.1 (E). The analysis generates K_d values of 3.0 ± 2.4 nM (A), 0.4 ± 0.2 nM (B), 2.6 ± 0.6 nM (C), 1.2 ± 0.3 nM (D), and 37.1 ± 6.3 nM (E).

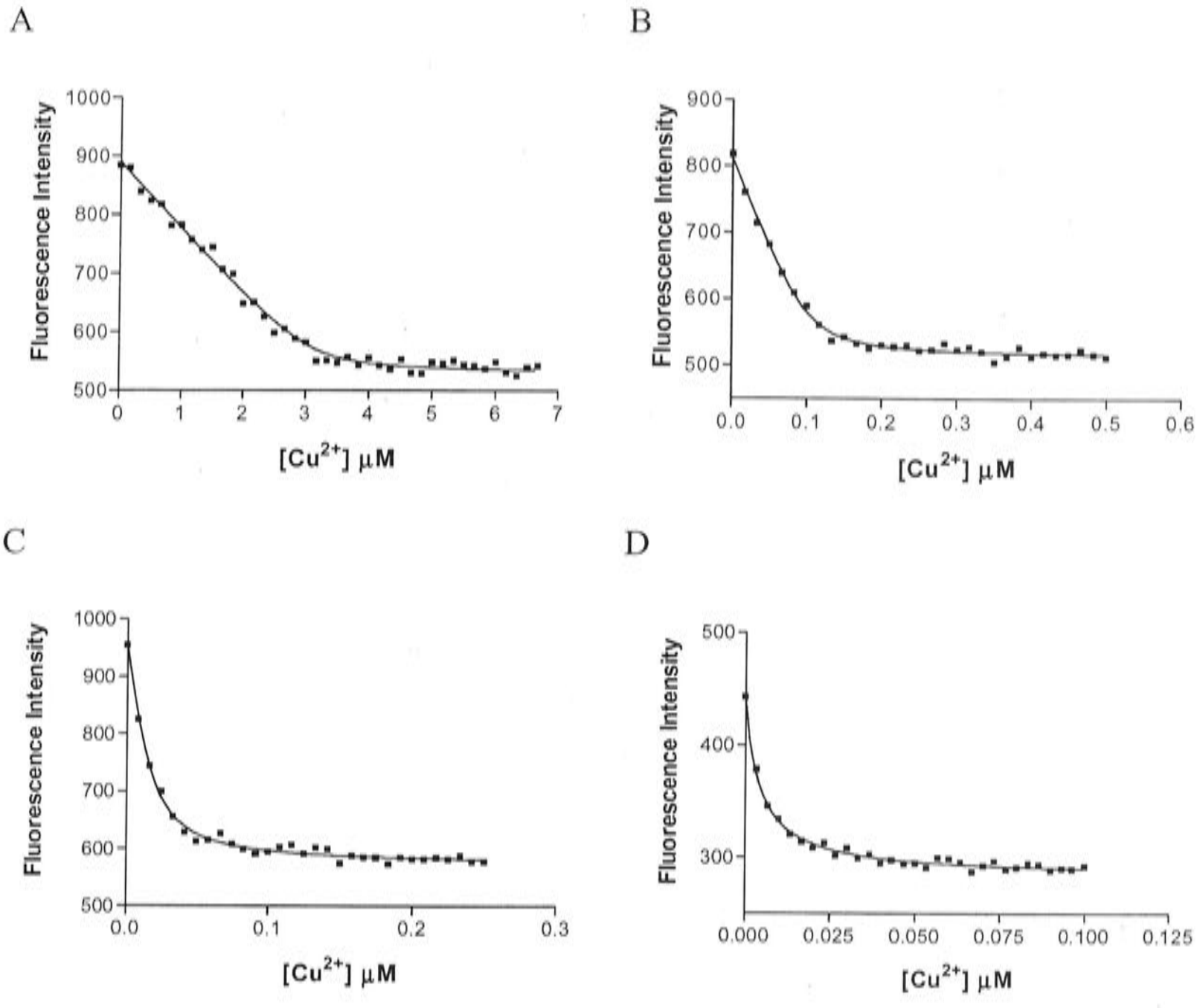

Figure 4.12: Fluorescence titration curves for copper binding to Msp4capC. Experiments were carried out at various concentrations of peptide: 5 µM (A), 0.5 µM (B), 0.25 µM (C) and 0.1 µM (D), titrated with 1 µL aliquots of 100 µM $Cu(Gly)_2$ in phosphate buffer pH 7.4. Squares represent the data points and the line results from nonlinear regression analysis according to Equation 4.2 (A, B, and C) and Equation 4.1 (D). The analysis generates K_d values of 18.6 ± 11.8 nM (A), 6.0 ± 1.4 nM (B), 5.8 ± 0.9 nM (C), and 4.3 ± 0.3 nM (D).

Table 4.3: Effect of peptide concentration on K_d values of copper binding to Msp1capC and Msp4capC peptides at pH 7.4.

Experimental conditions		Results			Fig no.
Peptide	[peptide]	K_d (nM)	Mo (µM)	R^2	
Msp1capC	5.00 µM	3.0 ± 2.4	5.511 ± 0.033	0.9974	4.11 A
	0.50 µM	0.4 ± 0.2	0.277 ± 0.002	0.9992	4.11 B
	0.25 µM	2.6 ± 0.6	0.131 ± 0.003	0.9981	4.11 C
	0.25 µM	1.2 ± 0.3	0.125 ± 0.002	0.9985	4.11 D
	0.10 µM	37.1 ± 6.3 (a)		0.9683	4.11 E
Msp4capC	5.00 µM	18.6 ± 11.8	3.125 ± 0.069	0.9932	4.12 A
	0.50 µM	6.0 ± 1.4	0.103 ± 0.005	0.9945	4.12 B
	0.25 µM	5.8 ± 0.9	0.017 ± 0.002	0.9919	4.12 C
	0.10 µM	4.3 ± 0.3 (a)		0.9903	4.12 D

(a): data were fitted to Equation 4.1.

4.4.6. Copper binding to mutant and variant Msp1 peptide

About 55% quenching was observed for Msp1 upon addition of copper (Figure 4.13). The same quenching percentage was also observed for Msp1N7A and Msp1Q10A, where the Ala residue replaces Asn and Gln, respectively. The similar quenching percentage suggests that Asn and Gln residues do not participate in copper binding. Furthermore, both K_d and C_s values of Msp1N7A and Msp1Q10A are the same as those of Msp1 (Figure 4.14 A-C, E-H and Table 4.4).

Addition of copper ions resulted in about 33% quenching for Msp1H2A (Figure 4.13). This substantial quenching of Msp1H2A (where His is replaced by Ala) suggests that copper can bind to the peptide even without the His residue. The titration curve for Msp1H2A (Figure 4.14 D) is not bi-phasic, suggesting that the copper-binding affinity for this peptide is much lower than for Msp1. To obtain a K_d value, the titration curve was fitted to a nonlinear regression analysis using Equation 4.1. The result (Figure 4.14 D and Table 4.4) shows the binding strength is reduced significantly with K_d value of 1560.0 ± 72.5 nM, or 100 times weaker than copper binding to Msp1.

An approximately 8% quenching was observed for the acetylated peptides (Msp1capN and Msp1capNC). The same value was observed for copper addition to the free amino acid Trp (as a control). As has been pointed out earlier (see section 4.4.4.1), the most likely explanation for the lack of quenching upon addition of copper ion to the N-terminally capped Msp1 is that copper ions require the imino group of Pro at the N-terminal end as an essential binding site. The fluorescence quenching simply does not occur as a consequence of the absence of binding.

Overall the results of fluorimetry experiments, in good agreement with FTIR (Chapter III), suggest that in Msp1 copper may bind to His and the imino group of Pro at the N-terminus. Copper may also bind to COO^- at the C-terminus. This is implied from the results discussed in section 4.4.4.3. The combined effect of copper binding to Msp1 (where His, free imino, and free COO^- exist together) was greater than the sum of binding to Msp1capNC (where only histidine exists) and to Msp1H2A (where the free imino and free COO^- exist). The consequence for removing the free imino group is greater than for removing the His group.

A

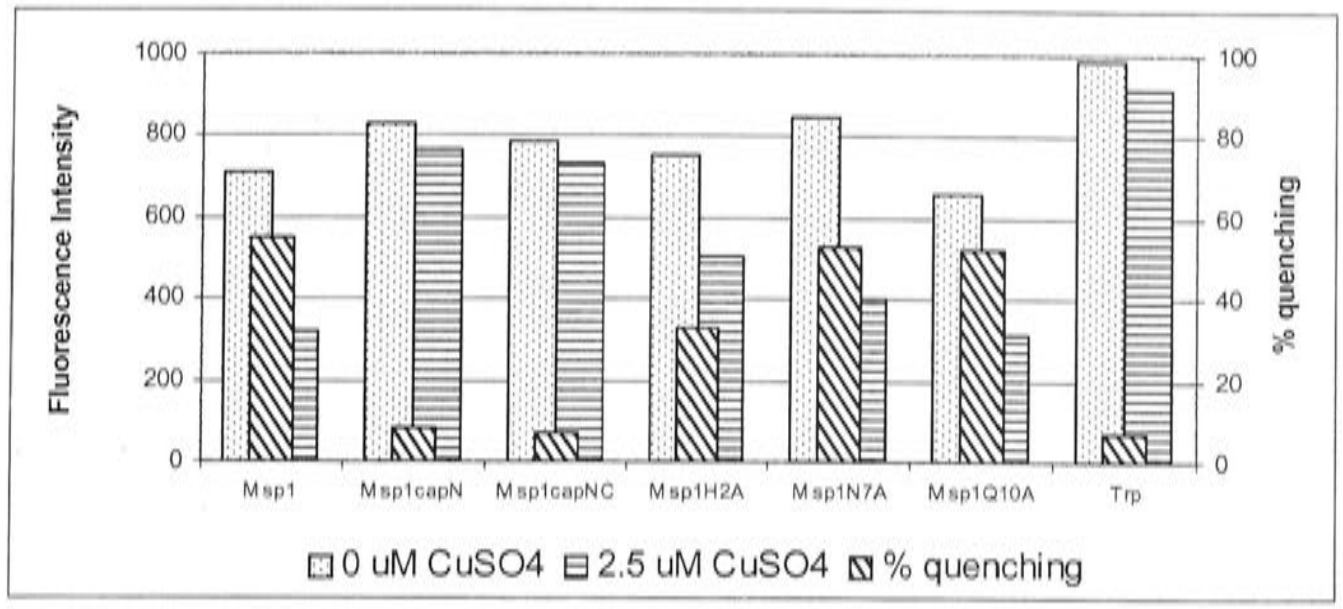

B

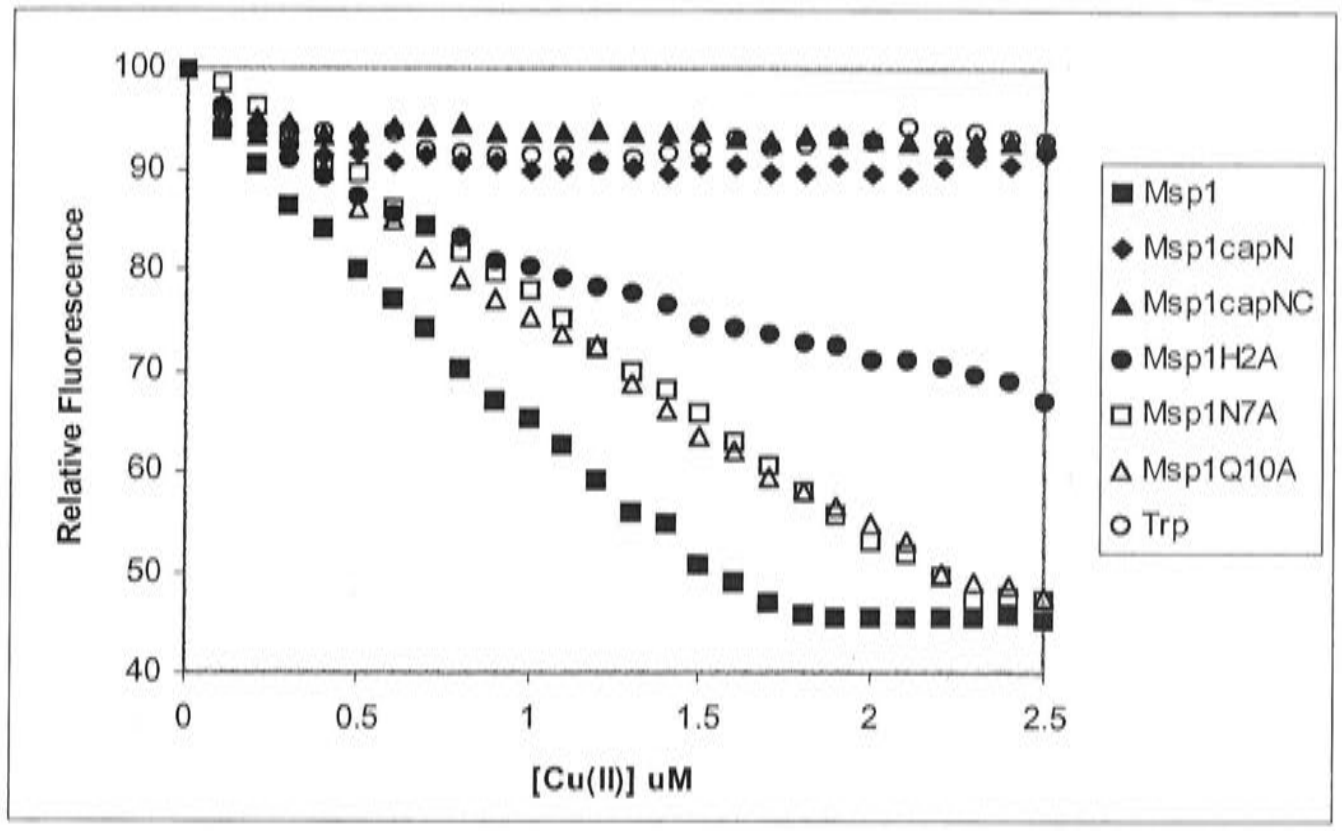

Figure 4.13: Copper binding to Msp1 and its mutant peptides. The data are presented as: (A) bar graphs of fluorescence intensity in the absence and presence of 2.5 μM $CuSO_4$ and its quenching percentage, (B) relative fluorescence intensity during copper (II) titration. Experiments were carried out in PBS buffer pH 7.4 and peptide concentration of 2.0 μM.

Table 4.4: K_d values of copper binding to Msp1 and its mutant peptides at pH 7.4.

Experimental conditions		Results			Fig no.
Peptide	[peptide]	K_d (nM)	C_s (μM)	R^2	
Msp1 (a)	2.0 μM	13.4 ± 3.9	1.506 ± 0.031	0.9938	4.14 A
Msp1 (b)	2.0 μM	8.3 ± 3.0	1.511 ± 0.023	0.9961	4.14 B
Msp1 (c)	2.0 μM	11.4 ± 3.9	1.581 ± 0.028	0.9951	4.14 C
Msp1H2A	2.0 μM	1560.0 ± 72.5	(d)	0.9968	4.14 D
Msp1N7A	2.0 μM	1.1 ± 0.8	1.514 ± 0.010	0.9991	4.14 E
Msp1N7A	2.0 μM	13.4 ± 6.5	2.277 ± 0.026	0.9983	4.14 F
Msp1Q10A	2.0 μM	3.8 ± 2.3	1.916 ± 0.019	0.9982	4.14 G
Msp1Q10A	2.0 μM	0.9 ± 0.9	2.292 ± 0.013	0.9994	4.14 H

(a), (b) and (c) are triplicates, (d): data were fitted to Equation 4.1.

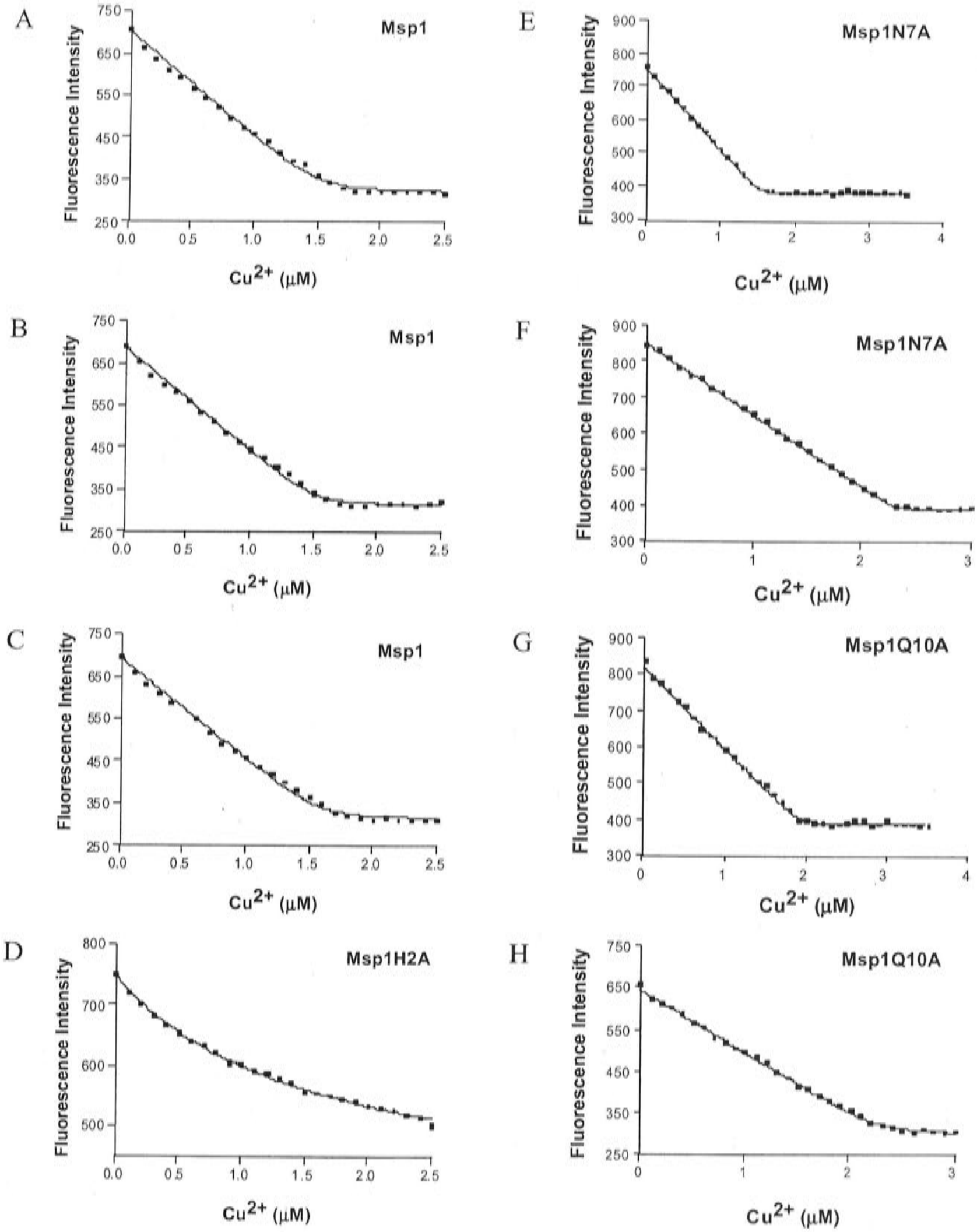

Figure 4.14: Fluorescence titration curves for copper binding to Msp1 and its mutant peptides. Experiments were carried out in PBS pH 7.4 and 2 μM concentration of Msp1 (A, B, and C), Msp1H2A (D), Msp1N7A (E & F) and Msp1Q10A (G and H). Copper ion is presented as $CuSO_4$ solution. Squares represent the data points and the line results from nonlinear regression analysis according to Equation 4.2 (A, B, C, E, F, G, and H) and Equation 4.1 (D). The analysis generates K_d values of 13.4 ± 3.9 nM (A), 8.3 ± 3.0 nM (B), 11.4 ± 3. 9 nM (C), 1560 ± 72.5 nM (D), 1.1 ± 0.8 nM (E), 13.4 ± 6.5 nM (F), 3.8 ± 2.3 nM (G), and 0.9 ± 0.9 nM (H).

The binding to the N- and C-terminal groups of the peptide is physiologically irrelevant, as these groups do not exist in the real protein. Therefore, the only relevant copper-

binding site that has been identified here is the His residue. In order to identify to which nitrogen atom of His the copper ion binds, experiments were conducted using His-methylated peptide as presented below.

4.4.7. Copper binding to Msp1 His-methylated peptide

The imidazole ring exists as two tautomeric forms depending on which nitrogen atom the proton binds to (for a more detailed explanation see section 3.4.1.4). Copper ions can bind to the unprotonated nitrogen, which can be either N_τ or N_π atom. To clarify which nitrogen binds copper in the repeats, we synthesized two peptides, each with either the N_τ or N_π atom methylated. In this way we can direct copper ion to bind to the unmethylated nitrogen and measure its copper-binding properties.

The copper-binding properties of Msp1His(1Me)capC is similar to that of Msp1capC peptide. The C_s values (Table 4.5) indicate two peptide molecules bind to one copper ion. The K_d value for copper binding to Msp1His(1Me)capC (7.89 ± 1.52 nM) at pH 6.0 is similar with that of Msp1capC peptide (8.2 ± 1.6 nM and 10.9 ± 1.7 nM, see Table 4.2). K_d values at pH 7.4 and 8.0, 0.03 ± 0.11 nM and 0.02 ± 0.21 nM, respectively (Table 4.5), are significantly lower (10 times) than those for copper binding to Msp1capC (see Table 4.2). This indicates that copper ion binds more strongly to Msp1His(1Me)capC peptide. However, the standard error for these two K_d values is very large (the quoted error is bigger than the quoted K_d value itself). As noted earlier, this large error is due to the experimental conditions (stoichiometric binding conditions) that are not suitable for accurate determination of K_d.

The titration experiment was also carried out for copper binding to Msp1His(3Me)capC peptide. Addition of copper ion to 0.5 μM Msp1His(3Me)capC produced significantly lower fluorescence quenching compared with that for Msp1His(1Me)capC. At pH 6.0 there is simply no quenching observed, while at pH 7.4 the quenching is very low and may not be accurate. As the pH is increased to 8.0, the observed fluorescence quenching increases and the data can be fitted to Equation 4.1. The analysis gave a K_d value of 1873 ± 539 nM. This K_d value is very much higher than that for Msp1His(1Me)capC and suggests very weak binding between copper and

Msp1His(3Me)capC. This weak binding indicates copper ions greatly prefer binding to the N_π atom rather than the N_τ atom.

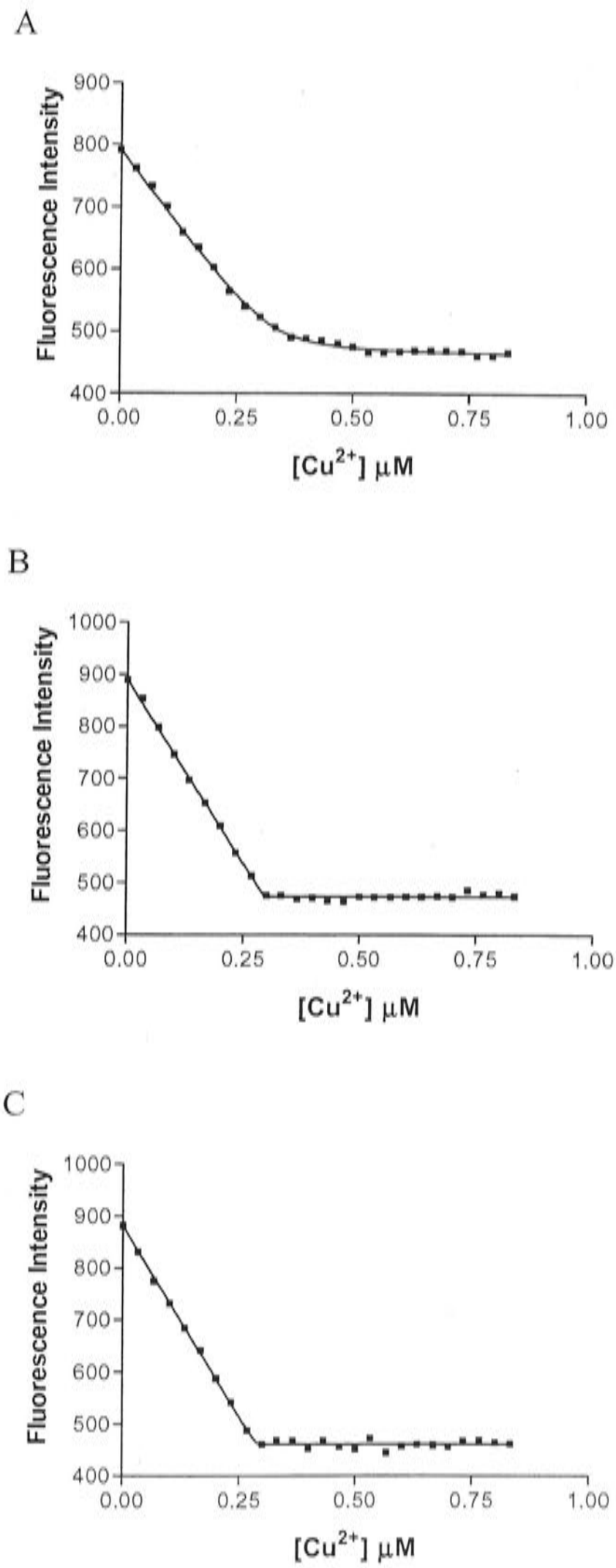

Figure 4.15: Fluorescence titration curves for copper binding to Msp1His(1Me)capC. Experiments were carried out with 0.5 µM peptide titrated with 1 µL aliquots of 100 µM $Cu(Gly)_2$ in phosphate buffer pH 6.0 (A), pH 7.4 (B) and pH 8.0 (C). Squares represent the data points and the line results from nonlinear regression analysis according to Equation 4.2. The analysis generates K_d values of 7.9 ± 1.5 nM (A), 0.03 ± 0.10 nM (B), and 0.02 ± 0.21 nM (C).

Table 4.5: K_d values of copper binding to Msp1 His-methylated peptides.

Experimental conditions			Results			Fig no
Peptide	[peptide]	pH	K_d (nM)	C_s (μM)	R^2	
Msp1His(1Me)capC	0.5μM	6.0	7.89 ± 1.52	0.328 ± 0.005	0.9987	4.15 A
		7.4	0.03 ± 0.11	0.293 ± 0.003	0.9989	4.15 B
		8.0	0.02 ± 0.21	0.287 ± 0.003	0.9979	4.15 C
Msp1His(3Me)capC	0.5 μM	8.0	1873 ± 539	(a)	0.9803	(na)

(na): figure not shown, (a): data were fitted to Equation 4.1.

4.4.8. Copper binding to repeat peptides with modified sequences

FTIR investigation (see Chapter III) has shown that replacement of Pro^3 with Gly^3 in the sequence of Ac-PH**P**GGSNWGQG-NH_2 (Msp1capNC) to produce Ac-PH**G**GGSNWGQG-NH_2 (Msp1P3GcapNC) significantly changes the binding properties of the N-terminally capped peptide. The peptide with Gly^3 binds copper ion, while the one with Pro^3 does not. A fluorescence titration experiment was carried out to investigate whether copper binding to the peptide with Gly^3 instead of Pro^3 will result in fluorescence quenching. As noted in Chapter I, literature data for mammalian PrP repeats suggests that the unprotonated nitrogen atom of the amide backbone of Gly^3 participates in copper binding. Therefore, lack of the unprotonated nitrogen atom might be predicted to result in reduction or abolition of binding in the marsupial repeat peptide. This subsection will also discuss copper binding to several other peptides with modified sequences: Msp_1strepcapNC (Ac-PQGGGTNWGQG-NH_2), Msp_4threpcapNC (Ac-PHGGSNWGQG-NH_2), and Hu1capNC (Ac-PHGGGWGQG-NH_2).

The results show that copper addition to these peptides does not result in quenching of Trp fluorescence intensity. FTIR shows they bind copper, except for Msp_1strepcapNC. Fluorescence measurements to detect binding rely on changes in the Trp microenvironment; if binding did occur but did not change the Trp environment, then there would be no quenching. The more obvious possibility for the absence of quenching is simply that there is no binding under these conditions of low (0.5 μM) peptide concentration at pH 7.4. It is possible that the binding is so weak that in order to be able to see the effect of the binding process on Trp fluorescence intensity the experiments need to be conducted at higher peptide concentration. Note that the FTIR experiments show binding takes place at 2.5 mM peptide concentration at pH 8.0 (see

Chapter III). However, due to time constraints, fluorimetry experiments at higher peptide concentration could not be done.

As noted in section 4.1, fluorescence quenching experiments have been used to study copper binding to the human PrP-repeat peptide (Hornshaw et al., 1995a; Jackson et al., 2001; Kramer et al., 2001). However, the peptides employed in those studies were not capped at their N- and C-termini. Copper binding to uncapped Hu1 peptide (PHGGGWGQ) was not investigated in this study. Nevertheless, a fluorescence quenching was predicted to occur upon copper addition to uncapped Hu1 peptide, based on observation in this study that quenching occurred upon addition of copper to uncapped Msp1 peptide.

As mentioned in Chapter I, several studies reported copper binding to capNC octarepeat peptide (Ac-PHGGGWGQ-NH_2) using methods other than fluorimetry. These have employed a rather high concentration of peptide, as required for each method. Raman spectroscopy used 20 mM peptide (Miura et al., 1996; Miura et al., 1999), CD used 398 μM peptide (Aronoff-Spencer et al., 2000) and 230 μM peptide (Bonomo et al., 2000), EPR used 1 mM peptide (Aronoff-Spencer et al., 2000), potentiometry used 1 mM, and NMR used 5.2 mM peptide (Luczkowski et al., 2002). Lower peptide concentration was also employed in CD experiments for peptide fragments of octarepeat (50 μM Ac-HGG-Et and 50 μM Ac-HGGG-Et) and octarepeat N-terminally extended by one residue (50 μM Ac-QPHGGGWGQ-Et) (Garnett and Viles, 2003). At this lower concentration, copper binding to these peptides was still observed. However, the concentration of peptide for the fluorimetry experiments (0.1–5 μM) is still much lower than the concentration employed in those reports. Overall, the phenomena observed in this study and those in the literature indicate that the mode of copper binding to PrP repeats depends on the concentration of the peptide.

4.5. Conclusions

The fluorimetry experiments allowed determination of copper-binding affinities (K_d) of PrP repeats of marsupial origin. The K_d values are much lower than those for other PrP repeats from mammals and chicken reported in the literature and determined using the fluorescence spectrophotometry method. Copper binding to Msp peptides is affected by

pH and peptide length. The K_d and stoichiometry of binding have been shown to depend on the peptide concentration. The dependence of K_d and stoichiometry on peptide concentration indicates that there is some other process occurring besides metal binding upon addition of copper ions. Probably, at certain peptide concentrations, the association between peptide molecules occurs as a result of copper binding. This suggestion is supported by the results from FTIR experiments, in which upon addition of copper some of the peptide (Msp1) molecules presumably form an intermolecular antiparallel β-sheet structure.

Fluorimetry experiments also provide some clues as to which groups and which amino acid residues participate in copper binding. The results suggest that the imino group of Pro at the N-terminus participates in the binding. The COO^- group at the C-terminus participates in the binding, and was shown to have a role in determining the binding stoichiometry. The absence of this group resulted in reduction of the number of copper ions bound per peptide molecule, or increase in the number of peptide molecules bound to one copper ion.

The His residue has also been identified as a copper-binding site. The absence of the His residue resulted in a 100-fold reduction in binding strength. Copper ions preferably bind to the N_π atom of the imidazole ring of His, rather than to the N_τ atom. Experiments show that copper ions bind strongly to N_τ-methylated His peptide, but very weakly to N_π-methylated peptide.

Initially it was thought that mutation of Pro^3 into Gly^3 of the sequence ^{1}PHPGGSNWGQ^{10} would reduce the role of the free imino group of ^{1}Pro, as has been observed in FTIR experiments (Chapter III). However, fluorescence experiments could not detect quenching upon addition of copper ions to this capNC peptide, or to Hu1capNC. This leads to the suggestion that the mode of copper binding in PrP-repeat peptide depends on the concentration of the peptide.

Chapter V

Fluorescence Resonance Energy Transfer

As reviewed in Chapter I, structural features of the PrP-repeat region, either as a complex with copper or by itself, have been intensively studied using a range of biophysical techniques. In its copper-free form, only one molecular model of the repeat region is available (Yoshida et al., 2000), while a number of models of the structure of the repeat region as a copper complex have been reported (Stockel et al., 1998; Miura et al., 1999; Viles et al., 1999; Aronoff-Spencer et al., 2000; Bonomo et al., 2000; Jackson et al., 2001; Burns et al., 2002; Luczkowski et al., 2002).

As shown by the NMR structures (Donne et al., 1997; Riek et al., 1997; Lopez Garcia et al., 2000; Zahn et al., 2000), the N-terminal region of PrP containing the repeats does not adopt a single defined conformation. There is some disagreement on the structure of the copper-free form of mammalian PrP repeats. Several studies showed it is unstructured (Hornshaw et al., 1995a; Miura et al., 1996; Viles et al., 1999; Bonomo et al., 2000; Whittal et al., 2000; Gustiananda et al., 2002). However, other studies report the presence of poly-L-proline type II left-handed helix (Smith et al., 1997) or loop and β-turn structure (Yoshida et al., 2000).

This chapter reports results from use of the fluorescence resonance energy transfer (FRET) method, which is able to probe one feature of the repeat region of PrP: the average distance between Trp and the N-terminal residue of the peptide.

5.1. Introduction

FRET is a technique that has been widely used for measuring distances between two points, either within or between molecules. The proximity of two points of interest in the protein molecule can be measured by labeling them with different chromophores. One is called the donor, which is the chromophore that initially receives the energy and transfers it to the other chromophore, which is called the acceptor. The donor must have a fluorescent property while the acceptor does not necessarily fluoresce. If the energy transfer occurs from the donor to the acceptor, the fluorescence of the donor (both intensity and lifetime) decreases, while the fluorescence of the acceptor, if it

fluoresces, increases. The distance between donor and acceptor can be calculated by employing the Förster equation (Förster, 1948), which relates the efficiency of transfer with distance (for reviews see Stryer, 1978; Wu and Brand, 1994; dos Remedios and Moens, 1995; Selvin, 1995).

Although FRET is usually used for measuring distance in a protein that adopts a defined conformation, in this study FRET is employed for PrP-repeat peptides, which are unstructured and likely adopt a range of conformations, dictated by their environment.

5.2. Aims

Aims of this study is to measure the distance between one Trp residue (donor) and the N-terminus of the peptide that had been labeled with the dansyl group (acceptor). In the case where the peptide possesses more than one Trp, a mutant with a single Trp residue was created, by replacing other Trp(s) with Phe. For the purpose of discussion, a correlation of the results with molecular dynamics (MD) simulations undertaken by Dr. Peter Cummins and analyzed by Dr. John Liggins in our group, and a summary of FRET results for an extended set of the peptides done by Dr. John Liggins, are also reported briefly.

5.3. Materials and methods

5.3.1. Sample preparation

All peptides and their dansylated forms (Table 5.1) were chemically synthesized and supplied by the Biomolecular Resources Facility (BRF) at the John Curtin School of Medical Research, Australian National University. The procedure for syntheses is described in Chapter II Materials and Methods.

The concentrations of the nondansylated peptides were determined using UV/Vis spectrophotometry based on the Trp absorption maximum at 280 nm (A_{280}) and extinction coefficient (ε_{280}) of 5500 M^{-1} cm^{-1} (Pace and Schmid, 1997). The concentration of the dansylated peptides and the degree of labeling were determined based on the dansyl absorption maximum at 331 nm (A_{331}) and extinction coefficient (ε_{331}) of 4000 M^{-1} cm^{-1}, and a correction factor for absorption by dansyl at 280 nm of

0.386 (Haughland, 2001). Hence, for 1 cm path length cuvette, the peptide and dansyl concentrations are:

$$[\text{peptide}] = \{A_{280} - (A_{331} \times 0.386)\} / 5500 \qquad \text{(Equation 5.1)}$$

$$[\text{dansyl}] = A_{331} / 4000 \qquad \text{(Equation 5.2)}$$

The degree of labeling (DOL) was calculated by using the formula

$$\text{DOL} = [\text{peptide}]/[\text{dansyl}] \times 100\% \qquad \text{(Equation 5.3)}$$

The degree of labeling for all dansylated peptides was found to be 100%.

For FRET measurement, peptide concentrations were 5 μM in universal buffer (multicomponent buffer, which is a mixture of 25 mM citric acid, 25 mM KH_2PO_4, 25 mM sodium tetraborate, 25 mM Tris, 25 mM KCl) (Perrin and Dempsey, 1974) at pH 3.0, 5.0, 6.5, 7.2, and 9.5.

5.3.2. Fluorescence measurements

A steady-state method was employed, in which the fluorescence emission intensity of peptide in a 5 mm path length quartz cuvette with maximum volume 0.5 mL was measured using a Perkin Elmer LS 50B spectrofluorimeter. Measurements were made to monitor the intrinsic fluorescence of the Trp residue in the nondansylated peptide, and in the dansylated peptide undergoing FRET from Trp to dansyl.

Trp residues are capable of undergoing homotransfer, i.e. an energy transfer process between Trp groups (Weber and Shinitzky, 1970). To prevent the homotransfer, Trp is excited at 295 nm. However, in these experiments, there is only one Trp residue per peptide and initial experiments indicated that the FRET distance does not differ between measurements with excitation at 280 nm and 295 nm. As the fluorescence emission intensity with excitation at 280 nm is significantly higher and, hence, provides higher sensitivity for excitation at 280 nm rather than at 295 nm, 280 nm excitation was used, with band slit width 5 nm. Emission spectra were obtained between 300-550 nm and emission intensities at 355 nm (Trp emission maximum) and 535 nm (dansyl emission maximum) were recorded. The temperature was set constant at 25 ^{O}C by means of a circulating water bath, except where the effect of temperature was investigated when it was varied (15, 20, and 25 ^{O}C).

Table 5.1. Pairs of peptides for measuring FRET distances. Nondansylated peptides are peptides that contain donor only, which is an intrinsic Trp (W) residue. Peptides are amidated and acetylated at the N- and C-termini respectively, except for Msp1 where the N- and C-termini are uncapped and Msp1capN where only the N-terminus is capped. Dansylated peptides are peptides that contain donor (Trp) and acceptor, which is the dansyl group attached to the N-terminus. Except for DansMsp1, which has a free alpha carboxyl group, all dansylated peptides are amidated at the C-terminus.

Distance between	Nondansylated peptides	Dansylated peptides	Size
W8 and Dansyl in Msp1	Msp1 NH-PHPGGSN**W**GQG-COOH	DansMsp1 Dansyl-PHPGGSN**W**GQG-COOH	11
W8 and Dansyl in Msp1capN	Msp1capN AcN-PHPGGSN**W**GQG-COOH	DansMsp1 Dansyl-PHPGGSN**W**GQG-COOH	11
W8 and Dansyl in Msp1capNC	Msp1capNC AcN-PHPGGSN**W**GQG-CONH2	DansMsp1capC Dansyl-PHPGGSN**W**GQG-CONH2	11
W8 and Dansyl in Msp2F18capNC	Msp2F18capNC AcN-PHPGGSN**W**GQPHPGGSNFGQG-CONH2	DansMsp2F18capC Dansyl-PHPGGSN**W**GQPHPGGSNFGQG-CONH2	21
W18 and Dansyl in Msp2F8capNC	Msp2F8capNC AcN-PHPGGSNFGQPHPGGSN**W**GQG-CONH2	DansMsp2F8capNC Dansyl-PHPGGSNFGQPHPGGSN**W**GQG-CONH2	21
W28 and Dansyl in Msp3F8,F18capNC	Msp3F8,F18capNC AcN-(PHPGGSNFGQ)$_2$PHPGGSN**W**GQG-CONH2	DansMsp3F8,F18capC Dansyl-(PHPGGSNFGQ)$_2$PHPGGSN**W**GQG-CONH2	31
W6 and Dansyl in Hu1capNC	Hu1capNC AcN-PHGGG**W**GQG-CONH2	DansHu1capC Dansyl-PHGGG**W**GQG- CONH2	9
W6 and Dansyl in Hu2F14capNC	Hu2F14capNC AcN-PHGGG**W**GQPHGGGFGQG-CONH2	DansHu2F14capC Dansyl-PHGGG**W**GQPHGGGFGQG-CONH2	17
W14 and Dansyl in Hu2F6capNC	Hu2F6capNC AcN-PHGGGFGQPHGGG**W**GQG-CONH2	DansHu2F6capC Dansyl-PHGGGFGQPHGGG**W**GQG-CONH2	17

5.3.3. Calculation of donor-acceptor apparent distance

Experimental data were analyzed using the Förster equation (Förster, 1948), which relates energy transfer efficiency (E) with distance (R) between donor and acceptor pairs:

$$R^6 = R_o^6 (E^{-1} - 1) \qquad \text{(Equation 5.4)}$$

Where R_o is the Förster distance (in Å) at which the transfer efficiency is 50% and specific for a particular donor-acceptor pair, and defined as:

$$R_o = (J K^2 Q_o n^{-4})^{1/6} \times 9.7 \times 10^3 \qquad \text{(Equation 5.5)}$$

The value of R_o depends on J, the spectral overlap integral, K^2 (kappa squared), the orientation factor for a dipole-dipole interaction, n, the refractive index of the medium between the donor and acceptor, and Q_o, the quantum yield of fluorescence of the energy donor in the absence of acceptor.

The value of K^2 cannot be directly measured and is the major uncertainty in the calculation of distance. Its value depends on the relative orientations of the donor and acceptor transition dipoles; it is 0 if all angles are perpendicular, and 4 if both transition moments are in line with the separation vector. Provided that both donor and acceptor can undergo unrestricted isotropic motion and rotate freely, K^2 assumes a numerical value of 2/3. Dos Remedios and Moens (1995) argue that the assumption of a value of 2/3 for K^2 appears to be valid for small peptides and small proteins, and its uncertainty in the determination of FRET distances may not be as critical as originally thought (dos Remedios and Moens, 1995). The Trp and dansyl groups should have considerable motional freedom as they are attached to the rest of the peptide molecule via a single covalent bond. Assuming that $K^2 = 2/3$ for the Trp and dansyl pair, the value of R_o is 21 Å (Dunn et al., 1981); this value was used in the calculation of distances.

As the presence of an energy acceptor in the vicinity of an excited energy donor provides an additional mode for the de-excitation process from donor quenching, E is calculated from the equation:

$$E = 1 - I_{DA} / I_D \qquad \text{(Equation 5.6)}$$

where I_{DA} is the fluorescence intensity of the donor in the presence of acceptor, and I_D is the fluorescence intensity of the donor only.

5.4. Results and discussion

5.4.1. Spectral overlap between Trp and dansyl

The fluorescence emission spectrum of Trp appreciably overlaps the absorption spectrum of dansyl bound to a representative Msp peptide, as shown in Figure 5.1.A. Such effective overlap is necessary for efficient FRET, as illustrated in Figure 5.1.B, which shows the steady-state fluorescence spectra of the dansylated and nondansylated forms of Msp1 peptide. The λ_{max} value for Trp emission intensity of 355 nm indicates the Trp residue is highly exposed to solvent as the aqueous Trp amino acid emits at 355 nm (Schmid, 1997). The significant decrease in Trp emission intensity for the dansylated peptide indicates substantial energy transfer. The similarity of the λ_{max} values and general spectral shape for the dansylated and nondansylated forms suggests that introduction of the dansyl group does not change the environment around the Trp residue, which is still highly exposed to solvent. This result also provides some confidence that attachment of the dansyl group to the N-terminus of PrP-repeat peptides does not perturb their structure greatly.

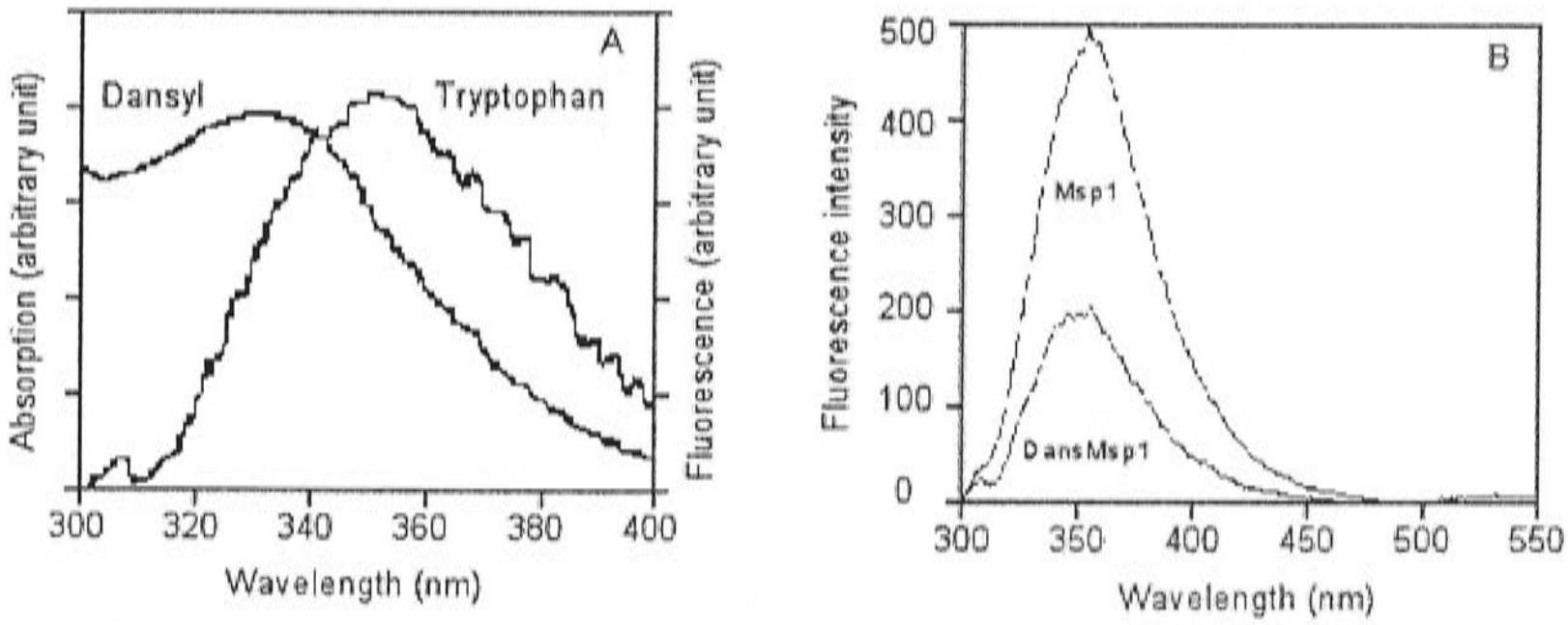

Figure 5.1: Spectral overlap between Trp and dansyl, and typical data from FRET experiments. (A). Spectral overlap between the Trp emission spectrum (λ_{max} 355 nm, λ_{exc} 280 nm) and the absorption spectrum of dansyl (λ_{max} 355 nm) in the DansMsp1capC peptide. The absorption and emission units are arbitrary. (B). Typical data from FRET experiments, which show the Trp emission intensity (λ_{max} 355 nm, λ_{exc} 280 nm) of 5 μM DansMsp1 is lower than that of 5 μM Msp1. Energy transfer also causes a sensitized emission of dansyl fluorescence (λ_{max} 535 nm), which appears as a small bump around 500–550 nm.

5.4.2. CD spectra of dansylated peptide

A further check for possible perturbation was made by running CD spectra of dansylated and nondansylated forms of two Msp peptides and Hu peptide, as shown in Figure 5.2. The CD spectra of nondansylated peptides (Msp1capNC, Msp2F8capNC, and Hu1capNC) show the characteristics of disordered structure, with a strong negative band around 200 nm, and a small maximum around 220 nm accompanied by a very weak negative band near 230 nm. For reference, disordered peptide is reported to have a strong negative band just below 200 nm, with a weak positive or negative band around 218 nm accompanied by a very weak negative band near 235 nm (Johnson, 1990; Woody, 1994; Woody, 1995).

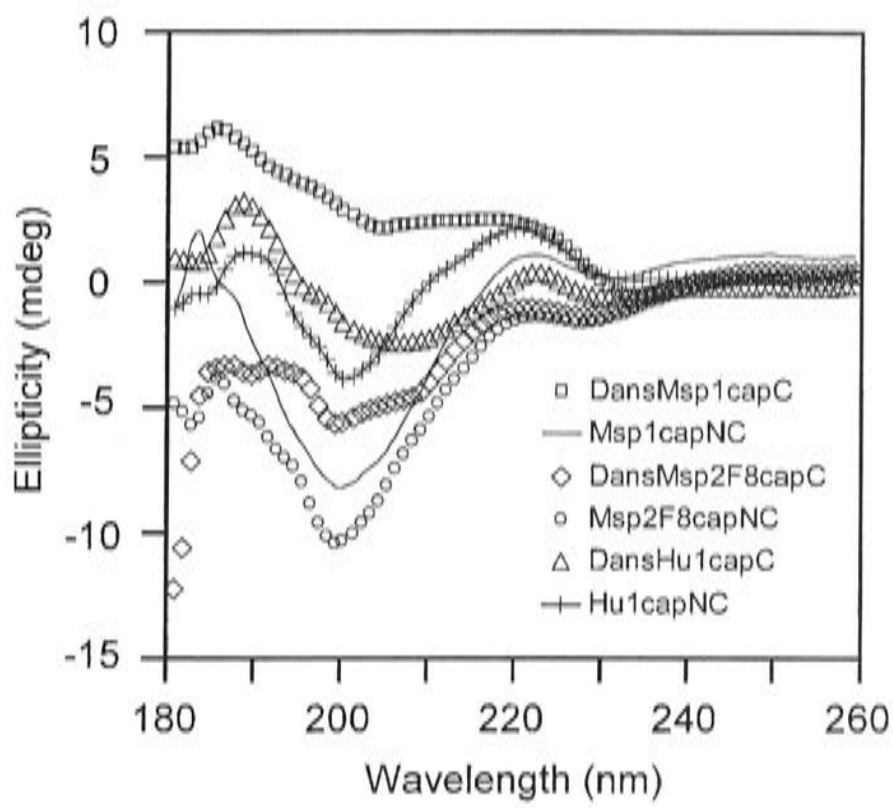

Figure 5.2: CD spectra of dansylated and nondansylated peptides. Spectra were taken from dansylated peptides (200 μM DansMsp1capC, 100 μM DansMsp2F8capC, and 200 μM DansHu1capC) and nondansylated peptides (200 μM Msp1capNC, 100 μM Msp2F8capNC, and 200 μM Hu1capNC) in H_2O at pH 5.0. Measurements are taken at constant temperature 25 ^{O}C, with path length cell 1 mm.

Although spectral changes are apparent for the dansylated forms, the spectra do not resemble those of any category of secondary structure other than random coil/disordered polypeptide. This evaluation, however, has to be taken cautiously because aromatic rings including the naphthalene group in dansyl, and in some cases the aromatic side chains of peptides, can contribute to the CD spectrum in the far UV region (Woody, 1994). Other work has also reported the tendency of the naphthalene ring in the dansyl group to affect the CD spectra of peptides in the region of 190-250 nm (Stella et al., 2002).

Based on the above indications from CD and the Trp emission spectra of little structural perturbation upon dansyl attachment, a number of pairs of dansylated and nondansylated peptides to measure FRET distances between Trp and the N-terminal residue of marsupial and human PrP-repeat peptides (see Table 5.1) were used. This pair of probes has previously been used to measure the distance between Trp and the N-terminal residue of small-disordered peptides (19 residues) (Lakowicz et al., 1994).

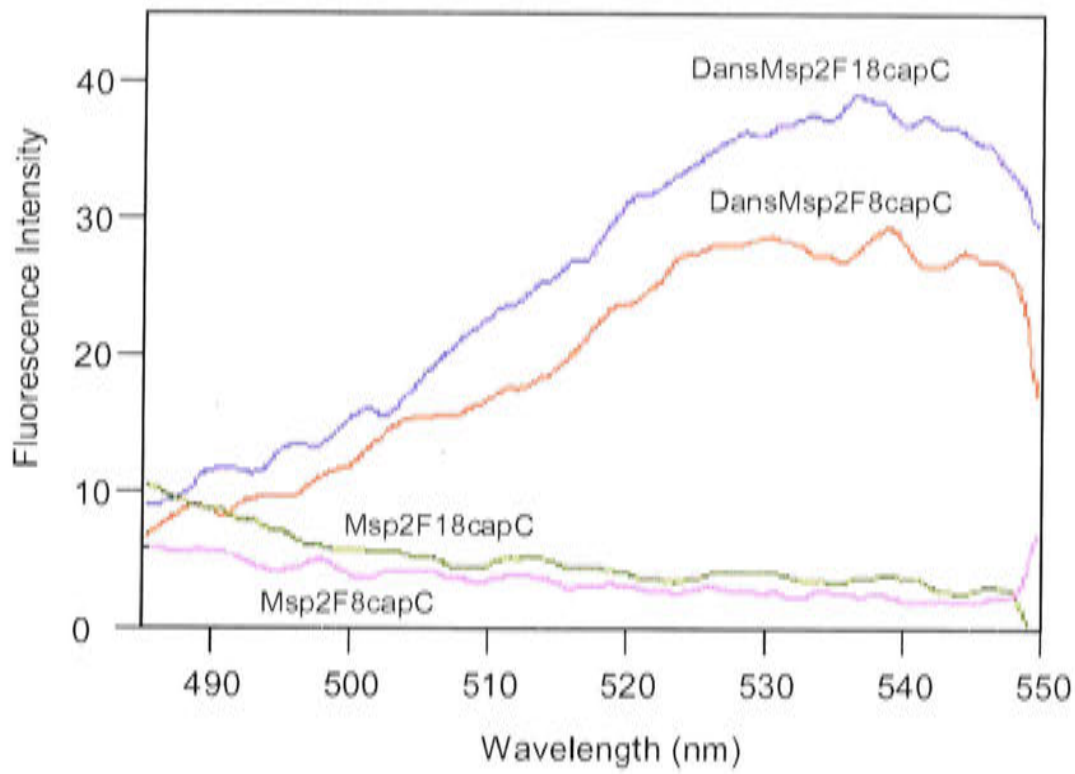

Figure 5.3: Fluorescence emission intensity of dansyl upon energy transfer from Trp. The dansyl emission intensity of DansMsp2F8capNC is lower than that of DansMsp2F18capNC as the distance between the acceptor (Trp) and the donor (dansyl) in the first peptide is longer than that in the second peptide. Msp2F8capNC and Msp2F18capNC do not emit fluorescence in this wavelength region, as shown by the flat baselines underneath the two spectra.

5.4.3. Dansyl fluorescence at 535 nm as other evidence for energy transfer

Figure 5.1.B shows that energy transfer also causes dansyl fluorescence, which has a λ_{max} value of 535 nm. The increase in intensity of acceptor emission upon energy transfer is called the sensitized emission, which can be used as another way to measure the extent of energy transfer (Selvin, 1995) because it also depends on the distance between donor and acceptor as shown in Figure 5.3. Figure 5.3 shows the dansyl fluorescence of dansylated and nondansylated forms of two Msp2 peptides (Msp2F8capNC and Msp2F18capNC). The dansyl emission intensity of DansMsp2F18capC is higher than that of DansMsp2F8capC, indicating, as expected, that the distance between Trp^{8} and dansyl in Msp2F18capNC is shorter than the distance between Trp^{18} and dansyl in Msp2F8capNC. Although this sensitized emission could be used to quantify the energy transfer, the sensitivity of measurement would be

very low as the intensity of the 535 nm band is very low, suggesting that the quantum yield of the dansyl attached to Msp peptides is very small. For that reason, in these experiments, the energy transfers were quantified by monitoring the decrease of the Trp fluorescence intensity rather than the increase of the dansyl fluorescence intensity.

5.4.4. pH effect on the Trp fluorescence emission intensity of dansylated and nondansylated peptides

As shown in Figure 5.4, the fluorescence intensity (λ_{ex} 280 nm, λ_{em} 335 nm) of dansylated and nondansylated peptides was pH dependent within the 3.0 to 9.5 range, indicating effects from protonation and deprotonation of some groups. The intensity of dansylated peptide is highest at pH 3.0, but falls to roughly constant from pH 5.0 (Figure 5.4.A). The pattern for nondansylated peptide is the reverse; it is lowest at pH 3.0 and rises until it is roughly constant from pH 6.5 (Figure 5.4.B).

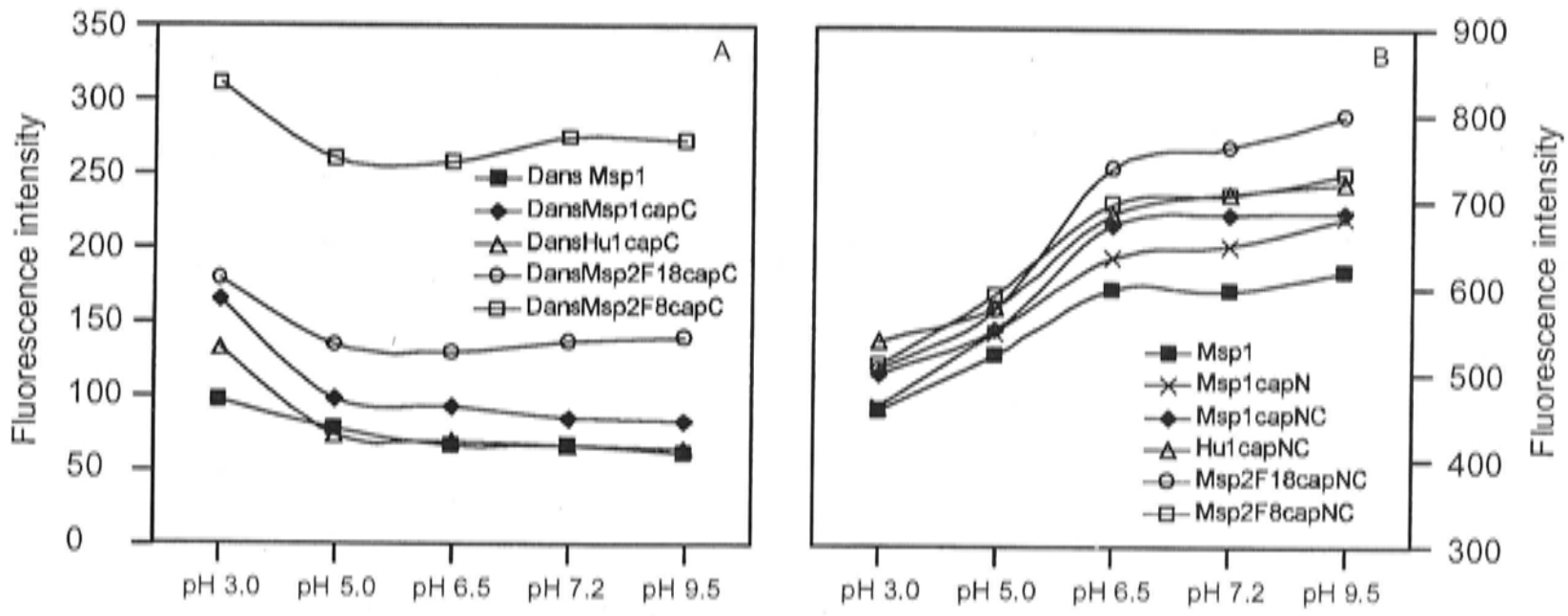

Figure 5.4: pH effect on fluorescence emission intensity of dansylated and nondansylated peptides. (A). Fluorescence emission intensity of dansylated peptides. (B). Fluorescence emission intensity of nondansylated peptides. All peptide concentrations were 5 μM in universal buffer pH 3.0, 5.0, 6.5, 7.2 and 9.5. The solutions were excited at 280 nm with band slit width 5 nm and the intensity at 355 nm was monitored while the temperature was maintained at 25 ^{O}C.

Trp fluorescence arises from the indole ring of its side chain, and the decrease in intensity at lower pH has been ascribed to a loss of aromaticity in the indole cationic form (Pesce, 1971 p.82); this ionization explains the pH dependence of nondansylated peptides in Figure 5.4.B. The different pH dependence of the dansylated peptides in Figure 5.4.A is due to compounding emission at 335 nm from protonated dansyl, which has a pK_a around 4 for the dimethylamino substituent (Lagunoff and Ottolenghi, 1966).

Thus, although the neutral dansyl group emits at 535 nm (λ_{ex} 331 nm), its protonated form has strong emission at 335 nm (λ_{ex} 280 nm). When the dansyl group is protonated, its intensity at 335 nm increases and its intensity at 535 nm decreases. The reverse happens when dansyl is deprotonated (Lagunoff and Ottolenghi, 1966). Thus, the intensity at 355 nm in dansylated peptides at pH 3.0 (Figure 5.4.A) is the highest due to a large contribution from the dansyl fluorescence. Due to this complication at low pH, the FRET measurements were restricted to the pH range 6.5 to 9.5.

5.4.5. pH dependence of FRET distances

The pH dependence of the FRET distances at pHs 6.5, 7.2, and 9.5 at 25 ^{O}C was measured for peptide sets 1-5 and 7 in Table 5.1, which includes the Msp1 set of uncapped, N-terminally capped, and N- and C-terminally capped forms, Msp2F18capNC and Msp2F8capNC, and Hu1capNC.

Results for the calculated FRET distances between Trp^8 and dansyl for the Msp1 set are shown in Table 5.2. These were obtained from duplicate measurements of the Trp emission intensities for both dansylated and relevant nondansylated forms (Table 5.1) at 355 nm (λ_{ex} 280 nm), calculating the energy transfer efficiencies using Equation 5.6, and hence, calculating the distance using Equation 5.4, assuming R_o is 21 Å (Dunn et al., 1981).

The FRET distance in the Msp1 peptide set (free Pro for nondansylated reference peptide) is slightly longer than that in the other two peptides (Msp1capN and Msp1capNC). This effect may be due not only to ionization but also to a hydrophobic effect from acetylation in capN peptides. The distance in Msp1capN is similar to that in Msp1capNC, indicating that amidation of the C-terminus does not affect the distance as much as acetylation of the N-terminus.

Table 5.2 also shows some trends for pH dependence of FRET distance: at pH 9.5 < 6.5 < 7.2 for Msp1 and Msp1capN; pH 9.5 < 6.5, 7.2 for Msp1capNC. The duplicates at pH 9.5 seem to be the most consistent as shown by smaller errors compared with those at pH 6.5 and 7.2. This inconsistency in the results at lower pH, especially at pH 6.5, is likely linked to His ionization.

Table 5.2: FRET distance between Trp^8 and dansyl in Msp1, Msp1capN, and Msp1capNC peptides. The FRET distances (R values) are averages of duplicate measurements. The table also presents the protonation states of the peptides based on pK_a values for the α-carboxyl (pK_a 2.34), α-imino (pK_a 10.96), and the imidazole side chain of His (pK_a 6.0) taken from the electronic sources stated below.
http://themerckindex.cambridgesoft.com/TheMerckIndex/AdditionalTables/pdfs/AminoAcidsAbbreivationsandpK.pdf.

pH	Msp1		Msp1capN		Msp1capNC	
	Protonation state	R (Å)	Protonation state	R (Å)	Protonation state	R (Å)
6.5	NH_2^+–PHPGGSN**W**GQG–COO^-	15.15 ± 0.26	AcN–PHPGGSN**W**GQG–COO^-	14.67 ± 0.29	AcN–PHPGGSN**W**GQG–$CONH_2$	14.90 ± 0.24
7.2	NH_2^+–PHPGGSN**W**GQG–COO^-	15.47 ± 0.36	AcN–PHPGGSN**W**GQG–COO^-	15.01 ± 0.40	AcN–PHPGGSN**W**GQG–$CONH_2$	14.91 ± 0.19
9.5	NH_2^+–PHPGGSN**W**GQG–COO^-	14.83 ± 0.13	AcN–PHPGGSN**W**GQG–COO^-	14.35 ± 0.09	AcN–PHPGGSN**W**GQG–$CONH_2$	14.52 ± 0.07

Table 5.3: Effect of pH on FRET distances of Msp and Hu PrP-repeat peptides. FRET distances (Å) between the dansyl group (attached to the N-terminal Pro^1) and Trp^8 in Msp1capNC and Msp2F18capNC, Trp^{18} in Msp2F8capNC, and Trp^6 in Hu1capNC at 25 ^oC. The distances are averages of duplicate measurements.

pH	Hu1capNC	Msp1capNC	Msp2F18capNC	Msp2F8capNC
6.5	14.22 ± 0.07	14.90 ± 0.24	16.26 ± 0.25	19.44 ± 0.24
7.2	14.19 ± 0.37	14.91 ± 0.19	16.04 ± 0.01	19.45 ± 0.02
9.5	13.54 ± 0.09	14.52 ± 0.07	15.84 ± 0.10	19.33 ± 0.14

The fact that the distance between Trp^8 and dansyl in the Msp1 set peptide at pH 9.5 is the shortest is in good agreement with two phenomena observed in FTIR experiments (Chapter III). Firstly, upon increasing pH from 6.0 to 9.0, the intensity of the 1360 cm^{-1} band increases, indicating that the Trp residue moves into a more hydrophobic environment, probably getting closer to the Pro side chain or to the N-terminal part of the peptide. Secondly, upon increasing pH from 6.0 to 9.0, the amide I band shifts to lower frequency, indicating some structural modification, which results in a more folded structure so that Trp is closer to the N-terminal part of the peptide.

5.4.6. Comparison of FRET distances in Msp1capNC, Msp2capNC, and Hu1capNC peptides

FRET distances at pHs 6.5, 7.2, and 9.5 for the two longer Msp peptides (Msp2F18capNC and Msp2F8capNC) and the shorter Hu1capNC peptide are shown in Table 5.3. Although there is some evidence for the distances for the Msp1 set in Table 5.2 and the short Hu1capNC peptide in Table 5.3 to be lower at pH 9.5 than at pH 6.5 or 7.2, this effect diminishes for the longer peptides, Msp2F18capNC and Msp2F8capNC. Distances at pHs 6.5 and 7.2 are very similar for the N- and C-capped peptides. In general, there appears to be little effect from pH variation.

The results in Table 5.3 begin to show the variability in the FRET distances as a function of distance in sequence space between the donor and acceptor, as well as a modulating effect from total peptide length. Thus, at pH 7.2, although the sequence distance for the Msp2F18capNC peptide, i.e. Trp^8 to dansyl, is the same as in the Msp1capNC peptide, the results show a FRET distance of ~16 Å which is ~1.1 Å longer than in Msp1capNC. In the Msp2F8capNC peptide where FRET measures the distance between dansyl and Trp^{18}, i.e. 10 residues more in sequence length than for Msp2F18capNC, the FRET distance of approximately 19.5 Å is longer by only ~ 3.5 Å. This indicates that the peptide chain loops back upon itself, by shortening the distance between Trp^{18} and the N-terminus. The presence of Pro residues, which can bend the peptide chain, in the second repeat (positions 11 and 13) of Msp2F8capNC, could cause the peptide to fold and, hence, reduce the FRET distance. The results in Table 5.3 also show that in the shortest peptide Hu1capNC, where the FRET measurement is between Trp^6 and dansyl, the average FRET distance of approximately 14.2 Å (pH 6.5 and 7.2)

is shorter by only ~ 0.7 Å, compared with the distance between Trp^8 and dansyl in Msp1capNC of 14.9 Å.

5.4.7. The FRET distance indicates the peptides are loosely compacted

In general, the experimental FRET distances between Trp and dansyl are much lower than their theoretical distances in a fully extended peptide chain; these were estimated in the following way. The length of the peptide backbone between successive residues is 3.63 Å (Creighton, 1983 p.4). In a fully extended Msp1, the N-terminus and the Trp^8 residue is separated with 7 peptide bonds, and hence, the total backbone length is 25.41 Å. After addition of the lengths of the dansyl group and the Trp side chain, the total distance between the centres of the dansyl group attached to the N-terminus and the indole group of Trp^8 in the fully extended peptide chain is approximately 32.6 Å.

Thus, the shorter FRET distance in Msp1capNC (14.9 Å) indicates that the peptide is loosely folded. The Hu1capNC peptide is similarly loosely folded because the experimental FRET distance between Trp^6 residue and the dansyl group (14.2 Å) is less than the theoretical FRET distance in the fully staggered peptide (25.3 Å). The same behavior is observed for Msp2capNC, Msp3capNC, and Hu2capNC (Figure 5.5).

A factor that can stabilize a folded structure in PrP-repeat peptides is the interaction between Trp and His residues. This interaction has previously been observed in both the NOE data and NMR structure calculations of human octarepeat peptides, which indicate that the β-proton of His is in close proximity to the aromatic ring of Trp, which is 4 residues distant (Yoshida et al., 2000). The interaction of His and Trp has been mainly explained by cation-π interaction or π-π interaction (Gallivan and Dougherty, 1999), depending on the protonation state of the His residue. The latter interaction can also occur between aromatic residues in the form of π-stacking (Gazit, 2002). Yoshida et al. (2002) proposed that the cation-π interaction between His and Trp stabilizes a loop structure in human PrP-octarepeat peptide. Gazit (2002) proposed that a π-stacking interaction might occur in PrP-repeat peptides leading to the formation of amyloid fibrils through a self-assembly process, as is proposed for the formation of prion particles.

5.4.8. Temperature dependence of FRET distances

Experiments were carried out to investigate the effect of temperature on the structure of PrP-repeat peptides. Preliminary experiments for the Msp1capNC and Msp2F8capNC systems at 15, 20, and 25 ^{O}C at pHs 6.5, 7.2, and 9.5 were done to check for any differences in pH dependence of the FRET distances at lower temperatures. As the pH dependence at these temperatures (Table 5.4) shows similar trends, the temperature dependence studies, which were extended to both lower and higher temperatures, were restricted to pH 7.2. The results of duplicate experiments (experiments were conducted by Dr. John Liggins) at temperatures 5, 15, 25, 40, 55, 70 and 85 ^{O}C for the 7 set of the N- and C-terminally capped peptides in Table 5.1 are shown in Figure 5.5.

Table 5.4: Preliminary data on the effect of temperature on FRET distances. FRET distances between Dansyl and Trp^{8} in Msp1capNC and Trp^{18} in Msp2F8capNC at temperatures 15, 20, and 25 ^{O}C are averages of duplicate measurements.

pH	Msp1capNC			Msp2F8capNC		
	15 ^{O}C	20 ^{O}C	25 ^{O}C	15 ^{O}C	20 ^{O}C	25 ^{O}C
6.5	14.56 ± 0.14	14.85 ± 0.15	14.90 ± 0.24	19.15 ± 0.05	19.07 ± 0.19	19.44 ± 0.24
7.2	14.39 ± 0.20	14.41 ± 0.15	14.91 ± 0.19	19.10 ± 0.03	18.96 ± 0.13	19.45 ± 0.02
9.5	14.33 ± 0.01	14.47 ± 0.02	14.52 ± 0.07	18.93 ± 0.30	18.75 ± 0.11	19.33 ± 0.14

The tendency for the FRET distance in peptides with the same distance in sequence space between Trp and dansyl to be longer when they are attached to longer peptides is also observed in these experiments. Figure 5.5 shows that the FRET distances at the temperatures studied are as expected from the distance in sequence space modulated by the effect of the peptide length. The FRET distances of Trp^{6}-dansyl in Hu1capNC < Trp^{6}-dansyl in Hu2F14capNC < Trp^{8}-dansyl in Msp1capNC < Trp^{8}-dansyl in Msp2F18capNC < Trp^{14}-dansyl in Hu2F6capNC < Trp^{18}-dansyl in Msp2F8capNC < Trp^{28}-dansyl in Msp3F8F18capNC. However, starting at 60 ^{O}C, the FRET distance between Trp^{8}-dansyl in Msp1capNC becomes greater than that between Trp^{8}-dansyl in Msp2F18capNC.

Figure 5.5 also shows that FRET distances increase regularly with increasing temperature, indicating that the macroscopic average of the peptide conformation becomes more extended. However, at the highest temperature studied (85 ^{O}C), the

structures are still much less than fully extended. These results suggest that intramolecular interactions, as discussed in section 5.3.7, continue to hold the structure of the peptides together so that it does not collapse upon increasing temperature.

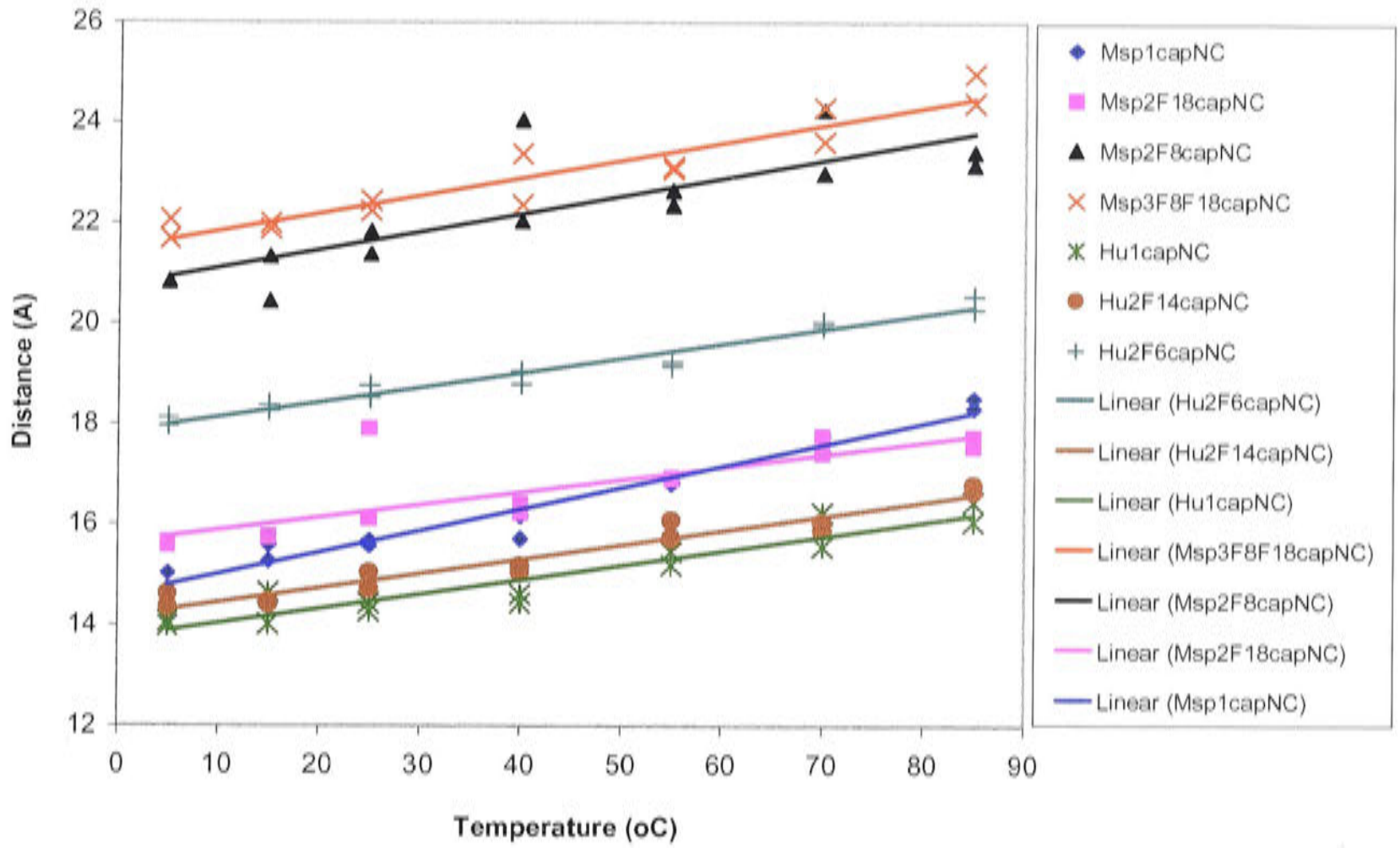

Figure 5.5: Temperature dependence of FRET distances at pH 7.2. The results of duplicate experiments (experiments were conducted by Dr. John Liggins) at temperatures 5, 15, 25, 40, 55, 70 and 85 ^{O}C for the 7 set of N- and C-terminally capped peptides. The symbols (diamond, square, triangle, etc.) represent the data points. The lines represent the linear trend of the data points fitted using the computer program GraphPad Prism 3. The slopes of the lines are as follows: Msp1capNC 0.043 ± 0.002 Å/^{O}C; Msp2F18capNC 0.025 ± 0.005 Å/^{O}C, Msp2F8capNC 0.036 ± 0.007 Å/^{O}C, Msp3F18capNC 0.035 ± 0.003 Å/^{O}C, Hu1capNC 0.029 ± 0.003 Å/^{O}C, Hu2F14capNC 0.029 ± 0.002 Å/^{O}C, and Hu2F6capNC 0.029 ± 0.002 Å/^{O}C.

It is possible that it is the interactions between Trp and His and aromatic residues in PrP-repeat peptides that cause the structure to remain slightly folded at the highest temperature studied (85 ^{O}C). The interaction between Trp and His in the form of a cation-π interaction is recognized as an important noncovalent binding interaction in structural biology (Gallivan and Dougherty, 1999). The cation-π interaction also contributes significantly to maintaining the stability of thermophilic proteins (Gromiha, 2002; Gromiha et al., 2002). The interaction of His-Trp has been reported to be the cause of an elevated pK_a for one His in barnase, which has a value of 7.75 (Loewenthal et al., 1991; Loewenthal et al., 1992). An alteration of the His side chain pK_a values was also reported in peptides, in which His and Trp residues engaged in cation-π

interactions, which stabilized α-helical structure in model Ala-based peptides (Fernandez-Recio et al., 1997). Thus, it is possible that this cation-π interaction stabilizes folded structure in PrP-repeat peptides, even at pH 7.2. Experiments to determine the apparent pK_a value of His are necessary to clarify this issue.

Figure 5.5 shows small but interesting trends in the rate of increase of distance with temperature, which is implied in the slope of the lines. As the slope reflects the stability of the structure of the peptides, the results in Figure 5.5 indicate that in terms of structural stability, Msp2F18capNC is the most stable, followed by the set of three Hu peptides, Msp2F8capNC and Msp3F8F18capNC, with Msp1capNC being the least stable. The paragraphs below will try to explain this phenomenon using the hypothesis of cation-π interaction.

Table 5.5 shows that the peptides where Trp is 4-residues distant from His generally have smaller slopes than peptides where Trp is 6-residues distant from His. The interaction of His and Trp in geometry of WH i,i+4 or HW i,i+4 was reported to be the most stabilizing one in α-helical peptides (Fernandez-Recio et al., 1997). The WH i,i+4 geometry was also proposed as a stabilizer for the loop structure in Hu PrP-octarepeat peptide (Yoshida et al., 2000). Table 5.5 also shows that the presence of Phe either 4- or 6- residues distant from His does not seem to influence the slopes. The literature suggests that the Trp residue is the most likely of the aromatics to be involved in a cation-π interaction (Gallivan and Dougherty, 1999). Thus, replacement of Trp with Phe would result in a decrease of the cation-π interaction in the mutant peptides relative to wild-type ones.

Thus, overall, the data suggest that in the wild-type Msp peptide, the structure of multi-decarepeat peptide is expected to be more stable than that of single-decarepeat peptide because in multi-decarepeats there is at least one cation-π interaction with geometry of WH i,i+4. For the same reason, the folded structure in Hu octarepeat peptide is predicted to be more stable than that in Msp decarepeat peptides.

Table 5.5: Temperature dependence of the FRET distances, and the geometry of the possible cation-π interactions in Msp and Hu PrP-repeat peptides. The possible cation-π interaction with geometry of HW i, i+4 or WH i, i+4 is presented in the shaded area.

Peptide	Sequence	Slope (Å/^{O}C)	Geometry
Msp1capNC	P***H***PGGSN**W**GQG	0.043 ± 0.002	HW i,i+6
Msp2F8capNC	P***H***PGGSN**F**GQP***H***PGGSN**W**GQG	0.036 ± 0.007	HF i,i+6; FH i,i+4; HW i,i+6
Msp3F8F18capNC	(P***H***PGGSN**F**GQ)$_2$P***H***PGGSN**W**GQG	0.035 ± 0.003	HF i,i+6; FH i,i+4; HF i,i+6; FH i,i+4; HW i,i+6
Hu2F6capNC	P***H***GGG**F**GQP***H***GGG**W**GQG	0.029 ± 0.002	HF i,i+4; FH i,i+4; HW i,i+4
Hu1capNC	P***H***GGG**W**GQG	0.029 ± 0.003	HW i,i+4
Hu2F14capNC	P***H***GGG**W**GQP***H***GGG**F**GQG	0.029 ± 0.002	HW i,i+4; WH i,i+4; HF i,i+4
Msp2F18capNC	P***H***PGGSN**W**GQP***H***PGGSN**F**GQG	0.025 ± 0.005	HW i,i+6; WH i,i+4; HF i,i+6

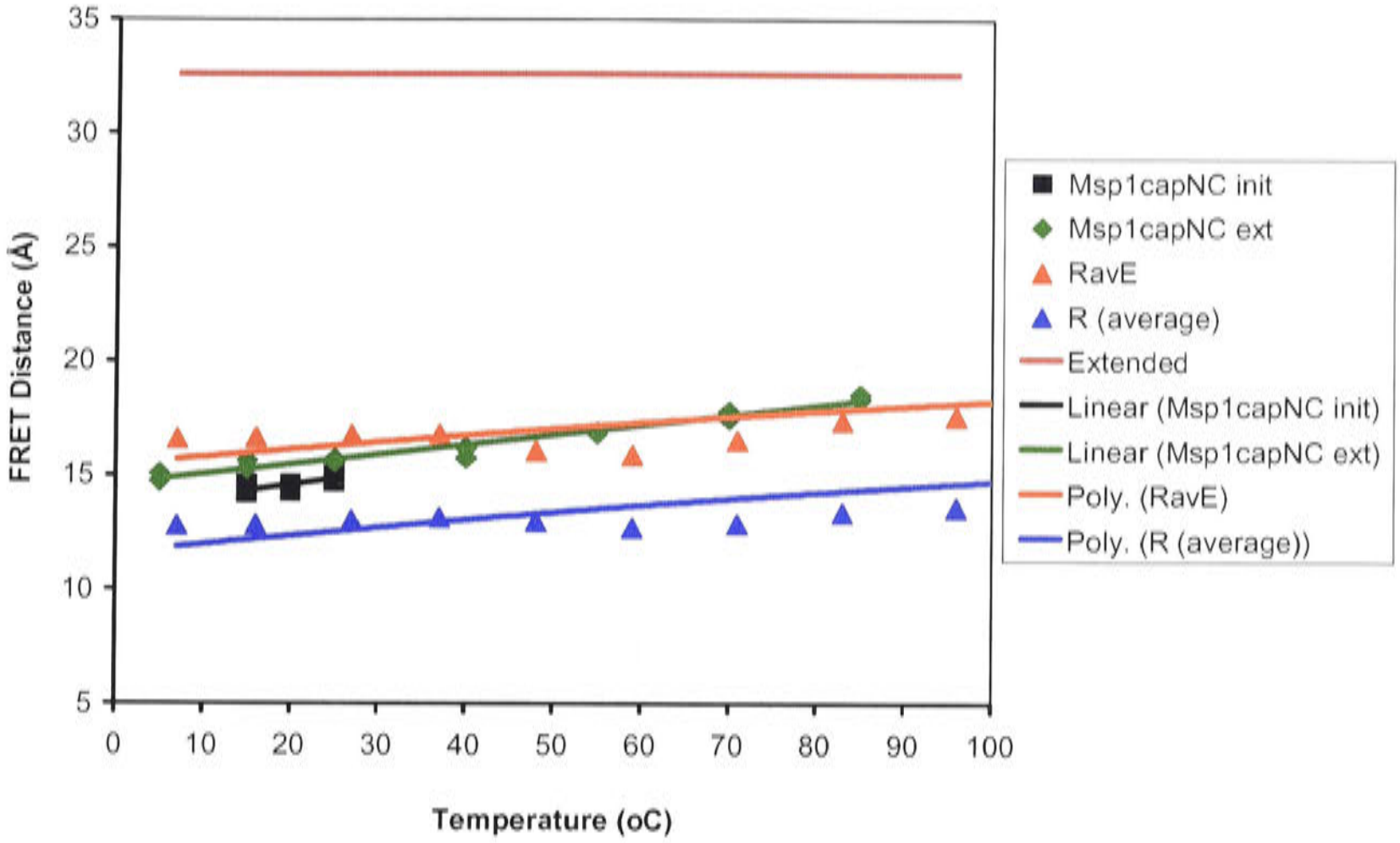

Figure 5.6: A comparison of experimental FRET distances and MD simulation results. Full details of the MD protocol will be reported elsewhere (Gustiananda, Liggins, Cummins, and Gready, paper in preparation). The replica-exchange molecular dynamics (REMD) simulation technique was used to sample effectively the conformational space of the peptide in solution. The REMD simulations were performed using 24 parallel trajectories (replicas) at temperatures distributed exponentially from a minimum value of 280 K to a maximum value of 620 K. The initial energy minimization and equilibration, and the REMD simulations were performed using the computer program, Molecular Orbital Programs for Simulations (MOPS) developed by Dr. Peter Cummins. Coordinates for analysis were collected every 0.1 ps (720,000 "snapshot" peptide structures in total). The 24 simulation temperatures translate to the experimental range 7 – 347 ^{O}C: (7, 16, 27, 37, 48, 59, 71, 83, 96, 109, 122, 136, 150, 165, 181, 197, 213, 230, 248, 266, 285, 305, 325 and 347 ^{O}C). The distance for each snapshot coordinate set was calculated between the mid-points of the bridging bonds of the naphthalene (dansyl) and the indole (Trp) rings. The extended chain estimate of 32.6 Å corresponds to the largest distance between the mid-points of the bridging bonds of the naphthalene and the indole rings obtained for a single snapshot. Msp1capNCinit represents the data points of the preliminary experiments over temperature range 15 - 25 ^{O}C. Msp1capNCext represents the data points of the later experiments (performed by Dr. John Liggins) over the extended temperature range of 5, 15, 25, 40, 55, 70 and 85 ^{O}C. R (average) is the average (from 2 ns to 3 ns of the simulation time) of the simulated Förster distance. For the simulation temperature of 27 ^{O}C, an R (average) value of 13.0 Å was obtained (average of 10,000 replicas), which is somewhat smaller than the experimental value of 15.6 Å at 25 ^{O}C. However, this is not the most informative way to compare the simulation with the experiment. The experimental Förster distance was calculated from the experimentally obtained transfer efficiency using the equation: $R = 21Å \times (E^{-1} - 1)$, where 21Å is the value of R_0 obtained assuming a kappa squared value of $^{2}/_{3}$. In order to really compare the simulation with the experiment, the same equation which was used to calculate the experimental value of R ($R = 21Å \times (E^{-1} - 1)$) was used to calculate a value of R (RavE) from the average simulated value of E; this was obtained from the formula $E = R_0^6 / (R_0^6 + R^6)$. Full details of the de novo calculation of kappa squared will be reported elsewhere (Liggins et al., manuscript in preparation). The values of RavE are in close agreement with the experimentally obtained values of R.

5.4.9. A comparison of FRET distances and MD simulation

MD simulations and analysis were performed by Dr. Peter Cummins and Dr. John Liggins. MD simulations were performed to provide an independent estimate of distance between the Trp and dansyl groups for comparison with the experimental results. The test system was dansylated Msp1.

As shown in Figure 5.6, there are two values of MD Förster distances, which were calculated in two different ways. The first value, R (average), was simply calculated directly as the 6^{th} root of the average value of R^6, in which R was measured directly from each snapshot coordinate set. The second value, RavE, was obtained from calculation of R from the average simulated values of E, which was obtained from back calculation of the first value, R (average) (see caption of Figure 5.6 for fuller details).

Förster distances calculated from the REMD simulation data for DansMsp1 are in remarkably close agreement with the experimental results for Msp1capNC/DansMsp1capC over the measured temperature range (5-85 ^{O}C), both in terms of absolute values and rates of increase with increasing temperature (Figure 5.6). The agreement is particularly striking when one compares the simulated and experimental values with the value for the fully extended polypeptide chain, of 32.6 Å.

5.4.10. Copper-ion binding and FRET distances

The results presented demonstrate that distances are reproducible and sensitive to experimental conditions; orderly T progression, some pH dependence. FRET can be used to monitor the structural changes in the protein or peptides as a result of ligand binding (dos Remedios and Moens, 1995). Previous chapters have presented results showing that copper ion binds to marsupial PrP-repeat peptides, and in so doing induces more folded structure. The FRET experiment, using dansyl and Trp as probes, to detect the structural changes in PrP-repeat peptides upon copper binding, is difficult to carry out mainly because under fluorimetry conditions the binding of copper to repeat peptides requires the free α-imino group of Pro at the N-terminus (see Chapter IV). Attachment of dansyl to the α-imino group of Pro at the N-terminus thus prevents the copper binding. Other pairs of probes would need to be introduced for the detection of structural changes associated with copper binding using the FRET method.

5.5. Conclusions

FRET has been found to be useful to investigate structural properties of PrP-repeat peptides. Inter-residual distances obtained from FRET experiments can be used as a distance constraint in structural models of PrP-repeat peptides derived from information compiled from various other spectroscopic techniques, or to validate MD simulations which can then be used to predict conformational distributions.

Trp-dansyl FRET has been found to be an efficient system for studying the PrP-repeat peptides. The method has excellent sensitivity because the initial intensity of Trp is high. This is because, in PrP-repeat peptides, Trp is solvent exposed and not undergoing thermal de-excitation, as it would be if buried in a protein. However, a major source of error is determination of concentration. Experience with two experimenters (myself and Dr. John Liggins) and repeat experiments show that small differences in concentration between dansylated and nondansylated samples may give variation of >0.5 Å; this error is not apparent in duplicates samples which were made from the same diluted stock.

Another potential source of error is the effect of dansyl attachment on both the Trp environment and on the structure of the peptide. The FRET method requires separate measurements of Trp emission intensity for nondansylated and dansylated pairs of peptides. As Trp intensity is very sensitive to the environment around the Trp residue, the method requires that this environment is unchanged in the dansylated peptide so that its intrinsic intensity is the same as in the reference nondansylated form. If this is not the case then the measured intensity decrease due to the resonance energy transfer to dansyl would contain other contributions and lead to errors in estimation of the Trp to dansyl distance from use of the Förster equation. Most applications of FRET involve folded proteins for which disturbance of the protein structure from dansylation is readily detectable, or can be minimized by optimum design of donor and acceptor positions if a high-resolution structure is available. For peptides lacking formal structure, such as studied here, there is no guidance in the literature on the effect of dansylation. In this study, CD was used to check for an effect. The CD spectra for the nondansylated form showed characteristic features of disordered structure. Although some spectral changes were apparent for the dansylated forms, the spectra are not consistent with any secondary structure category and most resemble random-coil or disordered polypeptide.

Hence, it is assumed that dansylation did not cause structural changes which would invalidate application of the FRET method.

FRET experiments and molecular dynamics simulations have shown that PrP-repeat peptide, either from marsupial or human, adopts disordered structure that is somewhat loosely folded. This structure is only moderately perturbed towards more extended conformations by increasing the temperature. The interaction of Trp-His through the cation-π interaction is proposed to be the major factor that stabilizes the folded structure in PrP-repeat peptides. The disposition of a four-residue interval between Trp and His is apparent in the more stable peptides.

The literature reports, and results in preceding chapters confirm, that PrP-repeat peptides adopt a random-coil structure, and do not adopt a single preferred stable conformation. This type of peptide will thus certainly have heterogeneity in the donor-acceptor distance; the MD simulations show that the peptide does not adopt a single preferred structure, but a distribution for which the average (see Figure 5.6 caption) is close to the FRET distance (Cummins et al., unpublished 2003). This heterogeneity cannot be detected by using the steady-state intensity measurements employed in this study. Such information in principle can be obtained by using fluorescence decay (time resolved) or fluorescence anisotropy decay experiments. However, it will be desirable to do such experiments to see if a large distribution of distances between chromophores is detectable, as fluorescence decay experiments have been applied to study the conformational dynamics of small flexible peptides such as RNase S-peptide (Maliwal et al., 1993), melittin (Lakowicz et al., 1994), galanin (Kulinski et al., 1997), and bradykinin (de Souza et al., 2000). Such distance distributions reflect the populations of peptide conformations, which coexist in equilibrium during the fluorescence lifetime.

Chapter VI

Electrospray Ionization Mass Spectrometry

Use of electrospray ionization mass spectrometry (ESI MS) for studying noncovalent protein complexes has been established for some time. ESI is a soft ionization technique for transferring protein molecules from their initial state in a sample (solution) to ionized states in gas phase, so that the molecular ions can be detected and mass analyzed. The gentleness of this ionization allows the noncovalent protein complex to survive the process without the protein undergoing any molecular fragmentation or complex dissociation. Although ESI MS detects the molecular ions in the gas phase, several recent studies suggest that a gas-phase measurement can reveal the complex properties in the solution phase (for reviews see Loo (1997) and Veenstra (1999)).

Due to its ability to measure accurately the molecular mass of the complex being studied, an important property of the complex that can be measured by ESI MS is the stoichiometry of the binding. Based on the mass difference between the complex and the apoprotein, the signals can be translated into stoichiometry (Hu and Loo, 1995). Some reports have also suggested that other complex properties such as dissociation constants (Bruce et al., 1995; Jorgensen et al., 1998; Whittal et al., 2000), conformational changes (Hutchens and Allen, 1992; Veenstra et al., 1998a; Veenstra et al., 1998b) and differentiation of cooperative vs. sequential binding (Hu and Loo, 1995) can be measured by ESI MS. However, careful and appropriate controls as well as interpretation of the data should be applied in such studies (Smith and Lightwahl, 1993).

6.1. Introduction

6.1.1. Principles of electrospray ionization mass spectrometry

There are three successive stages in ESI MS: spraying the liquid, forming ions from the highly charged droplets, and sampling and mass analysing the ions in a mass analyzer in vacuum (Mann, 1992). The first two stages are sketched in Figure 6.1 and the formation of molecular ions is described below.

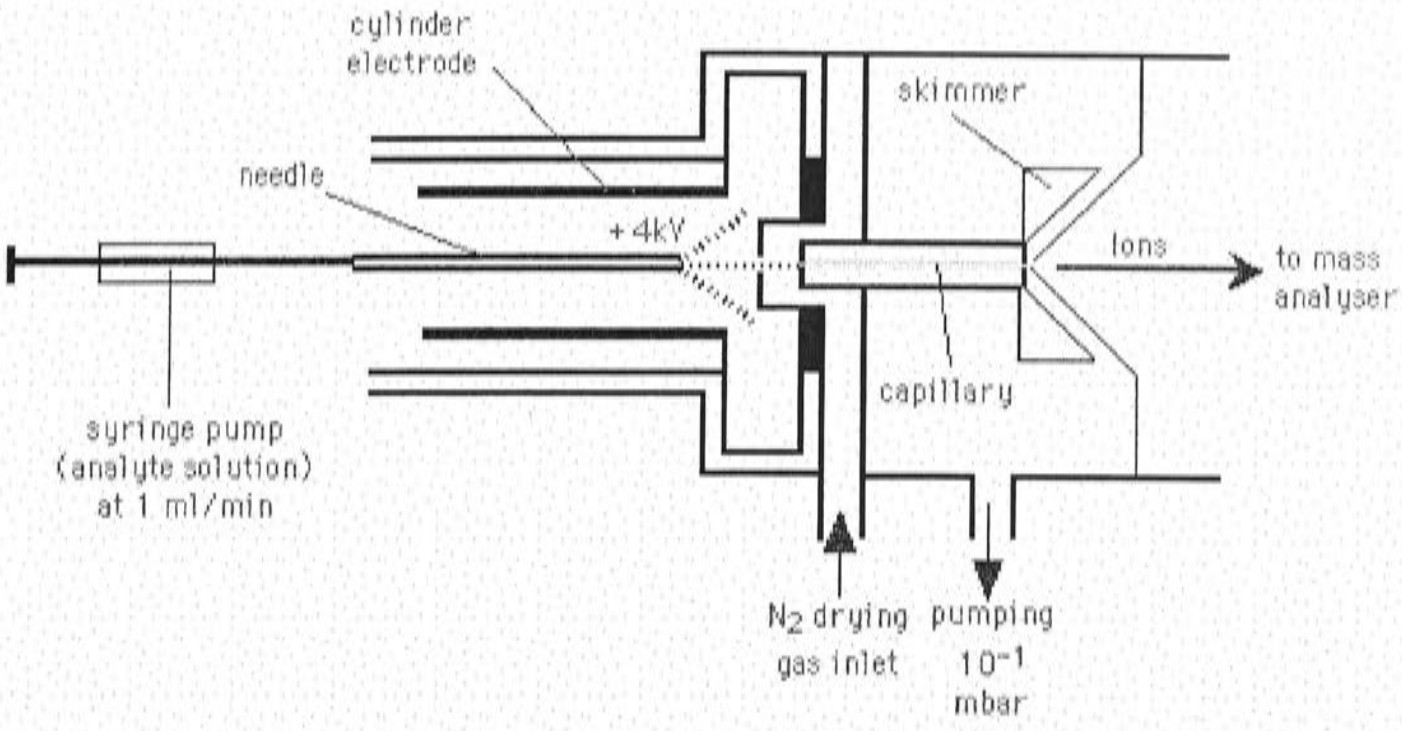

Figure 6.1: Schematic diagram of ESI MS process. The figure is taken from http://www-methods.ch.cam.ac.uk/meth/ms/theory/esi.html.

ESI MS produces singly or multiply charged ions directly from solution by creating a fine spray of highly charged droplets in the presence of a strong electric field. The sample solution is forced through a needle, which has a high electric field at the tip. This electric field is produced from the potential difference applied between the needle and the surrounding electrode. The high potential disperses the emerging liquid into a very fine spray of charged droplets, which all have the same polarity. Driven by the field, the charged droplets move away from the needle tip towards the end plate of the chamber located a few centimeters away. A drying gas flowing counter to the droplets' direction of motion helps to evaporate the solvent; this shrinks the droplets' size and increases the concentration of charge at the droplets' surface. At some point, the charge concentration at the droplet surface is so high that it exceeds the constraints of the surface tension of the droplets, which explode into smaller droplets with lower charge. The molecular ions are the final result of the repeated process of droplet shrinking and explosion. The molecular ions then enter the capillary and are focused into the mass analyzer through a series of lenses (Mann, 1992; Veenstra, 1999).

As the molecule has been transformed into a multiply charged ion, the mass spectrometry data (relative abundance of the various charge states of the molecule) are plotted against their mass-to-charge ratio (m/z). This is often referred to as a m/z spectrum. However for many applications (i.e. the spectra of mixtures) it is better that the data are transformed and displayed on a true molecular mass axis. The transformation process or deconvolution was carried out using software included within

the instrument software. The data plot on the true molecular mass axis is called the deconvoluted or transformed spectrum (Mann, 1992; Veenstra, 1999).

6.1.2. Mass spectrometry in the study of copper binding to PrP-repeat peptides

There are many examples of the application of mass spectrometry to the study of metal binding to peptides and proteins (Allen and Hutchens, 1992; Hutchens et al., 1992; Yu et al., 1993; Hu and Loo, 1995; Jiao et al., 1995; Moreau et al., 1995), and this method has also been applied to the study of copper binding to PrP repeats (Hornshaw et al., 1995b; Whittal et al., 2000; Kramer et al., 2001) (see Table 1.3 and 1.4 of Chapter I).

Using MALDI TOF (matrix assisted UV laser desorption/ionization time-of-flight) mass spectrometry, Hornshaw et al. (1995b) showed that synthetic peptides containing three or four copies of an octapeptide repeat sequence (PHGGGWGQ) preferentially bind copper over other metals with a stoichiometry of one copper per repeat. Peptides from the analogous region of chicken PrP, which contain an N-terminal repeat domain of the hexapeptide (NPGYPH), showed similar specificity and stoichiometry for copper binding (Hornshaw et al., 1995b).

Whittal et al. (2000) employed ESI MS to measure both the stoichiometry and binding affinity of copper ions to the repeat region of PrP, including pre- and post-repeat sequence. The stoichiometries of the complexes measured directly by ESI MS were pH dependent: a peptide containing four octarepeats chelated two copper ions at pH 6.0 but four at pH 7.4. Dissociation constants (K_d) for each copper ion binding to the octarepeat peptides were mostly in the low micromolar range. Copper ions also bound to the pre- and post-repeat sequence. In the C-terminally extended peptide (include post-repeat sequence), which has a fifth His residue, the binding of multiple copper ions at the higher pH occurs with a high degree of cooperativity. Whittal et al. also report the participation of free alpha amino group of the N-terminus in copper binding at higher copper concentration but not at lower copper concentration (Whittal et al., 2000).

In contrast to Whittal et al. (2000), Kramer et al. (2001) used ESI MS only to elucidate the stoichiometry of copper binding. They argued that ESI mass spectra for PrP and its peptides appear to reflect the situation in solution only qualitatively, not quantitatively.

The reported stoichiometry was four copper ions bound to human PrP_{60-91}, while binding of up to five copper ions was observed for the full-length murine PrP_{23-231} (Kramer et al., 2001).

6.2. Aims

In this project, ESI MS was used to detect noncovalent interactions between synthetic marsupial PrP-repeats peptide (Msp) (see Table 6.1) and copper ions as well as other metal ions. The method was also used to measure the copper-binding stoichiometry and elucidate the copper binding ability of some modified Msp1 peptides (peptides with single residue replacements by Ala and protection of N- and C-termini) (see Table 6.1). The data for copper binding ability of the modified Msp1 peptides should be able to provide information on the groups involved in copper binding. Therefore, the aim of using ESI MS is to determine the stoichiometry of the complex formation between copper and Msp peptides, screen the possible binding of other metals to Msp peptides, and identify the copper-binding sites.

6.3. Materials and methods

Table 6.1: Synthetic peptides used in the experiments

Peptide	Sequence	Size
Msp4	$(PHPGGSNWGQ)_4G$	41
Msp3	$(PHPGGSNWGQ)_3G$	31
Msp2	$(PHPGGSNWGQ)_2G$	21
Msp1	$(PHPGGSNWGQ)_1G$	11
Msp1H2A	$(PAPGGSNWGQ)_1G$	11
Msp1N7A	$(PHPGGSAWGQ)_1G$	11
Msp1Q10A	$(PHPGGSNWGA)_1G$	11
Msp1capN	Ac-$(PHPGGSNWGQ)_1G$	11
Msp1capC	$(PHPGGSNWGQ)_1G$-NH_2	11
Msp1capNC	Ac-$(PHPGGSNWGQ)_1G$-NH_2	11

6.3.1. Sample preparation

Typically, unless otherwise stated, the sample had final peptide concentration of 10 μM and $CuSO_4$ concentration of 100 μM in buffer. The buffer was either 10 mM ammonia/formic acid at pH 7.4 or 10 mM N-ethylmorpholine (NEM)/formic acid at pH 7.4. A 50 μL sample was injected into the ESI MS machine.

6.3.2. Choice of buffers

At the initial stage of the research, the buffer used was 10 mM ammonia/formic acid pH 7.4 for it is volatile and does not interact with copper ions. This buffer was also employed as a standard volatile buffer in the mass spectrometry laboratory of the Research School of Chemistry ANU. This buffer is recommended for use in pH ranges 7.0-10.0 (Perrin and Dempsey, 1974). However, over several hours during the ESI MS experiments, the sample solutions initially buffered at pH 7.4 became acidic (pH ~ 4.0). Due to this problem, the subsequent experiments used 10 mM N-ethylmorpholine (NEM)/formic acid buffer pH 7.4 instead. NEM does not interact with copper ions (Viles et al., 1999) and has been used in ESI MS experiments of copper binding to PrP-repeat peptides (Kramer et al., 2001). The NEM/formic acid buffer proved to be more stable than the ammonia/formic acid buffer in maintaining the pH at 7.4. However, the results of the experiments using ammonia/formic acid buffer are reported in this chapter (section 6.4.1, 6.4.2, and 6.4.3) to give an initial overview of the binding of copper and other metals to the peptide. These experiments were not repeated using NEM/formic acid buffer due to the time constraints of the thesis.

6.3.3. Conditions of data acquisition

Mass spectrometry of the peptides, with and without copper ions, was performed on a VG Quatro II Electrospray Ionization Mass Spectrometer in positive ion mode. The applied spray (capillary) voltage was 3.5 kV. Capillary temperature was set at 70 ^{O}C.

6.4. Results and discussion

6.4.1. Copper binding to Msp2, Msp3, and Msp4 peptides

ESI MS of the synthetic peptides containing several copies of the second repeat sequence of a marsupial PrP (Msp) resulted in the expected average masses for the apopeptides. Average mass units (amu) are Msp2, 2111; Msp3, 3129; and Msp4, 4147 (see Table 6.2 and Figures 6.2 and 6.3).

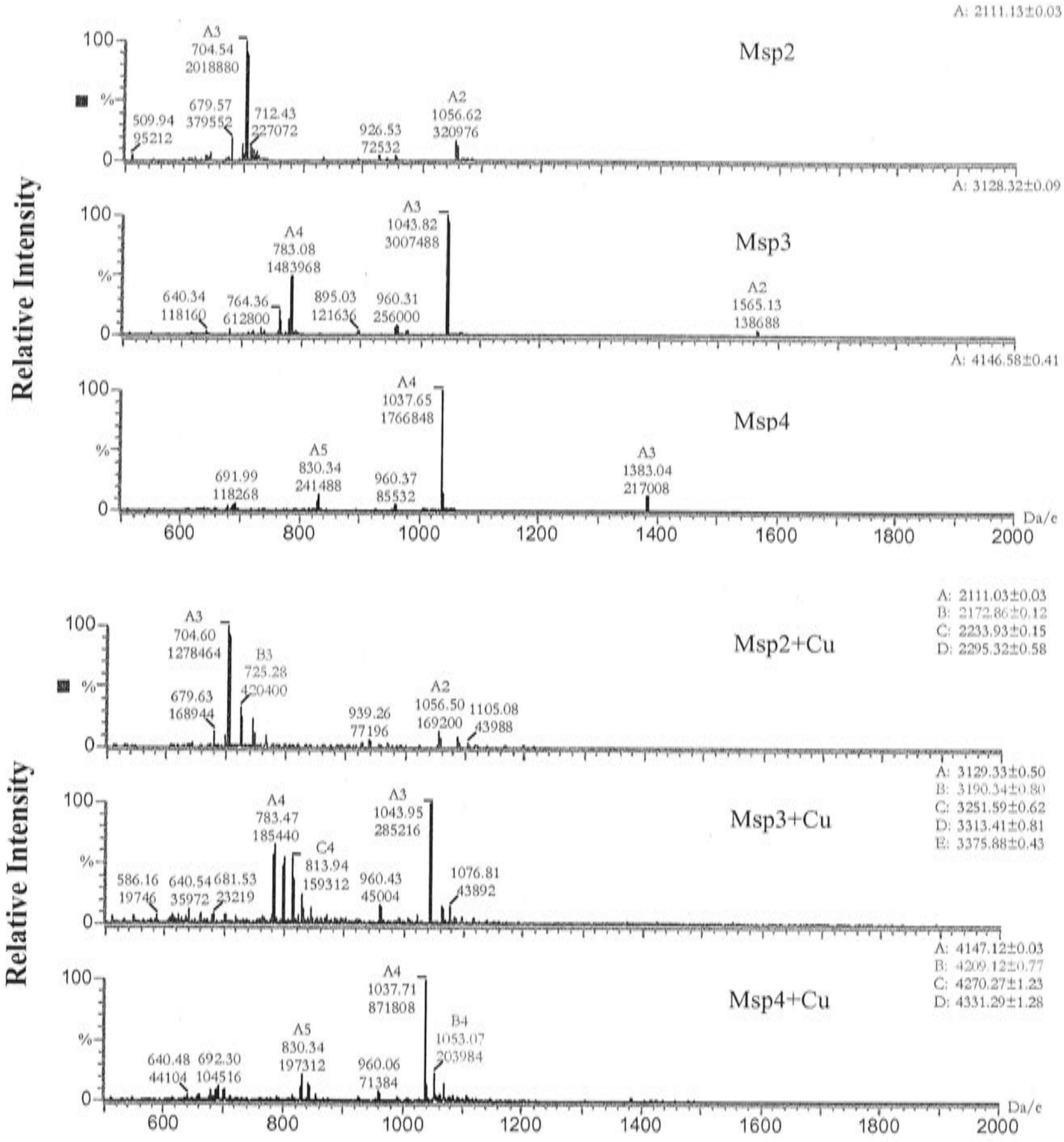

Figure 6.2: ESI MS data of copper binding to Msp peptides presented as mass/charge spectra. Mass/charge (m/z) (in Da/e) spectra were taken from 10 μM Msp peptides (Msp2, Msp3, and Msp4) in 10 mM ammonia/formic acid buffer pH 7.4 in the absence (upper panels) and presence (lower panels) of 100 μM $CuSO_4$. The most intense signal in the mass spectrum for Msp2 is $[Msp2+3H]^{3+}$, for Msp3 is $[Msp3+3H]^{3+}$, and for Msp4 is $[Msp4+4H]^{4+}$. Addition of copper ion does not change the most intense signal of the Msp peptides in the spectra. Addition of ten times molar ratio of copper to the Msp peptides did not change the charge states of the peptides, suggesting that the charge states are not derived from the bound metal ion. Increases in mass as a result of the addition of copper ions with no change in charge states suggests complex formation via noncovalent binding of copper to Msp peptides, rather than just cation adduction as a result of the electrospray process.

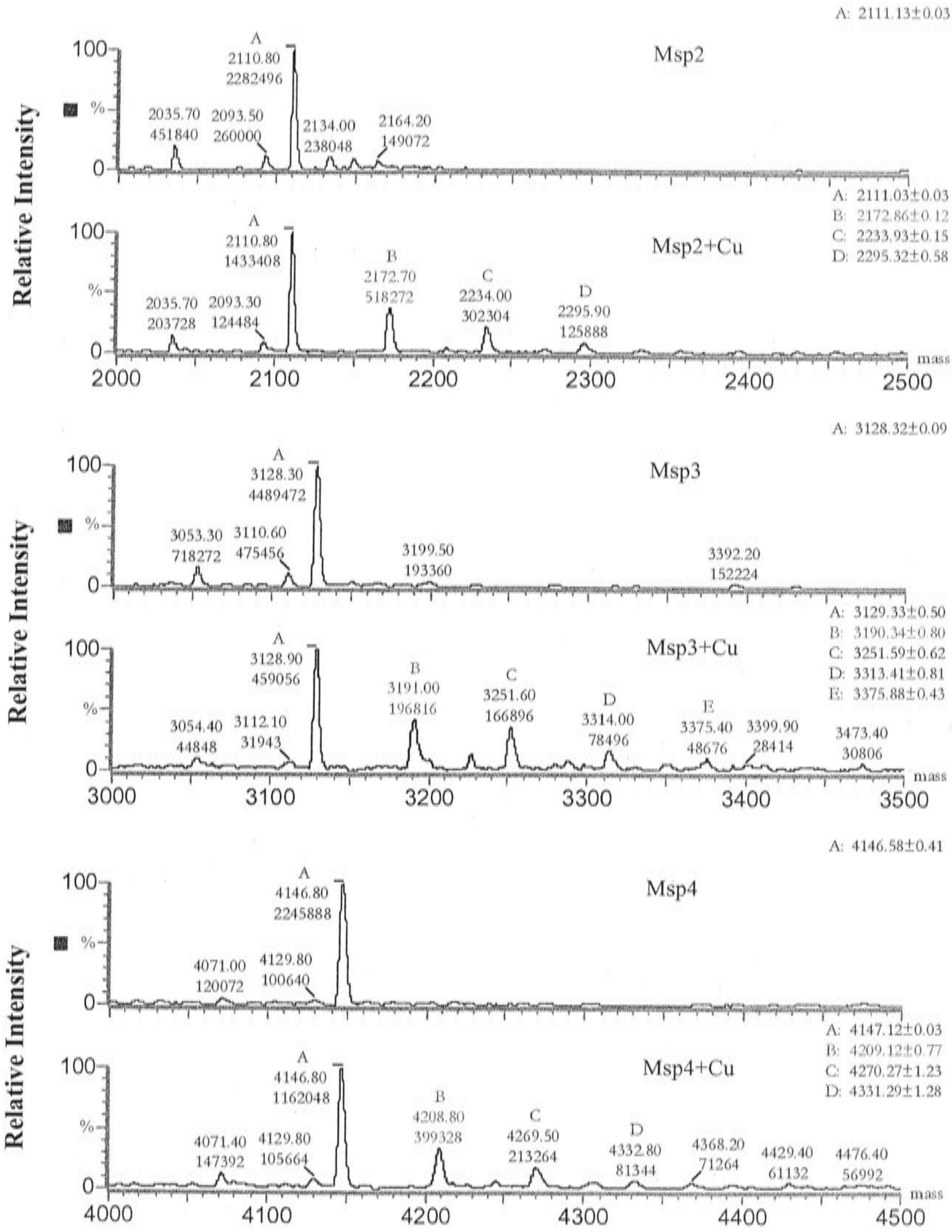

Figure 6.3: ESI MS data of copper binding to Msp peptides presented as transformed spectra. The spectra were taken from 10 µM Msp peptides (Msp2, Msp3, and Msp4) in 10 mM ammonia/formic acid buffer pH 7.4, in the absence and presence of 100 µM $CuSO_4$. When components have been identified in the m/z spectrum (Figure 6.2), the data system assigns charge states to each peak. The Transform algorithm uses this information to display the m/z spectrum on a true molecular mass axis. The average incremental difference in mass of approximately 61.5 between two neighboring molecular mass peaks suggests that the binding of one atom of copper releases two protons. The maximum number of copper ions that can be bound by Msp peptides is: three for Msp2, four for Msp3, and three for Msp4.

Addition of a 10-fold excess of $CuSO_4$ resulted in mass spectra of apopeptides with several additional peaks (see Figure 6.2 and 6.3). Table 6.3 and Figure 6.3 show that there is an increase of 61.5 amu in the molecular mass between neighboring peaks upon addition of copper, suggesting that the binding of one atom of copper releases two protons from the peptide molecule. The maximum numbers of copper ions that can be bound by Msp peptides are: three for Msp2, four for Msp3, and three for Msp4.

Table 6.2: Mass assignment for Msp peptides

Peptide	Sequences	Predicted Molecular Mass		Observed Molecular Mass
		Monoisotopic	Average	
Msp2	$(PHPGGSNWGQ)_2G$	2109.92	2111.18	2111.13±0.55
Msp3	$(PHPGGSNWGQ)_3G$	3127.36	3129.24	3128.32±0.09
Msp4	$(PHPGGSNWGQ)_4G$	4144.80	4147.29	4146.58±0.41

The most intense signals in the m/z spectra (see Figure 6.2 top) are: Msp2, $[Msp2+3H]^{3+}$; Msp3, $[Msp3+3H]^{3+}$; and Msp4, $[Msp4+4H]^{4+}$. Addition of copper did not change the most intense signal or the charge states of the peptides (see Figure 6.2 bottom). As just mentioned above, the m/z spectra (Figure 6.2) as well as the transformed spectra (see Figure 6.3) show that additional peaks emerge as a result of copper ions bound to Msp2, Msp3 and Msp4. It has been previously reported (Allen and Hutchens, 1992) that increases in mass as a result of the addition of metal ions with no change in charge states toward higher z values (lower m/z) suggest complex formation via noncovalent binding of metal to peptides, rather than just cation adduction as a result of the electrospray process. Thus, the additional peaks in the Msp spectra appear to reflect these peptide-copper complexes.

While the absence of a charge state shift towards higher z values upon addition of metal ions reflects the specific noncovalent interaction between peptides and metal ions, a charge state shift towards lower z values could reflect changes in conformation upon metal binding, in which the holopeptides are more folded or more structured than the apopeptides. Conformational changes reflected by changes in the charge envelope of the molecular ions have been previously reported in the literature (Hutchens and Allen, 1992; Veenstra et al., 1998a; Veenstra et al., 1998b). It has also been reported that addition of copper ions to full-length PrP, as well as to peptide corresponding to the N-

terminal tandem repeat region of PrP, resulted in a significant shift of the m/z peaks to lower charge z values, and thus higher m/z values. This suggests conformational changes associated with copper binding, resulting in a more folded conformation compared with the apopeptides or apoproteins (Whittal et al., 2000; Kramer et al., 2001).

The phenomenon of charge state shift towards lower z values was not observed in this study. Furthermore, under the experimental conditions, only small peaks of copper adducts were observed. The reason for only small peaks of copper adducts in the spectra is probably due to the pH being lower than 7.4, so that the binding of copper to the peptides is not optimum. As mentioned in section 6.3.2, the buffer used in these experiments is ammonium formate, which has a buffering capacity from pH 2.75-4.75 (pKa of formate is 3.75), so that it does not work well in maintaining the pH at 7.4. This pH effect, leading to the appearance of only small peaks of copper adducts, was reported by Whittal et al. (2000) for copper addition to ShaPrP(57-91) at pH 3.5: the free peptide peak (relative intensity around 80%) dominates the peaks for the copper adducts, which have relative intensities of less than 20% for one bound copper, around 5% for two bound, with the rest (three, four, and five copper ions) around 2%. Hence, it is important to use a buffer that works well at pH 7.4. As ESI MS requires the use of a volatile buffer, the choices are limited. Kramer et al. (2001) reported that the ESI MS of copper binding to PrP and its peptides is quite sensitive to the chosen buffer and introduced a new buffer system, N-ethylmorpholine (NEM). NEM has a pK_a of 7.7 and an effective pH range of 6.7-8.7.

There are two possible explanations for why the charge states do not shift towards lower z values in the Msp spectra of copper complexes. Firstly, copper ions do not bind optimally to the peptides as a result of lower pH, and, thus no conformational changes are induced. Secondly, it is possible that the conformation induced by copper ions is an open conformation such as a solvent-exposed α-helix structure, which is detected in FTIR experiments (see Chapter III). In this case, there would be no change in the charge envelope of the molecular ions as the residues or groups that carry the charges are still accessible and not buried within the molecule. These two possible explanations need to be clarified by repeat of the experiments using a reliable buffer, such as NEM, so that copper binding to Msp peptides will be optimum.

Table 6.3: Molecular mass assignment for Msp peptides (Msp2, Msp3, and Msp4) and their copper complexes observed by ESI MS

Peptide	No. of copper atoms bound (n)	[M-2nH+nCu] calculated	Mass observed	Incremental difference in mass
Msp2	0	2111.1808	2111.03±0.03	
				61.83
	1	2172.7109	2172.86±0.12	
				61.07
	2	2234.2410	2233.93±0.15	
				61.39
	3	2295.7711	2295.32±0.58	
		Average incremental difference in mass		61.43
Msp3	0	3129.2375	3129.33±0.50	
				61.01
	1	3190.7676	3190.34±0.80	
				61.25
	2	3252.2978	3251.59±0.62	
				61.82
	3	3313.8279	3313.41±0.81	
				62.47
	4	3375.3580	3375.88±0.43	
		Average incremental difference in mass		61.64
Msp4	0	4147.2943	4147.12±0.03	
				62
	1	4208.8244	4209.12±0.77	
				61.15
	2	4270.3545	4270.27±1.23	
				61.02
	3	4331.8846	4331.29±1.28	
		Average incremental difference in mass		61.39

6.4.2. Binding of other metal ions to Msp2

Msp2 was found to bind other metal ions such as calcium, zinc, magnesium and manganese (see Figures 6.4 and 6.5). As there is little evidence for significant binding of these ions to PrP-repeat peptides using other techniques, these ESI MS results suggest caution; it is likely that the additional peaks upon addition of metals in mass spectrometry are a result of non-specific ionic interaction *in the gas phase*. Note that similar behavior to the copper binding experiments was observed; the most intense signal did not change upon addition of the metal ions and the charge state remained the same before and after addition of metal ions, suggesting that the charge states are not derived from the bound metal ion.

Thus, as before, increases in mass as a result of the addition of the metals with no change in charge state suggests complex formation via noncovalent binding of metals to Msp2, rather than just cation adduction as a result of the electrospray process. The average incremental difference in mass of 61.5 (Cu), 38.02 (Ca), 63.54 (Zn), 22.22 (Mg), and 52.17 (Mn) between two neighboring peaks (see Figure 6.5 and Table 6.4) suggests that the binding of one metal atom releases two protons.

The MALDI-TOF mass spectrometry investigation reported by Hornshaw et al. (1995b) showed that the human octapeptide repeat sequence preferentially binds copper over other divalent metal ions such as zinc, manganese, cobalt, nickel, iron, calcium, and magnesium. This result was confirmed by fluorescence quenching experiments, which showed that only after addition of copper, and not other metal ions, was quenching significant (Hornshaw et al., 1995a). Whittal et al. (2000) also observed specificity of copper binding over that of zinc and nickel to the PrP repeats as monitored by ESI MS. Under identical experimental conditions, only peptides with added copper showed significant charge shift towards lower z values (higher m/z) as well as the appearance of metal-ion adducts with high relative intensity and reduced relative intensity of the metal-free species (Whittal et al., 2000). The specificity of copper binding for full-length $ShaPrP_{29\text{-}231}$ was shown by the lack of fluorescence quenching upon addition of other metals (Stockel et al., 1998).

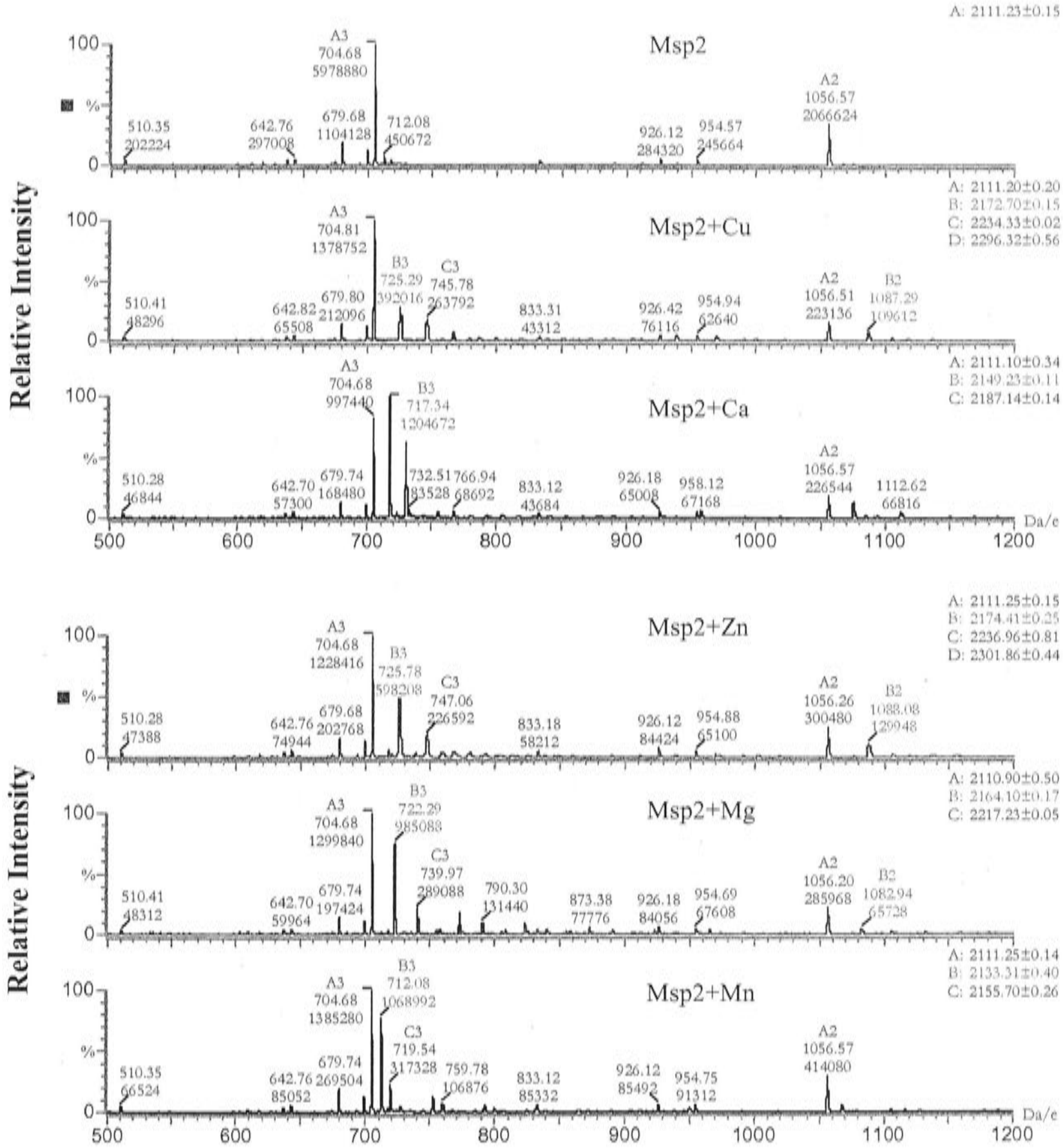

Figure 6.4: ESI MS data of binding of other metal ions to Msp2 peptide presented as mass/charge spectra. Mass/charge (m/z) (in Da/e) spectra were taken from 10 μM Msp2 in 10 mM ammonia/formic acid buffer pH 7.4 in the absence and presence of 100 μM $CuSO_4$, $CaCl_2$, $ZnCl_2$, $MgCl_2$, and $MnSO_4$. The most intense signal in the mass spectra for Msp2 is $[Msp2+3H]^{3+}$. Addition of metal ions does not change the most intense signal of Msp2 in the spectra. Addition of ten times molar ratio of metal ions does not change the charge states of the peptide, suggesting that the charge states are not derived from the bound metal ion.

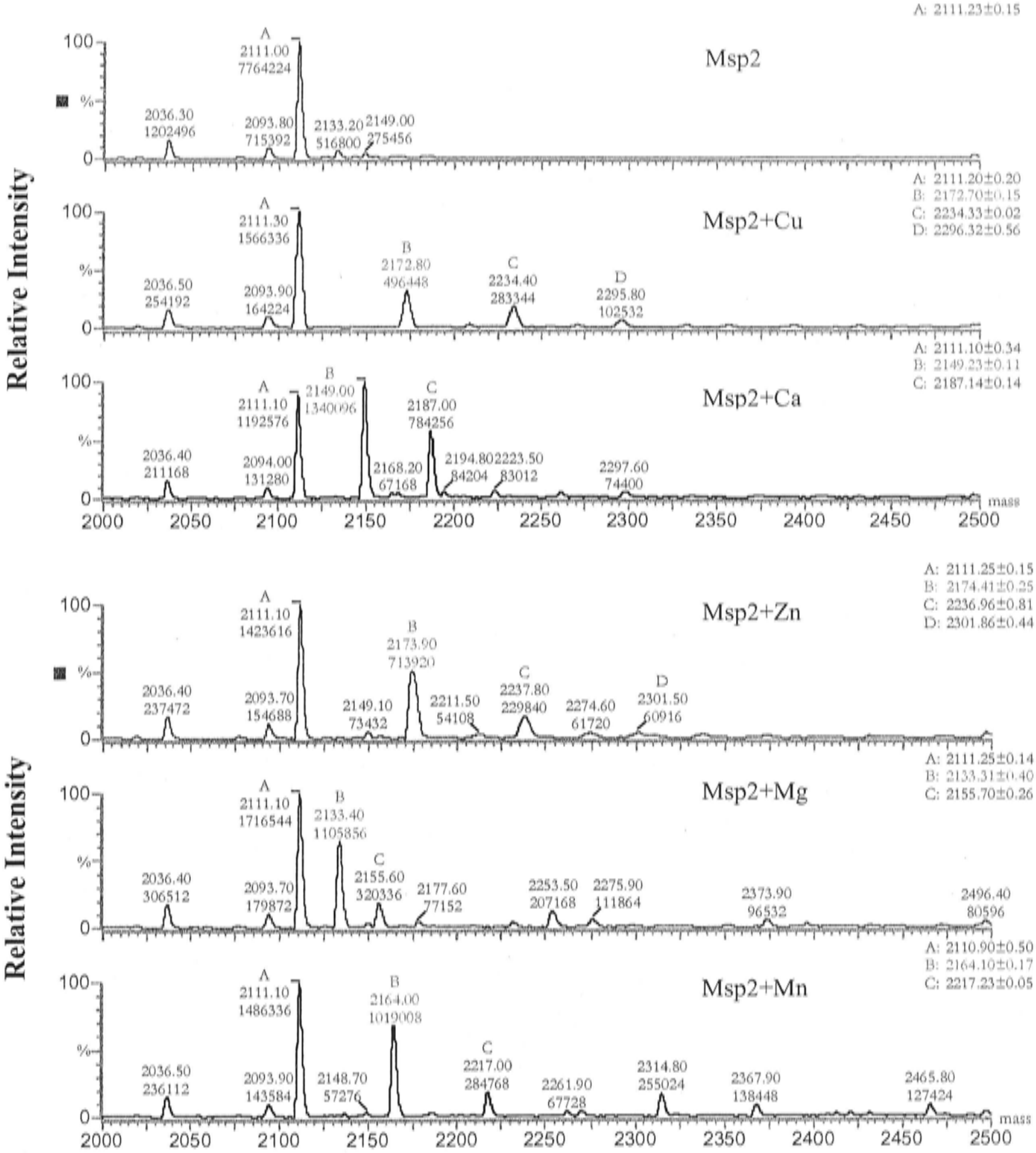

Figure 6.5: ESI MS data of binding of other metal ions to Msp2 peptide presented as transformed spectra. The spectra were taken from 10 μM Msp2 in 10 mM ammonia/formic acid buffer pH 7.4, in the absence and presence of 100 μM $CuSO_4$, $CaCl_2$, $ZnCl_2$, $MgCl_2$, and $MnSO_4$. When components have been identified in the m/z spectrum (Figure 6.4), the data system assigns charge states to each peak. The Transform algorithm uses this information to display the m/z spectrum on a true molecular mass axis. The average incremental difference in mass of 61.5 (Cu), 38.02 (Ca), 63.54 (Zn), 22.22 (Mg), and 52.17 (Mn) between two neighboring molecular mass suggests that the binding of one metal atom releases two protons.

Table 6.4: Molecular mass assignment for Msp2 and Msp2-metal complexes observed by ESI MS

Peptide or Complexes	No. of metal atoms bound (n)	[M-2nH+nmet] calculated	Mass observed	Incremental difference in mass
Msp2	0	2111.18	2111.23±0.15	
Msp2+Cu	0	2111.18	2111.20±0.20	
				61.5
	1	2172.71	2172.70±0.15	
				61.63
	2	2234.24	2234.33±0.02	
				61.99
	3	2295.77	2296.32±0.56	
		Average incremental difference in mass		61.71
Msp2+Ca	0	2111.18	2111.10±0.34	
				38.13
	1	2149.24	2149.23±0.11	
				37.91
	2	2187.30	2187.14±0.14	
		Average incremental difference in mass		38.02
Msp2+Zn	0	2111.18	2111.25±0.15	
				63.16
	1	2174.55	2174.41±0.25	
				62.55
	2	2237.93	2236.96±0.81	
				64.9
	3	2301.30	2301.86±0.44	
		Average incremental difference in mass		63.54
Msp2+Mg	0	2111.18	2111.25±0.14	
				22.06
	1	2133.47	2133.31±0.40	
				22.39
	2	2155.76	2155.70±0.26	
		Average incremental difference in mass		22.22
Msp2+Mn	0	2111.18	2110.90±0.50	
				53.2
	1	2164.10	2164.10±0.17	
				53.13
	2	2217.02	2217.23±0.05	
		Average incremental difference in mass		53.17

While there are many reports of the specificity of PrP and its N-terminal octapeptide repeats to bind copper (Hornshaw et al., 1995a; Hornshaw et al., 1995b; Stockel et al., 1998; Whittal et al., 2000), others have demonstrated the ability of octapeptide (Jackson et al., 2001) as well as full-length PrP (Brown et al., 2000) to bind other metal ions as well. Fluorescence quenching studies showed that other metal ions such as Zn(II),

Ni(II) and Mn(II) can bind to the N-terminal octapeptide of PrP with affinity three or more orders of magnitude more weakly than Cu(II) (Jackson et al., 2001). Substitution experiments demonstrated manganese could replace copper in the PrP molecule, indicating the ability of PrP to bind other metals (Brown et al., 2000).

So there is evidence in the literature to support the possibility that Msp peptides could bind other metal ions such as calcium, zinc, manganese, and magnesium. The binding of other metal ions to Msp peptides has been checked by FTIR experiments (see Chapter III), which suggests they can bind zinc, calcium, and magnesium ions but not manganese. The binding properties of these metal ions need to be characterized further.

6.4.3. Copper ion titration of Msp4

ESI MS experiments were carried out to titrate Msp4 with copper. Figure 6.6 shows the complete spectra while Figure 6.7.A shows an expanded view. Data for Cu/Msp4 molar ratio higher than 8 cannot be obtained due to instability in the electrospray at higher copper ion concentration. Blockage of the electrospray channel by copper hydroxide precipitation that occurs at pH 7.4 presumably caused such instability. Copper ion titration of Msp4 shows stepwise loading (of the binding sites), as depicted in Figure 6.7, suggesting that the sites are independent and identical. However, in the presence of up to 8 mol of copper per mol of Msp4, the Msp4 molecule was never totally bound in a complex. There could be two reasons for this. Firstly, there is probably an equilibrium established between uncomplexed and complexed forms. Fluorimetry experiments showed that the K_d of copper binding to Msp4 at pH 7.4 is of the order of nM. The ESI MS titration experiments were conducted at 10 μM Msp4 and varied concentration of copper ions (0 - 80 μM). As the highest copper concentration is 8 times the peptide concentration, all peptide should have bound copper ions. However, the data show that a large proportion of Msp4 molecules still exist as free peptide. Secondly, the pH of the solution is probably much lower than 7.4; as mentioned earlier, ammonium formate is not an effective buffer system to work at pH 7.4. At more acidic conditions, probably around pH 3.0-4.0, the affinity of copper binding to Msp4 will be reduced significantly. At this pH copper binding is weak, as reflected in the small peaks in the ESI mass spectrum.

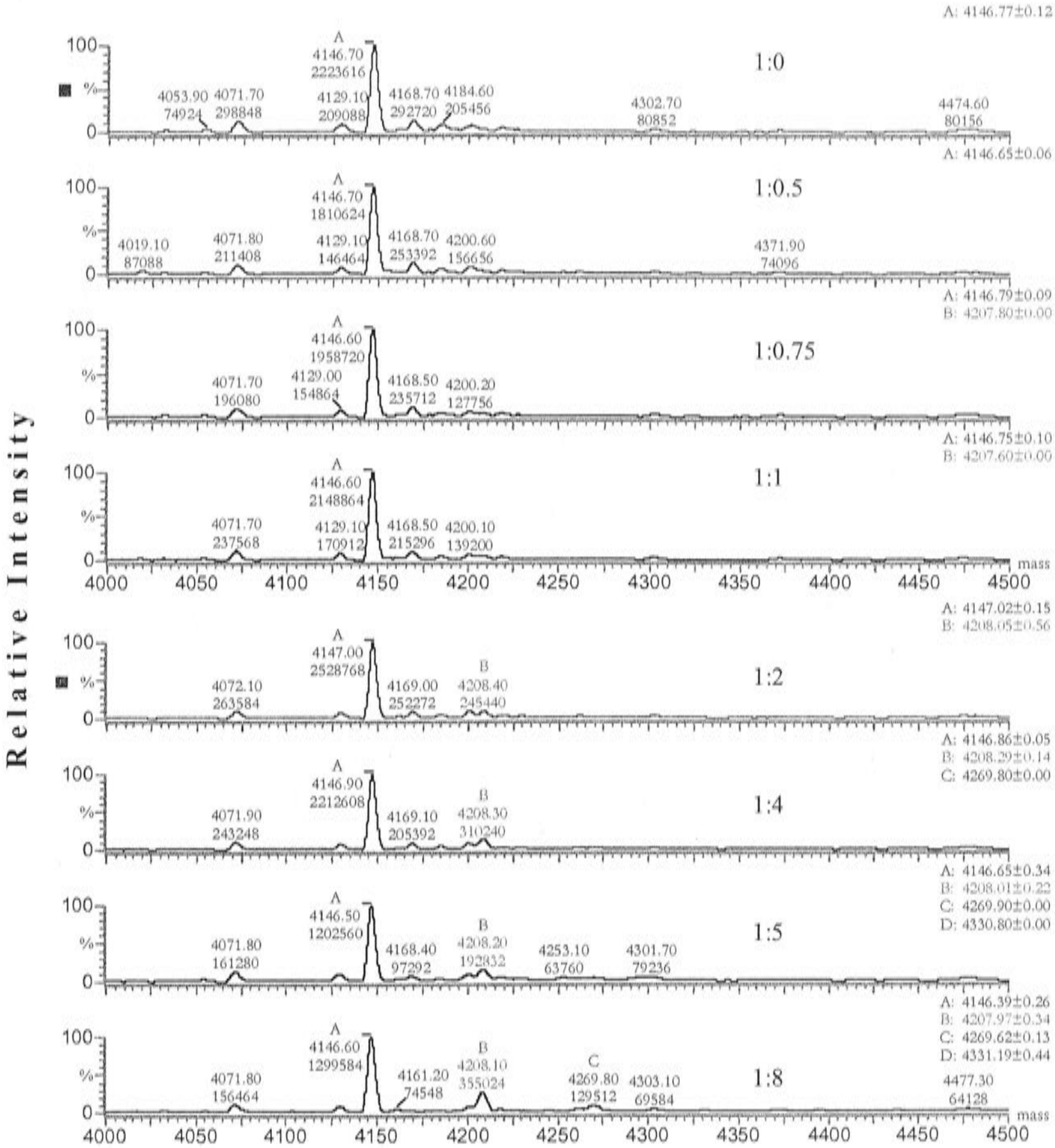

Figure 6.6: ESI MS data of copper ion distribution in copper Msp4 complex presented as transformed spectra. The spectra were taken from 10 μM Msp4 in 10 mM ammonia/formic acid buffer pH 7.4, in the absence (1:0) and presence of 5 μM (1:0.5), 7.5 μM (1:0.75), 10 μM (1:1), 20 μM (1:2), 40 μM (1:4), 50 μM (1:5), and 80 μM $CuSO_4$ (1:8). In the presence of up to 8 mol of copper/mol Msp4, Msp4 was never totally bound in a complex, although the intensity of the complexes increased as copper was added.

A

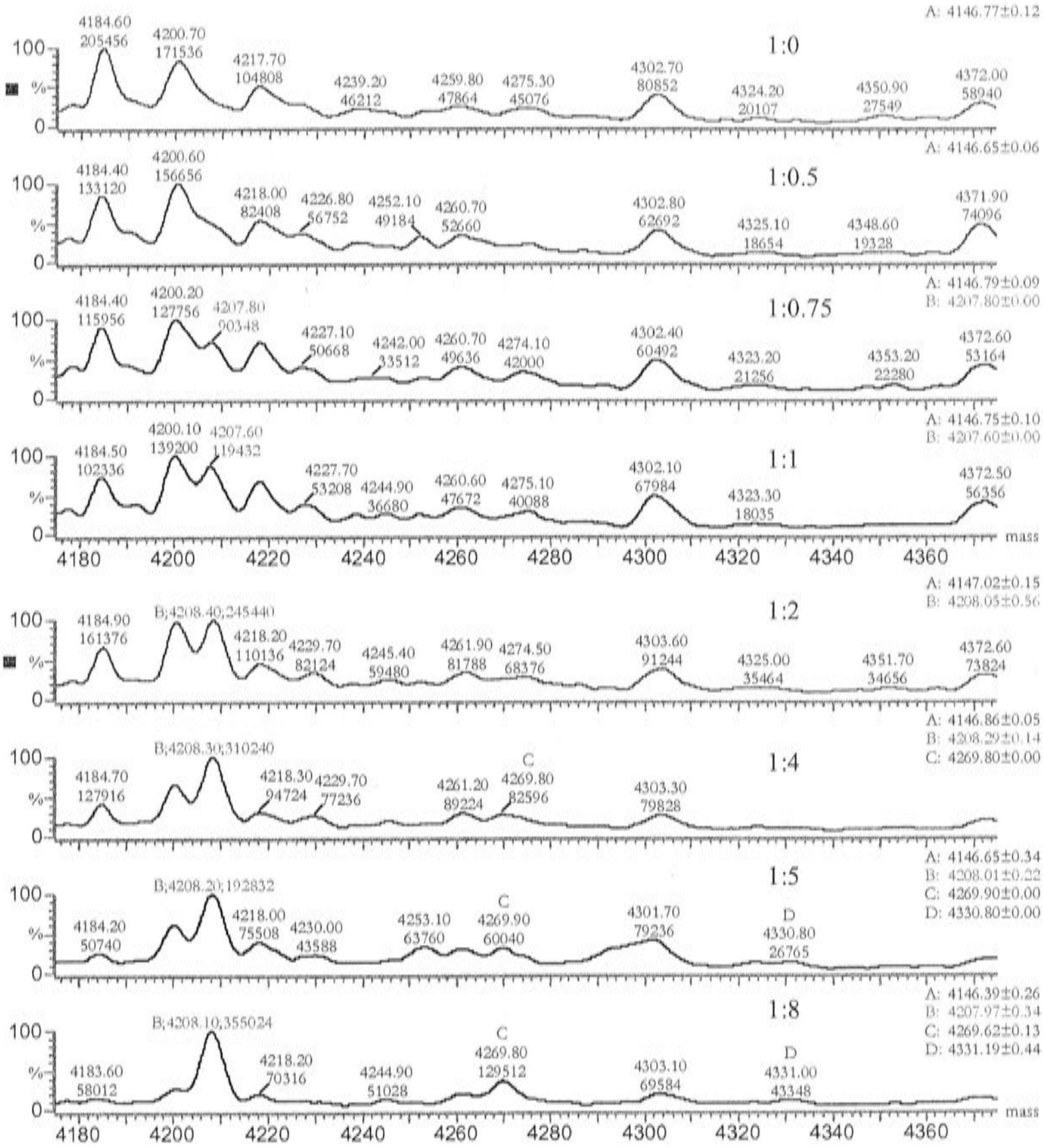

B

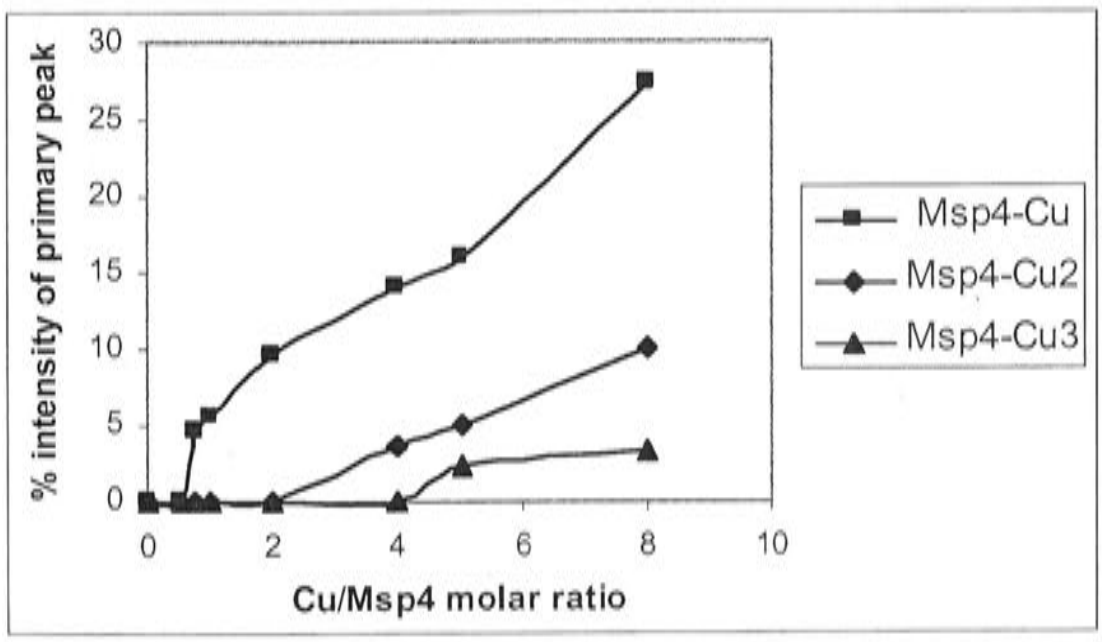

Figure 6.7: ESI MS data of copper ion distribution in copper Msp4 complex presented as detailed transformed spectra and saturation curves. A. Transformed spectrum displayed in detail to show the stepwise loading of the binding sites. B. Saturation curves of copper ion binding to Msp4 peptide. The stepwise loading of Cu^{2+} ion suggests that the sites are independent and identical.

6.4.4. Copper binding to Msp1 and its modified peptides

ESI mass spectra of modified Msp1 peptides and their copper complexes have been obtained (Figure 6.8 and Table 6.5). The experiments were conducted at pH 7.4 (NEM/formic acid buffer), with peptide concentration of 10 μM and copper ion concentration in the final solution of 100 μM.

The mass spectrum of Msp1 (Figure 6.8 A) shows the expected average mass of 1093.1. Upon addition of copper, a single peak representing the copper complex of Msp1 is observed at 1154.0 (see Figure 6.8 B), suggesting the stoichiometry of binding is one copper bound to Msp1, i.e. all Msp1 is found in its copper-complexed form.

To investigate possible copper-binding sites in Msp1, peptides which have the His, Asn, and Gln residues replaced by Ala (Msp1H2A, Msp1N7A, and Msp1Q10A respectively) were investigated by ESI MS. The possibility of copper binding to the free carboxylate group at the C-terminus as well as to the free imino group (Pro) at the N-terminus was also examined using peptides with the N- or C-terminus protected (Msp1capN or Msp1capC, respectively) and with both ends protected (Msp1capNC).

No additional peaks emerge as a result of copper addition to Msp1capN (compare Figure 6.8 C and D), which means that copper ions do not bind to this peptide. The result suggests that copper binding requires the free α-imino group as one of the binding sites. The involvement of the free α-amino group at the N-terminus in copper binding to $ShaPrP_{57-91}$ has been reported by Whittal et al. (2000), who also found that N-terminal acetylation of $ShaPrP_{23-98}$ caused some reduction in the stoichiometry of copper binding. The involvement of the free α-imino group was also observed in the fluorescence titration experiments (see Chapter IV) and in the FTIR experiments (see Chapter III), in which copper addition to the N-terminally capped Msp peptides does not cause spectral changes.

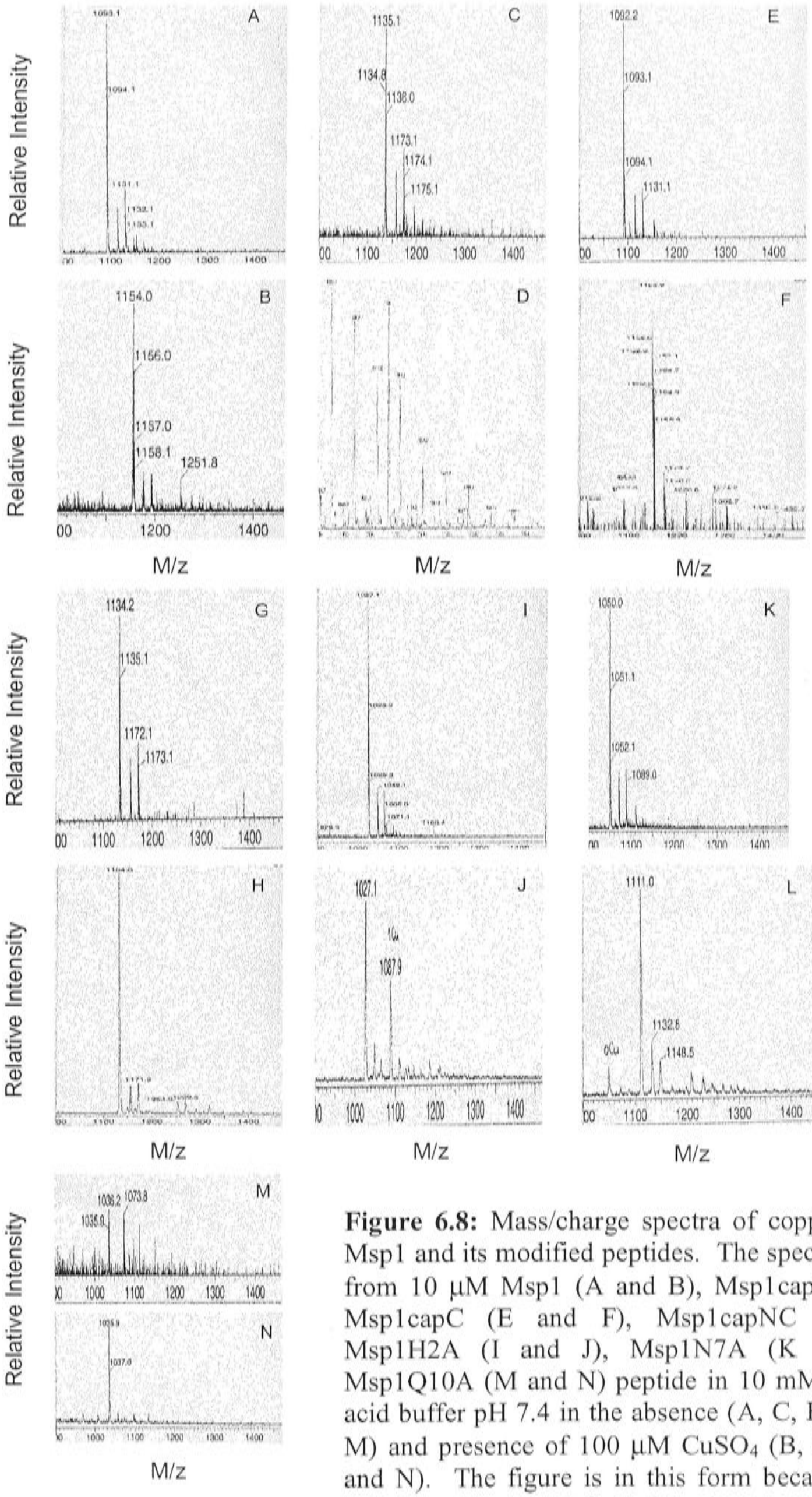

Figure 6.8: Mass/charge spectra of copper binding to Msp1 and its modified peptides. The spectra were taken from 10 μM Msp1 (A and B), Msp1capN (C and D), Msp1capC (E and F), Msp1capNC (G and H), Msp1H2A (I and J), Msp1N7A (K and L), and Msp1Q10A (M and N) peptide in 10 mM NEM/formic acid buffer pH 7.4 in the absence (A, C, E, G, I, K, and M) and presence of 100 μM $CuSO_4$ (B, D, F, H, J, L, and N). The figure is in this form because individual figures were scanned from the printout spectra.

Table 6.5: Molecular mass assignment for modified Msp1 peptides and their copper complexes observed by ESI MS.

Peptide or Complexes	No. of copper atoms bound (n)	[M-2nH+nCu] calculated	Mass observed	Figure No.
Msp1	0	1093.0	1093.1	6.8 A
Msp1+Cu	0	1093.0	none	6.8 B
	1	1154.5	1154.0	
	Average incremental difference in mass: 60.9			
Msp1capN	0	1135.0	1135.1	6.8 C
Msp1capN+Cu	0	1135.0	1135.1	6.8 D
	1	1196.5	none	
	Average incremental difference in mass: none			
Msp1capC	0	1092.0	1092.2	6.8 E
Msp1capC+Cu	0	1092.0	1092.0	6.8 F
	1	1153.5	1152.9	
	Average incremental difference in mass: 60.7			
Msp1capNC	0	1134.0	1134.2	6.8 G
Msp1capNC+Cu	0	1134.0	1134.0	6.8 H
	1	1195.5	none	
	Average incremental difference in mass: none			
Msp1H2A	0	1027.0	1027.1	6.8 I
Msp1H2A+Cu	0	1027.0	1027.1	6.8 J
	1	1088.5	1087.9	
	Average incremental difference in mass: 60.8			
Msp1N7A	0	1050.0	1050.0	6.8 K
Msp1N7A+Cu	0	1050.0	1050.0	6.8 L
	1	1111.5	1111.0	
	Average incremental difference in mass: 61.0			
Msp1Q10A	0	1036.0	1036.2	6.8 M
Msp1Q10A+Cu	0	1036.0	1035.9	6.8 N
	1	1097.5	none	
	Average incremental difference in mass: none			

The mass spectrum of Msp1capC shows a peak at 1092.2 (Figure 6.8 E). Upon addition of copper, a new peak at 1152.9, which represents a complex that binds one copper, is observed (Figure 6.8 F). The fact that in the absence of the α-carboxyl group the peptide (Msp1capC) still binds copper ion suggests this group does not participate in copper binding. This result is in good agreement with the FTIR (Chapter III) and fluorimetry (Chapter IV) data, which also show that copper binding to Msp1capC peptide still occurs.

Copper ions do not bind to Msp1capNC as shown in Figure 6.8 G and H. This result is also confirmed by the fluorescence quenching experiment (Chapter IV). The ESI MS

result again supports the suggestion that the α-imino group is essential for copper binding.

The ESI MS of Msp1H2A in the absence and the presence of copper (see Figure 6.8 I and J) indicates the involvement of His in copper binding. The spectra show that replacement of His with Ala resulted in a relative intensity of copper-free peptide twice as high as for the copper-complex peptide (Figure 6.8 J). Thus, the data suggest that the absence of the His residue caused reduction in copper-binding affinity. This is supported by the K_d value for copper binding to Msp1H2A obtained from fluorimetry, which is two orders of magnitude higher than the K_d for copper binding to Msp1. The ESI MS and fluorimetry data suggest that Msp1 peptide lacking the His residue is able to bind copper ion via a His-independent mechanism, probably involving the free α-imino group at the N-terminus together with the nitrogen atoms of deprotonated amide groups. The His-independent mechanism, which involves the free amino terminus, is also suggested by Whittal et al. (2000) for copper binding to $ShaPrP_{73-91}$.

Experiments were carried out to investigate the possibility of copper binding to the amide side chains of Asn and Gln. There is one additional peak observed in the ESI mass spectrum of Msp1N7A upon addition of copper (see Figure 6.8 K and L). The peak of copper-free Msp1N7A is also observed with relative intensity less than 1/6th that of the copper complex. These data suggest Asn plays a small role in copper binding. Gln replacement with Ala (Msp1Q10A) resulted in the absence of copper binding to the peptide (see Figure 6.8 M and N), suggesting that Gln is important for copper binding. Such involvement of the amide side chain of Gln residue in copper binding to a repeat region of PrP is the first to be reported. However, this observation is not consistent with FTIR and fluorimetry results reported here, both of which show Msp1Q10A binds copper ion well. The ESI MS experiment for copper binding to Msp1Q10A needs to be repeated to confirm if it is correct.

In summary, the ESI MS experiments show copper ions bind to the free imino end group of Pro and the imidazole side chain of His. Elimination of the free imino group abolishes binding entirely. Contrary to expectation, the replacement of His with Ala resulted in only 50% reduction in the population of the copper-bound species.

6.5. Conclusions

ESI MS experiments provide information on the copper-binding stoichiometry of Msp peptides. Experiments on copper binding to Msp2, Msp3 and Msp4 were performed in ammonium formate as suggested by the literature at the time. However, it is not an effective buffer at pH 7.4 and the real pH was lower. This caused copper binding to the Msp peptides to be sub-optimum, so that the population of copper complexed was very low. Under these conditions, the stoichiometry for copper binding to Msp2 is 3 copper ions, Msp3 4 copper ions, and Msp4 3 copper ions. The experiments need to be repeated with a more suitable buffer to work at pH 7.4, such as NEM.

The possibility of other metal ions binding to Msp2 has been investigated. While early reports in the literature suggested the specificity of copper binding to octapeptide (Hornshaw et al., 1995a; Hornshaw et al., 1995b; Whittal et al., 2000) and full-length PrP (Stockel et al., 1998), more recent reports suggested that other metal ions such as nickel could bind to the octapeptide (Jackson et al., 2001) and manganese to full-length PrP (Brown et al., 2000) under certain conditions. Msp2 has been shown to have capacity to bind other metal ions such as calcium, zinc, manganese and magnesium. However, this should be confirmed by other methods as ESI MS is prone to cation adduction, which results in non-specific binding. Although zinc, calcium, and magnesium binding to Msp peptides is confirmed by FTIR, the binding properties need to be characterized more fully.

Copper ion titration of Msp4 has revealed stepwise loading of the binding sites, suggesting that the sites are independent and identical. However, under the conditions where the pH of the solution is not maintained at 7.4 (due to the use of ammonium formate as a buffer), the peaks of copper-complexed Msp4 are very weak compared with those of copper-free Msp4; the number of copper-binding sites in Msp4 is thus inconclusive. The experiments need to be repeated using a more suitable buffer to work at pH 7.4.

ESI MS investigation of copper binding to modified Msp1 peptides has helped to define the groups forming the copper-binding site. The free α-imino group was found to be essential for copper binding; acetylation of the N-terminus abolished the copper binding

ability of the peptide. Replacement of His with Ala only partially reduced the copper binding ability of the peptide, indicating that the His role in copper binding is not as essential as the α-imino group of Pro. Together, these data indicate that the anchoring site for copper ion in Msp peptide is the α-imino group of Pro instead of the imidazole ring of His. This suggestion is in good agreement with results of FTIR (Chapter III) and fluorescence (Chapter IV) experiments.

Chapter VII

Other Approaches: Equilibrium Dialysis, Circular Dichroism, and Visible Absorption Spectroscopy

The purpose of this chapter is to present results from use of three other methods which were, however, not extensively employed due to time constraints. Nonetheless, some results were obtained which complement those from experiments described in previous chapters. The three methods, equilibrium dialysis (ED), circular dichroism (CD), and visible absorption spectroscopy, are well-established techniques to characterize complexes between copper and proteins.

7.1. Equilibrium dialysis

7.1.1. Introduction

Equilibrium dialysis (ED) is a traditional method commonly used to characterize the binding properties of macromolecules such as peptides and proteins. The technique allows measurement of the amount of ligand bound to a macromolecule. The measurement of the bound ligand is typically done through an indirect method, in which the total amount of ligand (bound plus free) and free ligand are the parameters to be measured in the experiment. The free ligand is dialyzed through a membrane until its concentration across the membrane reaches equilibrium. The membrane used in ED is semipermeable, such that it should be permeable to the ligand but impermeable to a macromolecule being studied. By measuring the concentration of ligand on one side of the membrane (e.g. contains free ligand and ligand bound to the macromolecule) and on the other side (free ligand only), the concentration of bound ligand can be calculated (Klotz, 1989). The diagram of the dialysis process is shown in Figure 7.1.

As mentioned in Chapter I, ED has been used to characterize copper-binding properties of PrP (Brown et al., 1997; Stockel et al., 1998). Recombinant PrP_{23-98}, which spans the entire N-terminal domain of human PrP that contains the four octapeptide (PHGGGWGQ) tandem repeat, at pH 7.4 binds 5 to 6 copper ions with dissociation constants (K_d) of 5.9 μM. Copper binding occurs with positive cooperativity, in which 3 to 4 copper ions bound cooperatively (Brown et al., 1997). ED has also been used to study copper-binding properties of the full-length Syrian hamster PrP ($ShaPrP_{29-231}$). At

slightly acidic condition (pH 6.0), $ShaPrP_{29-231}$ exhibits two binding sites specific for copper ion with a K_d of 14 μM (Stockel et al., 1998).

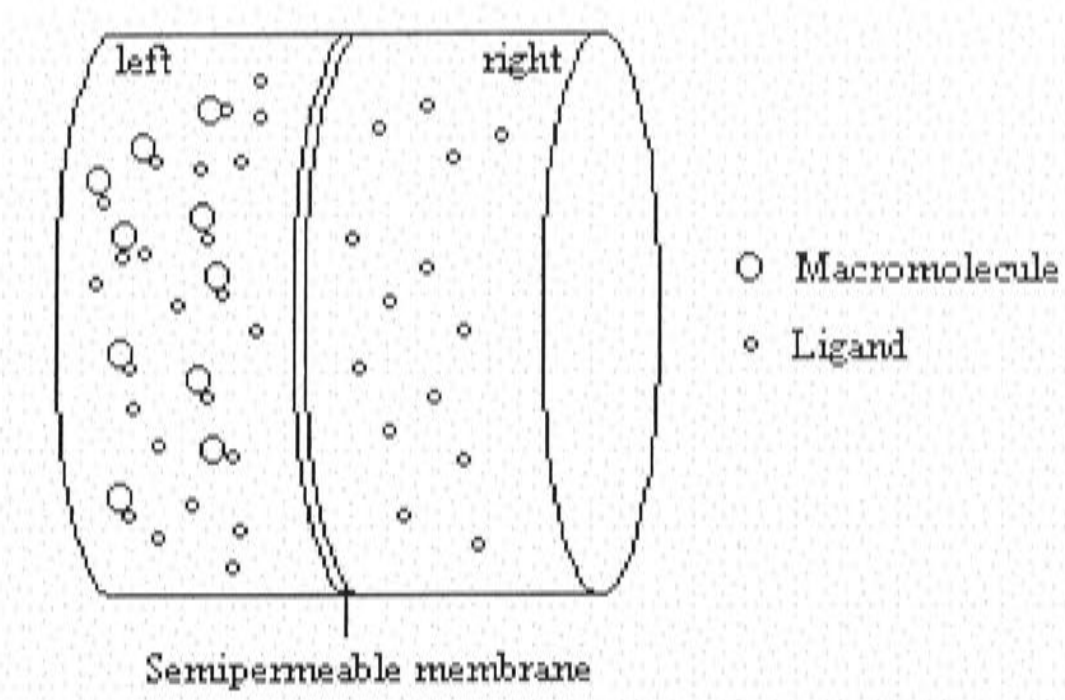

Figure 7.1: Illustration of equilibrium dialysis process. A semipermeable membrane is placed in the middle, so that there are two chambers. A solution of a macromolecule (i.e. protein) is placed in the left chamber and ligand solution in the right chamber. The solution is allowed to reach equilibrium, at which time the free-ligand concentration is the same in both chambers. If the amount of ligand in the left chamber (free plus bound) is measured as well as the amount of ligand in the right chamber (free ligand only), the amount of bound ligand can be determined by subtraction.

7.1.2. Aims

In this project, ED was used to demonstrate, directly, copper binding to Msp peptides. The binding properties of Msp4, Msp3, and Msp2 such as K_d and stoichiometry were extracted from the binding data. Due to its low molecular weight (MW), it is not possible to carry out ED experiments for copper binding to Msp1 (MW=1093), as the smallest pore-size membrane available in the market is 500 molecular weight cut off (MWCO). Although it is still smaller than the MW of Msp1, it is considered unsafe to use membrane with MWCO larger than 1/3 of the MW of peptide.

7.1.3. Materials and methods

7.1.3.1. Materials and apparatus

Synthetic peptides used in ED experiments are presented in Table 7.1. Copper used in equilibrium dialysis was supplied in the form of copper diglycine chelate ($Cu(Gly)_2$), which was made by combining solutions of $CuSO_4$ and amino acid glycine (mol ratio 1:2). The reason for using $Cu(Gly)_2$ is to prevent precipitation of copper as copper

hydroxide at pH 7.4, to mimic the in vivo situation and, because amino acid glycine competes for free copper, spurious binding to low-affinity sites is suppressed (Brown et al., 1997). The pH and ionic strength in both chambers was the same. The solution was maintained at pH 7.4 using 25 mM N-ethylmorpholine buffer (NEM), which was adjusted to pH 7.4 by HCl. The ionic strength was maintained at 0.15 by addition of 150 mM KCl (Brown et al., 1997). The membrane separating the two sides of dialysis chambers is a cellulose ester membrane with MWCO 1000 (for Msp4) and 500 (for Msp3 and Msp2), manufactured by Spectrum.

Table 7.1: Synthetic peptides used in the experiments

Peptide	Sequence	Size	MW
Msp4	$(PHPGGSNWGQ)_4G$	41	4147
Msp3	$(PHPGGSNWGQ)_3G$	31	3129
Msp2	$(PHPGGSNWGQ)_2G$	21	2111

The dialysis chambers (perspex) were made by the JCSMR workshop. The initial design had dimensions of: 16 mm inner diameter, 8 mm depth of inner chamber, and 1.6 mL half-cell volume (see Figure 7.2 A). The new dialysis chambers have dimensions of: 26 mm inner diameter, 3 mm depth of inner chamber, and 1.6 mL half-cell volume (see Figure 7.2 B). The improved design allows a larger membrane surface area with the same volume of solution inside half dialysis cells. A rotation apparatus (see Figure 7.2 C) was made by the JCSMR workshop to facilitate agitation during the dialysis. The rotation apparatus was equipped with clips to hold the dialysis cells during agitation.

7.1.3.2. Methods

Solutions containing different concentrations of $Cu(Gly)_2$ in 25 mM NEM buffer pH 7.4 and 150 mM KCl were prepared. 5 μM Msp peptide solution was also prepared in the same buffer (25 mM NEM pH 7.4 and 150 mM KCl). Cellulose ester membrane was cut into a round shape to fit the dialysis chamber. The membrane was placed between the two half dialysis cells, so that two compartments were formed. For each experiment 20 ED chambers were prepared. One compartment of each ED apparatus was filled with 1.25 mL $Cu(Gly)_2$ of variable concentration and the other compartment was filled

with 1.25 mL Msp peptide solution. A small air bubble was left in each compartment to facilitate mixing. The filled dialysis cells were agitated at 4 ^{O}C until equilibrium was reached - 6 days for MWCO 1000 and up to three weeks for MWCO 500. The two solutions in the compartments were then collected, and the copper concentrations were measured by inductively coupled plasma optical emission spectroscopy (ICP OES).

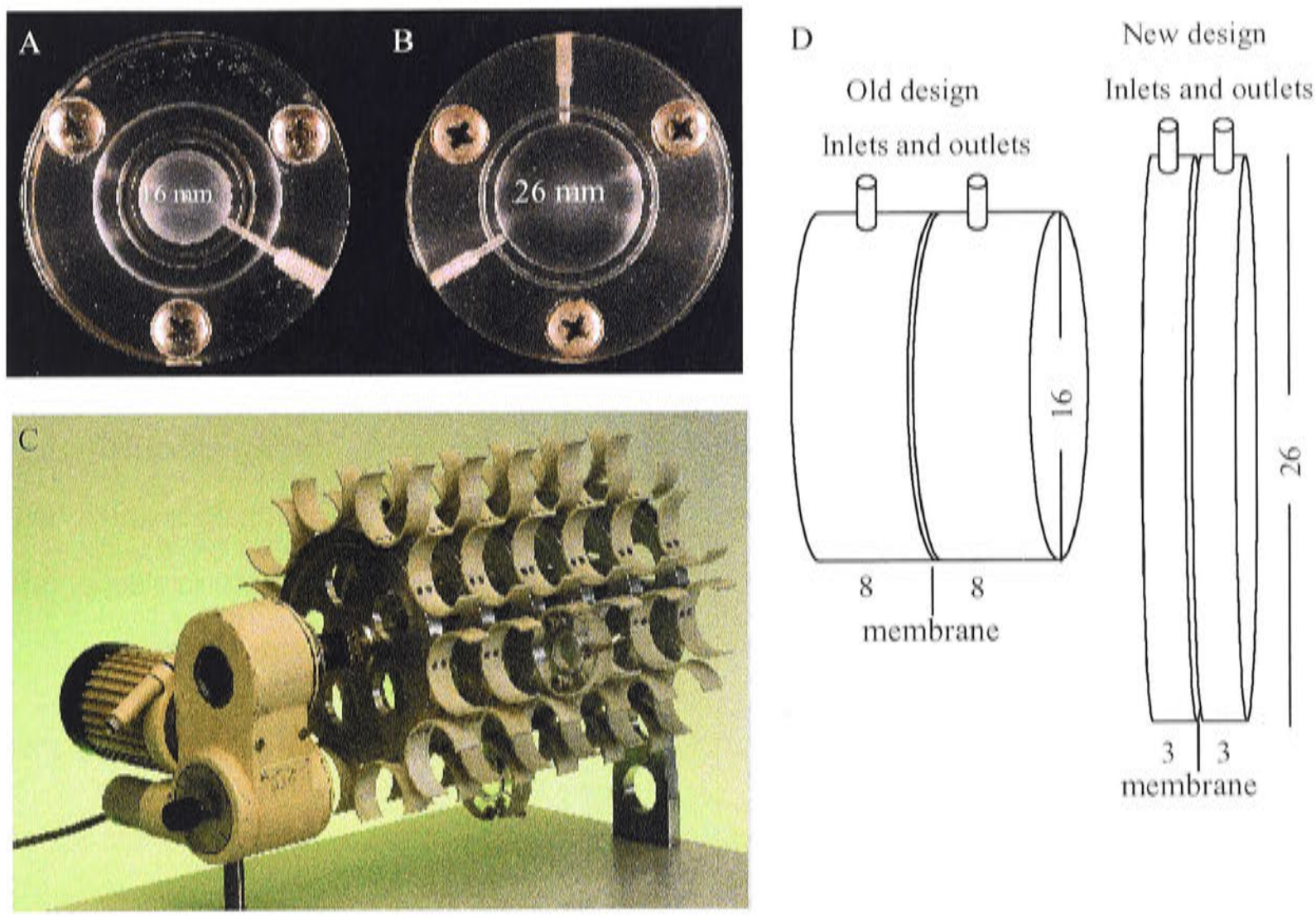

Figure 7.2: Design of dialysis chambers. (A) Initial design: inside diameter of 16 mm, 8 mm depth, and volume of 1.6 mL. (B) Improved design: inside diameter of 26 mm, depth of 3 mm, and volume of 1.6 mL. (C) Rotation device to facilitate agitation during dialysis. The rotation device was equipped with clips to hold the dialysis cells during agitation. (D) Diagram of the dialysis chambers showing the dimension of the chambers in mm. The inlets and outlets were used to add and remove solutions from the two compartments that were separated by the membrane. Peptide solutions were added to the left compartments (Msp-containing compartments) and copper solutions were added to the right compartments (Msp-free compartments).

Copper concentration in the Msp-containing compartment represents the total copper concentration $[Cu]_T$ (bound plus free copper) and copper concentration in the Msp-free compartment represents free copper concentration $[Cu]_f$. The extent of binding (ν) was calculated according to Equation 7.1,

$$\nu = [Cu]_b/[Msp] \qquad \text{(Equation 7.1)}$$

in which $[Cu]_b$ is the concentration of copper bound to the Msp peptide of concentration [Msp]. $[Cu]_b$ was calculated according to Equation 7.2.

$$[Cu]_b = [Cu]_T - [Cu]_f \qquad \text{(Equation 7.2)}$$

The binding data ν were then plotted against $[Cu]_f$ and analysed to get the dissociation constant (K_d) and the number of copper ions bound to the Msp peptide (n, stoichiometry).

7.1.4. Results and discussion

7.1.4.1. Design of the dialysis chamber

The old design was taken from an ED chamber used many years ago in JCSMR. This initial design (see Figure 7.2 A) resulted in very long times for copper ions to equilibrate across the dialysis membrane. According to Fick's law of diffusion (Equation 7.3), the rate of diffusion (d[Cu]/dt) is proportional to the area (A) across which diffusion occurs (from left ($[Cu]_L$) to right ($[Cu]_R$). For a given surface area, a larger volume of solution will require a longer equilibration time than a smaller volume of the same concentration;

$$-d[Cu]/dt = \{A([Cu]_L - [Cu]_R)\}/T \qquad \text{(Equation 7.3)}$$

where A is surface area of the membrane across which diffusion occurs, and T is the time for the diffusion process.

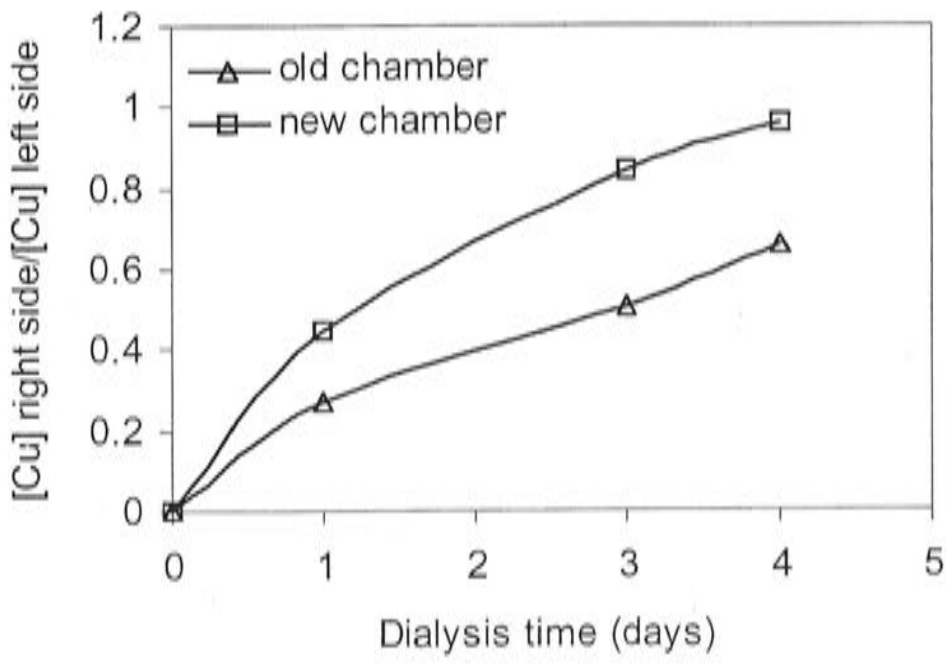

Figure 7.3: Effect of chamber design on copper diffusion. Old chamber design: inside diameter of 16 mm or membrane surface area of 804 mm^2. New chamber design: inside diameter of 26 mm or membrane surface area of 2123 mm^2. Dialysis experiments were carried out using 1000 MWCO membrane. 1.2 mL of 200 µM $Cu(Gly)_2$ in NEM pH 7.4 was placed in the right chamber, while the left chamber contained buffer only. Dialysis was stopped after 1, 3, and 4 days, and copper concentration in each chamber was measured using the ICP OES method.

Design of the dialysis cells with the same volume but larger membrane surface area should lead to a decrease in dialysis time. Improved design of the dialysis chamber (see Figure 7.2 B) was compared with the initial design for copper diffusion time (Figure 7.3). Figure 7.3 shows that copper diffusion in the improved design is 1.5 times faster than in the initial design. The design of the new chamber makes the membrane surface area larger while maintaining volume as the same for the old chamber.

7.1.4.2. Time for equilibration

In this experiment, the time necessary for establishing equilibrium was determined by investigating the copper diffusion across the dialysis membrane (MWCO 1000 and 500) in the absence of Msp peptides. By using the new design, equilibrium was reached after 5 days of dialysis for MWCO 1000 and after approximately 13 days for MWCO 500 (see Figure 7.4). In order to provide a safety margin, dialysis was carried out for 7 days when using MWCO 1000 and 18 days when using MWCO 500.

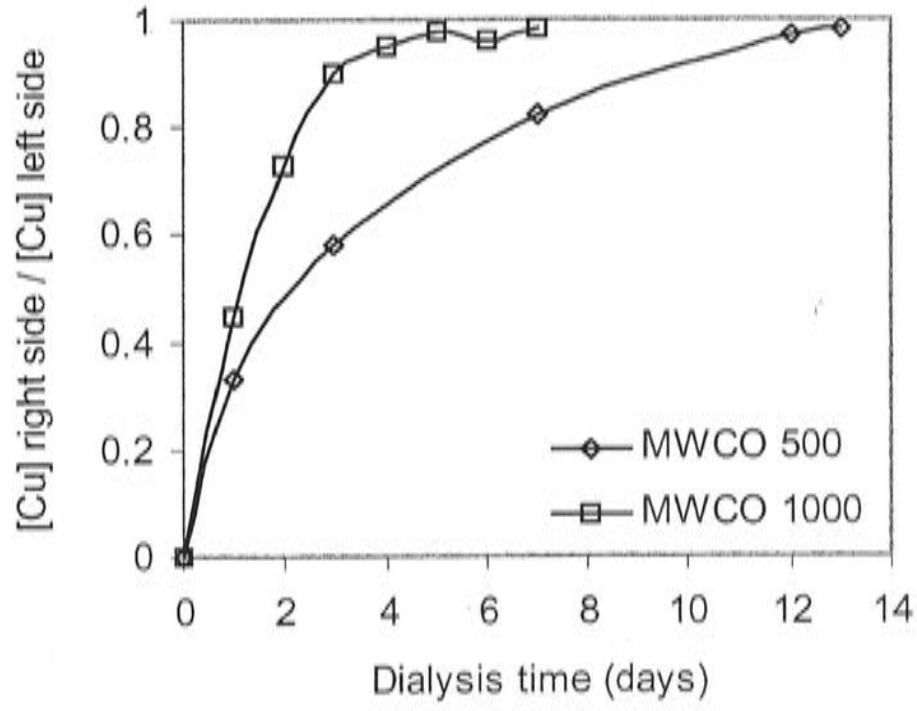

Figure 7.4: Time for copper diffusion across the dialysis membrane of MWCO 500 and MWCO 1000. 1.2 mL of 200 µM $Cu(Gly)_2$ in NEM pH 7.4 was placed in the right chamber, while the left chamber contained buffer only. Dialysis was stopped after days indicated, and copper concentration in each chamber was measured using the ICP OES method.

7.1.4.3. Copper binding to Msp peptides at pH 7.4

Figure 7.5 (top) shows the relative ratio of copper bound per Msp4 molecule plotted versus the free copper concentration. The maximum molar ratio of copper ions to Msp4 is between 2 and 2.5. The half-maximal binding observed for Msp4 is between 0.43 and

1.2 μM (average 0.73 μM). The data suggest that Msp4 molecule possesses two binding sites for copper with a dissociation constant of 0.73 μM. Figure 7.5 (bottom left) shows stoichiometry of one copper bound per Msp3 molecule, with a dissociation constant of 0.06 μM. A stoichiometry of two copper ions bound per Msp2 molecule and dissociation constant of 0.08 μM is shown in Figure 7.5 (bottom right).

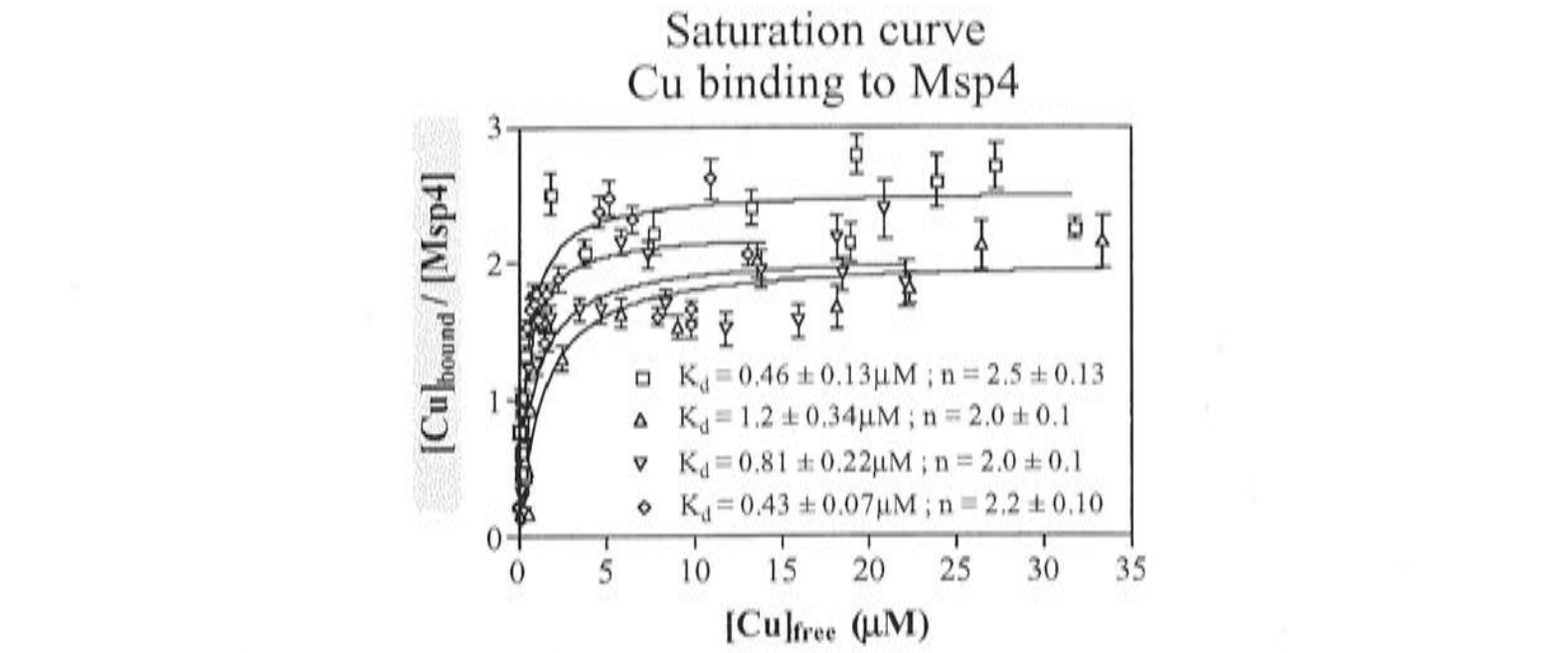

Figure 7.5: Binding of $Cu(Gly)_2$ to Msp peptides measured by equilibrium dialysis experiments. Saturation curve for copper binding to 5 μM Msp4 is the result of 4 sets of experiments (top). Saturation curve for copper binding to 5 μM Msp3 is the result of one set of experiments (bottom left). Saturation curve for copper binding to 5 μM Msp2 is the result of one set of experiments (bottom right). The data were fitted with saturation binding equation: $Y = (X \,.\, n)/(K_d + X)$ using the GraphPad Prism 3 program.

7.1.5. Conclusions from ED experiments

Thus, ED experiments show that 2 copper ions bind to Msp4, 1 copper ion binds to Msp3, and 2 copper ions bind to Msp2. This is not a regular pattern connecting the number of repeats with the number of copper ions bound. It is not clear why Msp2 binds more copper than Msp3. These stoichiometries of copper binding to Msp

peptides are not in agreement with results of other ED experiments on PrP repeats from human, where one copper ion bound to one repeat (Brown et al., 1998) or with stoichiometries for chicken and human PrP repeats determined by other methods (Table 1.4 of Chapter I).

The K_d values from equilibrium dialysis experiments are 0.73 μM for Msp4, 0.06 μM for Msp3 and 0.08 μM for Msp2. The K_d values for Msp4 are ~ 230 times higher than values from fluorimetry experiments (K_d of 3.2 nM for 0.5 μM Msp4). The K_d value for Msp3 is 15 times higher than its value from fluorimetry experiments (K_d of 4.0 nM for 0.5 μM Msp3), while that for Msp2 is 200 times higher than its value from fluorimetry experiments (0.4 nM for 0.5 μM Msp2). It should be pointed out that the ED experiments for copper binding to Msp3 and Msp2 were carried out for a very long time (up to three weeks). This is because a very small molecular weight cut off membrane (500 MWCO) needed to be used. The binding process takes place over a long time, which is good in one way as it provides a different scale time window for studying binding and should assure the system comes to equilibrium. The long time could be a source of error if during the process the peptide decays. However, the peptides are relatively stable and decay is unlikely.

7.2. Circular dichroism spectroscopy

7.2.1. Introduction

Circular dichroism (CD) measures differences in the absorption of left-handed polarized light versus right-handed polarized light by an optically active chromophore, which has structural asymmetry or chirality. Biological macromolecules such as peptides and proteins are composed of many optically active chromophore or chiral units, namely the asymmetric carbon atoms in their amino acid backbone. CD spectroscopy has therefore been used extensively to characterize the structure of proteins and peptides. The shape of the CD spectrum and the amplitude of the CD signal is characteristic for each type of secondary structure. The absence of regular structure in proteins results in zero CD intensity, while an ordered structure results in a spectrum, which can contain both positive and negative signals (for review see: (Johnson, 1988; Johnson, 1990; Woody, 1994; Woody, 1995)).

As noted in Chapter I, CD has been used to resolve the secondary structure of human octarepeats and chicken hexarepeats of PrP and the conformational changes associated with copper binding. The majority of the CD studies agree that PrP repeats are in random-coil form (Hornshaw et al., 1995a; Viles et al., 1999; Bonomo et al., 2000; Whittal et al., 2000), and take up more ordered structure, such as loop and turns, when the peptide binds to copper ions (Viles et al., 1999; Bonomo et al., 2000; Whittal et al., 2000). CD has also been used as a method to monitor the progress of binding between PrP-repeat peptides and the metal ion (Viles et al., 1999; Garnett and Viles, 2003). The magnitude of spectral changes that occur upon copper addition was then analyzed to get the K_d value as well as the stoichiometry.

7.2.2. Aims

In this project, CD was mainly used to probe the conformation of peptides containing several copies of the second-repeat sequence [$(PHPGGSNWGQ)_nG$, n = 1 and 2] of the N-terminal tandem repeat region of a marsupial PrP (Msp).

7.2.3. Materials and methods

7.2.3.1. Sample preparation

Unless otherwise stated, the sample for CD experiments was taken from a solution remaining from the FTIR experiments. The purpose of this was to ensure that both CD and FTIR spectra originated from the same sample as it was hoped the results from the CD experiments would complement the FTIR results, especially in terms of conformational changes. The peptide concentration was adjusted to 0.5 mM by diluting the FTIR samples accordingly. Blank solution was also prepared so that the concentration of salts (NaCl, NaOH, and HCl) was similar to that in the sample solution.

7.2.3.2. CD measurement.

CD spectra were recorded on a Jobin-Yvon Model CD6 instrument at 25 ^{O}C. Typically, a cell with 0.01 cm path length with two detachable windows was used for spectra recorded between 180 and 260 nm, with points sampled every 0.5 nm. Sample and blank solution were scanned 10 times. The data were processed using the CD6 dichrograph program. The blank spectrum was subtracted from the sample spectrum. The resultant spectrum was then smoothed. The measurement unit is θ (ellipticity in mdeg).

7.2.4. Results and discussion: CD spectral changes associated with copper binding to Msp peptides

CD spectra of Msp1capC (Figure 7.6.A), Msp2capC (Figure 7.6.C) and Msp2capNC (Figure 7.5.E) in the absence of copper ion at different pH values show the main features as an intense minimum at about 195 nm and positive band around 217 nm. This feature is typical of a disordered polypeptide backbone, and was also observed for PrP repeats from other species (Hornshaw et al., 1995a; Viles et al., 1999; Bonomo et al., 2000; Whittal et al., 2000; Garnett and Viles, 2003). No conformational changes associated with pH change are observed, despite some differences in band intensity: these could be due to inaccuracy in the determination of peptide concentration.

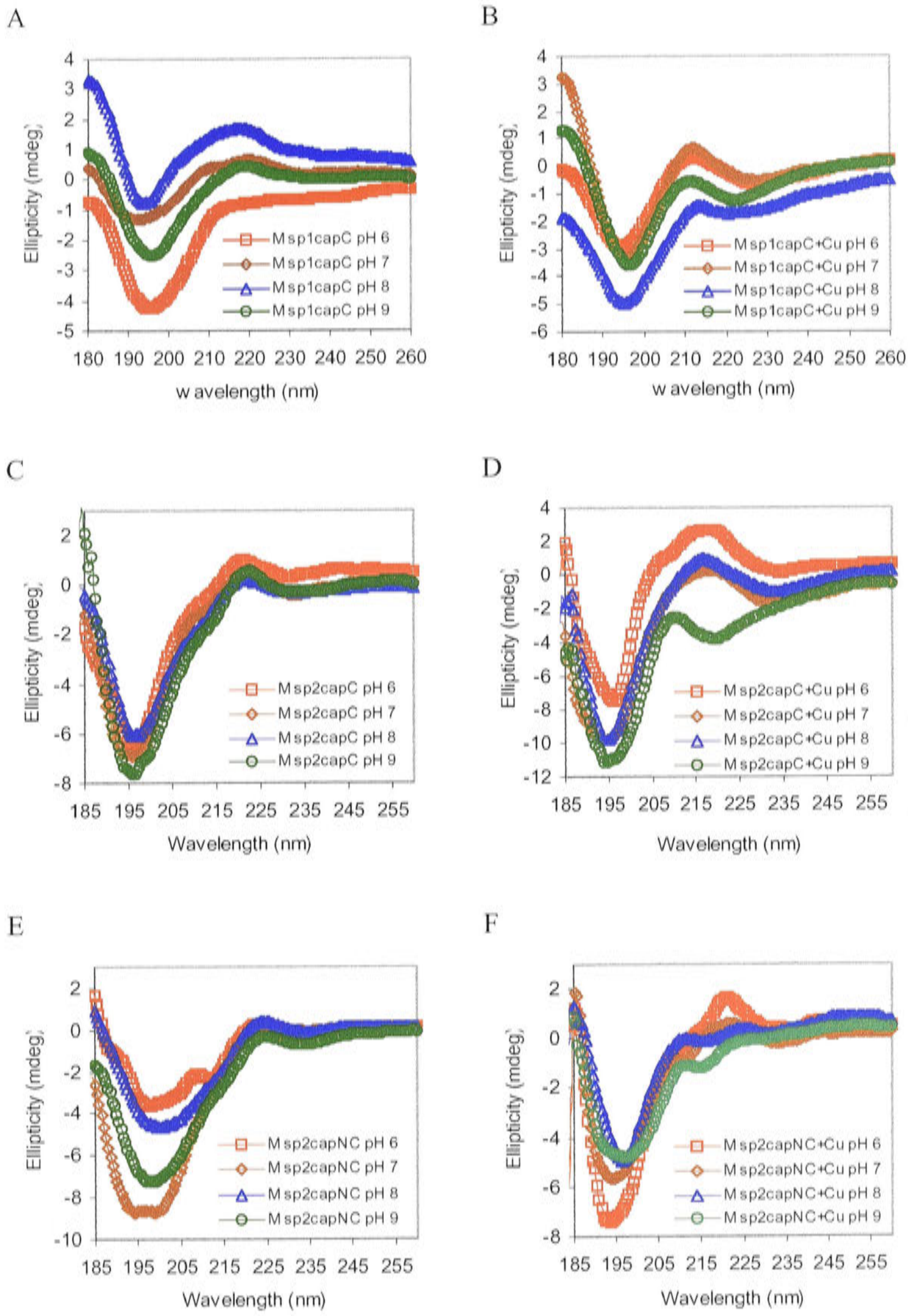

Figure 7.6: CD spectra of copper binding to Msp peptides. The spectra of 0.5 mM Msp1capC, Msp2capC, and Msp2capNC in the absence (A, C, and E, respectively) and presence (B, D, and F, respectively) of 2 mM $CuCl_2$ at pH 6.0, 7.0, 8.0, and 9.0. The samples were taken from solution remaining from FTIR experiments, which were then diluted appropriately.

Msp1capC+Cu. Copper addition to Msp1capC (Figure 7.6.B) resulted in some changes in the CD spectrum. At pH 6.0 and 7.0, a new weak negative band was observed at around 227 nm. Increasing the pH to 8.0 and 9.0 resulted in a blue shift of the new band, so that the band is now located around 222 nm. The new negative band at pH 9.0 is stronger than at any of the other three pHs, which indicates the stronger association between peptide and copper ions at this pH. However, a strong minimum band at 195 nm and weak positive band at 212 nm are still present in the spectra at all pHs. Overall, the spectral features are not consistent with any known CD spectrum of common secondary structure, i.e. α-helix or β-sheet.

The appearance of the new negative band at 222 and 227 nm is clearly associated with copper complexation of peptide molecule. The appearance of a new negative band at 222 nm is quite common and is always observed in the spectra of copper complexes of human PrP octarepeats (Viles et al., 1999; Bonomo et al., 2000; Whittal et al., 2000). However, the rest of the published spectral features are different from those of Msp1capC.

Msp2capC+Cu. Copper addition to Msp2capC resulted in the same effects as for Msp1capC. There is a new negative band around 230 nm observed at pH 6.0 to 8.0, which is blue shifted to 220 nm upon increasing pH to 9.0. As also observed in the copper complex of Msp1capC, the new negative band at pH 9.0 is stronger compared to the other three pHs. It clearly indicates this new band arises upon copper interaction with the peptide molecule, and that the interaction is stronger at pH 9.0.

Msp2capNC+Cu. The new negative band at around 230 nm does not appear in the spectra of Msp2capNC upon addition of copper ion at pH 6.0 and 7.0. This is consistent with previous observations in FTIR (Chapter III), which suggest that N-terminally capped peptide does not bind copper ion at these two pHs. Consistent with FTIR, the CD spectra show binding occurs only at basic pH (above 8.0) where a weak negative band at 215 nm appears and becomes stronger at pH 9.0.

7.2.5. Conclusions

The response of the complex toward increasing pH observed with CD is quite similar to that observed with FTIR. Both CD and FTIR indicated that copper interaction with the peptide was enhanced by increasing pH, so that at pH 9.0 the largest spectral changes occurred. By FTIR this strong interaction at pH 9.0, especially for multi-repeat peptide, was shown as a large shift of the amide I band toward lower frequency, which was assigned as solvent-exposed α-helical structure. For single-repeat peptide, the amide I band shift is not so prominent, and the band is assigned as random-coil structure.

Based on the FTIR results, CD spectra of the copper complex of Msp2capC were expected to show more helical structure at pH 9.0 than at lower pH. Also, the structure was expected to be more helical than the structure of the copper complex of Msp1capC peptide. In CD spectra, α-helix in (folded) proteins appears with two negative bands at 208 and 222 nm and a positive band at around 192 nm (Woody, 1994). The band at 220 nm for α-helix structure is assigned as the peptide n-π* transition component (Woody, 1994). The CD spectra of the copper complexes of Msp1capC and Msp2capC both show the negative ellipticity at 230 nm with band intensity appearing to be higher in Msp2capC than in Msp1capC. As pH is increased to 9.0, this band shifts to around 220 nm and increases in intensity. Again, the intensity of this band in Msp2capC is higher than that in Msp1capC. These data are in good agreement with that expected from FTIR.

Although the new negative band at around 220-230 nm suggests the presence of an increasing amount of helical structure for Msp2capC, the rest of the spectrum (Figure 7.6 B and D), which shows a negative band at 195 nm, does not resemble the usual CD spectrum for α-helical structure. Thus, although the appearance of the 230 nm band in copper complexes of Msp peptides might indicate α-helical structure, the dominant negative band at around 195 nm suggests the presence of a large amount of random-coil structure. Thus, in summary, conformational analysis suggests a mixture of helix and random-coil structure.

7.3. Visible absorption spectroscopy

7.3.1. Introduction

Visible absorption spectroscopy is a method to detect which atoms are bound to copper ions, based on the relationship between the ligand field around the central copper (II) and the position of the λ_{max} of copper complexes (Bryce and Gurd, 1966). These bands shift to shorter wavelength as the number of strong-field atoms that are bound to copper increases. In general, in copper complexes of peptides coordinating groups may be classified according to field strength as α-amino nitrogen > peptide bond nitrogen > imidazole nitrogen > oxygen (from C=O peptide or COO^- terminal) (Bryce and Gurd, 1966; Breslow, 1973).

Visible absorption spectroscopy has been used for the study of copper complexes of PrP repeats (Miura et al., 1999; Viles et al., 1999; Luczkowski et al., 2002). Viles et al. (1999) observed an absorption band at 625 nm with an extinction coefficient of 40 M^{-1} cm^{-1}, which was assigned as the 3N complex, where 2 nitrogen atoms from the imidazole ring of His and one nitrogen atom of a peptide bond coordinates to the copper ion.

Miura et al. (1999) reported λ_{max} of the copper complex of PHGGG located at 623 nm. Combined with Raman results, it was suggested that this band arises from one N_π atom of His and two nitrogen atoms of deprotonated amides in the triglycine segment, which are the equatorial ligands in this complex. The fourth equatorial ligand is a water molecule. For the copper complex of OP1 (PHGGGWGQ), the reported λ_{max} was 615 nm. As the value is close to that of the copper-PHGGG complex, the coordination of ligands in OP1 was suggested to be the same as for this pentapeptide. The 8 nm difference in the λ_{max} was attributed to a difference in coordination geometry or in the apical ligands. The λ_{max} for the copper complex of OP2 ($(PHGGGWGQ)_2$) depends on the concentration of copper ion. It changes from 610-613 to 597-599 nm with a transition midpoint at r=1, where it is the ratio of copper to peptide. It was suggested that at r below 1, each octapeptide unit independently binds copper, with structure very similar to that of OP1. Visible absorption spectra of the copper complex of OP4 ($(PHGGGWGQ)_4$) show λ_{max} at 607 and 600 nm at r=0.5 and 1, respectively. The λ_{max} values are close to those observed for the copper complex of OP2, indicating that the

primary equatorial ligands are the same as in the copper complex of the peptide described above. Miura et al. (1999) observed partial aggregation of the peptide, and the intermolecular association may be a cause of the blue shift from 607 nm at r=0.5 to 600 at r=1.

Luczkowski et al. (2002) observed a shift in the λ_{max} value upon increasing pH, indicating an increase in the number of ligands bound to the copper ion (Table 7.2). By monitoring λ_{max}, the species formed at each pH can be predicted, with support from other spectroscopic data.

According to Luczkowski et al. (2002), the proposed ligands in $CuH_{-1}L$ species are the terminal imino group of Pro (NH), a deprotonated amide nitrogen (N^-), and the nitrogen atom of the imidazole ring of His (N_{imid}). As pH increases above 8.0, more amide nitrogens deprotonate and coordinate to the copper ion. At this pH, the His residue no longer participates in the complex, so that now the coordination sphere was filled with NH, and 3 deprotonated amide nitrogens (3 x N^-). As the pH was raised above 10.0, the biuret complex, where the copper ion coordinates to deprotonated amide nitrogen atoms, is observed (4 x N^-).

Table 7.2: Visible absorption spectroscopic data for copper binding to PrP-octarepeat peptides. The peptide sequences were PHGGGWGQ-NH_2 and Ac-PHGGGWGQ-NH_2. Data were taken from Luczkowski et al. (2002).

Species	pH	λ_{max} (nm)	ε (M^{-1} cm^{-1})	Ligands
PHGGGWGQ-NH_2				
CuHL	2.0-4.0	596	18	
$CuH_{-1}L$	3.0-9.0	597	75	NH, N^-, N_{imid}
$CuH_{-2}L$	>6.0	588	98	
$CuH_{-3}L$	>8.0	541	114	NH, 3xN^-
$CuH_{-4}L$	>10.0	505	211	4xN^-
Ac-PHGGGWGQ-NH_2				
CuL	4.0-7.0	742	22	
$CuH_{-2}L$	6.0-10.0	621	97	
$CuH_{-3}L$	7.0-11.0	589	99	
$CuH_{-4}L$	>8.0	531	183	

7.3.2. Aims

In these experiments, visible absorption spectroscopy was used to probe the ligands in the copper complex of Msp3 peptide.

7.3.3. Experimental

7.3.3.1. Sample preparation

The sample used for these experiments was obtained from the remaining solution of FTIR samples of the copper complex of Msp3. All remaining solutions were combined so that the concentration of Msp3 and $CuCl_2$ in the solution for Vis absorption spectroscopy measurement was not exactly known. The pH of the solution was initially brought to 12.0 by addition of NaOH solution. The pH was then adjusted to the desired pH by addition of HCl. pH was measured using the Hanna pH meter equipped with a mini probe.

7.3.3.2. Spectrum measurement

Spectra of Msp3 solution in the presence of copper at various pHs were measured by UV/Vis spectrophotometry using the Varian Cary 1 Bio. The sample was placed in a 500 µL quartz cuvette of 1 cm path length. Spectra were taken in the region of 500-700 nm against water as a reference.

7.3.4. Results and discussion

Results in Table 7.3 show that the λ_{max} value shifts towards lower wavelength upon increasing pH, which indicates the involvement of more strong-field ligands in the copper coordination. FTIR and fluorescence spectroscopy data (Chapters III and IV) have previously assigned the possible groups of Msp1 that binds to copper ion, as the imino end group of Pro (NH), the nitrogen atom of the imidazole ring of His (N_{imid}) and amide nitrogen (N^-). As noted above, the order of the field strength is $NH > N^- > N_{imid}$ (Breslow et al., 1973). The shift of the λ_{max} towards lower wavelength upon increasing pH indicates the involvement of more amide nitrogens, as coordination to this group requires deprotonation of amide, which only occurs at high pH. Also the N^- group is a strong-field ligand that will shift the λ_{max} toward a lower value. Assignment of possible ligands at each λ_{max}, and at each pH, is presented in Table 7.3.

The involvement of NH and N_{imid} (pK_a 6.8-7.9 and 6.2, respectively (Creighton, 1983 p.7)) at pHs as low as 4.0 is in agreement with Luczkowski et al. (2000) who detected copper coordination to NH, N_{imid}, and N^- groups in C-terminally capped human PrP octarepeat peptide (Table 7.2).

Table 7.3: Visible absorption spectroscopic data for copper complexes of Msp3 peptide. The peptide sequence was $(PHPGGSNWGQ)_3G$.

Complex	pH	λ_{max}	Proposed Ligand
NH-$(PHPGGSNWGQG)_3$G-OH	4.0	631	NH, N_{imid}
	5.0	592	NH, N_{imid}, COO^-
	6.0	594	NH, N_{imid}, COO^-
	7.0	584	NH, N_{imid}, COO^-, N^-
	8.0	575	NH, N_{imid}, COO^-, N^-
	9.0	563	NH, N_{imid}, 2 x N^-

7.3.5. Conclusions

Although this was a rough preliminary experiment, it indicates that visible absorption spectroscopy is useful as a complementary method to assign binding sites for copper in Msp peptides. The blue shift that occurs upon increasing pH indicates the involvement of more nitrogen atoms of the peptide bond in the copper coordination sphere. Further study with simple peptides, such as Msp1, its mutants and other variants, will be able to provide more information about the copper-binding sites to complement the data from FTIR and other methods.

Chapter VIII

Concluding Essay:

Biophysical Properties of Marsupial PrP Repeats

The studies of marsupial PrP repeats presented in this thesis support the idea that this protein interacts with, and may play a role in, cellular metabolism of copper ion. The investigation was carried out using low-resolution spectroscopic methods plus the equilibrium dialysis technique, as there are several obstacles prohibiting the use of high-resolution techniques in the study of repetitive protein sequences.

The use of several spectroscopic methods is necessary to obtain information about all aspects of the biophysical properties of the peptide. However, various conditions – e.g. practicable ranges of peptide and copper ion concentrations, and types of buffer – specific to different methods might cause disagreement in the final results of study of the same property. Nevertheless, conformational and other properties of disordered polypeptides will be better understood if their dependence on environmental conditions is also known.

The sequence of possum decarepeat (PHPGGSNWGQ) was chosen as the main subject of this research as it was the only sequence then available. It is, however, expected to be typical of marsupial PrP-repeat sequences in its essential differences with mammalian PrP-repeat sequences. As shown in Table 1.1 of Chapter I, the PrP repeats of both marsupial species now known (brush-tailed possum and tammar wallaby) do not have the HGGGW segment, which is a feature of the consensus sequence of mammalian PrP repeats. Although the motif P[H/Q].GG.WGQ is conserved among the mammalian and marsupial sequences, this marsupial decarepeat used as the basis for these studies has a Pro inserted as its third residue (after H/Q), which cannot coordinate copper ion through its amide nitrogen.

The purpose of this chapter is threefold: (1). to provide a summary of the findings in the previous Chapters III to VII; (2) to provide explanatory notes on the consistent and conflicting results indicated in those chapters; and (3) to provide some suggestions for future research.

8.1. Structure of marsupial PrP repeats

8.1.1. Copper-free peptides

The NMR structure of a full-length marsupial PrP is not yet available. However, the accumulated spectroscopy data (FTIR, CD, fluorescence, and FRET spectroscopy) reported in this thesis suggest that the repeats region of marsupial PrP is unstructured in the absence of copper ion. This is in good agreement with the structure of copper-free peptide of PrP repeats from mammalians (Hornshaw et al., 1995a; Miura et al., 1996; Viles et al., 1999; Bonomo et al., 2000; Whittal et al., 2000) and chicken (Hornshaw et al., 1995a).

Although marsupial PrP-decarepeat peptides are unstructured, they are not staggered or fully extended but rather loosely folded as suggested by the FRET distance between Trp and the N-terminus (dansyl group attached) of the peptides. The FRET distance between Trp and the N-terminus in human PrP octarepeat peptide also shows that the peptide is loosely folded. The loose folding of human octarepeat is in agreement with the loops and turns structure in Yoshida et al.'s NMR model, which shows Trp is close to the N-terminus of one octarepeat (Yoshida et al., 2000).

Furthermore, Yoshida et al. (2000) suggest that cation-π (at acidic pH 6.5) interaction between the imidazole ring of His and the aromatic ring of Trp stabilizes this loop structure in human octarepeat peptide. However, π-π interaction at neutral or alkaline pH with neutral His seems possible also. Based on the theory of cation-π interaction, Yoshida et al. (2000) predict that a chicken hexarepeat PHNPGY will adopt the same loop structure because, just as in the case of human octarepeat, four residues make up the distance between His and the aromatic ring of Tyr (Yoshida et al., 2000). In the case of marsupial decarepeats (PHPGGSNWGQ), however, there is a 6-residue interval between Trp and His. Thus, in marsupial decarepeats peptide, the cation-π or π-π interaction would likely induce the formation of a larger loop structure.

8.1.2. Copper-complexed peptides

FTIR experiments show that copper ion addition to marsupial PrP-repeat peptides resulted in the formation of a more hydrogen-bonded structure, as the amide I band shifts significantly to lower frequency. The new frequency of the amide I band is

assigned as arising from a solvent-exposed α-helical structure (Haris and Chapman, 1995). The formation of α-helix structure was also observed in CD spectra, which show emergence of a negative band at 220-230 nm upon addition of copper ion to the peptides. Fluorescence spectrosocopy data, which show the wavelength maximum peak does not shift toward a lower wavelength upon addition of copper ion, support the conclusion of solvent-exposed structure in the complexes.

The presence of α-helix structure, resulting from copper addition, was also detected in human PrP repeats, which were studied using Raman spectroscopy (Miura et al., 1996). However, these results are in disagreement with a CD study which suggested no structural changes upon addition of copper ion (Hornshaw et al., 1995a). Yet, other CD experiments suggested the presence of turns and structured loops resulting from copper addition to repeat peptides (Viles et al., 1999; Bonomo et al., 2000; Whittal et al., 2000).

8.2. Dissociation constant (K_d) and stoichiometry of copper binding to marsupial PrP repeats

Stoichiometry and K_d of copper binding to marsupial PrP repeats have been determined by mass spectrometry, fluorescence spectrophotometry, and the equilibrium dialysis technique.

Mass spectra of copper binding to Msp2, Msp3, and Msp4 showed that the peak intensity of the copper complexes of peptide was much lower than that of the free peptide. In contrast with the dissociation constant of the copper complex determined by fluorescence spectrophotometry in the nM range (which will be discussed later), such low peak intensity indicates that the binding of copper to the peptides is very weak. The reason for these conflicting data is, perhaps, due to the use of ammonia/formic acid buffer in the mass spectrometry experiments. As discussed in Chapter VI, the ammonia/formic acid buffer is unreliable for maintaining the pH at 7.4, so that the pH of the solution is likely acidic by the time the sample is analyzed. Nevertheless, in this research these mass spectra revealed the first evidence of possible binding between copper ion and marsupial PrP repeats, which was then further investigated by using other methods. It should be noted that due to the aforementioned unreliable buffer, the

mass spectrometry experiments of copper binding to Msp2, Msp3, and Msp4 did not conclusively show the binding stoichiometry.

The fluorescence spectrophotometry experiments at 0.5 μM peptide concentration demonstrated a stoichiometry of 1 copper ion binding per 1 peptide molecule of Msp2, Msp3, and Msp4. Under the same experimental conditions at 0.5 μM peptide concentration, the stoichiometry is 1 copper ion binding per 2 peptide molecules of Msp1. The stoichiometry of copper ion binding to Msp1 does not change after the free COO^- group at the C-terminus of the peptide is amidated (Msp1capC). In the other three peptides (Msp2, Msp3, and Msp4), the elimination of the COO^- group (in C-terminally amidated peptides: Msp2capC, Msp3capC, and Msp4capC) decreases the copper-binding stoichiometry, as fluorimetry experiments show 1 copper ion binding per 2 peptide molecules of Msp2capC, 1:3 Cu(II)/Msp3capC, and 1:4 Cu(II)/Msp4capC. A marked decrease in the stoichiometry of copper binding per peptide molecule indirectly suggests COO^- group as a copper-binding site; this will be discussed further in the next section.

The stoichiometry of one copper binding to more than one molecule of peptide (Msp1 and all C-terminally amidated peptides) suggests the formation of multi-peptide complexes, which is not supported by results from other methods employed in this research. A method that can directly detect the formation of multi-peptide complexes is the analytical ultracentrifugation (AUC) technique. However, due to time constraints of this thesis, work using the AUC could not be pursued.

The fluorescence spectrophotometry experiments also show that the stoichiometry and K_d depend on peptide concentration. This indicates that peptide molecule association, which is reflected in the stoichiometry of copper binding noted above, follows the copper-binding process. Fluorimetry experiments of copper binding to Msp1capC at varied peptide concentrations show peptide molecule association occurs at low, not high, peptide concentration. As previously mentioned, at 0.5 μM peptide concentration the stoichiometry is 1 copper binding per 2 Msp1capC molecules. At 5 μM peptide concentration the peptide molecule association does not occur, as shown in the stoichiometry of 1 copper ion binding per 1 Msp1capC molecule. This suggests that the number of copper ions binding per peptide molecule at high peptide concentration is

twice that at low peptide concentration. This phenomenon is also observed in the copper complex of Msp4capC.

The equilibrium dialysis experiments show a stoichiometry of 2 copper ions binding per 1 Msp4 molecule. This is in disagreement with the fluorimetry result, which shows that 1 copper ion binds to 1 Msp4 molecule. The disagreement is probably caused by the peptide concentration used in the ED experiment (5 μM) which is 10 times higher than in the fluorimetry experiment (0.5 μM). Given this effect of concentration on the stoichiometry of binding, the fluorimetry experiment of copper binding to 5 μM Msp4 needs to be done to check whether consistent stoichiometry is now obtained. Nevertheless, as the stoichiometry data of copper binding to Msp4capC are available, the stoichiometry of copper binding to 5 μM Msp4 can be deduced as shown in Table 8.1 below.

Table 8.1: Effect of peptide concentration on the stoichiometry of binding between copper and Msp4. The predicted stoichiometry of copper binding to 5.0 μM Msp4 (shown in the shaded area) was deduced from Msp4capC data obtained from fluorescence experiments.

Peptide concentration	Stoichiometry in Msp4capC	Stoichiometry in Msp4
0.5 μM	1 Cu : 4 Msp4capC	1 Cu : 1 Msp4
5.0 μM	1 Cu : 2 Msp4capC	1 Cu : 1/2 Msp4

As noted in Chapter IV, and presented in Table 8.1, at 0.5 μM Msp4capC the stoichiometry is 1 copper ion binding per 4 peptide molecules, while at 5 μM peptide it is 1 copper ion binding per 2 Msp4capC molecules. At 0.5 μM peptide, the number of copper ions bound to Msp4 is 4 times that bound to Msp4capC peptide. At 5 μM peptide, the number of copper ions bound to Msp4 is predicted also to be 4 times that bound to Msp4capC peptide. Fluorescence spectrometry shows that at 5 μM peptide concentration the stoichiometry is 1 copper ion binding per 2 Msp4capC molecules. Thus, in Msp4, the stoichiometry should be 1 copper ion binding per 1/2 Msp4 molecule, or 2 copper ions binding per one Msp4 molecule, i.e. consistent with the results from the ED experiments.

As discussed in Chapter IV, the concentration of peptide used in the experiments to determine the K_d, is much higher than the K_d itself, resulting in low accuracy of the K_d determination, but high accuracy of the stoichiometry determination (Bagshaw and Harris, 1987). However, despite a very large error, the K_d values, which are in the nM range for copper binding to marsupial PrP-repeat peptides, are much lower than most K_d values for copper binding to other PrP repeats (from chicken and human) reported in the literature (Hornshaw et al., 1995a; Brown et al., 1997; Stockel et al., 1998; Viles et al., 1999; Whittal et al., 2000; Kramer et al., 2001). Some exceptions are K_d values of Garnett and Viles (2003) in the 10 μM to 10 nM range, and Jackson et al. (2001) who proposed a K_d in the fM range.

Thus, while results of both ED and fluorimetry experiments show the same copper-binding stoichiometry, the K_d value is still in dispute: the K_d from the fluorimetry experiments is in the nM range, while that from ED experiments is in the μM range. However, as the binding curves from the fluorescence experiments are measured under conditions of stoichiometric binding, the K_d value is determined to be much lower than 0.5 μM (peptide concentration used in fluorimetry experiments), but will have large error.

8.3. Proposed copper-binding mode in marsupial PrP repeats

Fluorescence titration experiments show the imino group of Pro at the N-terminus is very important in facilitating the binding between copper ions and the Msp peptides ($(PHPGGSNWGQ)_nG$, where n = 1, 2, 3, and 4), as acetylation of the N-terminus abolished binding between peptide and copper ion. On the other hand, replacement of the His residue with Ala caused only a 100 times increase of K_d, which means only a weakening of the binding. From this we can infer that the anchoring site for copper binding in Msp peptides is the imino group of Pro instead of the imidazole ring of the His residue. Once copper ion binds to the anchoring site, other ligands including the nitrogen atom of the imidazole ring of His complete the coordination sphere. Similar findings from FTIR and ESI MS experiments confirm that the imino group is the anchoring site for copper ion in Msp peptides.

However, in contrast to fluorimetry, FTIR experiments show that in the absence of the imino group of Pro, the binding between the N-terminally acetylated peptide and copper ion does occur but only at basic pH (pH≥8.0). The binding occurs via the His side chain as the anchoring site and other ligands, including the amide nitrogen, that complete the coordination sphere.

The involvement of the amide backbone in copper coordination is indicated in FTIR spectra. The factors that determine whether or not a particular main chain amide is involved in the binding are its position relative to the anchoring site and the steric hindrance of the side chain. Breslow (1973) reported that copper ion tends to coordinate with nitrogen atoms of the peptide bond, with simultaneous displacement of the peptide bond proton. The nearest peptide bond to the anchoring site will have the lowest pK and will most likely participate in copper binding, provided there is no steric hindrance (Breslow, 1973).

The His side chain residue has two nitrogen atoms that can participate in copper binding, namely N_π and N_τ. The fluorimetry experiments indicate copper ion strongly prefers binding to the N_π atom rather than to the N_τ atom, as the affinity of copper binding to Msp1His(1Me)capC at pH 8.0 is shown to be much higher than that for Msp1His(3Me)capC. Furthermore, copper ion addition to Msp1His(3Me)capC at pH 6.0 and 7.0 does not change the Trp fluorescence emission intensity, while addition to Msp1His(1Me)capC peptide does. This lack of change suggests that copper ion does not bind to the N_τ atom of the imidazole ring of His under these fluorimetry experimental conditions (pH 6.0-7.0 and 0.5 μM peptide concentration). The result is in contrast to the FTIR experiment, which shows that addition of copper changes the spectrum of both peptides at all pHs studied (pH 6.0-9.0). This discrepancy is probably due to the difference in peptide concentration used in each method, with the FTIR method requiring a 1,000 times higher peptide concentration than the fluorimetry method.

In order to propose a structure for the copper complex, information about the binding stoichiometry as well as the groups or atoms that bind to copper ion is needed. The difficulty is that the stoichiometry of binding is very much affected by the peptide concentration, as has been shown by the fluorimetry experiment. In the work presented

here, information on the stoichiometry is obtained from the fluorimetry experiments, which requires only μM concentration of the peptides. On the other hand, information on the binding sites is gained mostly from the FTIR experiments, which employed mM peptide concentration. However, the fluorimetry experiments to some extent also provide information about the binding sites that are in good agreement with the FTIR results, such as the importance of the imino group of Pro at the N-terminus and the imidazole side chain of His.

Titration data to study binding from the FTIR experiments are available only for copper binding to Msp1. However, the shape of the binding curve (Figure 3.35.B) shows the binding is not under stoichiometric conditions, but under equilibrium conditions, from which we can extract accurate information about the K_d, but not stoichiometry. The stoichiometry data at high peptide concentration, therefore, are deduced from fluorimetry titration of copper binding to various concentrations of Msp peptides (see section 4.4.5 of Chapter IV)

The data presented in Table 4.3 of Chapter IV, and discussed above in section 8.3, indicate an increase in the number of copper ions bound to the peptide molecule with increasing peptide concentration. From this data, the predicted complex that formed at high peptide concentration is 1:1 copper per Msp1, Msp1capC, and Msp1capNC peptide. The likelihood of 2 copper ions binding to 1 Msp1 molecule is less as there is only one potential anchoring site, which is the imino group of Pro at the N-terminus. The complexes of Msp2, Msp3, and Msp4 are more difficult to predict. However, given that copper binding requires the imino group of Pro at the N-terminus, it is likely that the stoichiometry is also 1 copper binding per 1 Mspn (n=2, 3, and 4) molecule. Nonetheless, there is also a possibility that both the imino group of Pro and the imidazole ring of His act as copper-anchoring sites in long repeats such as Msp4 which, as shown in the ED experiment, binds 2 copper ions.

8.3.1. Copper-binding mode in Msp1 and Msp1capC

As noted above, the anchoring site for peptide is the imino group of Pro. The binding of copper to the imino group will be accompanied by binding to the adjacent peptide bond nitrogen with concurrent displacement of the peptide bond proton (Breslow, 1973).

Therefore, in Msp1 (PHPGGSNWGQG) and Msp1capC (PHPGGSNWGQ-NH_2), the nitrogen amide of the His^2 residue will join the coordination sphere. Note that the involvement of the amide backbone in copper coordination is apparent in FTIR spectra. Another nitrogen atom comes from the imidazole ring of His^2. There are two nitrogen atoms of the imidazole ring with potential to be binding sites, but in this case, according to the FTIR spectra of copper complexes of Msp1 and Msp1capC and fluorescence titration spectrophotometry results, it is the N_π atom that is participating. The possible complex is shown in Figure 8.1. Copper ion binds the nitrogen atom of the imino group of Pro^1, the nitrogen atom of the main chain amide of His^2, and the nitrogen atom of the imidazole ring of His^2. In Msp1, the fourth ligand could be the oxygen atom of a water molecule or the α-carboxyl group at the C-terminus. In Msp1capC, the fourth ligand could be the oxygen atom of a water molecule.

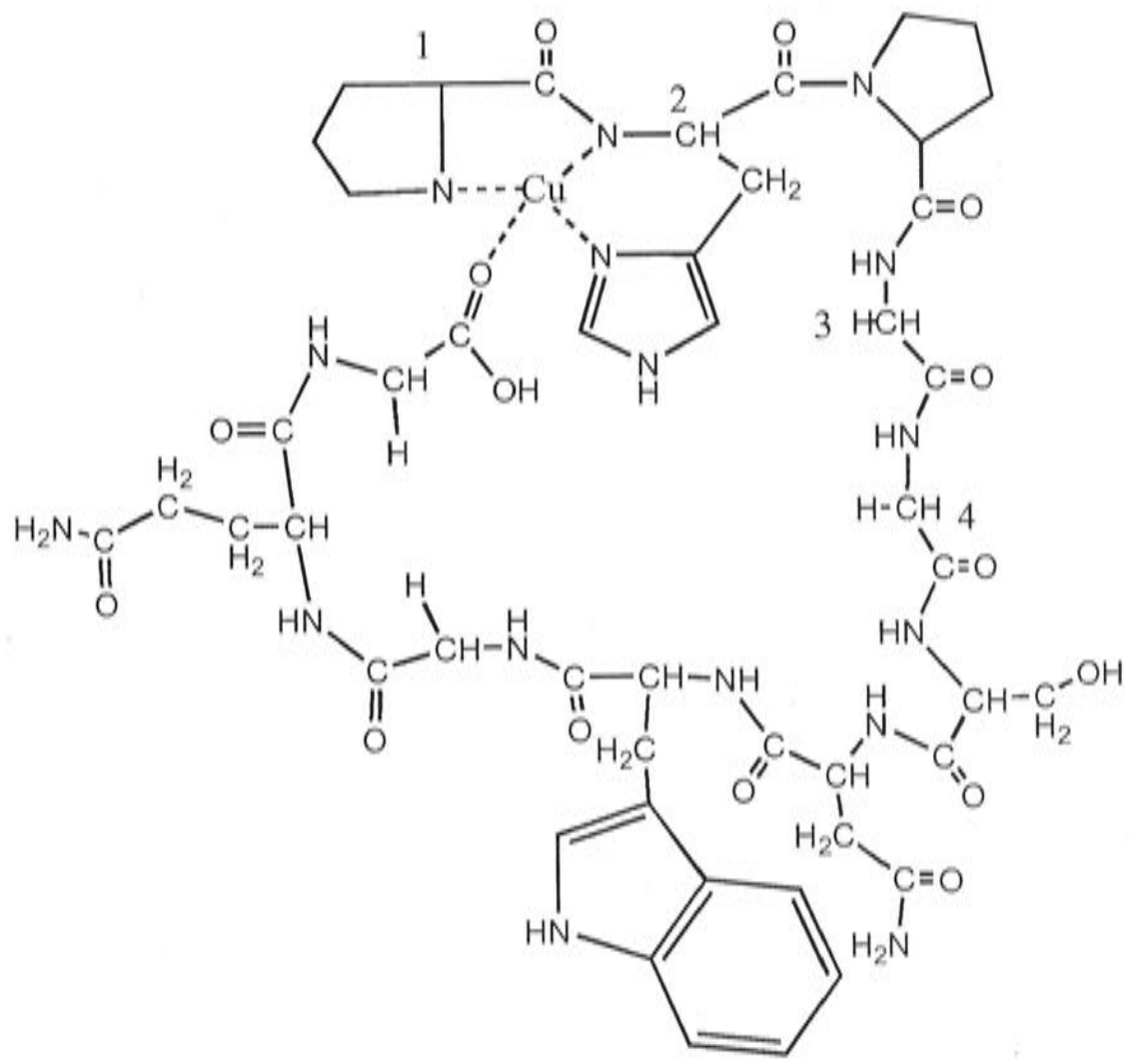

Figure 8.1: Copper-binding mode in $(PHPGGSNWGQ)_nG$ peptide at neutral pH. The C_α atoms of the first four residues were labeled. The figure shows that peptide binds copper ion via the nitrogen atom of the α-imino group of Pro^1, the nitrogen atom of the amide backbone of His^2, and the nitrogen (N_π) atom of the imidazole ring of His^2, resulting in the formation of 5- and 6-membered rings. The fourth ligand could be the oxygen atom from the α-carboxyl group at the C-terminus or a water molecule. At basic pH, other nitrogen atoms from the main chain amide backbone participate.

8.3.2. Copper-binding mode in Msp1capNC

In the absence of the α-imino group of Pro, the anchoring site for copper binding to marsupial PrP-repeat peptide is the imidazole ring of His. The deprotonated nitrogen atoms of the main chain amide will complete the coordination sphere. At the N-terminal side of the anchoring site, the nearest amide nitrogen coming from the His residue itself participates in the binding. However, the binding towards the N-terminus cannot move further than His^2, as the nitrogen atom of the main chain amide of Pro^1 does not have a proton to displace.

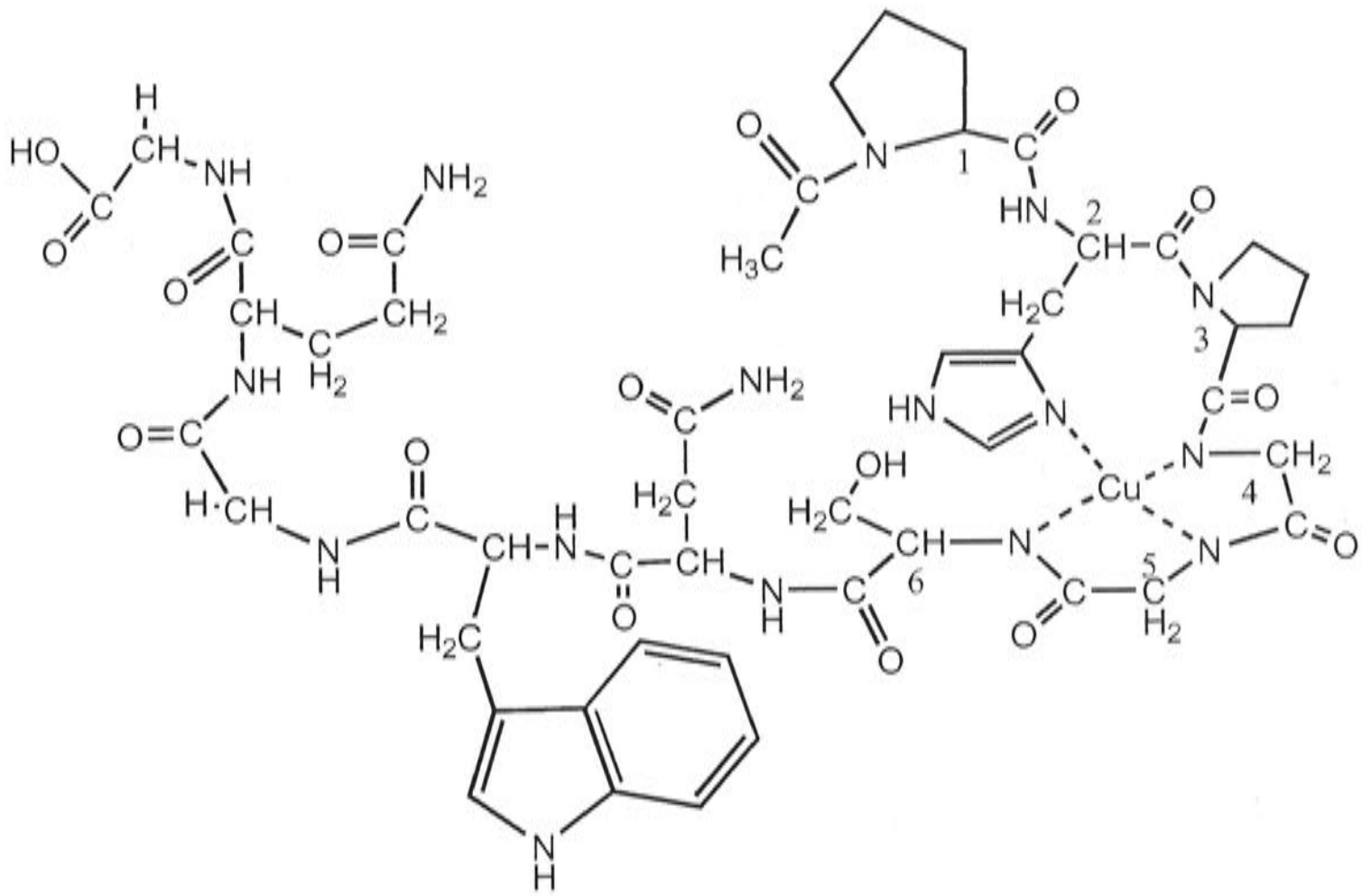

Figure 8.2: Copper-binding mode in Ac-$(PHPGGSNWGQ)_nG$ peptide at basic pH. The C_α atoms of the first six residues were labeled. The figure shows that the peptide binds copper ion via the nitrogen (N_π) atom of the imidazole ring of His^2, and 3 nitrogen atoms of the main chain amide backbone of Gly^4, Gly^5, and Ser^6 resulting in the formation of one 10- and two 5-membered rings.

Consequently the binding should move towards the C-terminus (forward binding). But, the fact that the third residue is Pro, for which the nitrogen amide cannot participate in coordination, the forward binding is blocked. Participation of the amide nitrogen further along towards the C-terminus is possible only at high pH. As mentioned above, the closer the peptide backbone to the anchoring site, the lower the pK for proton displacement, and vice versa (Breslow, 1973). As a consequence, the binding occurs only at basic pH (see Figure 3.6 of Chapter III), where the coordination of the imidazole ring of His^2 can be supported by coordination of the nitrogen atoms of main chain

amides of residues further towards the C-terminus, for instance Gly^4 and Gly^5. The fact that the binding occurs only at basic pH also indicates copper ion prefers binding to the nitrogen atom of the peptide bond rather than to the carbonyl oxygen atoms of the Pro^1 or Pro^3 residues.

The proposed binding site in Msp1capNC at basic pH is, therefore: the N_π atom of His^2 and nitrogen atoms of the main chain amides of Gly^4, Gly^5, and possibly Ser^6 as the pH is increased. The binding results in the formation of one 10-membered and two 5-membered rings (Figure 8.2).

8.3.3. Copper-binding mode in Msp1P3GcapNC

The sequence of the first half part of this peptide (^{1}PHGGGSNWGQG^{11}) is similar to that of the first half part of human PrP repeats (^{1}PHGGGWGQG^9). FTIR assignments have revealed that copper-binding sites in Msp1P3GcapNC will be the imidazole ring of His^2 (the anchoring site) and three nitrogen atoms of the main chain amide of Gly^3, Gly^4, and Gly^5, as shown in Figure 8.3. The participation of the nitrogen amide of Gly^3 is inferred from large FTIR spectral changes that occur upon addition of copper ion to Msp1P3GcapNC. Note that in wild-type peptide (Msp1capNC), where the third residue is Pro, the spectral changes upon copper ion addition are minimal.

The binding site proposed in Figure 8.3 is fairly similar to the proposed binding site for human PrP octarepeat according to the X-ray crystal structure of Burns et al. (2002) and the proposed model of Luczkowski et al. (2002). As mentioned in Chapter I, both papers proposed that copper ion binds to the N_π atom of His^2 and two nitrogen atoms of the main chain amide of Gly^3 and Gly^4 (Burns et al., 2002; Luczkowski et al., 2002). In addition to that, the XRD data show copper ion also binds to the peptidic oxygen atom of Gly^4 (Burns et al., 2002).

As shown in Figure 8.3, in Msp1P3GcapNC (^{1}PHGGGSNWGQG^{11}) copper ion binds to the N_π atom of the imidazole side chain of His^2 residue and 3 nitrogen atoms of the main chain amide backbone of Gly^3, Gly^4, and Gly^5. It is possible that the Gly^5 residue is not the ligand for copper, but that the amide backbone participation comes from the oxygen atom (of Gly^4) rather than the nitrogen atom (of Gly^5). However, there are no

data to support the involvement of the oxygen carbonyl in the copper coordination sphere.

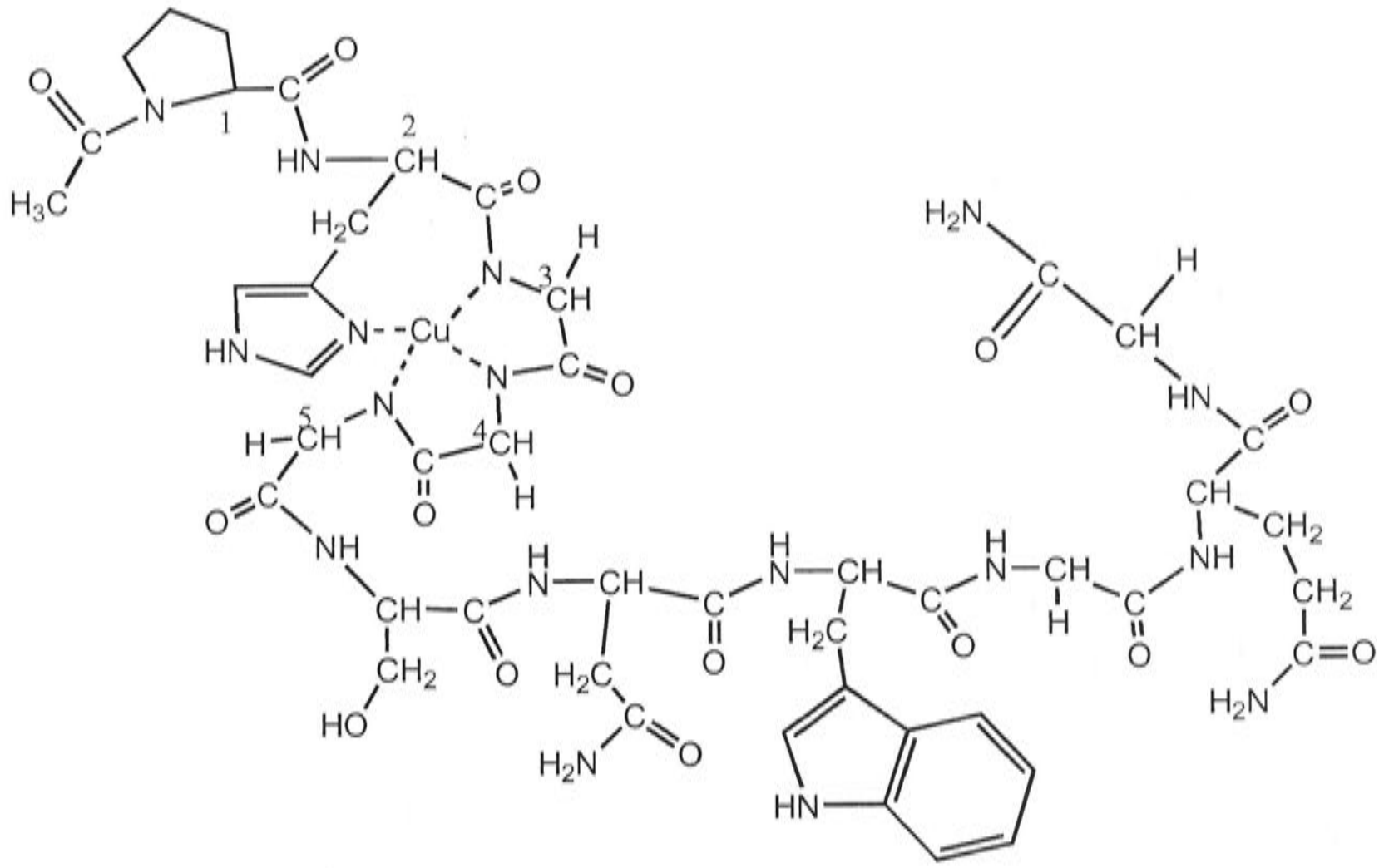

Figure 8.3: Copper-binding mode in Msp1P3GcapNC (Ac-PHGGGSNWGQG-NH_2) peptide at neutral and slightly basic pH. The C_α atoms of the first five residues were labeled. The figure shows the peptide binds copper ion via the nitrogen (N_π) atom of the imidazole ring of His^2, and 3 nitrogen atoms of the main chain amide backbone of Gly^3, Gly^4, and Gly^5 resulting in the formation of one 7- and two 5-membered rings.

The fact that copper ion binds this mutant peptide better than the wild type indicates the HGGG segment as a copper-binding unit at neutral and slightly basic pH. As noted, this cannot be replaced by HPGG because the Pro residue cannot donate its nitrogen main chain amide for copper coordination. Recent literature points out the specificity of this HGGG segment in binding of copper ion (Garnett and Viles, 2003; Luczkowski et al., 2003). None of the marsupial (Windl et al., 1995; Premzl and Gready, 2003, personal communication) or avian (Gabriel et al., 1992) PrP repeats have this segment.

Copper binding to the tammar wallaby PrP repeats, in which the third repeat (PHAGGSNWGQ) contains the HAGG segment (Premzl and Gready, 2003, personal communication), should be studied to establish further the copper-binding specificity of the HGGG segment and to provide a comparison with the properties of possum PrP repeats.

8.4. Copper-binding mode in Hu1capNC

As mentioned in the previous section, the copper-binding mode in Hu1capNC would be similar to that of Msp1P3GcapNC. The coordination involved the imidazole ring of His^2, the three nitrogen atoms of the main chain amides coming from Gly^3, Gly^4, and Gly^5, as shown in Figure 8.4.

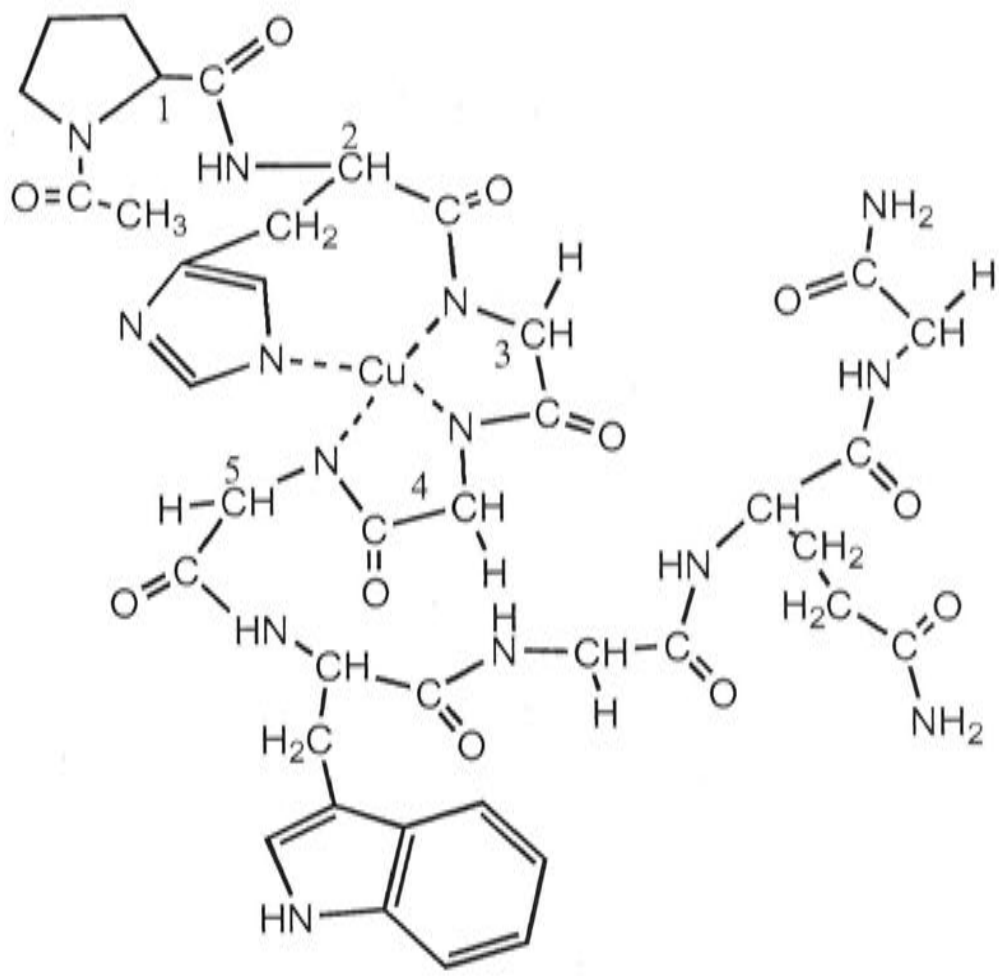

Figure 8.4: Copper-binding mode in Hu1capNC (Ac-PHGGGWGQG-NH_2) peptide at neutral and slightly basic pH. The C_α atoms of the first five residues were labeled. The figure shows the peptide binds copper ion via the nitrogen (N_τ) atom of the imidazole ring of His^2, and 3 nitrogen atoms of the main chain amide backbone of Gly^3, Gly^4, and Gly^5 resulting in the formation of one 8- and two 5-membered rings.

The nitrogen of the imidazole ring of His that participates in copper coordination comes from the N_τ rather than the N_π atom, as suggested by FTIR spectra. This is in contrast to the binding site proposed by Miura et al. (1999) for human repeat, in which, at pH 8.0, copper ion binds the N_π atom of the imidazole ring of His. This difference may be due to the ratio of peptide and copper ion concentration in the FTIR experiments (1:4 of peptide per copper ion) being much higher than in the Raman experiments [1:1 (20 mM peptide per 20 mM copper ions]. As mentioned in Chapter III, in this FTIR experiment, the peptide concentration was 2.5 mM and the copper ion concentration was 10 mM. Thus, this phenomenon indicates that for Hu1capNC peptide the concentration ratio of copper influences the coordination environment. This suggestion, however, is not

confirmed, as there are no experimental data for this concentration ratio-dependent binding mode.

8.5. Suggestion for future studies

The work presented in this thesis has resolved some questions regarding the copper-binding properties of PrP repeats from species other than human, other eutherian mammals, or birds. But, several issues still need further investigation. The first issue is whether the copper-binding modes in multi-decarepeat marsupial PrP peptide will be the same as those for the single-decarepeat peptide. For that matter, the stoichiometry of copper binding to multi-decarepeats peptide needs to be clarified. A second issue is whether the preference of copper ion binding to the N_π or N_τ atom of the imidazole ring of the His residue is a function of the concentration ratio of peptide and copper ion. A third issue is whether the copper-binding properties of the actual sequence of the marsupial PrP-repeat peptide are similar to the properties of the consensus-decarepeat peptides studied in this thesis. A fourth issue that needs to be investigated further is the cation-π or π-π interaction between His and Trp in PrP-repeat peptides, and the influence of such interactions in the folding of the repeats and the stability of the peptide conformation.

References

Allen, M. H. and Hutchens, T. W. (1992). Electrospray-ionization mass spectrometry for the detection of discrete peptide/metal-ion complexes involving multiple cysteine (sulfur) ligands. *Rapid Communications in Mass Spectrometry* **6**: 308-312.

Aronoff-Spencer, E., Burns, C. S., Avdievich, N. I., Gerfen, G. J., Peisach, J., Antholine, W. E., Ball, H. L., Cohen, F. E., Prusiner, S. B. and Millhauser, G. L. (2000). Identification of the Cu^{2+} binding sites in the N-terminal domain of the prion protein by EPR and CD spectroscopy. *Biochemistry* **39**: 13760-13771.

Arrondo, J. L. and Goni, F. M. (1999). Structure and dynamics of membrane proteins as studied by infrared spectroscopy. *Progress in Biophysics and Molecular Biology* **72**: 367-405.

Baldwin, M. A., Cohen, F. E. and Prusiner, S. B. (1995). Prion protein isoforms, a convergence of biological and structural investigations. *Journal of Biological Chemistry* **270**: 19197-19200.

Barth, A. (2000). The infrared absorption of amino acid side chains. *Progress in Biophysics and Molecular Biology* **74**: 141-173.

Bagshaw, C. R. and Harris, D. A. (1987). Measurement of Ligand Binding to Proteins. In Bashford, C. L. and Harris, D. A. (Eds.), *Spectrophotometry & spectrofluorimetry : a practical approach*. Oxford, IRL Press Limited. Pp.91-113.

Bonomo, R. P., Imperllizzeri, G., Pappalardo, G., Rizzarelli, E. and Tabbi, G. (2000). Copper(II) binding modes in the prion octapeptide PHGGGWGQ: a spectroscopic and voltammetric study. *Chemistry* **6**: 4195-4202.

Breslow, E. (1973). Metal-Protein Complexes. In Eichhorn, G. L (Ed.), *Inorganic Biochemistry* vol 1. New York, Elsevier Scientific Publishers Company. Pp. 227-249.

Brimacombe, D. B., Bennett, A. D., Wusteman, F. S., Gill, A. C., Dann, J. C. and Bostock, C. J. (1999). Characterization and polyanion-binding properties of purified recombinant prion protein. *Biochemical Journal* **342**: 605-613.

Brown, D. R. and Besinger, A. (1998). Prion protein expression and superoxide dismutase activity. *Biochemical Journal* **334**: 423-429.

Brown, D. R., Hafiz, F., Glasssmith, L. L., Wong, B. S., Jones, I. M., Clive, C. and Haswell, S. J. (2000). Consequences of manganese replacement of copper for prion protein function and proteinase resistance. *EMBO Journal* **19**: 1180-1186.

Brown, D. R., Qin, K., Herms, J. W., Madlung, A., Manson, J., Strome, R., Fraser, P. E., Kruck, T., von Bohlen, A., Schulz-Schaeffer, W., Giese, A., Westaway, D. and Kretzschmar, H. (1997). The cellular prion protein binds copper in vivo. *Nature* **390**: 684-687.

Brown, D. R., Schmidt, B. and Kretzschmar, H. A. (1998). Effects of copper on survival of prion protein knockout neurons and glia. *Journal of Neurochemistry* **70**: 1686-1693.

Brown, D. R., Wong, B. S., Hafiz, F., Clive, C., Haswell, S. J. and Jones, I. M. (1999). Normal prion protein has an activity like that of superoxide dismutase. *Biochemical Journal* **344**: 1-5.

Bruce, J. E., Anderson, G. A., Chen, R. D., Cheng, X. H., Gale, D. C., Hofstadler, S. A., Schwartz, B. L. and Smith, R. D. (1995). Bio-affinity characterization mass spectrometry. *Rapid Communications in Mass Spectrometry* **9**: 644-650.

Bryce, G. F. and Gurd, F. R. N. (1966). Visible spectra and optical rotatory properties of cupric ion complexes of L-Histidine-containing peptides. *The Journal of Biological Chemistry* **241**: 122-129.

Burns, C. S., Aronoff-Spencer, E., Dunham, C. M., Lario, P., Avdievich, N. I., Antholine, W. E., Olmstead, M. M., Vrielink, A., Gerfen, G. J., Peisach, J., Scott, W. G. and Millhauser, G. L. (2002). Molecular features of the copper binding sites in the octarepeat domain of the prion protein. *Biochemistry* **41**: 3991-4001.

Byler, D. M. and Susi, H. (1986). Examination of the secondary structure of proteins by deconvolved FTIR spectra. *Biopolymers* **25**: 469-487.

Cereghetti, G. M., Schweiger, A., Glockshuber, R. and Van Doorslaer, S. (2001). Electron paramagnetic resonance evidence for binding of Cu^{2+} to the C-terminal domain of the murine prion protein. *Biophysical Journal* **81**: 516-525.

Chirgadze, Y. N., Fedorov, O. V. and Trushina, N. P. (1975). Estimation of amino acid residue side-chain absorption in the infrared spectra of protein solutions in heavy water. *Biopolymers* **14**: 679-694.

Cohen, F. E. and Prusiner, S. B. (1998). Pathologic conformations of prion proteins. *Annual Review of Biochemistry* **67**: 793-819.

Creighton, T. E. (1983). *Proteins: structures and molecular principles*. New York, W.H. Freeman and Company.

de Souza, E. S., Hirata, I. Y., Juliano, L. and Ito, A. S. (2000). End-to-end distance distribution in bradykinin observed by Förster resonance energy transfer. *Biochimica et Biophysica Acta* **1474**: 251-261.

Donne, D. G., Viles, J. H., Groth, D., Mehlhorn, I., James, T. L., Cohen, F. E., Prusiner, S. B., Wright, P. E. and Dyson, H. J. (1997). Structure of the recombinant full-length hamster prion protein PrP(29-231): the N terminus is highly flexible. *Proceedings of the National Academy of Sciences USA* **94**: 13452-13457.

dos Remedios, C. G. and Moens, P. D. (1995). Fluorescence resonance energy transfer spectroscopy is a reliable "ruler" for measuring structural changes in proteins. Dispelling the problem of the unknown orientation factor. *Journal of Structural Biology* **115**: 175-185.

Dunn, B. M., Pham, C., Raney, L., Abayasekara, D., Gillespie, W. and Hsu, A. (1981). Interaction of alpha-dansylated peptide inhibitors with porcine pepsin: detection of complex formation by fluorescence energy transfer and chromatography and evidence for a two-step binding scheme. *Biochemistry* **20**: 7206-7211.

Fernandez-Recio, J., Vazquez, A., Civera, C., Sevilla, P. and Sancho, J. (1997). The tryptophan/histidine interaction in alpha-helices. *Journal of Molecular Biology* **267**: 184-197.

Flechsig, E., Shmerling, D., Hegyi, I., Raeber, A. J., Fischer, M., Cozzio, A., von Mering, C., Aguzzi, A. and Weissmann, C. (2000). Prion protein devoid of the octapeptide repeat region restores susceptibility to scrapie in PrP knockout mice. *Neuron* **27**: 399-408.

Ford, M. J., Burton, L. J., Morris, R. J. and Hall, S. M. (2002). Selective expression of prion protein in peripheral tissues of the adult mouse. *Neuroscience* **113**: 177-192.

Förster, T. (1948). Intermolecular energy migration and fluorescence. *Annual Physics* **2**: 55-75.

Gabriel, J. M., Oesch, B., Kretzschmar, H., Scott, M. and Prusiner, S. B. (1992). Molecular cloning of a candidate chicken prion protein. *Proceedings of the National Academy of Sciences USA* **89**: 9097-9101.

Gallivan, J. P. and Dougherty, D. A. (1999). Cation-π interactions in structural biology. *Proceedings of the National Academy of Sciences USA* **96**: 9459-9464.

Garnett, A. P. and Viles, J. H. (2003). Copper binding to the octarepeats of the prion protein. Affinity, specificity, folding, and cooperativity: insights from circular dichroism. *Journal of Biological Chemistry* **278**: 6795-6802.

Gazit, E. (2002). A possible role for π-stacking in the self-assembly of amyloid fibrils. *FASEB Journal* **16**: 77-83.

Gonzalez-Iglesias, R., Pajares, M. A., Ocal, C., Espinosa, J. C., Oesch, B. and Gasset, M. (2002). Prion protein interaction with glycosaminoglycan occurs with the formation of oligomeric complexes stabilized by Cu(II) bridges. *Journal of Molecular Biology* **319**: 527-540.

Gromiha, M. M. (2002). Influence of cation-π, interactions in mesophilic and thermophilic proteins. *Journal of Liquid Chromatography & Related Technologies* **25**: 3141-3149.

Gromiha, M. M., Thomas, S. and Santhosh, C. (2002). Role of cation-π interactions to the stability of thermophilic proteins. *Preparative Biochemistry & Biotechnology* **32**: 355-362.

Gustiananda, M., Haris, P. I., Milburn, P. J. and Gready, J. E. (2002). Copper-induced conformational change in a marsupial prion protein repeat peptide probed using FTIR spectroscopy. *FEBS Letters* **512**: 38-42.

Harada, I., Miura, T. and Takeuchi, H. (1986). Origin of the doublet at 1360 and 1340 cm^{-1} in the Raman spectra of tryptophan and related compounds. *Spectrochimica Acta Part A-Molecular Spectroscopy* **42 A**: 307-312.

Haris, P. I. and Chapman, D. (1992). Does Fourier-transform infrared spectroscopy provide useful information on protein structures? *Trends in Biochemical Sciences* **17**: 328-333.

Haris, P. I. and Chapman, D. (1995). The conformational analysis of peptides using Fourier transform IR spectroscopy. *Biopolymers* **37**: 251-263.

Haris, P. I., Lee, D. C. and Chapman, D. (1986). A Fourier transform infrared investigation of the structural differences between ribonuclease A and ribonuclease S. *Biochimica et Biophysica Acta* **874**: 255-265.

Hasegawa, K., Ono, T. and Noguchi, T. (2000). Vibrational spectra and ab initio DFT calculations of 4-methylimidazole and its different protonation forms: infrared and Raman markers of the protonation state of a histidine side chain. *Journal of Physical Chemistry* **B 104**: 4253-4265.

Hasnain, S. S., Murphy, L. M., Strange, R. W., Grossmann, J. G., Clarke, A. R., Jackson, G. S. and Collinge, J. (2001). XAFS study of the high-affinity copper-binding site of human PrP^{91-231} and its low-resolution structure in solution. *Journal of Molecular Biology* **311**: 467-473.

Haughland, R. P. (2001). *Handbook of Fluorescent Probes and Research Products*. 8th ed. Eugene, Molecular Probes Inc.

Heimburg, T., Schunemann, J., Weber, K. and Geisler, N. (1999). FTIR-Spectroscopy of multistranded coiled coil proteins. *Biochemistry* **38**: 12727-12734.

Hornshaw, M. P., McDermott, J. R., Candy, J. M. and Lakey, J. H. (1995a). Copper binding to the N-terminal tandem repeat region of mammalian and avian prion protein: structural studies using synthetic peptides. *Biochemical and Biophysical Research Communications* **214**: 993-999.

Hornshaw, M. P., McDermott, J. R. and Candy, J. M. (1995b). Copper binding to the N-terminal tandem repeat regions of mammalian and avian prion protein. *Biochemical and Biophysical Research Communications* **207**: 621-629.

Hu, P. F. and Loo, J. A. (1995). Determining calcium-binding stoichiometry and cooperativity of parvalbumin and calmodulin by mass spectrometry. *Journal of Mass Spectrometry* **30**: 1076-1082.

Hutchens, T. W. and Allen, M. H. (1992). Differences in the conformational state of a zinc-finger DNA-binding protein domain occupied by zinc and copper revealed by electrospray ionization mass spectrometry. *Rapid Communications in Mass Spectrometry* **6**: 469-473.

Hutchens, T. W., Nelson, R. W., Allen, M. H., Li, C. M. and Yip, T. T. (1992). Peptide-metal ion interactions in solution: detection by laser desorption time-of-flight mass spectrometry and electrospray ionization mass spectrometry. *Biological Mass Spectrometry* **21**: 151-159.

Ismail, A. A., Mantsch, H. H. and Wong, P. T. (1992). Aggregation of chymotrypsinogen: portrait by infrared spectroscopy. *Biochimica et Biophysica Acta* **1121**: 183-188.

Jackson, G. S., Murray, I., Hosszu, L. L. P., Gibbs, N., Waltho, J. P., Clarke, A. R. and Collinge, J. (2001). Location and properties of metal-binding sites on the human prion protein. *Proceedings of the National Academy of Sciences USA* **98**: 8531-8535.

Jackson, M., Haris, P. I. and Chapman, D. (1989). Conformational transition in poly(L-lysine): studies using Fourier transform infrared spectroscopy. *Biochimica et Biophysica Acta* **998**: 75-79.

Jackson, M., Mantsch, H. H. and Spencer, J. H. (1992). Conformation of magainin-2 and related peptides in aqueous solution and membrane environments probed by Fourier transform infrared spectroscopy. *Biochemistry* **31**: 7289-7293.

Janek, K., Rothemund, S., Gast, K., Beyermann, M., Zipper, J., Fabian, H., Bienert, M. and Krause, E. (2001). Study of the conformational transition of A β(1-42) using D-amino acid replacement analogues. *Biochemistry* **40**: 5457-5463.

Jiao, C. Q., Freiser, B. S., Carr, S. R. and Cassady, C. J. (1995). An electrospray ionization mass spectrometry study of copper adducts of protonated ubiquitin. *Journal of the American Society for Mass Spectrometry* **6**: 521-524.

Jobling, M. F., Huang, X., Stewart, L. R., Barnham, K. J., Curtain, C., Volitakis, I., Perugini, M., White, A. R., Cherny, R. A., Masters, C. L., Barrow, C. J., Collins, S. J., Bush, A. I. and Cappai, R. (2001). Copper and zinc binding modulates the aggregation and neurotoxic properties of the prion peptide PrP106-126. *Biochemistry* **40**: 8073-8084.

Johnson, W. C. Jr. (1988). Secondary structure of proteins through circular dichroism spectroscopy. *Annual Review of Biophysics and Biophysical Chemistry* **17**: 145-166.

Johnson, W. C., Jr. (1990). Protein secondary structure and circular dichroism: a practical guide. *Proteins* **7**: 205-214.

Jorgensen, T. J. D., Roepstorff, P. and Heck, A. J. R. (1998). Direct determination of solution binding constants for noncovalent complexes between bacterial cell wall peptide analogues and vancomycin group antibiotics by electrospray ionization mass spectrometry. *Analytical Chemistry* **70**: 4427-4432.

Jung, C. (2000). Insight into protein structure and protein-ligand recognition by Fourier transform infrared spectroscopy. *Journal of Molecular Recognition* **13**: 325-351.

Klotz, I. M. (1989). Ligand-protein binding affinities. In Creighton, T. E. (Ed), *Protein function: a practical approach*. Oxford, IRL Press. Pp.25-54.

Knaus, K. J., Morillas, M., Swietnicki, W., Malone, M., Surewicz, W. K. and Yee, V. C. (2001). Crystal structure of the human prion protein reveals a mechanism for oligomerization. *Nature Structural Biology* **8**: 770-774.

Kramer, M. L., Kratzin, H. D., Schmidt, B., Romer, A., Windl, O., Liemann, S., Hornemann, S. and Kretzschmar, H. (2001). Prion protein binds copper within the physiological concentration range. *Journal of Biological Chemistry* **276**: 16711-16719.

Kulinski, T., Wennerberg, A. B., Rigler, R., Provencher, S. W., Pooga, M., Langel, U. and Bartfai, T. (1997). Conformational analysis of galanin using end to end distance distribution observed by Förster resonance energy transfer. *European Biophysics Journal* **26**: 145-154.

Lagunoff, D. and Ottolenghi, P. (1966). Effect of pH on the fluorescence of dimethylaminonaphthalenesulphonate (DNS) and several derivatives. *Comptes-rendus des Travaux Carlsberg Laboratories* **35**: 63-83.

Lakowicz, J. R. (1983). *Principles of fluorescence spectroscopy*. New York, Plenum Press.

Lakowicz, J. R., Gryczynski, I., Laczko, G., Wiczk, W. and Johnson, M. L. (1994). Distribution of distances between the tryptophan and the N-terminal residue of melittin in its complex with calmodulin, troponin C, and phospholipids. *Protein Science* **3**: 628-637.

Loewenthal, R., Sancho, J. and Fersht, A. R. (1991). Fluorescence spectrum of barnase: contributions of three tryptophan residues and a histidine-related pH dependence. *Biochemistry* **30**: 6775-6779.

Loewenthal, R., Sancho, J. and Fersht, A. R. (1992). Histidine-aromatic interactions in barnase. Elevation of histidine pK_a and contribution to protein stability. *Journal of Molecular Biology* **224**: 759-770.

Lopez Garcia, F., Zahn, R., Riek, R. and Wuthrich, K. (2000). NMR structure of the bovine prion protein. *Proceedings of the National Academy of Sciences USA* **97**: 8334-8339.

Luczkowski, M., Kozlowski, H., Legowska, A., Rolka, K. and Remelli, M. (2003). The possible role of Gly residues in the prion octarepeat region in the coordination of Cu^{2+} ions. *Journal of the Chemical Society-Dalton Transactions* **4**: 619-624.

Luczkowski, M., Kozlowski, H., Stawikowski, M., Rolka, K., Gaggelli, E., Valensin, D. and Valensin, G. (2002). Is the monomeric prion octapeptide repeat PHGGGWGQ a specific ligand for Cu^{2+} ions? *Journal of the Chemical Society-Dalton Transactions* **11**: 2269-2274.

Maliwal, B. P., Lakowicz, J. R., Kupryszewski, G. and Rekowski, P. (1993). Fluorescence study of conformational flexibility of RNase s-peptide: distance-distribution, end-to-end diffusion, and anisotropy decays. *Biochemistry* **32**: 12337-12345.

Mann, M. (1992). Electrospray Mass Spectrometry. In Gross, M. L. (Ed), *Mass spectrometry in the biological sciences: a tutorial*. Netherlands, Kluwer Academic Publishers. Pp. 145-163.

Miura, T., Hori-i, A. and Takeuchi, H. (1996). Metal-dependent α-helix formation promoted by the glycine-rich octapeptide region of prion protein. *FEBS Letters* **396**: 248-252.

Miura, T., Hori-i, A., Mototani, H. and Takeuchi, H. (1999). Raman spectroscopic study on the copper(II) binding mode of prion octapeptide and its pH dependence. *Biochemistry* **38**: 11560-11569.

Miura, T., Satoh, T., Hori-i, A. and Takeuchi, H. (1998). Raman marker bands of metal coordination sites of histidine side chains in peptides and proteins. *Journal of Raman Spectroscopy* **29**: 41-47.

Moreau, S., Awade, A. C., Molle, D., Legraet, Y. and Brule, G. (1995). Hen egg white lysozyme-metal ion interactions: investigation by electrospray ionization mass spectrometry. *Journal of Agricultural & Food Chemistry* **43**: 883-889.

Muga, A., Surewicz, W. K., Wong, P. T. and Mantsch, H. H. (1990). Structural studies with the uveopathogenic peptide M derived from retinal S-antigen. *Biochemistry* **29**: 2925-2930.

Ozer, I. and Tacal, O. (2001). Method dependence of apparent stoichiometry in the binding of salicylate ion to human serum albumin: a comparison between equilibrium dialysis and fluorescence titration. *Analytical Biochemistry* **294**: 1-6.

Pace, C. N. and Schmid, F. X. (1997). How to determine the molar absorbance coefficient of a protein. In Creighton, T. E. (Ed.), *Protein structure: a practical approach*. Oxford, IRL Press. Pp.253-259.

Pan, K. M., Baldwin, M., Nguyen, J., Gasset, M., Serban, A., Groth, D., Mehlhorn, I., Huang, Z., Fletterick, R. J., Cohen, F. E. and Prusiner, S. B. (1993). Conversion of α-helices into β-sheets features in the formation of the scrapie prion proteins. *Proceedings of the National Academy of Sciences USA* **90**: 10962-10966.

Pan, T., Wong, B. S., Liu, T., Li, R., Petersen, R. B. and Sy, M. S. (2002). Cell-surface prion protein interacts with glycosaminoglycans. *Biochemical Journal* **368**: 81-90.

Panick, G., Malessa, R. and Winter, R. (1999). Differences between the pressure- and temperature-induced denaturation and aggregation of β-lactoglobulin A, B, and AB monitored by FT-IR spectroscopy and small-angle X-ray scattering. *Biochemistry* **38**: 6512-6519.

Pauly, P. C. and Harris, D. A. (1998). Copper stimulates endocytosis of the prion protein. *Journal of Biological Chemistry* **273**: 33107-33110.

Perrin, D. D. and Dempsey, B. (1974). *Buffers for pH and metal ion control*. London, Chapman and Hall.

Pesce, A. J. Rosen, C. -G. and Pasby, T. L. (1971). *Fluorescence spectroscopy: an introduction for biology and medicine*. New York, Marcel Dekker Inc.

Prusiner, S. B. (1998). Prions. *Proceedings of the National Academy of Sciences USA* **95**: 13363-13383.

Qin, K. F., Yang, Y., Mastrangelo, P. and Westaway, D. (2002). Mapping Cu(II) binding sites in prion proteins by diethyl pyrocarbonate modification and matrix-assisted laser desorption ionization-time of flight (MALDI-TOF) mass spectrometric footprinting. *Journal of Biological Chemistry* **277**: 1981-1990.

Quaglio, E., Chiesa, R. and Harris, D. A. (2001). Copper converts the cellular prion protein into a protease-resistant species that is distinct from the scrapie isoform. *Journal of Biological Chemistry* **276**: 11432-11438.

Riek, R., Hornemann, S., Wider, G., Glockshuber, R. and Wuthrich, K. (1997). NMR characterization of the full-length recombinant murine prion protein, mPrP(23-231). *FEBS Letters* **413**: 282-288.

Schmid, F. X. (1997). Optical spectroscopy to characterize protein conformation and conformational changes. In Creighton, T. E. (Ed.), *Protein structure: a practical approach*. Oxford, IRL Press. Pp.261-297.

Selvin, P. R. (1995). Fluorescence resonance energy transfer. *Methods in Enzymology* **246**: 300-334.

Shiraishi, N., Ohta, Y. and Nishikimi, M. (2000). The octapeptide repeat region of prion protein binds Cu(II) in the redox-inactive state. *Biochemical and Biophysical Research Communications* **267**: 398-402.

Shyng, S. L., Lehmann, S., Moulder, K. L. and Harris, D. A. (1995). Sulfated glycans stimulate endocytosis of the cellular isoform of the prion protein, PrP^{C}, in cultured cells. *Journal of Biological Chemistry* **270**: 30221-30229.

Simonic, T., Duga, S., Strumbo, B., Asselta, R., Ceciliani, F. and Ronchi, S. (2000). cDNA cloning of turtle prion protein. *FEBS Letters* **469**: 33-38.

Smith, C. J., Drake, A. F., Banfield, B. A., Bloomberg, G. B., Palmer, M. S., Clarke, A. R. and Collinge, J. (1997). Conformational properties of the prion octa-repeat and hydrophobic sequences. *FEBS Letters* **405**: 378-384.

Smith, R. D. and Lightwahl, K. J. (1993). The observation of non-covalent interactions in solution by electrospray ionization mass spectrometry: promise, pitfalls and prognosis. *Biological Mass Spectrometry* **22**: 493-501.

Stella, L., Venanzi, M., Carafa, M., Maccaroni, E., Straccamore, M. E., Zanotti, G., Palleschi, A. and Pispisa, B. (2002). Structural features of model glycopeptides in solution and in membrane phase: a spectroscopic and molecular mechanics investigation. *Biopolymers* **64**: 44-56.

Stockel, J., Safar, J., Wallace, A. C., Cohen, F. E. and Prusiner, S. B. (1998). Prion protein selectively binds copper(II) ions. *Biochemistry* **37**: 7185-7193.

Stryer, L. (1978). Fluorescence energy transfer as a spectroscopic ruler. *Annual Review of Biochemistry* **47**: 819-846.

Sumudhu, W., Perera, S. and Hooper, N. M. (2001). Ablation of the metal ion-induced endocytosis of the prion protein by disease-associated mutation of the octarepeat region. *Current Biology* **11**: 519-523.

Sunde, M. and Blake, C. C. (1998). From the globular to the fibrous state: protein structure and structural conversion in amyloid formation. *Quarterly Reviews of Biophysics* **31**: 1-39.

Surewitz, W. K. and Mantsch, H. H. (1988). New insight into protein secondary structure from resolution-enhanced infrared spectra. *Biochimica et Biophysica Acta* **952**: 115-130.

Susi, H. and Byler, D. M. (1983). Protein structure by Fourier transform infrared spectroscopy: second derivative spectra. *Biochemical and Biophysical Research Communications* **115**: 391-397.

Susi, H. and Byler, D. M. (1986). Resolution-enhanced Fourier transform infrared spectroscopy of enzymes. *Methods in Enzymology* **130**: 290-311.

Tasumi, M. (1979). Interaction of metal ions with peptides in aqueous medium as studied by infrared and Raman spectroscopy. In Theophanides, T. M. (Ed.), *Infrared and Raman spectroscopy of biological molecules*. Dordrecht, D. Reidel Publishing Company. Pp. 225-240.

Torreggiani, A., Bonora, S. and Fini, G. (2000a). Raman and IR spectroscopic investigation of zinc(II)-carnosine complexes. *Biopolymers* **57**: 352-364.

Torreggiani, A., Tamba, M. and Fini, G. (2000b). Binding of copper(II) to carnosine: Raman and IR spectroscopic study. *Biopolymers* **57**: 149-159.

Van Rheede, T., Smolenaars, M. M., Madsen, O. and De Jong, W. W. (2003). Molecular evolution of the Mammalian prion protein. *Molecular Biology and Evolution* **20**: 111-121.

Veenstra, T. D. (1999). Electrospray ionization mass spectrometry in the study of biomolecular non-covalent interactions. *Biophysical Chemistry* **79**: 63-79.

Veenstra, T. D., Johnson, K. L., Tomlinson, A. J., Craig, T. A., Kumar, R. and Naylor, S. (1998a). Zinc-induced conformational changes in the DNA-binding domain of the vitamin D receptor determined by electrospray ionization mass spectrometry. *Journal of the American Society for Mass Spectrometry* **9**: 8-14.

Veenstra, T. D., Johnson, K. L., Tomlinson, A. J., Kumar, R. and Naylor, S. (1998b). Correlation of fluorescence and circular dichroism spectroscopy with electrospray ionization mass spectrometry in the determination of tertiary conformational changes in calcium-binding proteins. *Rapid Communications in Mass Spectrometry* **12**: 613-619.

Viles, J. H., Cohen, F. E., Prusiner, S. B., Goodin, D. B., Wright, P. E. and Dyson, H. J. (1999). Copper binding to the prion protein: structural implications of four identical cooperative binding sites. *Proceedings of the National Academy of Sciences USA* **96**: 2042-2047.

Viles, J. H., Donne, D., Kroon, G., Prusiner, S. B., Cohen, F. E., Dyson, H. J. and Wright, P. E. (2001). Local structural plasticity of the prion protein. Analysis of NMR relaxation dynamics. *Biochemistry* **40**: 2743-2753.

Warner, R. G., Hundt, C., Weiss, S. and Turnbull, J. E. (2002). Identification of the heparan sulfate binding sites in the cellular prion protein. *Journal of Biological Chemistry* **277**: 18421-18430.

Weber, G. and Shinitzky, M. (1970). Failure of energy transfer between identical aromatic molecules on the excitation at the long wavelength edge of absortion spectrum. *Proceedings of the National Academy of Sciences USA* **65**: 823-830.

Whittal, R. M., Ball, H. L., Cohen, F. E., Burlingame, A. L., Prusiner, S. B. and Baldwin, M. A. (2000). Copper binding to octarepeat peptides of the prion protein monitored by mass spectrometry. *Protein Science* **9**: 332-343.

Windl, O., Dempster, M., Estibeiro, P. and Lathe, R. (1995). A candidate marsupial PrP gene reveals two domains conserved in mammalian PrP proteins. *Gene* **159**: 181-186.

Wong, B. S., Pan, T., Liu, T., Li, R., Gambetti, P. and Sy, M. S. (2000). Differential contribution of superoxide dismutase activity by prion protein in vivo. *Biochemical and Biophysical Research Communications* **273**: 136-139.

Wong, B. S., Pan, T., Liu, T., Li, R., Petersen, R. B., Jones, I. M., Gambetti, P., Brown, D. R. and Sy, M. S. (2000). Prion disease: A loss of antioxidant function?. *Biochemical and Biophysical Research Communications* **275**: 249-252.

Wong, C., Xiong, L. W., Horiuchi, M., Raymond, L., Wehrly, K., Chesebro, B. and Caughey, B. (2001). Sulfated glycans and elevated temperature stimulate PrP^{Sc}-dependent cell-free formation of protease-resistant prion protein. *EMBO Journal* **20**: 377-386.

Woody, R. W. (1994). Circular dichroism of peptides and proteins. In Nakanishi, K. Berova, N. and Woody, R. W. (Eds.), *Circular dichroism principles and applications*. New York, VCH Publishers Inc.

Woody, R. W. (1995). Circular dichroism. *Methods in Enzymology* **246**: 34-71.

Wootton, J. C. (1994). Non-globular domains in protein sequences: automated segmentation using complexity measures. *Computational Chemistry* **18**: 269-285.

Wootton, J. C. (1994). Sequences with 'unusual' amino acid compositions. *Current Opinion in Structural Biology* **4**: 413-421.

Wopfner, F., Weidenhofer, G., Schneider, R., von Brunn, A., Gilch, S., Schwarz, T. F., Werner, T. and Schatzl, H. M. (1999). Analysis of 27 mammalian and 9 avian PrPs reveals high conservation of flexible regions of the prion protein. *Journal of Molecular Biology* **289**: 1163-1178.

Wright, P. E. and Dyson, H. J. (1999). Intrinsically unstructured proteins: re-assessing the protein structure-function paradigm. *Journal of Molecular Biology* **293**: 321-331.

Wu, P. and Brand, L. (1994). Resonance energy transfer: methods and applications. *Analytical Biochemistry* **218**: 1-13.

Yoshida, H., Matsushima, N., Kumaki, Y., Nakata, M. and Hikichi, K. (2000). NMR studies of model peptides of PHGGGWGQ repeats within the N-terminus of prion proteins: a loop conformation with histidine and tryptophan in close proximity. *Journal of Biochemistry* **128**: 271-281.

Yu, X., Wojciechowski, M. and Fenselau, C. (1993). Assessment of metals in reconstituted metallothioneins by electrospray mass spectrometry. *Analytical Chemistry* **65**: 1355-1359.

Zahn, R., Liu, A., Luhrs, T., Riek, R., von Schroetter, C., Lopez Garcia, F., Billeter, M., Calzolai, L., Wider, G. and Wuthrich, K. (2000). NMR solution structure of the human prion protein. *Proceedings of the National Academy of Sciences USA* **97**: 145-150.